UNITED KINGDOM · CHINA · MALAYSIA

Development of a Chitosan Based Glucose Responsive Nanoparticulate Insulin Delivery System

Asantewaa Yaa, B.Pharm, MPhil Pharmacy

Thesis submitted to the University of Nottingham in fulfilment of the requirements for the Degree of Doctor of Philosophy

October 2013

To my beloved mother Mrs Georgina Baffour Gyawu, my lovely husband Mr Kofi Osei, my adorable son Stephen Alfred Nhyiraba Osei, my dearest grandmother, Victoria Addai and my entire family. Thank you for being there for me through the thick and the thin of the period of my research

This thesis is the result of the author's original except for quotations and citations which have been duly acknowledged. It has not been previously or concurrently submitted for any degree at the University of Nottingham Malaysia Campus or any other institution.

Signed:

Date:

ACKNOWLEDGEMENTS

If I have ten thousand tongues I will continually sing praises to my maker, I am thankful to God for how far He has brought me, He has been with me every step along the way and today if what He promised me years ago is in sight, all I can say is a big thank you to Him.

I would like to express my sincere appreciation to my supervisor Assoc. Prof. Nashiru Billa for his immense support through the admission process and the course of this challenging research. Your fatherly love, your constructive criticism, support and your advice are invaluable, I am indeed a better person than what I used to be and your guidance through this process has churned the best out of me.

I would like to express my sincere thanks to my co-supervisor, Prof. Clive Roberts for his support throughout my study on the UK campus. Thank you for the encouragement and the faith you had in me that propelled me to reach out for the best, you never gave up on me and your time and effort you put into my project is deeply appreciated. I will also like to thank Dr. Jonathan Burnley and Dr. John Aylott as part of the supervisory team, your patience, unlimited encouragement and corrections helped the channelling of my project on the right course. I would like to thank Prof Stephen Doughty (Vice-Provost Teaching and Learning) for his support during the initial stages of study and also for being my internal assessor, along with Dr. Kok Wai Ling for their guidance and encouragement as well as contributing their precious time to be my internal assessors. My sincere thanks to Dr Andrew Morris, the Head of the School Pharmacy (Malaysia Campus), who in one way or the other contributed to the success of this project. Thanks to the Graduate school of the University of Nottingham Malaysia Campus for the training courses which I found to be very resourceful throughout my research.

My kindest appreciation goes to Prof Mak Joon, the Dean of the School of Postgraduate Studies and Research of International Medical University for his approval to run some analyses.

Many thanks to Dr. David Scurr, Dr. Christopher Parmenta, Prof. Chen, Paul Cooling and Catherine Ortori all of the University of Nottingham UK Campus, for helping me in the different aspects of my work, the technical knowledge imparted by you all is deeply appreciated.

Many thanks to all the lab technicians, the academic and non-academic staff in the School of Pharmacy University of Nottingham, Malaysia campus, the diverse ways you contributed to the success of this project is really appreciated.

My sincere thanks is also extended to the UNMC/Nottingham Malaysia Intercampus Doctoral Award Scheme (MIDAS) Scholarship for providing the financial support needed in the course of the project.

My sincere thanks goes to all my lab mates in drug delivery group (UNMC), the LBSA lab group (UNUK) and all my friends who have been supportive and helping me in completing the project in various ways, notably Mogana Sundari A/P Rajagopal, Lau Hui ling, Hilda Amekyeh and Dr. Adeyinka Temitope Aina. This journey has all been successful with your immense contribution in all aspects.

Finally I want to thank my family and friends in Ghana, to Mr Edward Bagyiri thank you for your support from such a distance, to Professor Ofori Kwakye I really appreciate your encouragement, Thelma Ohene Agyei, thank you for your sisterly love and encouragement. To my sister and brothers Dr. Mrs Sandra Osei Agyei, Kwame Mireku, Lemuel Wiafe Akenteng and Kwaku Afriyie Baffour Gyawu you give me a great reason to climb the highest and toughest mountains in life. A special thanks to my mum and dad (Mr and Mrs Baffour-Gyawu), to my

grand mum and grand dad (Victoria Addai and Stephen Boahene, Mr and Mrs Tagoe and to my in laws Prof. and Mrs Osei, you have all given me diverse reasons to pursue this dream and your constant advice, encouragement and prayers has seen me through. Lastly, I will like to thank my husband Mr Kofi Osei. Your patience, love, understanding, care and support is invaluable, you have indeed proved to me that Love helps us overcome all our fears.

Thank you all for making this project successful.

TABLES OF CONTENTS **Page**

LIST OF TABLES

Page

LIST OF FIGURES

Page

LIST OF EQUATIONS

Page

ABSTRACT

Research into responsive polymeric insulin delivery systems for the management of diabetes mellitus is gaining increasing interest due to the rise in the incidence rate and the burden of daily multiple subcutaneous insulin injections that needs to be endured by the patient. The present study attempted to formulate a nanoparticulate glucose responsive insulin delivery system from a natural polymer chitosan, using a safe glucose sensor, phenyl boronic acid (PBA), which is known to interact with glucose. In the present project, a new method for the production of chitosan tripolyphosphate (TPP) nanoparticles via ultrasonication was developed and optimised. The electrostatic method of tagging PBA onto chitosan was unsuccessful, but the method of N-reductive alkylation of introducing the PBA was successful. Evidence of PBA bonding on to chitosan was assessed by FTIR, ToF-SIMS, DSC and glucose adsorption sensitivity measurements. Glucose adsorption sensitivity to PBA-bonded chitosan polymer was directly related to the amount of PBA functionality within the conjugates and the physical nature of the matrices (porous or crystalline) as revealed by scanning electron microscopy (SEM). The nanoparticles showed glucose concentration dependent swelling with swelling decrease at a glucose concentration above 2.5mg/ml. Encapsulation of insulin into the nanoparticulate matrix was achieved by both the ionotropic gelation and polyelectrolyte complexation methods. Smaller particles with z-average between 140 – 150nm, lower Pdi and zeta potential between 17.5-19.1mV were characteristic of particles produced by PEC, whilst slightly larger particles with z-averages between 170-200nm, higher Pdi and zeta potential between +17.6-21.6mV were noticed for the particles produced by ionotropic gelation. Higher encapsulation of insulin of about 90% was achieved using the PEC method as compared to 34% from the ionotropic gelation series. The amount of drug encapsulated in both methods was pH dependent. *In vitro*

glucose dependent insulin release studied on PEC formulations showed a glucose and fructose concentration dependent release which was affected by the buffer system used. Lower insulin release from higher concentration of the sugars was attributed to the formation of bidentate interaction between the diols in the sugar and PBA, which restricts further expansion of the nanoparticles and hence reduces insulin release. This was confirmed by the SEM images of the nanoparticles after exposure to buffer, glucose and fructose in buffers at pH 7.4. Nanoparticles exposed to fructose showed more spherical and intact matrices whilst the buffer samples showed fragmented particles. The samples exposed to glucose showed some degree of fragmentation but not high as compared to that of nanoparticles exposed to buffer. The release of insulin from this formulation was therefore dependent on a complex interplay between the components of the buffer and the amount of sugar present.

CHAPTER 1

INTRODUCTION

1.1 General overview of diabetes and nanoparticulate delivery system

According to The World Health Organization (WHO), the number of people with diabetes is on the rise due to aging, urbanisation and more importantly, increased level of inactivity and increasing prevalence of obesity (WHO|Diabetes, 2013). Depending on the stream of management, there are two forms of the disease; Type I and Type II *diabetes mellitus*. Type I diabetes comes about due to the loss of pancreatic function. The loss of pancreatic function may be due to disease or injury to the pancreas which ultimately leads to loss of optimum glycaemic control. Thus, insulin needs to be injected subcutaneously three to four times daily to compensate for the needs of the body (Shaw *et al*. 2010; Kitagawa *et al*. 1994).

Management of Type I diabetes requires adequate skills and proper glucose monitoring since fluctuations in glucose concentration in the body can be fatal. On the other hand, in Type II diabetes there is a decrease in the body's secretion and sensitivity to insulin, which is usually caused by obesity. Proper life-style modifications usually ensure adequate glycaemic control (Gerstein and Haynes 2001; Owens *et al*. 2003).

With regard to Type I diabetes and in the in the light of the above constraints, many researchers have embarked on the design of insulin-containing delivery systems, with the aim of delivering insulin to the body in response to the variation of glucose concentration. In such delivery systems, it is often desirable to effect prolonged insulin delivery ideally through a feedback mechanism and ideally, these systems should not require invasive interventions. Many of such

attempts have been made in the designing of such delivery systems and various mechanisms of glucose sensation have been pursued. Some of these include insulin delivery systems based on hydrogels with a specific glucose sensing moiety (Matsumoto *et al*. 2003; Zha *et al*. 2011; Motornov *et al*. 2010).

Many researchers have utilised the combination of glucose oxidase with pH-sensitive hydrogels to sense changes in glucose concentration and regulate insulin release, henceforth within the pH-sensitive hydrogels containing glucose oxidase; glucose is converted to gluconic acid by glucose oxidase, thus lowering the pH in the hydrogels and hence the swelling of the hydrogels leading to insulin release. Thus, the pH-sensitive hydrogels containing glucose oxidase is made to control insulin release in response to the glucose concentration (Albin *et al*. 1985; Hassan *et al*. 1997; Parker *et al*. 1999; Traitel *et al*. 2000; Gu *et al*. 2013)

Another mechanism proposed is based on insulin-releasing hydrogels where moieties such as lectins act as the glucose sensing moiety. These proteins have unique carbohydrate-binding properties, and are very useful for the fabrication of glucose-sensitive systems. Therefore, some researchers have focused on the glucose-binding properties of concanavalin A (Con A), a lectin possessing four binding sites (Yin *et al*. 2010). The mechanism here is based on insulin being released from the hydrogel complex with Con A, in response of free glucose, based on the competitive and complementary binding properties of insulin and glucose to Con A (Brownlee and Cerami 1979; Kimiko *et al*. 1990; Obaidat and Park 1997).

The susceptibility of proteins to degradation by proteolytic enzymes and their inherent instability is a major drawback in their usage as glucose sensing moieties. Furthermore, the immunogenic reaction induced by lectins is also of concern.

Due to some of these drawbacks discussed, current research is beginning to focus on the formulation of glucose-sensitive hydrogels without biological components such as proteins, and rather utilising complex formation with glucose-sensing chemical moieties. One group of compounds with such glucose sensing moiety are the boronic acids. Boronic acids in the form of hydroxyboronate anion form a complex with cis-1,2 or 1,3-diol (Bachelier and Verchere 1995) and glucose being a diol has both groups, hence boronic acids will have the ability to reversibly bind the cis diols in glucose (figure 1.1).

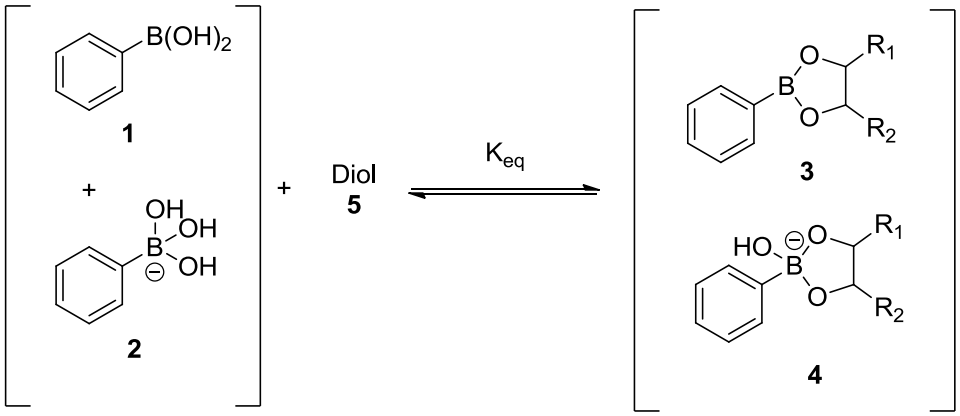

Figure 1.1 Reversible binding of boronic acid to diols (Springsteen and Wang 2002)

Boronic acids have been used in the development of feedback controlled drug delivery polymers as saccharide sensors and their potential applications pharmaceutically have been widely explored in enzyme inhibition, boron neutron capture therapy and antibody mimics for cell surface polysaccharides (Yang *et al*. 2003).

Figure 1.2 summarises some of the potential uses of boronic acids. Boronic acids have been studied and proven to be safe for use as glucose sensors (Yang *et al*. 2003; Kikuchi *et al*. 1996; Kataoka *et al*. 1994).

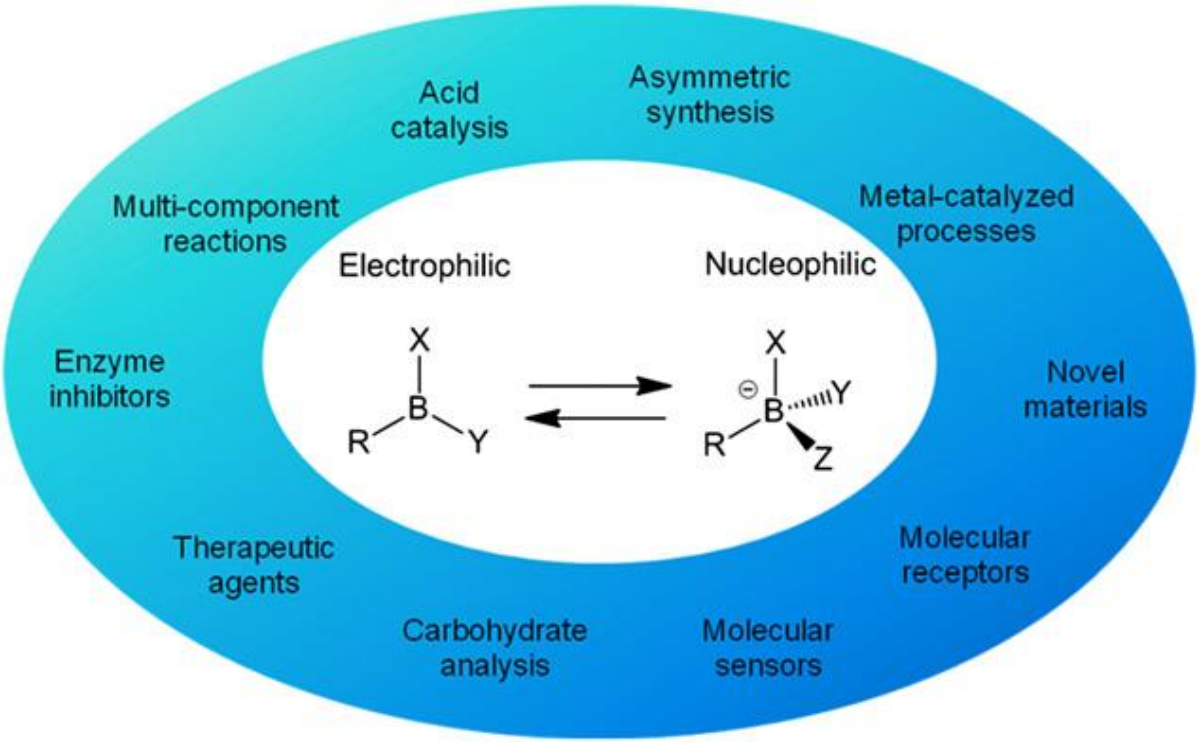

Figure 1.2 Various uses of boronic acids (Cambre and Sumerlin 2011)

Nanoparticles are receiving considerable attention in the delivery for therapeutic drugs. The literature emphasises the advantages of nanoparticles over microparticles (McClean *et al*. 1998) and liposomes (Soppimath *et al*. 2001). The submicron size of nanoparticles offers a number of distinct advantages over microparticles, including relatively higher intracellular uptake compared with microparticles. Other important advantages of nanoparticles as drug carriers include: high carrier capacity (many drug molecules can be incorporated in the particle matrix); feasibility of incorporation of both hydrophilic and hydrophobic substances and possibility of variable routes of administration. The nanoparticulate carriers can also be designed to enable controlled

(sustained) drug release (Agnihotri *et al*. 2004; Uner and Yener 2007). Nanoparticles are readily produced by various methods depending on the polymer being used. The formulated nanoparticulate delivery system must be compatible and desirably biodegradable and the formulation process must be simple and reproducible.

Chitosan is a well-studied polymer that has proven biodegradable and biocompatible properties (Kean and Thanou 2010). In the present study, we aimed to formulating glucose responsive insulin containing nanoparticles using chitosan as the parent polymer and boronic acid as the glucose sensing moiety by adopting a robust and yet a simple method. Nanoparticles have the highest surface area-to-volume ratio of any dosage form. This approach is unique, in that several of the previously proposed models were formulated as polymer strips or microparticles. Majority utilised synthetic polymers which are mostly non-biodegradable. The system presented in this study is based on a natural polymer in conjunction with a safe glucose sensing moiety.

1.2 Review of *diabetes mellitus*

Diabetes is a metabolic disorder which occurs when the pancreas does not produce enough insulin, or when the body cannot effectively utilise the insulin it produces. This leads to an increased concentration of glucose in the blood (hyperglycaemia) with disturbed carbohydrate, fat and protein metabolism (Amos *et al*. 1997; DiPiro *et al*. 2005).

1.2.1 Epidemiology and global estimates

According to WHO, the number of people with diabetes is increasing due to population growth, aging, urbanisation, and increasing prevalence of obesity and physical inactivity. 347 million people worldwide have diabetes (WHO, Diabetes, 2013). The world prevalence of diabetes among adults (20–79 years) was 6.4%, affecting 285 million adults in 2010 and is estimated to increase to 7.7% and 439 million adults by 2030. Between 2010 and 2030, there will be a 69% increase in numbers of adults with diabetes in developing countries and a 20% increase in developed countries. These predictions, based on a larger number of studies than previous estimates, indicate a growing burden on the management of diabetes, particularly in developing countries (Zimmet *et al*. 2001; Shaw *et al*. 2010). WHO projects that diabetes will be the 7th leading cause of death in 2030 (WHO | Diabetes, 2013).

Current estimates suggest that, globally, the number of people with diabetes will rise from 151 million in the year 2000, to 221 million by the year 2010, and to 300 million by 2025 *(Amos et al*. 1997; King *et al*. 1998). This rise is predicted to occur virtually in every nation, with the greatest increase expected in developing countries. Type II diabetes will account for nine patients in every ten of these diagnoses. This explosive increase in the prevalence of Type II diabetes,

and the consequences of its complications and associated disorders, represents the greatest health care challenge facing the world today (Zimmet *et al*. 2001).

1.2.2 Classification of *diabetes mellitus*

1.2.2.1 Type I and Type II *diabetes mellitus*

Type I diabetes occurs as a result of deficiency of insulin due to the destruction of pancreatic cells and this usually progresses to the stage of absolute insulin deficiency. In the majority of Japanese patients with Type I diabetes, an autoimmune process is thought to play a major role in cell destruction. Auto-antibodies to islet cell antigens are detected in many patients (70– 90%), particularly at the early stages (Kitagawa *et al*. 1998). Typically, it occurs in young subjects with acute onset, but may occur at any age, sometimes with slow progression (Fajans 1990). Occasionally, before the occurrence of clinical symptoms or hyperglycaemia, auto-antibodies or the loss of acute insulin response to intravenous glucose may be detected.

Most patients previously labelled as "Non-Insulin Dependent *Diabetes Mellitus*" (NIDDM) have now been grouped into Type II category. In this type, the mass of pancreatic cells and their function are preserved to some extent and insulin injection is seldom required. Both decreased insulin secretion and decreased insulin sensitivity (insulin resistance) are involved in its pathogenesis. The relative role of these two factors varies between patients. With regard to insulin secretion, the acute insulin response to a glucose load is characteristically defective. The majorities of patients are obese or have been obese in the past (Kitagawa *et al*. 1998).

Typically, Type II diabetes develops after middle age, but may occur in younger people. Screening by urinalysis of large number of school children has revealed that Type II diabetes has been steadily increasing since the 1970s. The incidence of Type II diabetes is very low under the age of 10 years, but exceeds the incidence of Type I diabetes in mid-teens. About 80% of them are obese (Kitagawa *et al*. 1994).

1.2.2.2 Gestational *diabetes mellitus* (GDM)

GDM is a state of glucose intolerance occurring or detected for the first time during pregnancy. Thus, pregnancy is a diabetogenic factor. Etiologically, many GDM patients probably share common genetic susceptibilities with Type I or Type II diabetes, and the deterioration of glucose tolerance is precipitated by the metabolic effect of pregnancy. The reason to treat GDM as an independent category is its clinical importance which requires special consideration. During pregnancy, glucose intolerance milder than 'diabetic type' may affect the infant and mother adversely. Glucose intolerance during pregnancy is often normalised after delivery, but such cases are at higher risk of developing diabetes in the future (Kim *et al*. 2002; Jovanovic 2001).

1.2.3 Complications of *diabetes mellitus*

There are lots of complications that arise with *diabetes mellitus*, due to the different metabolic derangement that the body is subjected to. It affects the vascular system; leading to peripheral neuropathy, retinopathy, hypertension and coronary heart disease, the renal system; leading to microalbuminuria and nephropathy. All these complications make diabetes a condition worth giving attention to and its management done with care and discipline on the patient's side (DiPiro *et al*. 2005).

1.2.4 Management of *diabetes mellitus*

The management of this condition is multifaceted. It requires quality medical attention and discipline also from the patient. The discipline stems out of the needed lifestyle modification by the patient for adequate glycaemic control.

Multiple daily injection of insulin is the main stream of therapy for Type I diabetes coupled with lifestyle modification by the patient. Their diet and general health needs to be monitored; any complication related to the condition also needs to be attended to (Gerstein and Haynes 2001).

Type II management is multifaceted, requiring weight reduction, calorie restriction and patient education. Adequate self-management remains the cornerstones of management of Type II diabetes. However, many patients are unable to sustain satisfactory long-term glycaemic control after achieving a temporary response, and medical treatment such as oral hypoglycaemic including the biguanides (metformin), sulphonylureas (glizone), glucose oxidase inhibitors (acarbose), metiglinides (repaglinde) and the thiazolidines (pioglitazone), or insulin are subsequently needed, depending on the severity and the stage of the disease (Guthrie 1997; Balfour and McTavish 1993; Bailey 1993; Saltiel and Horikashi 1995). Recently, new breeds of antidiabetic drug called the SGLT-2 inhibitors (dapagliflozin, canagliflozin) are under study and not yet approved by the FDA. These can be used in conjunction with other oral hypoglycaemics (Shah *et al*. 2012). Results produced so far shows their possible use in the management of Type II diabetes.

1.3 Insulin

Insulin is a polypeptide hormone formed, after elimination of C peptide by hydrolysis. It comprises of 51 amino acids in the form of two chains of 21 and 30 amino acids, connected by two disulphide bridges (figure 1.3). It has a molecular weight of 5808 Dalton. It is secreted by the ß cells of the islets of Langerhans of the pancreas (Structural Biochemistry).

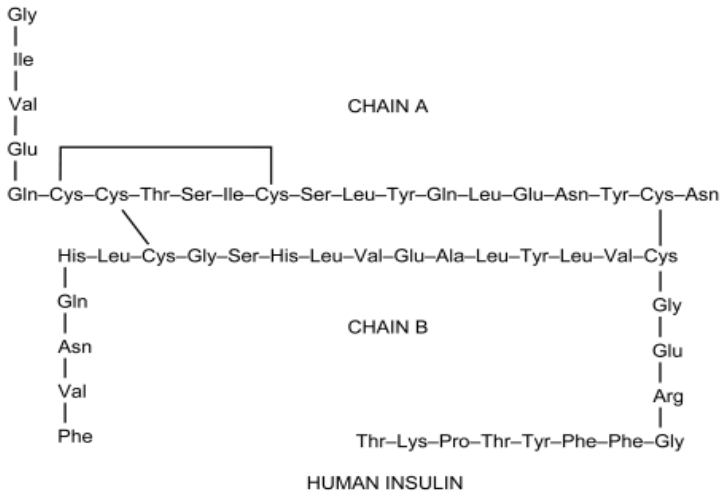

Figure 1.3 Amino acid sequence of human insulin (Insulin: Martindale)

It is the central hormone that regulate the energy and glucose metabolism in the body and causes cells in the liver, muscle, and fat tissue to take up glucose from the blood, storing it as glycogen in the liver and muscle. It restrains the use of fat as an energy source (Fajans 1990; Rave *et al*. 2000). When insulin is absent, glucose is not taken up by body cells, and the body begins to use fat as an energy source.

Figure 1.4 shows the hexameric 3D structure of insulin, coordinated by two zinc ions. It is believed to be the form in which insulin is stored in the beta-cells of the islets of Langerhans prior to release. It belongs to the group of peptides called IGF (insulin like growth factors) or somatomedins (Insulin: Martindale, 2013). However, its structure varies slightly between species and it has been noted that, insulin from animal differs in strength (carbohydrate metabolism) from that of humans. Porcine insulin is especially close to the human version (Richter and Neises 2003).

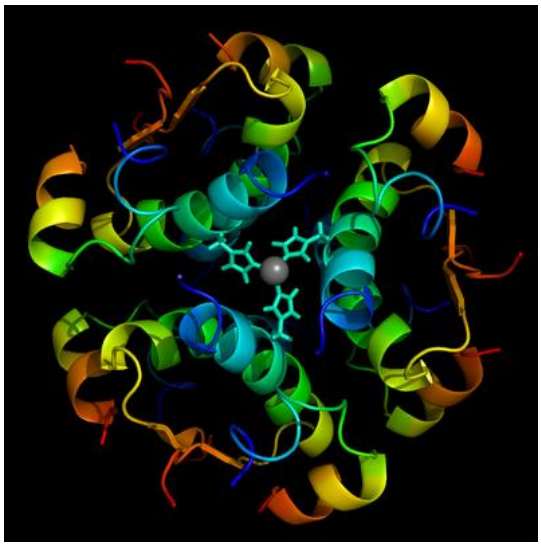

Figure 1.4 Hexameric 3D structure of insulin ("Beautiful proteins", 2013)

Subcutaneously injected Insulin is the mainstream therapy for Type I diabetes and sometimes for uncontrolled Type II *diabetes mellitus.* The dosage normally depends on the type of insulin being used and the extent of the condition (Kennedy 1991).

1.3.1 Classification of insulin

Insulin may be classified as rapid-acting, very rapid-acting, intermediate-acting, and long-acting, based on the number of hours until "peak" therapeutic effect. Peak action occurs when the concentration of insulin is greatest in the blood and has its greatest glucose-lowering effect.

Rapid and very rapid -acting insulin are often used before eating to control the large rise of blood glucose that often occurs after a meal. Ideally, short-acting insulin is taken approximately 30-45 minutes before the meal. Their duration of action is about 2 hours. Example is Humulin® and Insulin Lispro® by Eli Lilly (DiPiro *et al*. 2005; "Insulin Basics", 2013.).

Intermediate-acting insulins are absorbed 3-4 hours after injection and have their peak action after 7-9 hours. Again, there is considerable variation as the duration of action may be as much as 12-16 hours after injection. Used in the morning, its peak therapeutic effects could be observed in the afternoon. One of the best uses of this type of insulin is its injection at bedtime to control the morning glucose of the next day. An example is the Neutral Protamine Hagedorn® (NPH) insulin (also known as Humulin N, and Isophane insulin) produced by Novo Nordisk (DiPiro *et al*. 2005).

Long-acting insulin has a peak effect occurring after 10-12 hours and its duration of action may be 16-18 hours. It is not a popular insulin, but may be individuals in whom intermediate-acting insulins taken at bedtime act too quickly, resulting in hypoglycaemic reactions during the night. By its use, one can slow down the peak action by an hour or two, often preventing hypoglycaemia at night, but controlling the fasting sugar of the next day. Examples are Ultra Lente insulin, Human Ultra Lente (DiPiro *et al*. 2005; "Insulin Basics", 2013.).

1.3.2 Storage

Insulin is highly unstable and therefore it is recommended that unopened insulin be refrigerated (2^{o}C to 8^{o}C) prior to use. Once the insulin is in use, the manufacturer-recommended expiration dates will vary based on the insulin and delivery device. For financial reasons, patients may attempt to use insulins longer than their expiration dates, but careful attention must be paid to monitoring glycaemic control and signs of insulin decay such as clumping, precipitation and discoloration.

1.4 Routes of insulin delivery

The main mode of insulin delivery has been via subcutaneous route. The motivation for the search for an alternative route of delivery is to contribute to the avoidance of the burden of multiple subcutaneous injections, which will in turn improve compliance and improve the pharmacokinetics of insulin. More acceptable alternative routes of insulin administration have been and are being investigated including the dermal and oral route, however only the pulmonary and buccal insulin has become a feasible commercialised alternative thus far (Kumria and Goomber 2011).

1.4.1 Gastrointestinal route

This route is the most convenient way of delivering drugs and the administration of insulin by this route is attractive and has a potential of being utilised for insulin delivery. However, the acidic conditions in the stomach make it unfavourable for the delivery proteins, due to the susceptibility of proteins and peptides like insulin to degradation by the acidic conditions in the

stomach and enzymatic activities in the small intestines. Thus, the delivery of peptides via the oral route therefore presents its own challenges. Moreover, the gastrointestinal mucosa prevents absorption of large hydrophilic peptides. Several strategies, alone or in combination, have been developed to increase intestinal absorption of peptides such as insulin. They include the use of permeation enhancers such as bile salts and fatty acids, associated or not with enzyme inhibitors like aprotinin (Bendayan *et al*. 1994; Mesiha *et al*. 2002), liposomes, emulsions, mucobioadhesives and polymer-based delivery systems (Kisel *et al*. 2001). The use of polymers in encapsulating insulin into microspheres which degrade in the liver to release insulin has also been studied. All these strategies have achieved partial success and need further investigation (Reis and Damgé 2012).

1.4.2 Intranasal and pulmonary route of delivery

The epithelial surface of the of the nasal cavity offers a possible route for insulin delivery, but the main barriers to absorption include the active mucociliary clearance mechanism and the proteolytic enzymes present.

The respiratory tree offers the greatest potential for the delivery of polypeptides such as insulin, due to its high vascularisation and vast surface area. Until the dynamics of aerosol was recognised, there was not significant progress in the field of attempting to deliver insulin via inhalation (Owens *et al*. 2003). Though this route is a promising route of delivery, there are key factors that affect the delivery and efficiency of inhaled insulin via the route. These are the breathing pattern, the presence of air flow obstruction, interstitial lung disease, smoking, exercise and the patient's dexterity to handling delivery devices.

1.5 Insulin delivery devices

Historically, patients injected insulin subcutaneously using glass syringes with detachable needles, but these needles were large and made injections very painful. The discovery of disposable plastic 'diabetic syringes' with a fixed needle was an advancement which made injections less painful. Biphasic insulin therapy also solved the problem of dosage inaccuracies caused by improper mixing of short- and longer-acting insulin using the syringe.

The last five years have seen an increase in the range of insulin delivery devices. These devices have helped in the revolution of insulin self-care and comes in various forms such as, syringes, pens (Novo Nordisk and the Lily pens), insulin pumps and jet injectors (Owens *et al*. 2003).

1.5.1 Pulmonary insulin delivery devices

Current pulmonary drug delivery systems include a variety of pressurised metered dose inhalers (pMDI), dry powder inhalers (DPI), nebulizers and aqueous mist inhalers (AMI).

The Nektar/Exubera device is a DPI which uses compressed air to disperse an insulin powder formulation into a spacer reservoir prior to inhalation (Owens *et al*. 2003; Rave *et al*. 2000), but the marketing of this product has been discontinued due to fear of risk of causing lung toxicity on long term use (Heinemann 2008). Currently there is only one buccal insulin formulation being marketed. It is a liquid formulation that delivers insulin directly into the buccal mucosa. The deposition of the drug on the buccal mucosa allows the developers get over the earlier concerns about the risk of lung toxicity that was raised regarding Exubera® (Guntu and Dhand 2007; Kumria and Goomber 2011).

1.6 Insulin assay

1.6.1 Development of qualitative and quantitative assay for insulin

Biological assays were developed to assess the potency of insulin based on the measurement of the hypoglycaemic response in rabbits and convulsive response in mice because of the lack of knowledge of insulin's chemical structure after its discovery by Banting and Best in 1921. Variations of these approaches have been used since to validate the potency of insulin in pharmaceutical preparations. When Banting and co-workers found that insulin induced convulsions in rabbits when they are hypoglycaemic, the amount of insulin which produced convulsions in a rabbit in 2-4 h was defined as a unit of activity (Marks 1925). The method was adopted by the United States Pharmacopoeia and is still retained after a number of refinements in experimental design and analysis.

Unfortunately, the use of an anaesthetic in the procedure whilst obtaining blood for glucose measurement was known to have effect on the mouse's apparent response to insulin and some developmental work would be necessary before the technique could be changed.

1.6.2 Improvements in sensitivity of assay methods

The mouse convulsion and the rabbit and mouse blood glucose methods are sufficiently sensitive to detect insulin at the concentrations found in pharmaceutical preparations. Although they are the only currently internationally accepted assay methods, many other bio-assays for the analysis of insulin have been developed over the years for research and assay purposes. Among the more sensitive methods includes one developed by Bornstein (1950) in which adrenalectomised and hypophysectomised rats rendered alloxan diabetic were demonstrated to be sensitive to as little as 50 micro-units of insulin, whereas a normal intact mouse is sensitive to only 200 times that

amount. However, the skilled surgery required for the Bornstein technique made it generally unsuitable for routine insulin assays. About the same time, fairly sensitive *in vitro* methods were developed for the assay of insulin. It was shown by Groen *et al*. (1952) that, there was a relationship between insulin concentration and glucose uptake in the rat diaphragm. This method was sensitive to about 10 micro-units of insulin. Another method was developed by Winegrad and Renold (1958) based on the glucose uptake by the rat epididymal fat pad and that method was sensitive to 30 micro-units of insulin. However, according to Wright (1960), several substances, for example, free fatty acids and adrenalin, interfere with the diaphragm method and it was further shown by Riesler (1967) that, proteolytic enzymes leaked out of the cut muscle fibres to degrade the insulin. Also several authors have queried the specificity of the fat pad assay, so in spite of being very sensitive to insulin, both types of *in vitro* assay lacked precision and specificity.

1.6.2.1 Radioimmunoassay procedures

Yalow and Berson (1960) devised a sensitive, precise and specific radioimmunoassay for the determination of insulin at physiological concentrations. The radioimmunoassay technique of Hales and Randle (1963) was examined in Wellcome's Laboratories where a large number of insulin stability samples were considered to be the ideal proving ground for this method. But the results obtained were disappointing as they did not always correlate with biological potencies obtained for the same samples. It was also suspected that thermally induced changes in the configuration of the insulin molecule were causing some changes in molecular conformation, such as mono- or di-desamidation, leading to immunoassay values which in Wellcome's hands were falsely low or in other hands were falsely high, depending on the antibody used. As the

radioimmunoassay could not be shown to correlate with clinical or in vitro efficacy, and because of the real difficulty of reagent standardisation, it was not considered suitable for adoption by the regulatory authorities. However, the radioimmunoassay technique has been regularly used for fresh samples to monitor insulin activity during manufacture and purification. This technique costs about one sixth of the current *in vivo* bio-assay method and has the added advantage of not using animals. Therefore, it is the method of choice for in-process samples. Other insulin-orientated radioimmunoassay techniques have also been utilised at Wellcome to determine the amounts of hormone impurities, such as proinsulin, glucagon and pancreatic polypeptides, in order to ensure that they are present only in the lowest concentration possible in the finished product.

1.6.3 Current trends

The improvements in technology have over the last few years, opened the door to a new era of insulin testing. Firstly, improvements in manufacturing and purification processes have resulted in the production of very pure, virtually single component insulins. This was followed in 1986 by the establishment of separate international standards for human, bovine and porcine insulins by the World Health Organization.

Secondly, the advent of HPLC columns with greater resolving power has enabled further development by workers in this field to precisely assay insulins. This enables species to be identified and the proteins in the formulations can be separated and quantified. The procedure involves the introduction of insulin formulations to an ultra-pore column and the reading of the peaks produced. Using this technique, peaks of insulin and desamido insulin can be identified and quantified. It is the insulin and desamido insulin components which contribute to the

biological activity and calculation of the areas under the peaks produced by these can provide a quantitative analysis of the insulin and insulin-like components present in the formulations.

1.6.3.1 HPLC methods for insulin assay

Much work has been done on the use of HPLC as method for assaying insulin. The main variation in the methods has been the choice of column, the nature of mobile phases and the type of detection system used. In the assay of insulin, most work utilises reversed phase columns with large pore sizes (300 Å). The mobile phases ranges from the aqueous systems such as buffers and salt solutions, with the organic phase being mainly acetonitrile with modifiers like triflouroacetic acid (TFA) and diethyleneamine. The mode of detection of insulin is usually by ultra violet (UV) absorption at a wavelength of 214 nm (Moslemi *et al*. 2003; Kunkel *et al*. 1997), but the detection of insulin by fluorescence is achievable by labelling the insulin with fluorescein isothiocyanate (FITC) (Fisher and Smith 1986; Oliva *et al*. 2000; Sawicka *et al*. 2006). Mercoloni *et al.* (2008) and Sato *et al*. (1996) have however reported the use of fluorescence as the detection mode for insulin without labelling with FITC.

1.7 Review of nanoparticulate delivery system (NPDS)

Nanoparticulate delivery systems are defined as solid, submicron-sized drug carriers that may or may not be biodegradable (Couvreur *et al*. 1988;1995). The term nanoparticle is a collective name for both nanospheres and nanocapsules. Nanospheres have a matrix type of structure. Drugs may be absorbed at the sphere surface or encapsulated within the particle.

NPDS can be vesicular systems in which the drug is confined to a cavity consisting of an inner liquid core surrounded by a polymeric membrane (Couvreur *et al*. 1995). In this case, the active substances are usually dissolved in the inner core but may also be adsorbed to the capsule surface.

Nanoparticles are receiving considerable attention as drug carriers. The literature emphasises the advantages of nanoparticles over microparticles (Xuan *et al*. 2005) and liposomes (Soppimath *et al*. 2001). The submicron size of nanoparticles offers a number of distinct advantages over microparticles, including relatively higher intracellular uptake compared with microparticles. In terms of intestinal uptake, apart from their particle size, nanoparticle nature and charge properties seem to influence the uptake by intestinal epithelia. Intestinal uptake of nanoparticles prepared from hydrophobic polymers seems to be higher than that of particles with more hydrophilic surfaces (Jung *et al*. 2000); thus more hydrophilic particles may be rapidly eliminated from the gastrointestinal tract. Generally, nanoparticles based on hydrophobic polymers such as polystyrene, uncharged and positively charged, provide an affinity to follicle-associated epithelia as well as to absorptive enterocytes, whereas negatively charged polystyrene nanoparticles show only low affinity to any type of intestinal tissues. In contrast, nanoparticles based on negatively charged hydrophilic polymers, show a strong increase in bioadhesive properties and are absorbed by both M cells and absorptive enterocytes. A combination of both

nanoparticle surface charges and increased hydrophilicity of the matrix material seem to affect the gastrointestinal uptake in a positive sense (Fleige *et al*. 2012).

1.8 Methods used for the preparation of chitosan nanoparticles

In the present work, chitosan was selected as the polymer of choice because it is well-studied biocompatible and biodegradable. Chitosan is made from the deacetylation of chitin, a naturally occurring and abundantly available biocompatible polysaccharide mainly from marine crustaceans. The applications of chitin are limited compared to chitosan because chitin is chemically inert (Anthonsen *et al*. 1993). Acetamide group of chitin can be converted into amino group to give chitosan which is carried out by treating chitin with concentrated alkali solution. Chitosan is presented as powder, paste or film and in molecular weights.

Many methods have been proposed for preparing nanoparticles; and these methods can be classified into two main categories according to whether the formulation requires a polymerisation reaction or is achieved directly from a macromolecule or preformed polymer (Couvreur *et al*. 1995).

The polymerisation methods can be further classified into emulsion and interfacial polymerisation and there are two types of emulsion polymerisation—organic and aqueous—depending on the continuous phase. Nanoparticles can also be prepared directly from preformed synthetic or natural polymers and by desolvation of macromolecules (Pinto Reis *et al*. 2006).

Chitosan nanoparticles have been developed to encapsulate proteins such as bovine serum albumin, tetanus and diphtheria toxoid (Soppimath *et al*. 2001), vaccines (Vila *et al*. 2004), anticancer agents (Janes *et al*. 2001), insulin (Jintapattanakit *et al*. 2007), and nucleic acids (

Mao *et al*. 2001). Chitosan has also been reported to have considerably enhanced the absorption of peptides such as insulin and calcitonin across the nasal epithelium (Illum *et al*. 1994).

1.8.1 Ionic or ionotropic gelation

This technique involves the introduction of a cross-linking agent e.g. tripolyphosphate (TPP), into aqueous phase containing chitosan under magnetic stirring, thus leading to the formation of chitosan nanogels (Calvo *et al*. 1997). The process results in the controlled gelation of chitosan in the form of spherical, homogeneous and compact nanoparticles, characteristics that are expected to benefit the performance of the system both *in vivo* and *in vitro* (Liu and Gao 2009; Seda Tığlı Aydın and Pulat 2012).

1.8.2 Polyelectrolyte complex formation (PEC)

This is another method that has been used in the production of chitosan nanoparticles containing proteins. It is a mild method used to prepare nanoparticles at ambient temperature without the use of sonication and organic solvents. Thus, it is a suitable procedure used to encapsulate protein and peptides drugs that are sensitive to different stress factors. Bayat *et al*. (2008) , formulated insulin nanoparticles from chitosan and its quartenized derivatives by direct electrostatic interaction between the negatively charged insulin and positively charged chitosan and its quartenized derivatives. The manipulation of these PEC systems were pH dependent (Dakhara and Anajwala 2010).

1.9 Characterisation of nanoparticles

Nanotechnology offers many advantages to traditional drug design, delivery and medical diagnostics. However, nanomedicines present considerable challenges for preclinical development. Nanoparticle constructs intended for medical applications consist of a wide variety of materials, and their small size, unique physicochemical properties and biological activity often require modification of standard characterisation techniques. A rational characterisation strategy for nanomedicines includes physicochemical characterisation, sterility and, biodistribution (absorption, distribution, metabolism and excretion (ADME) and toxicity characterisation, which includes both *in vitro* tests and *in vivo* studies.

1.9.1 Physicochemical characterisation

Nanoparticle characterisation is necessary to relate the ultimate performance of particle with its physical properties and also establish understanding and control of nanoparticle synthesis and applications. Characterisation is done by using a variety of techniques, mainly drawn from material science.

The morphology and size of nanoparticles are very important in their characterisation. Many researchers working on nanoparticles indeed need to prove that the particles are nano in dimension. Size measurements are normally done using Photon Correlation Spectroscopy (PCS), which is also called dynamic light scattering. The system operates on the principle that, when a monochromatic light beam, such as a laser, is shone onto a solution with spherical particles in Brownian motion, the particles cause a Doppler Shift when the light hits the moving particle, changing the wavelength of the incoming light. This change is related to the size of the particle.

This method can give important details such as the computation of the sphere size distribution and give a description of the particle's motion in the medium, measuring the diffusion coefficient of the particle and using the autocorrelation function (López-León *et al*. 2005). The principles of measurement on different machines are the same, what differ is the make and the models of the instrument.

The morphology of nanoparticle is also an important parameter that needs to be assessed. Common techniques used are electron microscopy which includes Scanning Electron Microscopy (SEM), Transmission Electron Microscopy (TEM) and Atomic Force Microscopy (AFM).

The SEM uses a focused beam of high-energy electrons to generate a variety of signals at the surface of solid specimens. The signals that are derived from the electron-sample reveal information about the sample including the morphology (texture), chemical composition, and orientation of materials making up the sample. Areas ranging from approximately 1 cm to 5 microns in width can be imaged in a scanning mode using conventional SEM techniques (magnification ranging from 20x to approximately 30,000x, spatial resolution of 50 to 100 nm) (Alexander *et al*. 2009).

The TEM operates based on the sample principle as the light microscope but uses electrons for imaging other than light. Because TEM uses electrons and low wavelength beams, it is possible to get a resolution a thousand times better than with a light microscope. Objects that are a few angstroms (10^{-10} m) such as details in cell or different materials down to the near atomic level can be seen on the TEM (Transmission electron microscope, 2013).

SEM is based on scattered electrons while TEM is based on transmitted electrons. SEM focuses on the sample's surface and its composition whereas TEM provides the details about internal composition. Therefore, TEM can show many characteristics of the sample, such as morphology, crystallisation, stress or even magnetic domains. On the other hand, SEM shows only the morphology of the samples (Transmission electron microscope, 2013).

AFM can help achieve atomic resolution by using a sharp specially made cantilever tip. Images obtained by AFM can distinguish two closely spaced atoms. The image is created by quantifying the forces between the probe (cantilever tip) and the sample surface. Highly resolved three dimensional images can be obtained and normally, these images are free from large artefacts. In electron microscopy, special sample preparation is needed; also the sample viewing chamber must be under vacuum but AFM requires neither a vacuum environment nor any special sample preparation. Samples can also be viewed in the liquid medium and this implies that samples can be analysed in a near original condition (Grobelny *et al*. 2011). The resolution and power of viewing is also instrument-dependent. In each instance, the real shape of the nanoparticles can be discerned and if there is aggregation, it can also be observed.

The zeta potential of a particle is the overall charge that the particle acquires in a particular medium and can be measured on a Zetasizer® instrument. The magnitude of the measured zeta potential is an indication of the repulsive force that is present and can be used to predict the long-term stability of the product. If all the particles in suspension have a large negative or positive zeta potential then they will tend to repel each other and there is no tendency for the particles to come together. However, if the particles have low zeta potential values then there is no force to prevent the particles coming together and flocculating. The effect of the pH, concentration of an

additive or the ionic strength of the medium on the zeta potential and rheological properties can give information in formulating the product to give maximum stability.

Other physicochemical characterisation that can be done on nanoparticles iclude powder x-ray diffraction (XRD), fourier transform infrared spectroscopy (FTIR), matrix-assisted laser desorption/ionisation, time-of-flight mass spectrometry (MALDITOF), ultraviolet-visible spectroscopy and nuclear magnetic resonance (NMR) (Boonsongrit *et al*. 2008; Harish Prashanth and Tharanathan 2006). Each of these can harness valuable information with regard to the physical properties of the nanoparticles and its ultimate performance.

1.10 Polymeric controlled release drug delivery systems

The discovery and development of newer and more therapeutically efficient drugs have led to significant attention being focused on the development of methods by which these active substances are to be administered or delivered.

In conventional drug delivery, the drug concentration in the blood rises when the drug is taken, later and declines. Since each drug has a plasma level above which it is toxic and below which it is ineffective, the plasma drug concentration in a patient at a particular time depends on compliance with the prescribed routine. Controlled-release devices can be used to maintain the drug in the desired therapeutic range with just a single dose, thus localising delivery of the drug to a particular body compartment and reducing the systemic drug level. This gives the possibility of preserving medications that are rapidly destroyed by the body. There is also a reduction in the need for follow-up care and this increases patient comfort and/or improves compliance (Kost and Langer 2001).

The type of material used for controlled release can be classified as, biodegradable, non-biodegradable, non-biodegradable but soluble. These materials can be fabricated into microspheres, matrices and membranes. They are normally administered via the parenteral, implantation, oral and transdermal routes. Some of these delivery modules have been successfully commercialised (Soppimath *et al*. 2001; Allen and Cullis 2004).

1.10.1 Stimuli responsive polymeric drug delivery systems

The present research pursuit is aimed at developing a stimuli responsive delivery system sensitive to glucose concentration. The review below looks at the historic and future perspectives in research in this area.

In recent years, several research groups have been developing responsive systems which will be able to mimic the normal physiological process in which the amount of released drug is controlled according to the physiological needs of the individual. These responsive polymeric delivery systems can be classified as open or closed loop systems, depending on the mechanism of input and the how the output is effected. In the open-loop systems, the information about the controlled variable is not automatically used to adjust the system inputs to compensate for the change in the process variables. In closed-loop systems the controlled variable is detected and as a result the system output is adjusted accordingly. Open-loop systems are known as pulsed or externally regulated and the closed-loop systems as self-regulated (Kost and Langer 2001). The externally controlled devices apply external triggers in the form of magnetic, ultrasonic, thermal, and electric energy. On the other hand, self-regulated devices release rates are normally controlled by feedback information without any external intervention (Fleige *et al*. 2012).

1.10.1.1 Externally regulated delivery systems

In these modules, drug delivery is controlled by the application an external stimuli. These are reviewed below.

1.10.1.1.1 Magnetically modulated systems

In these release systems, drug release is controlled by the application of a magnetic field to the carrier of the drug and hence based on the design; the drug is released for pharmacological action. Studies have demonstrated that insulin and other molecules could be continuously released by embedding the hormone in a carrier like ethylenevinylacetate copolymer (Creque *et al*. 1980). These researchers conducted *in vitro* studies to characterise the parameters affecting the release rates, and later a single subcutaneous implant which decreased the glucose levels of diabetic rats for 105 days was designed (Brown *et al*. 1986). This group took a further initiative for the designing of a delivery system for use in diabetes. *In vitro* studies have also been conducted showing that the polymer-protein matrices containing magnetic beads exhibited enhanced release rates when placed in an oscillating external magnetic field (Edelman *et al*. 1985; Kost *et al*. 1987).

In vivo studies showed that when polymeric matrices containing insulin and magnetic beads are implanted in diabetic rats, glucose levels can be repeatedly decreased on demand by application of an oscillating magnetic field. A design comprising of polymeric matrix containing insulin and magnet was studied in diabetic rats. Here, it was discovered that blood glucose level dropped more than half of the initial concentration when exposed to external magnetic field. In the absence of the magnetic field, the blood glucose level remained high over the 51-day

implantation period. The researchers observed that, every time the magnetic field was applied, the blood glucose level reduced (Kost *et al*. 1987).

1.10.1.1.2 Ultrasonically modulated systems

Kost *et al*. (1988) suggested the feasibility of ultrasonically controlled polymeric delivery systems in which release rates of substances can be repeatedly modulated at will from a position external to the delivery system. Both bio-erodible and non-erodible polymers were investigated as drug carrier matrices. The bioerodible polymers evaluated were polyglycolide, polylactide, poly bis(p-carboxyphenoxy) alkaneanhydrides and their copolymers with sebacic acid. The releasing agents were p-nitroaniline, p-aminohippurate, bovine serum albumin and insulin.

Appreciable polymer erosion and drug release were observed when the bio erodible samples were exposed to ultrasound. The systems response to the ultrasonic triggering was quick, that is within 2 minutes and reversible. There was an enhanced release also in the non-erodible systems when they were exposed to ultrasound, but this time the release was diffusion dependent.

Kost *et al*. (1989) observed that, the release rates of zinc bovine insulin from ethylenevinylacetate copolymer matrices were 15 times higher when exposed to ultrasound compared to the unexposed periods. It has also been demonstrated that the extent of enhancement can be regulated by the intensity, frequency or duty cycle of the ultrasound.

Ultrasound was also evaluated as an enhancer for drug delivery through the skin. Tyle and Agrawala (1989) reviewed the topic of phonophoresis defined as the movement of drugs through living intact skin and into soft tissue under the influence of an ultrasonic perturbation. Studies

performed in the laboratories on the effect of ultrasound on implantable drug delivery devices provided the impetus to conduct studies to evaluate the systemic effect of ultrasound on drug permeation through the skin and explore its applicability as transdermal drug delivery enhancer or trigger when needed (Kost *et al*. 1989; Levy *et al*. 1989).

A novel ultrasound-responsive doxorubicin (DOX)-loaded nanoparticulate system has been developed, using poly(D,L-lactide-co-glycolide)-methoxypoly(ethylene glycol) (PLGA- PEG) complexing doxorubicin with a high encapsulation efficiency. Nanodroplets were formulated and were stabilised by a PEG shell. These nanodroplets were transformed into nanobubbles at 37 °C. Little amounts of drugs were released without the application of ultrasound. The nanodroplets demonstrated lower toxicity than the free drug (Du *et al*. 2011; Fleige *et al*. 2012).

1.10.1.1.3 Thermoresponsive delivery systems

Thermoresponsive hydrogels such as N-substituted polyacrylamide have been of interest in the field of controlled drug delivery (Okano *et al*. 1990). The thermosensitive hydrogels can be classified into two groups based on the origin of thermosensitivity in aqueous swelling *(Bae et al*. 1989; Hirokawa and Tanaka 1984). The first is based on polymer-water interactions, especially specific hydrophobic–hydrophilic balancing effects and the configuration of side groups. The other is based on polymer–polymer interactions in addition to polymer–water interactions.

Huffman *et al*. (1986) synthesised hydrogels based on N-isopropylacrylamide (NIPAAm) or N-isopropylacrylamide-methacrylic copolymers cross-linked with methylene-bis-acrylamide

(MBAAm). This group of researchers studied the absorption and release of vitamin B12, myoglobin and chymotrypsin from these hydrogels as a function of temperature. These gels were responsive to temperature changes and therefore the quick response of the gel surface to temperature changes may be utilised as an on–off switch for drug release (temperature changes prevent drug release due to instant surface shrinking).

Bae *et al.* (1989) reported that, there was some degree of insulin permeability through thermo sensitive hydrogels based on poly (N-acryloylpyrolidine) and its copolymers with styrene or 2 hydroxyethylmetacrylate cross-linked by ethyleneglycoldimethacrylate. The cross-linked poly(N-acryloylpyrolidine) homopolymer exhibited thermo sensitivity in water swelling, with weak mechanical strength, which restricted its practical application to diffusion experiments. The incorporation of a hydrophobic monomer into the polymer improved the mechanical strength and lowered the overall swelling level as well as the thermo sensitivity. It was observed that, insulin permeation through the copolymers could be regulated by changing the membrane composition and temperature. The permeability was mainly affected by the degree of hydration, regardless of chemical composition and temperature. The rate of insulin permeation through poly(hydroxyethylmethacrylate) increased with an increase in temperature, but in contrast the rate of insulin permeation through poly(N-acryloylpyrolidine) copolymers increased with a decrease in temperature. Therefore, temperature responsive polymers can also be used for drug delivery.

1.10.1.1.4 Electrically controlled responsive systems

D'Emanuele *et al.* (1988), proposed a drug delivery device which consisted of a polymer reservoir with a pair of electrodes placed across the rate-limiting membrane. By altering the magnitude of the electric field between the electrodes the authors proposed to modulate the drug release rates in a controlled and predictable manner. A linear relationship was found between electrical current and propanolol hydrochloride permeability through poly (2-hydroxyethylmethacrylate) (PHEMA) membranes. Buffer ionic strength as well as electrode polarity were found to have a significant effect on the drug permeability.

Grimshaw *et al.* (1989), demonstrated four distinct electrochemical and electromechanical mechanisms for selective controlled transport of proteins and neutral solutes across hydrogel membranes: (1) electrically and chemically induced swelling of a membrane to alter the effective pore size and permeability; (2) electrophoretic augmentation of solute flux within a membrane; (3) electroosmotic augmentation of solute flux within the membrane; and (4) electrostatic partitioning of charged solutes into charged membranes. Electric fields can cause changes in membrane ionisation states affecting membrane hydration and permeability. Eisenberg and Grodzinsky (1987) altered the restricted diffusion of sucrose through collagen membranes via electrodiffusion (effect of the electric field on concentration profiles within the membrane), producing flux changes up to 25%. Weiss *et al* (1986) produced a 16-fold increase in the permeability of similar PMMA membranes to 10 kDa dextran by using the electrolysis reaction at a platinum cathode to alter bash pH and, hence, membrane hydration.

The mechanisms described for electrically controlled membrane permeability are of current interest in the field of electrically controlled or enhanced transdermal drug delivery for example iontophoresis (Banga and Chien 1988). Over the past 60 or more years, the principles of

iontophoresis have been applied for localised drug delivery to muscles and joints (Okabe *et al.* 1986*;* Chien *et al*. 1987).

Current/voltage conditions for the iontophoretic application should: (1) be sufficiently high to provide a desired delivery rate; (2) not produce any harmful effects on the skin including a permanent alteration in the skin permeability; (3) establish a quantitative relationship between the flux and applied current/voltage; and (4) maintain constancy of the current/voltage during the experimental period. In addition, the drug should be electrochemically stable (Behl *et al*. 1989).

In order to overcome charge build up, irritation and burning of the skin in the area of prolonged continuous current electrode application, a pulsed current approach was evaluated. In this approach the current was turned on and off in short intervals. Using the pulsed current iontophoresis, the skin could tolerate much higher voltage and current conditions (Behl *et al*. 1989).

Films containing negatively charged Prussian Blue (PB) nanoparticles and positively charged gentamicin were prepared by Leprince *et al.* (2010). When oxidised, the negative charge of the PB nanoparticles changed to neutral, which led to the dissolution of the film. Control over the drug dosage was demonstrated by tuning the film thickness as well as the magnitude of the applied voltage. Drug release kinetics was changed to achieve different release by applying different electric potential profiles. The *in vitro* efficacy of this mode of drug delivery was confirmed by using a strain of *Staphylococcus aureus* (Schmidt *et al*. 2010; Fleige *et al*. 2012).

1.10.1.1.5 Chemically controlled delivery systems

1.10.1.1.5.1 pH and ionic strength responsive drug delivery systems

Several studies have been performed on polymers whose charge density depends on pH and ionic composition of the outer solution (Gumbleton and Schmaljohann 2006). Altering the pH of the solution will cause swelling or deswelling of the polymer. Polyacidic polymers will be unswollen at low pH, since the acidic groups become protonated and hence unionised. However at higher pH, the polyacid polymer swells. The opposite holds true for polybasic polymers, since the ionisation of the basic groups will increase with decreasing pH. Thus, drug release from reservoir or matrix devices made from these polymers will display release rates that are pH dependent (Kirstein *et al*. 1985; Fleige *et al*. 2012).

The pH range of fluids in various segments of the gastrointestinal tract may provide environmental stimuli for responsive drug release. Fildes (1976) developed a membrane to bypass the rumen of the cow which allowed release of its drug in the cow's fourth stomach. This polymeric membrane was highly impermeable at the rumen pH (pH 7), the rumen pH, but swelled at pH 4, which is the fourth stomach's pH.

1.10.1.1.5.2 Enzyme-sensitive hydrogels

Biodegradable polymers have become increasingly useful in biomedical fields because of their high potential for tissue engineering and drug delivery systems (Chasin and Langer 1991; Hollinger 1995). There are some specific enzymes that can digest specific polymers and this implies that sensitive hydrogels can be formulated from specific biodegradable polymers that can be degraded by these specific enzymes.

Some enzymes are used as important signals for diagnosis to monitor several physiological changes and specific enzymes in specific organs have become useful signals for site-specific drug delivery. Therefore, enzyme-sensitive hydrogels are promising candidates as enzyme sensors and enzyme-sensitive drug delivery systems since the incorporated drugs will only be released at specific sites. For example, the microbial enzymes that are predominantly present in the colon can be used as signals for site-specific delivery of drugs to the colon. Hovgaard and Brøndsted (1995) focused on the fact that microbial enzymes in the colon, such as dextranases, can degrade the polysaccharide dextran. They prepared dextran hydrogels cross-linked with diisocyanate for colon-specific drug delivery. The dextran hydrogels were degraded *in vitro* by a model dextranase, as well as *in vivo* in rats and in a human colonic fermentation model. Release of a drug from the dextran hydrogels could be controlled by the presence of dextranase. Drug release from the dextran hydrogels in the absence of dextranase was observed to be based on simple diffusion processes, however in the presence of dextranase it was mainly governed by the degradation of the dextran. Thus, it follows that dextran hydrogels are dextranase-sensitive and may hold promise as intelligent systems for colon-specific drug delivery.

Azoreductase is also useful for colon-specific drug delivery as it is an enzyme produced by the microbial flora of the colon. Few researchers have used azoaromatic bonds which can be degraded by azoreductase in the colon to construct azoreductase-sensitive hydrogels for colon-specific drug delivery. Kopecek *et al*. (1994) used azoaromatic bonds as cross-linking agents to prepare hydrogels and these hydrogels were pH-sensitive and biodegradable as they contained both acidic co monomers and azoaromatic cross-links. The hydrogels could protect protein drugs against digestion by proteolytic enzymes in the stomach. In the colon, azoreductase becomes accessible to the cross-links in the swollen hydrogels and can degrade the matrix to release the

protein drugs. These studies are examples showing that the combination of enzyme sensitivity with pH sensitivity enables site-specific drug delivery (Fleige *et al*. 2012).

1.10.1.1.5.3 Glucose responsive drug delivery systems

Glucose sensitive hydrogels are very useful in the development of self-regulated insulin delivery systems and enables the construction of artificial pancreas that administers the necessary amount of insulin in response to the rise in blood glucose concentration.

One of such system is that which combines glucose oxidase with pH-sensitive hydrogels to sense glucose and regulate insulin release. Within these pH-sensitive hydrogels is embedded or entrapped glucose oxidase. In contact with glucose, the glucose is converted to gluconic acid by glucose oxidase, this lowers the pH in the hydrogels (figure 1. 5). The lowering of the pH within the hydrogel leads to swelling of the hydrogel and hence insulin release. Thus, the pH-sensitive hydrogels containing glucose oxidase can be used to control insulin release in response to the glucose concentration (Miyata *et al*. 2002).

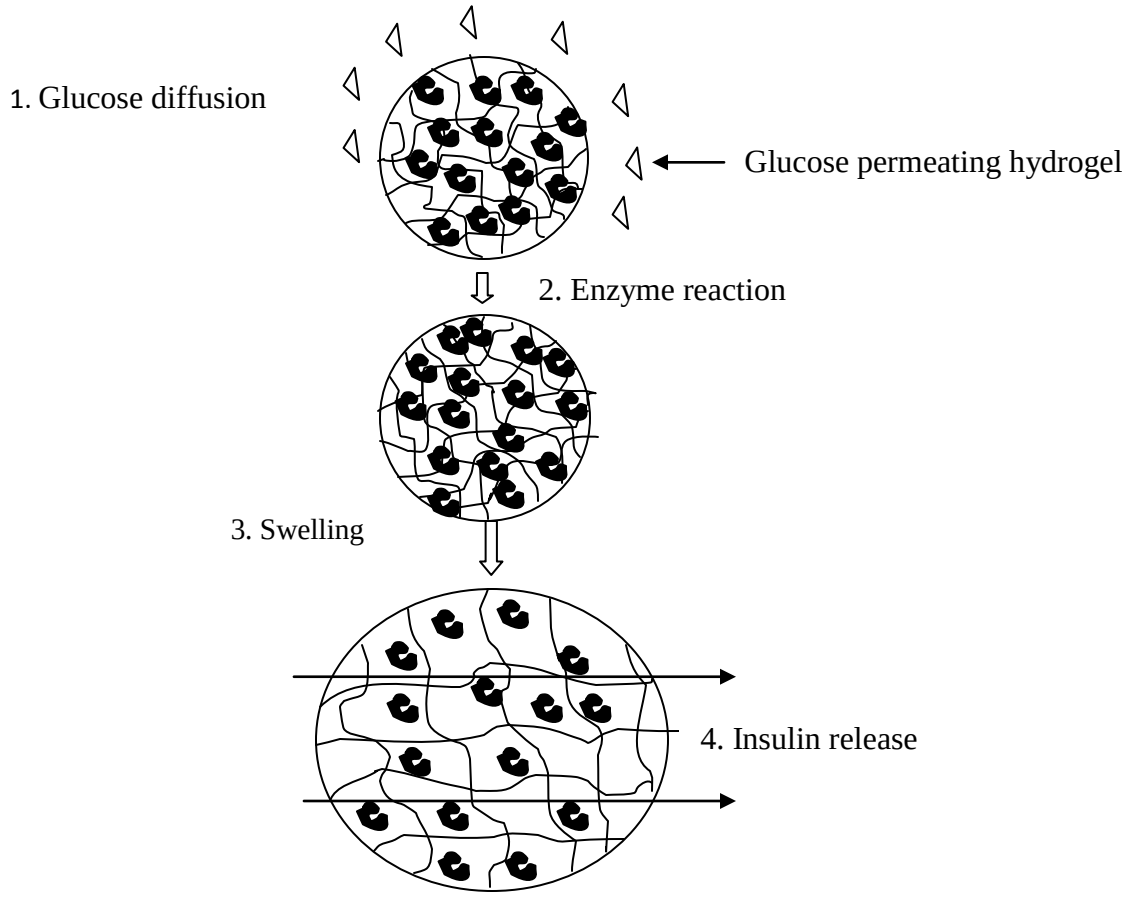

Figure 1.5 Mechanism of insulin release from a glucose oxidase loaded hydrogel. (Modified from Miyata *et al*. 2002)

For example Ishihara *et al*. (1984) combined a copolymer membrane of N, N-diethylaminoethyl methacrylate (DEA) and 2-hydroxypropyl methacrylate (HPMA) with a cross-linked poly(acrylamide) membrane, in which glucose oxidase and insulin were immobilised. The presence of glucose enhanced insulin permeability through the membrane which contained glucose oxidase. This glucose-sensitive insulin permeation was achieved based upon the combination of an enzymatic reaction with a pH-sensitive swelling. In this system, glucose diffuses into the membrane and is catalysed by glucose oxidase, resulting in the conversion of glucose to gluconic acid. The insulin permeation through the membrane was strongly dependent upon the glucose concentration. Furthermore, Ishihara *et al*. (1986) investigated insulin release

from polymer capsules containing insulin and glucose oxidase. Insulin release was inhibited in the absence of glucose, but was strongly enhanced in the presence of glucose.

Albin *et al*. (1985, 1987) entrapped glucose oxidase within hydroxyethyl methacrylate-N, N-dimethylaminoethyl methacrylate copolymer hydrogel membranes to construct a glucose-sensitive insulin delivery system. As in the other hydrogels reviewed earlier, the addition of glucose resulted in swelling of the membranes and an enhanced permeation of insulin from a reservoir via diffusion through the swollen hydrogel membranes.

Parker *et al*. (1999) and Hassan *et al*. (1997) copolymerised methacrylic acid (MAAc) with poly(ethylene glycol) monomethacrylate in the presence of activated glucose oxidase in order to prepare glucose-sensitive poly(methacrylic acid-g-ethylene glycol) (poly(MAAc-g-EG)) hydrogels. Carboxyl groups of MAAc formed a complex with etheric groups of ethylene glycol (EG) at a low pH, but the complex dissociated at a high pH, due to ionisation of the carboxyl groups. Therefore, the poly(MAAc-g-EG) hydrogels collapsed at a low pH, due to complexation between carboxyl groups and etheric groups, but were swollen at a high pH. Thus, poly(MAAc-g-EG) hydrogels showed pH-sensitivity caused by formation and dissociation of the complex in response to pH changes. The glucose oxidase-loaded poly(MAAc-g-EG) hydrogels showed a slower swelling rate at high glucose concentrations as seen in hyperglycemic conditions (200–500 mg/dl) than that at the lower glucose concentrations of normal blood (80 mg/dl). It is postulated that the poly(MAAc-g-EG) hydrogels squeeze out insulin during their collapse in the presence of glucose. Thus, the poly(MAAc-g-EG) hydrogels containing glucose oxidase showed a glucose-sensitivity resulting from the combination of the catalytic reaction of glucose oxidase and the pH-sensitive complex formation between carboxyl and etheric groups. Consequently,

glucose-sensitive insulin release can be achieved by using pH-sensitive hydrogels containing insulin and glucose oxidase (Qi *et al*. 2009).

Lectins, which are carbohydrate-binding proteins, interact with glycoproteins and glycolipids on the cell surface and induce various effects, such as cell agglutination, cell adhesion to surfaces, and hormone-like action. The unique carbohydrate-binding properties of lectins are very useful for the fabrication of glucose-sensitive systems. Therefore, some researchers have focused on the glucose-binding properties of Con A, a lectin possessing four binding sites.

Brownlee *et al.* (1979) and Kim *et al*. (1990) were pioneers in the development of glucose-sensitive insulin release systems using Con A. Their strategy was to synthesise a stable, biologically active glycosylated insulin derivative able to form a complex with Con A. The glycosylated insulin derivative could be released from its complex with Con A in the presence of free glucose, based on the competitive and complementary binding properties of glycosylated insulin and glucose to Con A. Furthermore, Makino *et al.* (1990), bound the self-regulated insulin delivery systems, enclosed in polymer membranes to soluble bead immobilised or cross-linked to Con A. Polymer membranes or microcapsules containing Con A and succinyl-amidophenyl-glucopyranoside insulin (SAPG-insulin) quickly controlled the release of SAPG-insulin in response to changes in the glucose concentration, based on the mechanism of the competitive and complementary binding properties of SAPG-insulin and glucose to Con A. Polymer membranes and microcapsules containing Con A and SAPG-insulin were used as self-regulated insulin release devices *in vitro* and could be optimised for use *in vivo* studies. These studies provided new concepts with regard to the competitive and complementary binding

properties of glucose derivatives and glucose to Con A, as well as their suitability for the fabrication of glucose-sensitive hydrogels (Makino *et al*. 1991)

Novel glucose-sensitive hydrogels were prepared using complex formation between Con A and the pendant glucose groups of PGEMA to produce cross-linked points in the hydrogels (Nakamae *et al.*, 1994). The Con A-entrapped PGEMA hydrogels were obtained by copolymerisation of a monomer with pendant glucose (GEMA) and a divinylmonomer in the presence of Con A. The density of cross-linkage of the resultant Con A-entrapped PGEMA hydrogels increased with increasing Con A concentration, suggesting that Con A acts as a cross-linking agent. The immersion of Con A-entrapped PGEMA hydrogels in an aqueous glucose solution resulted in their swelling and the swelling ratios were strongly dependent upon the glucose concentration (figure 1.6).

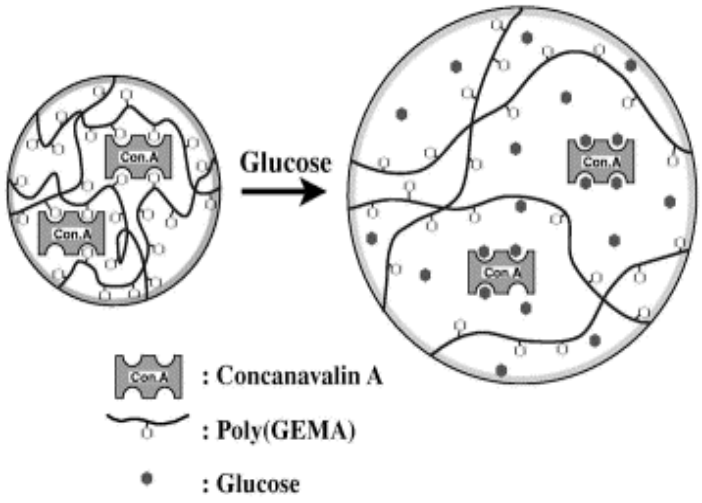

Figure 1.6 Schematic representation of glucose-sensitive swelling changes in a poly(GEMA)–Con A hydrogel (Miyata *et al*. 2002)**.**

Compressive modulus measurements revealed that the cross-linking density of Con A-entrapped PGEMA hydrogels decreased with increasing glucose concentration. The glucose-sensitive

swelling of Con A-entrapped PGEMA hydrogels was due to the presence of free glucose, which resulted in the dissociation of the complex via competitive exchange. Thus, the Con A-entrapped PGEMA hydrogels were able to recognise a specific monosaccharide and induce structural changes. These results suggest that Con A-entrapped PGEMA hydrogels have many potential applications as a novel glucose sensor and as new closed-loop insulin delivery system.

Lee and Park (1996) and Obaidat and Park (1996) prepared a type of hydrogel capable of sol–gel phase-reversible transitions based upon changes in the glucose concentration. It was shown that the mixture of a vinylpyrrolidinone-allylglucose copolymer with Con A led to the immediate formation of hydrogels, due to complex formation between pendant glucose groups and Con A. The addition of free glucose led to a phase transition of the hydrogel into the sol state. The concentration of free glucose in the environment had to be at least four times that of pendant glucose to induce the phase transition from gel to sol. The gel-sol phase transition in response to the free glucose concentration was repeated more than 10 times without any problems. The hydrogel was able to sense changes in the glucose concentration of the environment and respond to them in a reversible manner. Obaidat and Park (1997) also investigated the release of lysozyme and insulin as model proteins through glucose-sensitive hydrogel membranes using a diffusion cell. Porous poly(hydroxyethyl methacrylate) (PHEMA) membranes were used to sandwich glucose-containing polymers and Con A between the donor and receptor chambers of the cell. The release rate of the proteins from the receptor chamber to the donor chamber was strongly dependent upon the free glucose concentration. Their studies demonstrate that the glucose-sensitive sol–gel phase transition can be used to regulate insulin release in response to the free glucose concentration in the environment.

Kokufuta *et al* (1991), combined the carbohydrate-binding properties of Con A with the temperature-sensitive property of poly(N-ispropylacrylamide) (PNIPAAm) to prepare saccharide-sensitive hydrogels. Con A was loaded on a cross-linked PNIPAAm hydrogel that underwent a volume phase transition at 34°C. The Con A-loaded PNIPAAm hydrogel was shown to swell abruptly in the presence of the ionic saccharide dextran sulphate at temperatures close to the volume phase transition point. The abrupt swelling of the Con A-loaded PNIPAAm hydrogel caused by the ionic saccharide dextran sulphate was attributed to the ionic osmotic pressure exerted by the ionised saccharide. The replacement of the ionic saccharide dextran sulphate with a non-ionic saccharide led to the collapse of the hydrogel to its native volume. The temperature-sensitive property of PNIPAAm in the hydrogel contributed to a dramatic change in the swelling ratio, due to a shift in volume phase transition by complex formation.

All of the preceding studies utilised proteins, such as glucose oxidase or lectins, for the fabrication of glucose-sensitive hydrogels. The use of proteins and biological components within drug delivery systems has obvious draw-backs. Therefore this current project opts for the use of glucose-sensitive hydrogels without biological components such as proteins, but instead complex formation between a phenylboronic acid group and glucose.

Phenylboronic acid (PBA) and its derivatives form complexes with polyol compounds, such as glucose in aqueous solution. The complex between phenylboronic acid and a polyol can be dissociated in the presence of a competing polyol which is able to form a stronger complex. This means that complex formation between PBA and a polyol compound has many potential applications as a glucose-sensitive material.

Kitano *et al.* (1991) synthesised copolymers with PBA moieties (poly(NVP-co-PBA)) by copolymerising N-vinyl-2-pyrrolidone (NVP) and 3-(acrylamido)phenylboronic acid (PBA). Due to the reversible complex formation between PBA of poly(NVP-co-PBA) and poly(vinyl alcohol) (PVA), the competitive binding of phenylboronic acid with glucose and PVA could be utilised to construct a glucose-sensitive system. The formation and dissociation of the poly(NVP-co-PBA)/PVA complex could be investigated by observing the change in viscosity. The viscosity measurements revealed that poly (NVP-co-PBA) formed a complex with PVA in the absence of glucose. However, the complex dissociated in the presence of glucose. These results led to the concept of a glucose-sensitive insulin release system using poly (NVP-co-PBA) and PVA. The presence of free glucose resulted in swelling of the poly(NVP-co-PBA)/PVA complex hydrogel, due to complex dissociation (figure 1.7).

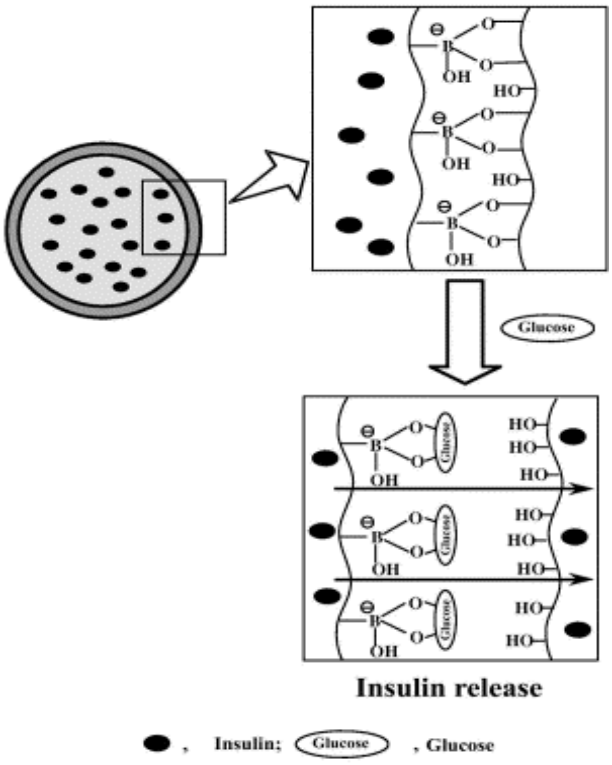

Figure 1.7 Concept of a glucose-sensitive insulin release system using PVA/poly(NVP-co-PBA) (polymer capsule type) (Kitano *et al*. 1991)

It was difficult for the researchers to use the poly(NVP-co-PBA)/PVA complex as a glucose-sensitive insulin release system, because of its intrinsic instability at a physiological pH of 7.4. To stabilise complex formation between phenylboronic acid and glucose at a physiological pH of 7.4, amino groups were introduced either into the polymer or in the vicinity of the PBA moiety (Kataoka *et al*., 1994). Furthermore, a glucose-sensitive hydrogel possessing both PBA and amino groups was prepared for the development of a novel glucose-sensitive insulin delivery system at physiological pH by Shiino *et al*. (1995). This glucose-sensitive insulin delivery system was based upon the complex formation between gluconated insulin and the PBA groups in the hydrogel. The gluconated insulin was released from the hydrogel in the presence of free glucose, which induced the dissociation of the complex. This system released insulin in response to the glucose concentration at a physiological pH.

PBA exists in equilibrium between the uncharged and the charged form. Complex formation between the uncharged form and glucose was shown to be unstable because of its high susceptibility to hydrolysis, while charged PBA groups were able to form a stable complex with glucose (figure 1.8). Complex formation between the charged PBA groups and glucose caused a shift in the equilibrium towards an increase of charged PBA groups. Therefore, the total amount of charged PBA groups increased and uncharged groups decreased when glucose was added. (Kost and Langer, 2001)

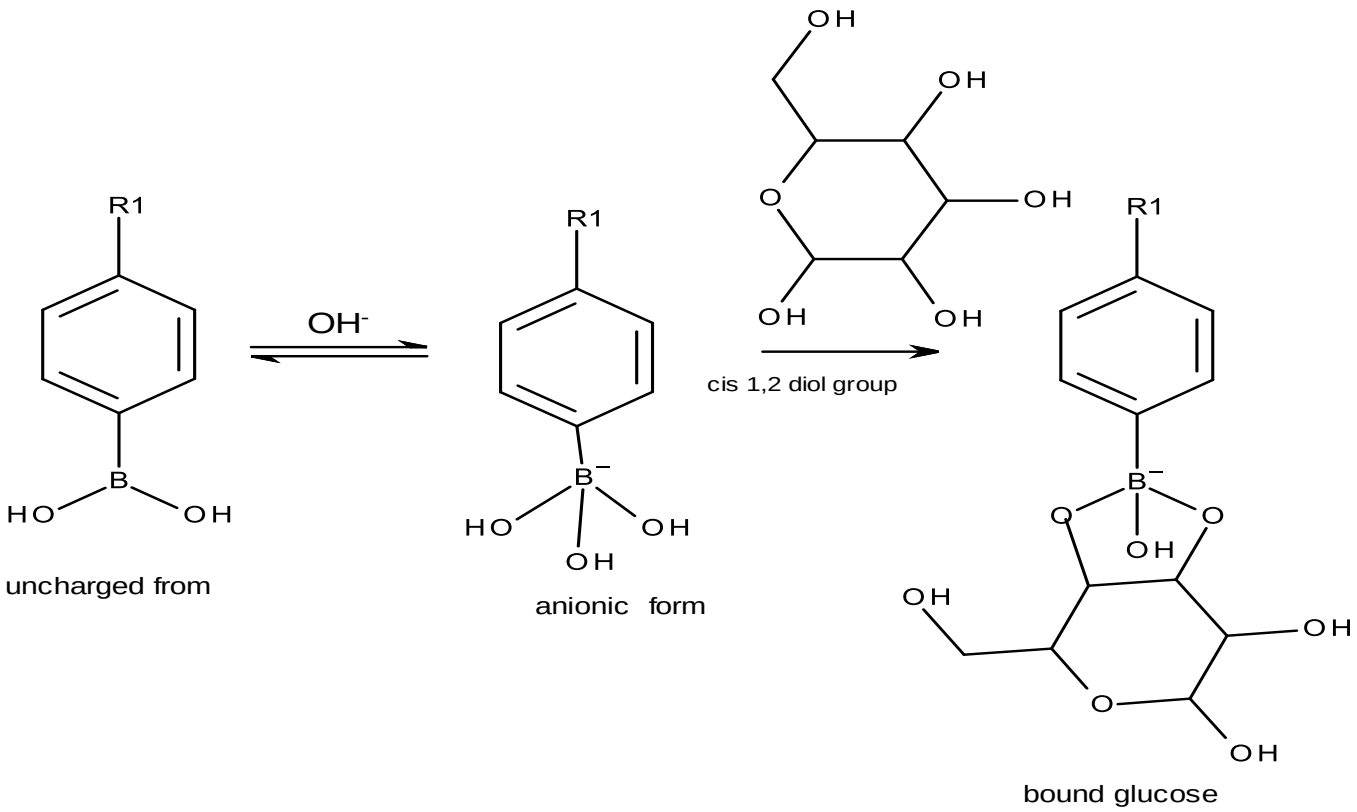

Figure 1.8 Reversible binding between boronic acid and cis diol in aqueous media

Wu *et al*. (2011) have investigated the utilisation of PBA-bonded chitosan nanoparticles as a vehicle for controlled insulin release. They attributed insulin release from the nanoparticles to glucose sensitivity of the PBA moiety and the molecular weight of the polymer.

In the current project, PBA was functionalised onto chitosan using a simple chemical reaction process (one pot reaction) which differs from the method used by Wu *et al.* (2011) in the above study. However we recognise that in order to enhance the sensitivity of the PBA-chitosan conjugates, the surface area must be increased. Therefore in our approach, we have sought to increase the surface area of the conjugate by also fabricating our chitosan PBA conjugates into nanoparticles, using methods that are reproducible, scalable and relatively simple.

1.11 Objectives of current project

In the light of the above review, the main objective of this project was to design and develop an insulin-containing glucose responsive nanoparticulate delivery system, such that the system will be able to release insulin in response to changes in external glucose concentration.

In order to achieve these objectives, the research was sectioned into the following aspects.

1. Identification of polymers and sensing moieties to be used.
2. Functionalisation or incorporation of sensing moiety onto polymer.
3. Characterisation of functionalised polymer.
4. Synthesis and characterisation of responsive nanoparticles out of the functionalised polymer.
5. *In vitro* analyses of the responsive polymers and the nanoparticles as a function of external media.

These aspects are reviewed in detail into the separate chapters that follow.

CHAPTER 2

PREPARATION OF CHITOSAN TRIPOLYPHOSPHATE (TPP) NANOPARTICLES BY IONOTROPIC GELATION

2.1. Introduction

Ionotropic gelation is one of the simplest approaches that have been utilised by several researchers in the preparation of chitosan nanoparticles. This technique is based on the principle that polyelectrolytes can cross link in the presence of counter ions to form hydrogels. The polyanions form a meshwork of structures by combining with the polyvalent cations and hence inducing gelation through binding with mainly the anion blocks. These hydrogel can be produced by dropping polyanion solution into an aqueous solution of a polyvalent cation. Different drugs and biomolecules can be loaded into these hydrogels during the production where they become enmeshed (Sarmento *et al*. 2006; Sadeghi *et al*. 2008). The use of chitosan, alginates and gellan gum for the encapsulation of drugs are based on the principle of ionotropic gelation.

There are different types of cross-linkers and a choice may be made based on safety profiles and degree of cross-linking. Chitosan nanoparticles and microparticles have been prepared by chemical cross-linking with glutaraldehyde, glyoxal and ethylene glycol diglycidyl ether. Although these were found to be efficient cross-linkers, they were not preferred in the present study owing to their physiological toxicity (Akbuga and Durmaz 1994; Berger *et al.* 2004).

Due to the polycationic nature of chitosan, it can interact with different negatively charged species such as tripolyphosphate (TPP) and sodium sulphate.

The interaction between TPP and chitosan leads to the spontaneous formation of biocompatible nanoparticles, which can be efficiently employed in the delivery of different drugs like proteins

and vaccines. The cross-linking density, crystallinity and hydrophilicity of cross-linked chitosan can allow modulation of drug release and extend its range of potential applications in drug delivery (Bhumkar and Pokharkar 2006).

Ionotropic gelation of chitosan with TPP involves the addition of aqueous TPP to the aqueous phase containing chitosan under magnetic stirring, thus leading to the formation of chitosan nanogels (Calvo *et al*., 1997). The process results in the controlled gelation of chitosan in the form of spherical, homogeneous and compact nanoparticles, characteristics that are expected to benefit the performance of the system both *in vivo* and *in vitro*. The use of magnetic stirring in the production of nanoparticles is time consuming and requires the use of large volumes of material.

Notwithstanding, the present work was aimed at the preparation of nanoparticles by employing ultrasonication; a process which imparts high frequency energy to induce electrostatic interaction. We theorised that due to the intense energy transmitted, the duration of preparation and the time required for the formation of the nanoparticles would be short. The optimal conditions to obtain desirable chitosan TPP nanoparticles were investigated.

2.2 MATERIALS AND METHODS

2.2.1 Materials

Low molecular weight chitosan, purchased from Sigma (Sigma-Aldrich Co. LLC, St Louis, Missouri, USA). Sodium tripolyphosphate (TPP), purchased from Thermofischer Scientific, Acetic acid, purchased from Merck, Millipore filtered, 18 Ω pure water, all other chemicals were of reagent grade.

2.3 Methods

2.3.1 Nanoparticle preparation by ultrasonication

Chitosan /TPP nanoparticles were prepared based on the ionotropic gelation of the polyanion and the polycation. Various concentrations of chitosan (1-10 mg/ml) were prepared by dissolving the required amount of chitosan in 1% acetic acid. The chitosan solution was then filtered and used for subsequent investigations. The ratios of chitosan to TPP studied were (3:1, 4:1, 5:1, 8:1 and 10:1). 5 ml of the chitosan solution was measured into a glass vial, clamped and the 13 mm diameter probe of the high intensity ultrasonicator (Vibra Cell, Sonics, VCX 750, USA) (figure 2.1) inserted into the chitosan solution (whilst ensuring that the tip of the probe does not touch the bottom of the vial). 5 ml of the TPP solution (prepared by dissolving the required amount of TPP in purified water) was added drop wise into the chitosan solution whilst the ultrasonicator was operated for 1 minute.

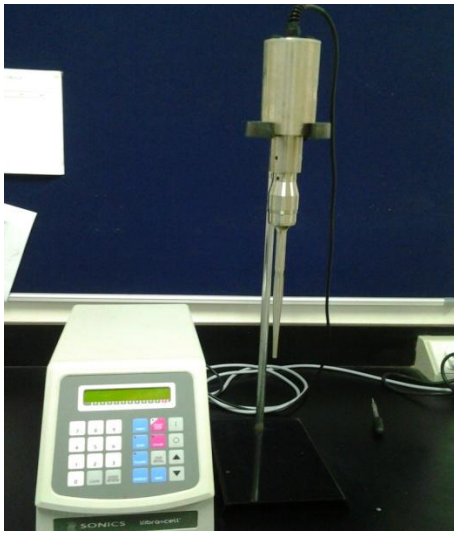

Figure 2.1: Image of the probe ultrasonicator (Vibra Cell, Sonics, VCX 750, USA)

2.3.2 Effect of ultrasonication amplitude on z-average and Pdi of nanoparticles

For the effect of ultrasonication amplitude on z-average and Pdi of nanoparticles, 5 ml of chitosan solution and 5 ml of TPP solution at a ratio of chitosan to TPP 3:1. The amplitude of ultrasonication was varied between 20% - 40% (150-300 Watts) and its effect on the z-average, Pdi and zeta potential of the nanoparticles were investigated using a Zetasizer Nano ZS® (Malvern, UK) equipped with a 4Mw He- Ne laser (633 nm). Each analysis was carried out at 25^{o}C and performed in triplicate and data expressed as mean ± standard deviation.

Calculation for ultrasonication power output

Maximum power output of the probe ultrasonicator = 750Watts at 100% amplitude of ultrasonication, if ultrasonicator is operated at 40% amplitude, Power output = $\frac{40}{100}$ *x 750 = 300 Watts.*

2.3.3 Effect of time of ultrasonication and volume of formulation on the final temperature and z-average of nanoparticles

For the effect of time of ultrasonication and the total volume of the formulation on the final temperature and z-average of nanoparticles, different total volumes of nanoparticle formulation (10- 50 ml) were prepared and the time of ultrasonication was varied between 1-5 minutes. The chitosan to TPP ratio in each preparation was fixed at 3:1 and the chitosan concentration fixed at 5 mg/ml. The final temperature of each formulation was then recorded using a digital probe thermometer and the z-average measured by Zetasizer Nano ZS® (Malvern, UK) equipped with a 4Mw He- Ne laser (633 nm). Each analysis was carried out at 25^{o}C and performed in triplicate and data expressed as mean ± standard deviation.

2.3.4 Effect of pH of chitosan solution on z-average, Pdi and zeta potential of the nanoparticles

Prior to formulation, the pH of the chitosan solution (5 mg/ml) was adjusted to pH between 3.50 and 6.00. 5 ml of the pH adjusted solution was measured into a 20 ml glass vials and 5 ml of TPP added drop wise to the chitosan solutions whilst ultrasonicating at 40% amplitude (300 Watts) for 1 minute. The ratio of chitosan to TPP was fixed at 3:1. The z-average, Pdi and zeta potential was measured using a Zetasizer Nano ZS (Malvern, UK) equipped with a 4Mw He- Ne laser (633 nm). Each analysis was carried out at 25^{o}C and performed in triplicate and data expressed as mean ± standard deviation.

2.3.5 Effect of concentration of chitosan and TPP on the z-average, Pdi and zeta potential of the nanoparticles

Various ratios of the chitosan to TPP (3:1, 4:1, 5:1, 8:1 and 10:1) were prepared such that the concentration of chitosan in solution was varied between 1.0 mg/ml to 10.0 mg/ml and the TPP concentration in solution also from 0.33 mg/ml to 3.0 mg/ml. 5 ml of the TPP solution was added drop wise into 5 ml of chitosan solution in accordance with the ratio of study whilst ultrasonicating at an amplitude of 40% (300 Watts) for 1 minute. The z-average, Pdi and zeta potential was measured using a Zetasizer Nano ZS® (Malvern, UK) equipped with a 4Mw He-Ne laser (633 nm). Each analysis was carried out at 25^{o}C and performed in triplicate and data expressed as mean ± standard deviation.

2.3.6 Stability behaviour of chitosan TPP nanoparticles produced by magnetic stirring and ultrasonication

For the effects magnetic stirring on the stability of chitosan TPP nanoparticles, 3 mg/ml of chitosan solution was prepared in 1% acetic acid and pH adjusted to 5.5 and filtered. A 1 mg/ml solution of TPP was also prepared in purified water and filtered. 10 ml of the chitosan solution was measured into a beaker and placed on an HTS- 1003 magnetic stirrer operated at 800 rpm. The stirrer was started and 10 ml of the TPP was added drop wise into the chitosan solution, the resulting nanoparticulate suspension was allowed to stir for 30 minutes.

For the effects of ultrasonication on stability of the nanoparticles, 5 ml of the filtered chitosan solution pH adjusted to 5.5 was measured into a clean vial. 5 ml of the TPP was added drop wise

into the chitosan whilst ultrasonicating at 40% amplitude (300 Watts) for one minute. The formation of a clear colloidal dispersion was indicative of the formation of the nanoparticles.

The various formulations were stored at ~25^{o}C and ~4^{o}C (temperature measured by using a TFA Dostmann Wertheim digital thermo-hygrometer). The z-average, Pdi and zeta potential were measured weekly over a month using a Zetasizer Nano ZS® (Malvern, UK) equipped with a 4Mw He- Ne laser (633 nm). Each analysis was performed in triplicate and data expressed as mean ± standard deviation.

2.4 Physical characterisation of nanoparticles

2.4.1 Photon correlation spectroscopy and zeta potential

Photon correlation spectroscopy studies were carried out on the nanoparticles using the Zetasizer Nano ZS® (Malvern, UK) equipped with a 4Mw He- Ne laser (633 nm). The parameters of the nanoparticles measured were z-average, Pdi and the zeta potential. Particle size analysis was evaluated using intensity distribution and hence the z-average diameter is an intensity mean diameter; the pdi is the parameter describing the width and variation within the distribution. The zeta potential is the measurement of the surface charge of the nanoparticles.

This parameter is analysed by software based on the Henry equation:

$$U_E = \frac{2\varepsilon\zeta \mathrm{F(Ka)}}{3\eta} \quad \text{..... Equation 2.1}$$

(Where ε is the dielectric constant of the dispersant, $F(\kappa a)$ is the Henry function and η is the viscosity) through the determination of the electrophoretic mobility of the sample.

Prior to analysis, undiluted or diluted (1:10) sample was added to the clear disposable zeta cell and measurements performed. Each analysis was carried out at 25^{o}C and performed in triplicate and data expressed as mean ± standard deviation.

2.4.2 Scanning electron microscopy (SEM)

Nanoparticle morphology was studied using a field emission electron microscope (FESEM) (Model, Quanta 400F, FEI Company, USA) Samples of nanoparticle in solution were placed on carbon tapes mounted on metal stubs and air dried for 24 hours and examined on the FESEM without coating.

2.5 RESULTS AND DISCUSSION

2.5.1 Effect of ultrasonication amplitude on the z-average, Pdi and zeta potential of nanoparticles

The ultrasonicator works on the principle of generating alternating low-pressure and high-pressure waves in fluids, leading to the formation and violent collapse of small vacuum bubbles. This phenomenon is termed ultrasonic cavitation. This phenomenon in liquids causes high speed liquid jets of up to 1000 km/h. Such jets press liquid at high pressure between the particles and separate them from each other. Smaller particles are accelerated with the liquid jets and collide at high speeds. These effects are used for the deagglomeration and milling of micrometre and nanometre-size materials as well as for the disintegration of cells or the mixing of reactants. It is therefore desirable to optimise the amplitude of ultrasonication so that nanoparticles with desirable properties can be prepared.

The selection of final amplitude for the production of the nanoparticles was determined by factors such reproducibility of desirable z-average and Pdi. Figure 2.2 shows the effect of the difference in amplitude on the z-average and the Pdi of nanoparticles.

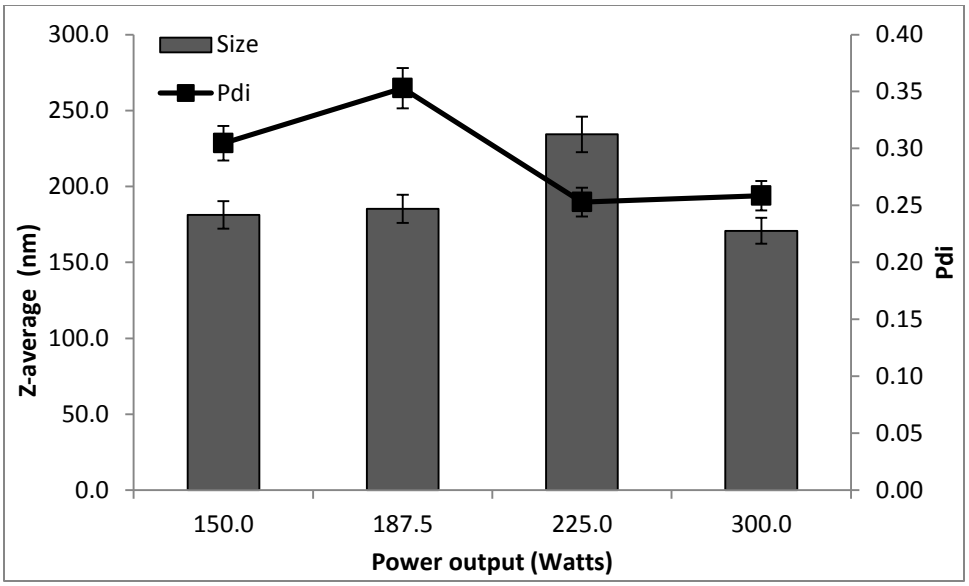

Figure 2.2: Effect of amplitude (power output) of ultrasonication on the z-average and Pdi of nanoparticles

The amplitude of 40% (300 Watts) appears to be the optimum, because at this magnitude, smaller particles were produced with a lower Pdi. The amplitude of 40% (300 Watts) was therefore selected for further work.

A critical look at figure 2.2, brings to light an evidence of a gradual z-average increase as the magnitude of the amplitude of ultrasonication increased to 30%, (225 Watts), this can be explained based on the principle that, as the amplitude increases more cavitations are created and these dampen the efficiency of energy transmission and hence reduces the ultrasonic effect (Mason, 1999) hence causing a z-average increase. At very high amplitude however, the energy transmitted may surpass the dampening effects thereby resulting in particle size reduction. The changes in particle size and polydispersity could have also resulted from ultrasonic-mediated depolymerisation of chitosan chains (Tang *et al*. 2003).

2.5.2 Effect of ultrasonication time and the total volume of formulation on the final temperature and the z-average of nanoparticles

Temperature is an important factor that needs to be controlled when formulating products that are thermo labile like proteins. The method developed for the production of nanoparticles by ultrasonication was intended to be used for the production of a nanoparticulate product encapsulating insulin. Since insulin is a protein and susceptible to degradation at high temperatures (Oliva *et al*. 2000), the temperature increment caused by the ultrasonication process of making the insulin containing nanoparticle could not be overlooked. Also the effect of processing temperature on the z-average and Pdi of nanoparticles needed to be understood and controlled so that products of desirable quality could be made. Hence, to analyse the effect of ultrasonication time and volume of material on the above mentioned physical properties of the nanoparticles, different total volumes of the formulation (10- 50 ml) were subjected to various ultrasonication times between 1-5 minutes and the result is presented in figure 2.3 and table 2.1.

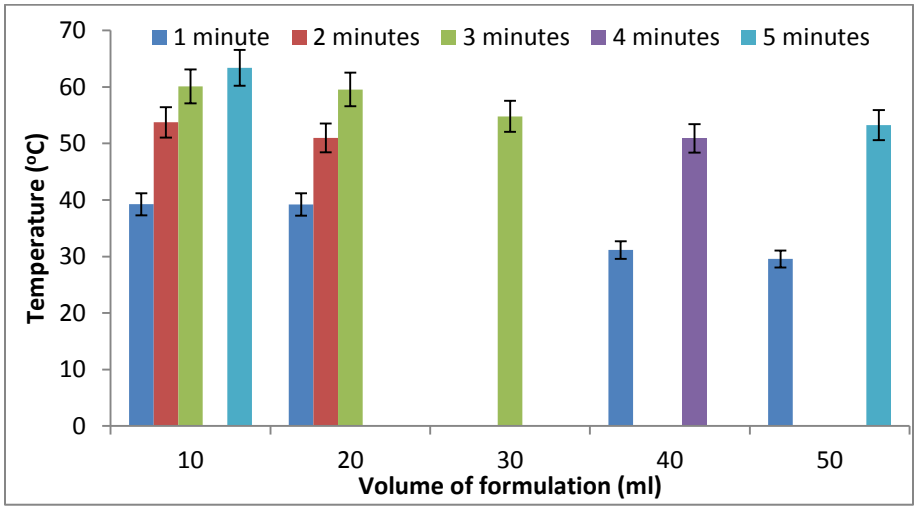

Figure 2.3 Effect of ultrasonication time and the total volume of formulation on the final average temperature of nanoparticulate suspension

There was an increase in temperature as the ultrasonication time was increased, irrespective of the total volume formulation (table 2.1). Interestingly, there was an initial decrease in z-average as the ultrasonication time was increased. However it was observed at 10 ml, this initial decrease in z-average was followed by increase on extended ultrasonication. It follows that ultrasonication causes reduction in z-average however on extended ultrasonication, an increase in z-average is observed. A similar observation was made by Chuah *et al*. (2013) on curcumin containing nanoparticles made by ultrasonication.

Table 2.1 Effect of ultrasonication time and the total volume of formulation on the final average temperature and the z-average of nanoparticles

Total volume of formulation (ml)	Time of sonication (minutes)	Average temperature recorded after sonication	Z-average (nm)
10	1	39.25±1.65	254.10±4.60
	2	53.75±1.85	212.00±4.70
	3	60.10±2.70	224.65±13.65
	5	63.40±3.50	285.80±10.80
20	1	39.20±0.40	280.70±2.90
	2	51.00±1.10	229.25±4.45
	3	59.57±0.55	223.73±4.04
30	3	54.80±0.30	233.13±1.15
40	1	31.15±0.45	276.19±2.21
	4	50.90±0.70	217.30±2.40
50	1	29.55±0.15	288.40±1.90
	5	53.25±0.85	224.20±1.00

2.5.3 The effect of the pH of chitosan solution on the z-average, Pdi and zeta potential of nanoparticles

A review of literature suggests that, the optimum pH for the formulation of chitosan nanoparticles by ionotropic gelation is about 5.5 (Ma *et al*. 2002). This is in view of the fact that, at this pH more than 90% of the amine groups of chitosan are protonated (Mao *et al*. 2006). However the effect of variation of pH on the z-average, zeta potential and Pdi appears to be lacking in the literature. Therefore we investigated the effect of the initial pH of chitosan solution on the aforementioned properties of the nanoparticles. In all instances pH adjustments were carried out with 4M NaOH.

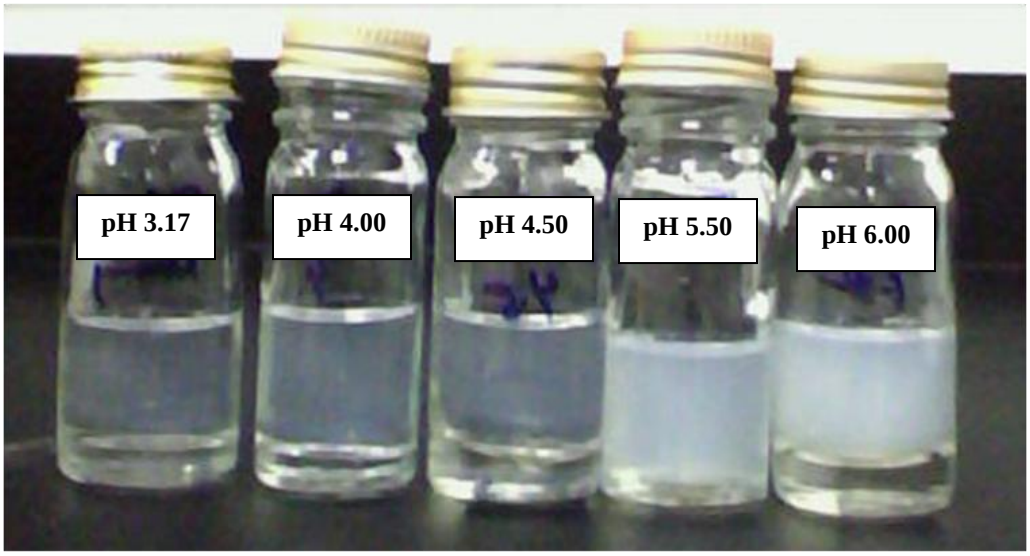

Figure 2.4: Image of chitosan TPP nanoparticle suspensions as a function of pH

Figure 2.4 shows solutions of chitosan TPP nanoparticles that were produced at different pH. It can be seen that, the opalescence of the solutions increased with increasing pH. The opalescent appearance of the solution is reported to be indicative of the formation of nanoparticles (Wu *et al*. 2005; Seda Tığlı Aydın *et al*. 2012). This phenomenon can be explained on the basis that, chitosan being a polycation has its amine groups protonated at acidic pH and therefore as pH

increases there is further protonation. This favours the interaction of the phosphate groups of the TPP with the amine groups of the chitosan leading to an increase in the degree of cross linking between chitosan and TPP. More of such interactions means that more nanoparticles would be produced and hence the observed trend in the opalescence. There is also an increase in the cross-linking density as the number of amine sites available for cross-linking is increased leading to a more compact chitosan TPP matrix. However, as pH was increased (beyond pH 6), there was an increase in the opalescence of the nanoparticulate solution with observable aggregates. This increase in opalescence may not be due to the interaction of the amine groups of chitosan with the phosphate groups of TPP, but rather, due to deprotonation of the amine groups of chitosan leading to precipitation of the chitosan out of solution since protonation is the mechanism that maintains the chitosan in solution.

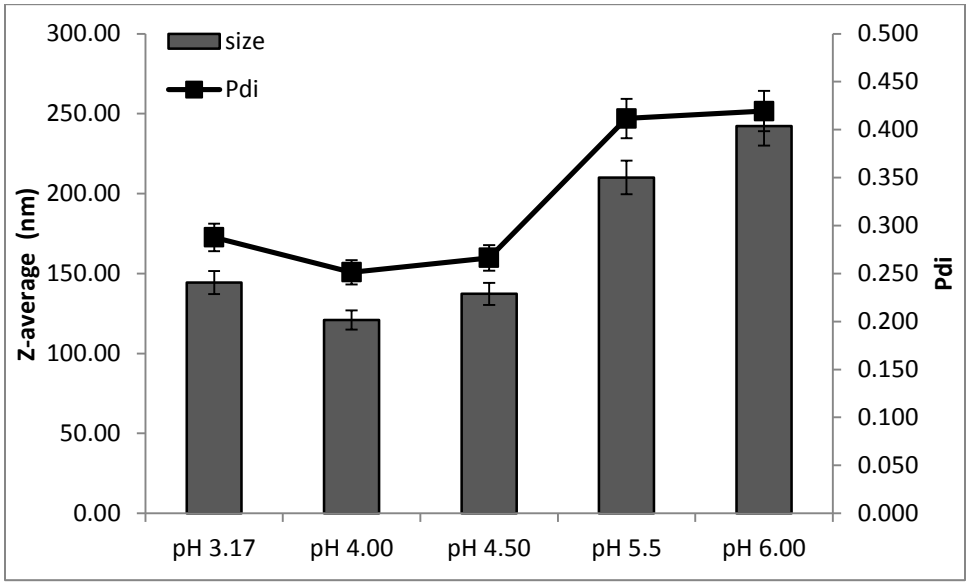

Figure 2.5: The effect of pH of chitosan solution on the z-average and Pdi of nanoparticles

The z-average range of the nanoparticles falls between 120-250 nm, however we observed there was an initial decrease in z-average when pH was increased to 4.0 from 3.17 (figure 2.5). The

less protonated amine groups in the chitosan at pH 3.17 may have resulted in the formation of loose matrices which may have reflected in the z-average increase. However as the pH increased above 4.0 a gradual z-average increase was observed (figure 2.5). In most of the reports in the literature, a pH of 5-5.5 has been used in the formation of nanoparticles by ionic gelation from chitosan and TPP whilst encapsulating different drugs (Janes *et al*. 2001; Ma *et al*. 2002). Clearly, in the present study a pH of 4.0 appears to be optimum in terms of size and Pdi. Hence pH can be controlled and varied to yield a specific desirable size of nanoparticles. Though the size and Pdi are rightly affected by the pH, the molecular weights of the chitosan also affect the size. Hence, a pH 4 being optimum for our system that employs low molecular weight chitosan may not apply to other molecular weights chitosan.

The Pdi shows the degree of polydispersity or homogeneity within the nanoparticulate system. Though sizes measured are in the nanometre region the interparticulate difference is very important. Wide variability within the particle sizes may affect the drug loading and drug releasing efficiency of the delivery system. Figure 2.5 generally shows an increase in the Pdi as the pH of chitosan solution was increased, though there was an initial increase at pH 3.17 and after dropping slightly at pH 4 and then increasing again. Values close to 0 indicate homogeneous dispersion, whereas those greater than, 0.3 generally indicate heterogeneity. The trend in the current investigation can be explained from the point of view that, at pH approaching neutral to alkaline region there is decreased propensity of chitosan to interact with TPP coupled with the increased possibilities of deprotonation of amine groups of chitosan within the formed nanoparticles. This scenario is likely to manifest in the production of nanoparticles with varied degree of chitosan TPP interaction and hence varied z-average which sums up with increased Pdi.

The zeta potential is an important parameter in nanoparticulate formulation because it can be used to predict the stability of the nanoparticles via their propensity towards agglomeration. In figure 2.6, the zeta potential of the nanoparticle decreased as the pH of the chitosan solution was increased.

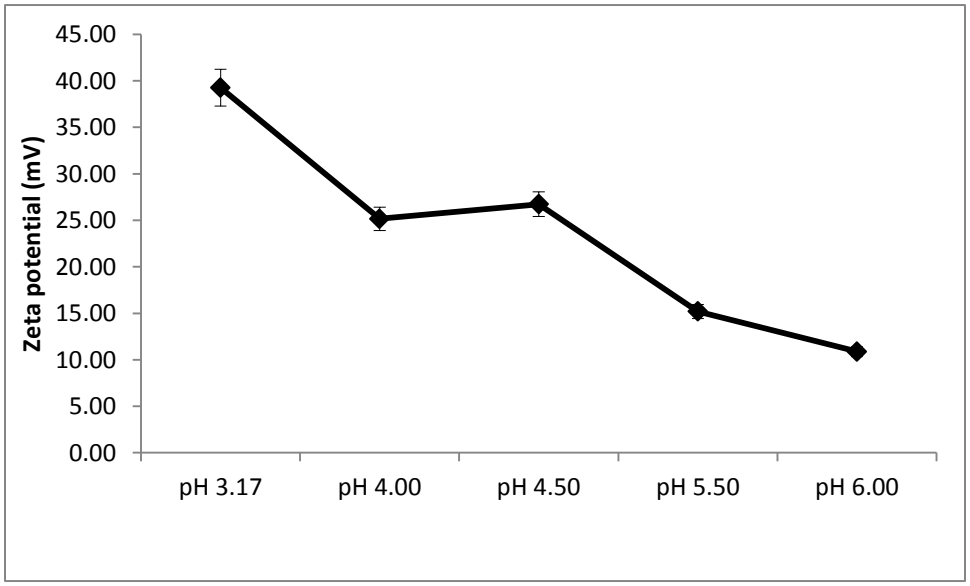

Figure 2.6: The effect of pH of chitosan on the zeta potential of nanoparticles

The zeta potential of the chitosan TPP nanoparticles are normally positive due to the protonated amine groups in the chitosan. An increase in pH increases the chances of the nanoparticles to agglomerate due to deprotonisation of the amine groups of chitosan as explained earlier. This result is in concert with the data on the effects of pH on z-average and Pdi depicted in figure 2.5.

It must be added that, a decrease in the zeta potential means that the nanoparticles have a higher possibility of agglomerating due to decreased surface charge. Therefore, the observed increase in Pdi and z-average with increase in pH can be seen as resulting from increased deprotonation of amine groups of chitosan with concomitant decrease in zeta potential.

In nanoparticle formulation quality and quantity are factors that cannot be overlooked. Hence careful consideration must be given to the choice and amount of starting materials to be used. This careful selection of amount of starting materials should give a formulation with desirable properties and good yield. The recovery of nanoparticles for further analysis is always a point of interest, very low concentrations of starting materials may lead to no yield at all.

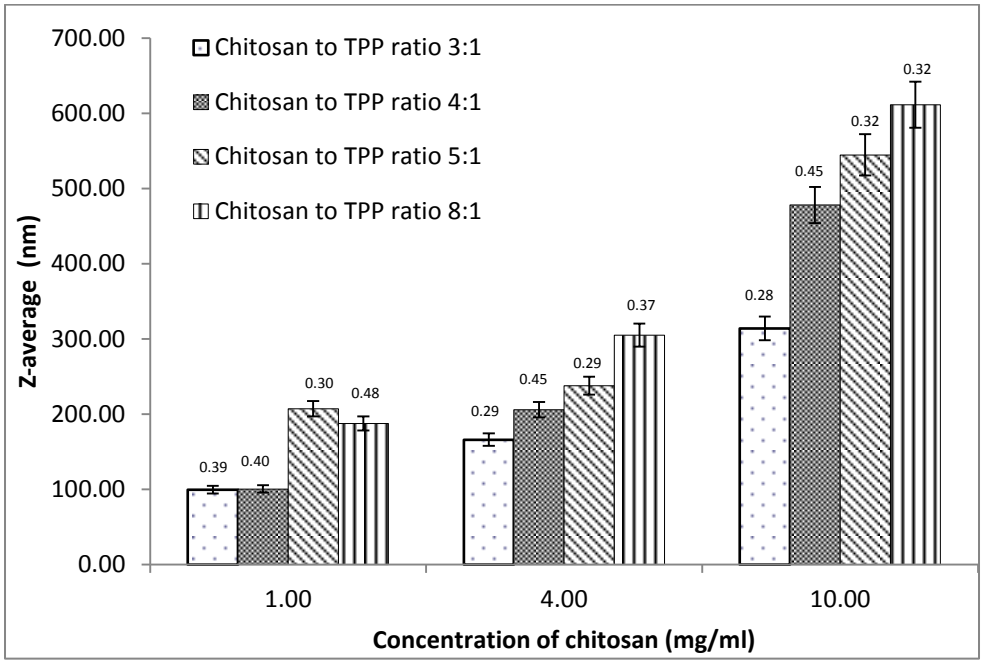

Figure 2.7: Pdi (indicated on top of bars) and z-average of nanoparticles as function of chitosan concentration at different chitosan to TPP ratios

Figure 2.7 shows that, as the concentration of chitosan was increased in the different formulations, there was a gradual increase in the z-average. At the lowest ratio of chitosan 3:1, the smallest particles are produced as compared to the ones produced at higher chitosan to TPP ratios. The increase in z-average of the nanoparticles can be attributed to an increase in the amount of the amine groups available for cross linking with the phosphate groups of TPP. However, there would be residual of amine groups since most of the phosphate groups of TPP would have reacted with the excess of the amine groups of chitosan. This will lead to the

production of nanoparticles with loosely knit matrices. Such matrices are likely to lose their integrity more readily which results in the production of polydisperse particle (Hasanovic *et al*. 2009).

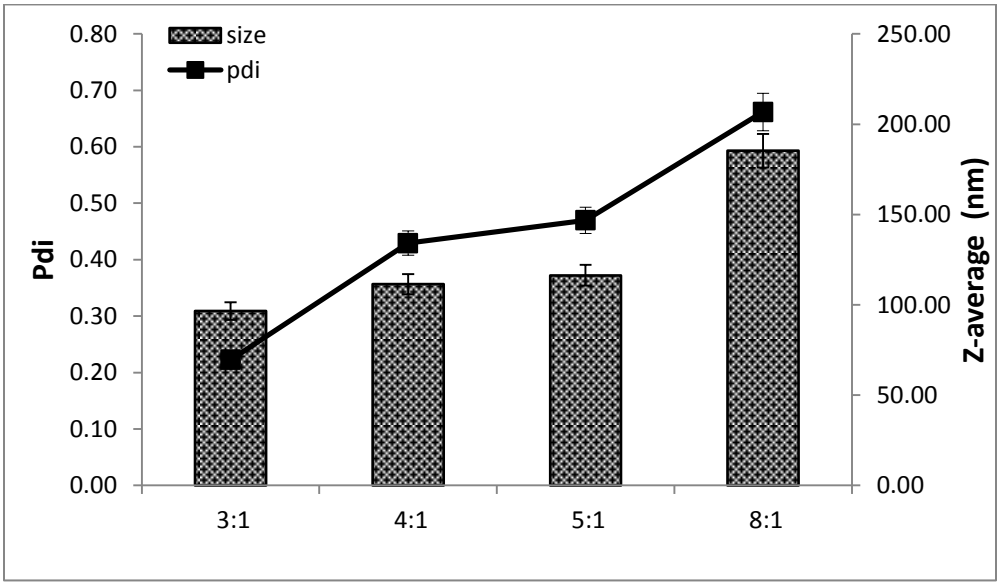

Figure 2.8: Pdi and z-average of nanoparticles prepared from 1 mg/ml chitosan solution at different chitosan to TPP ratio

In the production of chitosan microspheres, He *et al*. (1998) observed that when more cross-linking agent was used, the microspheres were regular, and particle sizes were smaller. This appears to be in agreement with observation made in the present study. From figure 2.8, it can be seen that, as the concentration of chitosan increased, particle size also increased.

Separately, visual images of nano formulations were taken at 3, 5, 8 and 10 mg/ml of chitosan and these are depicted in figure 2.9. It can be observed that as the concentration of chitosan was increased the solution became more opalescent. At all cross-linking densities, the concentration of 1 mg/ml – 4 mg/ml chitosan produced gave smaller particle sizes between 90 nm – 300 nm, whilst that of 10 mg/ml gave larger particles. The production of larger particles as the concentration was increased can be attributed to the limited space of particle movement within the solution and hence potential particles agglomeration. Smaller interparticulate distance increases the chances of the individual nanoparticulate interaction, hence an increased propensity towards agglomeration.

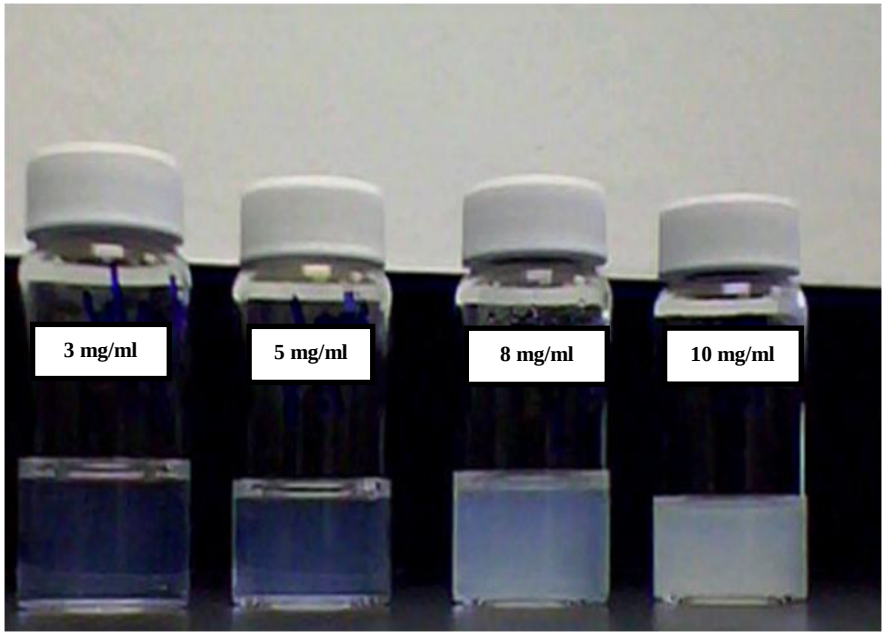

Figure 2.9: Image of chitosan TPP nanoparticles showing variation in opalescence as the concentration of chitosan increases

It was expected that, the high zeta potential of chitosan nanoparticles which was recorded as above 40 mV should be able to make the various preparations less susceptible to aggregation, but it was observed that at chitosan concentration of 10 mg/ml larger particles were produced. In this

respect, the distance between individual nanoparticles was reduced and hence the surface charge was ineffective. Though the zeta potential read was high, the reduction in the interparticulate distance with more material occupying small volume could be the cause of the observation in the change in size of particles prepared at a 10 mg/ml chitosan concentration. Also the effective power transmitted through the sample to cause cavitations that produces smaller particles during the ultrasonication process may have reduced due to the observed increase in viscosity of the chitosan solution as the concentration of chitosan was increased.

Nanoparticles can be produced from very low concentrations of chitosan and TPP, but the process of recovery is a real challenge. Therefore we need to be cognisant of the concentration of the starting materials, in view of possible low nanoparticle recovery. From the present study it was noted that, at a 1 mg/ml concentration of chitosan, very low nanoparticle recovery was observed but chitosan concentration of 5 mg/ml produced particles with good recovery. At 10 mg/ml, larger particles were produced which negates the good recoveries observed. Therefore initial concentrations between 1 mg/ml and 5 mg/ml of chitosan seemed to produce smaller particles with appreciable Pdi and zeta potential and this working concentration range was adapted for subsequent work. As observed by Pan *et al*., 2002, the particle size and other parameters of nanoparticles could be controlled by varying the concentration of the counter ions and this has also been proved by this current work.

Figures 2.10 (a-b) shows the SEM images of chitosan TPP nanoparticles produced by ultrasonication. The images shows the tendency of some of the nanoparticles to agglomerate. Figure 2.10b shows image of nanoparticles produced from a chitosan concentration 8 mg/ml, the population of nanoparticle is increased as compared to figure 2.10a of samples produced from 3 mg/ml chitosan.

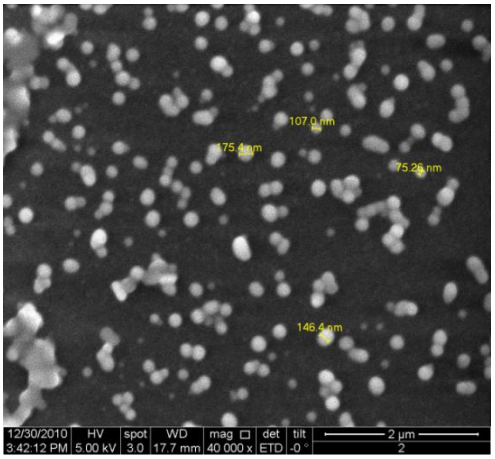

Figure 2.10a: SEM image of chitosan TPP nanoparticles. Chitosan to TPP ratio of 3:1 (3 mg/ml)

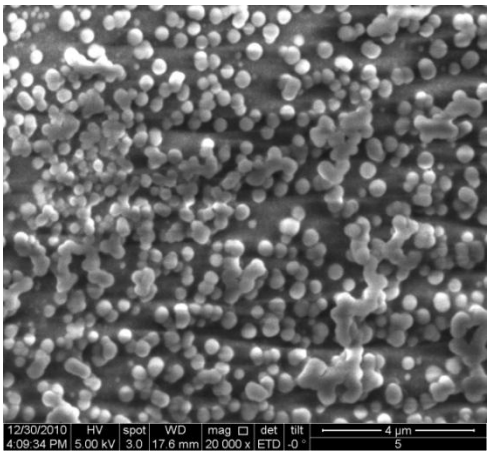

Figure 2.10b: SEM image of chitosan TPP nanoparticles. Chitosan to TPP ratio of 3:1 (8 mg/ml)

2.5.4 Stability behaviour of chitosan TPP nanoparticles produced by ultrasonication and magnetic stirring

The conventional method for producing chitosan TPP nanoparticles has been via magnetic stirring. In the present work, we developed and optimised a method for the production of chitosan TPP nanoparticles via ultrasonication. In the light of this modification, there was a need to assess the stability nanoparticles produced by ultrasonication as compared to that of the stability of the conventional.

The colloidal stability of chitosan TPP nanoparticles produced via both magnetic stirring and ultrasonication was studied over a period of one month. The samples were subjected to different storage conditions as described under section 2.5.3 and the z-average, zeta potential and Pdi were studied. Since the stability of chitosan TPP nanoparticles produced via magnetic stirring has already been studied (López-León *et al*. 2005), we only subjected nanoparticles produced by the newly optimised method to basic stability assessment as normally done on the nanoparticle produced by magnetic stirring. Chitosan degrades in biological environments due to enzymatic action, however it has been discovered that, chitosan nanoparticles formulated via ionotropic gelation lose their integrity in aqueous media even in the absence of enzymes (López-León *et al*. 2005).

The nanoparticles produced by the two methods were initially assessed with regards to their z-average, Pdi and zeta potential. The samples were then stored at 25^{o}C (room temperature) and 4^{o}C (refrigerator). The z-average, Pdi, and zeta potential were measured weekly over a period of a month and any changes in the physical appearance was also recorded.

Figure 2.11 shows the z-average results obtained with samples stored at 25^{o}C and 4^{o}C. It can be seen that, for the two types of nanoparticles prepared by the above stated methods, the particle size for nanoparticles stored at room temperature showed a significant increase in z-average over the weeks.

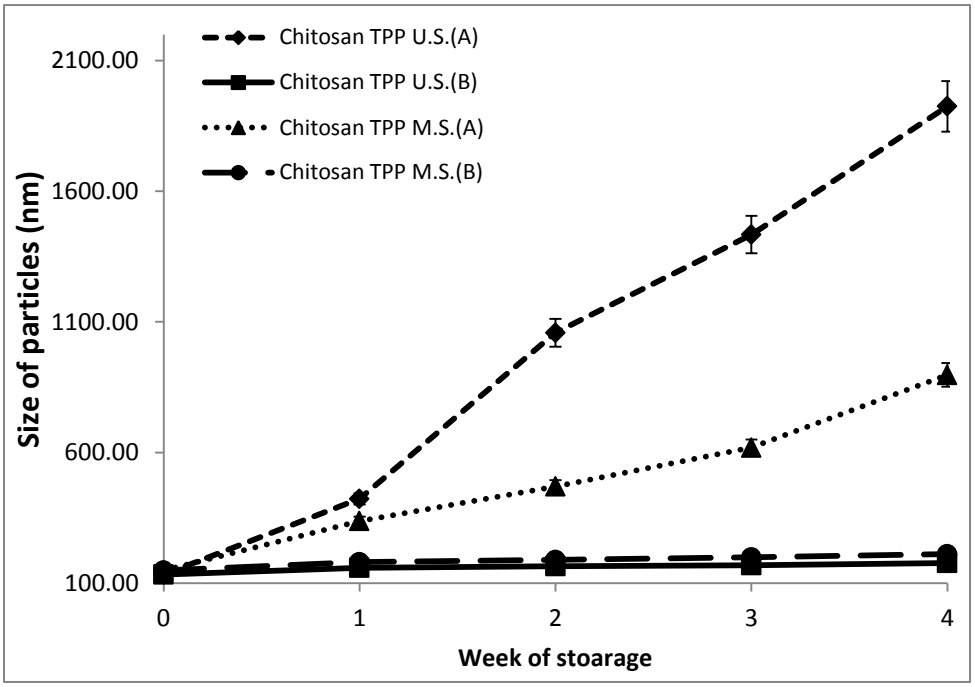

Figure 2.11 Z-average of nanoparticles stored at different conditions as a function of time.

- U.S. = Chitosan TPP nanoparticles prepared by ultrasonication
- M.S. = Chitosan TPP nanoparticles prepared by magnetic stirring
- (A) = Nanoparticles stored at 25^{o}C
- (B) = Nanoparticles stored at 4^{o}C

For chitosan TPP nanoparticles prepared by ultrasonication, by the end of the 4th week of storage the z-average increase was more than 8 fold the original, with a significant increase in the Pdi as seen in figure 2.12 and a similar observation in z-average increase was also made for the magnetic stirred samples. The increase in z-average seemed more pronounced in the ultrasonicated system than the magnetic stirred system and the progression of z-average increase was slow for the samples prepared by magnetic stirring. Since matrices formed from chitosan

depend on how tightly knit the matrices are, there is a possibility that, the matrices in the ultrasonicated samples loosened up quickly than those made prepared by magnetic stirring.

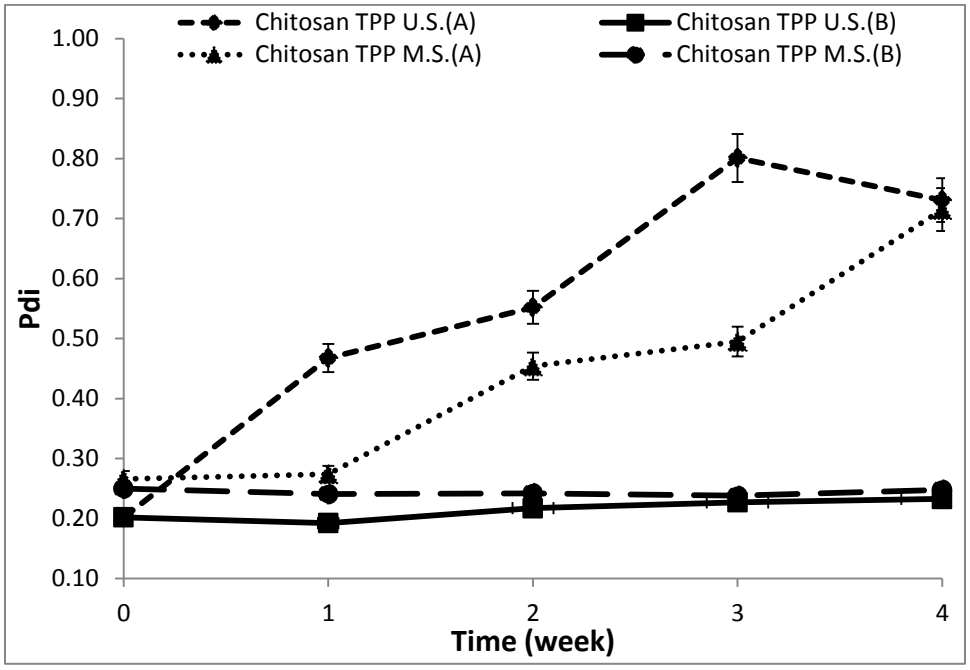

Figure 2.12 Average Pdi of nanoparticles stored at different conditions as a function of time

- U.S. = Chitosan TPP nanoparticles prepared by ultrasonication
- M.S. = Chitosan TPP nanoparticles prepared by magnetic stirring
- (A) = Nanoparticles stored at 25^{o}C
- (B) = Nanoparticles stored at 4^{o}C

It may seem that the energy involved in the formation of nanoparticles via ultrasonication is higher than that of production by magnetic stirring. This energy caused the formation of smaller particles, but the matrices of these particles may not have been tightly knit as compared to those of the magnetic stirred samples. Also, the duration of ultrasonication had to be restricted due to the associated increase in temperature generated, which undesirably caused increase in the z-average of particles. The loss of the matrices integrity leads to changes in the particles spherical shape. The significant increase in the Pdi (figure 2.12) also confirms the heterogeneity on the system. Heterogeneous systems are not favourable because these systems contain particles with

wide variability of sizes and this variability will affect the drug loading and drug release. This will in turn affect the usefulness of the nanoparticles as a drug delivery system.

From figure 2.11 and 2.12, it can be seen clearly that, samples stored at 4^{o}C showed great stability than samples stored at room temperature. The z-average and Pdi changes in the samples stored at 4^{o}C did not show significant increase as compared to those stored at 25^{o}C. Temperature relationship with Brownian motion of particles has been used to explain possible aggregation in nanoparticulate systems (Tsai *et al*. 2011). Lower temperatures reduce the brownian motion of particles, thereby reducing their kinetic energy. These reductions lead to an increase in interparticulate distance which reduces the tendency for particles to collide with each other and aggregate. Hence this may explain the significant difference seen in the stability of samples stored at 25^{o}C and those stored at 4^{o}C.

The zeta potential of both formulations remained stable over the weeks of storage as no drastic changes were observed. Nanoparticulate systems with zeta potential values above |25| mV are considered stable and those having values below this stipulated range are liable to aggregation caused by van der Waal inter particle attractions. Zeta potential is a parameter used in ascertaining the state of the nanoparticle surface charge and this can help in determining the stability of a nanoparticle suspension, i.e. to what degree aggregation will occur over time.

From figure 2.13, the zeta potential of the nanoparticles prepared by either method and stored at 25^{o}C or 4^{o}C showed little variation during storage over 1 month, albeit a slight rise in values for nanoparticles prepared by magnetic stirring. These changes are however insignificant and is a feature that may be worth exploring in subsequent modification to the formulation.

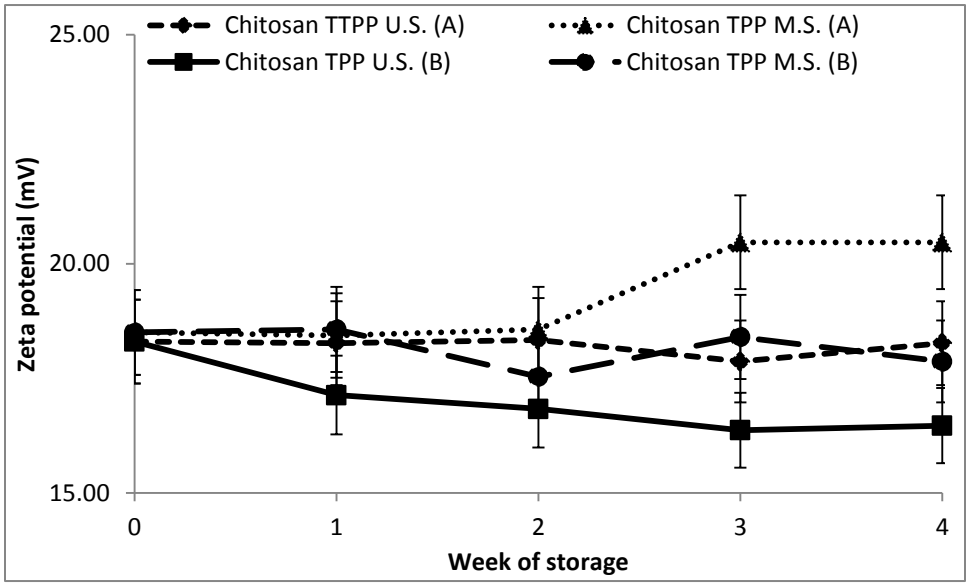

Figure 2.13 Average zeta potential of chitosan nanoparticles stored at different conditions as a function of time.

- U.S. = Chitosan TPP nanoparticles prepared by ultrasonication
- M.S. = Chitosan TPP nanoparticles prepared by magnetic stirring
- (A) = Nanoparticles stored at 25^{o}C
- (B) = Nanoparticles stored at 4^{o}C

Figure 2.14 (a and b) shows images of samples stored at 25^{o}C and 4^{o}C for 4 weeks, formulated using magnetic stirring and ultrasonication respectively. For nanoparticles by both methods it can clearly be seen that the opalescence of the samples stored at room temperature was greater than those stored at 4^{o}C. An increase in the turbidity is indicative of the presence of larger aggregates in samples. In addition, it is clear from the image that the nanoparticle prepared by ultrasonication was more turbid than the magnetic stirred one.

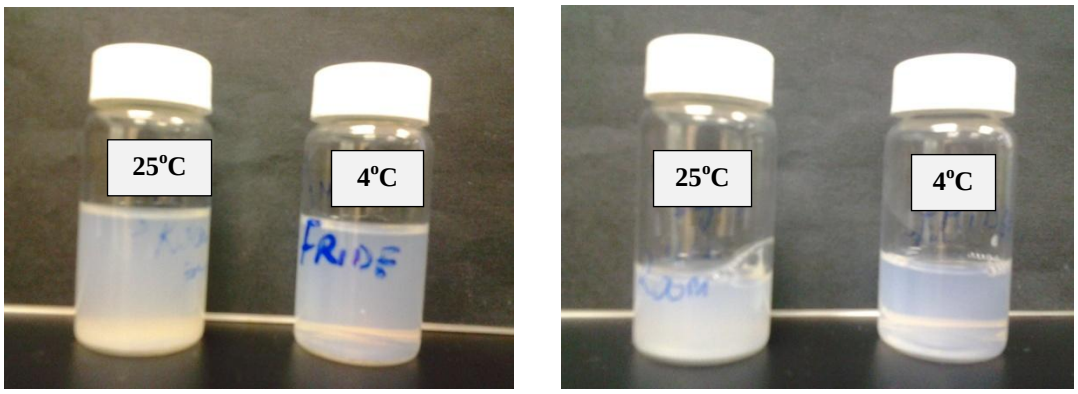

(a) (b)

Figure 2.14: Visual images of chitosan nanoparticles formulated by magnetic stirring (a) and (b) ultrasonication after storage at 25°C and 4°C for one month

Figure 2.15 – 2.18 shows the z-average distribution by intensity of the formulation stored at the different temperature over the period one month.

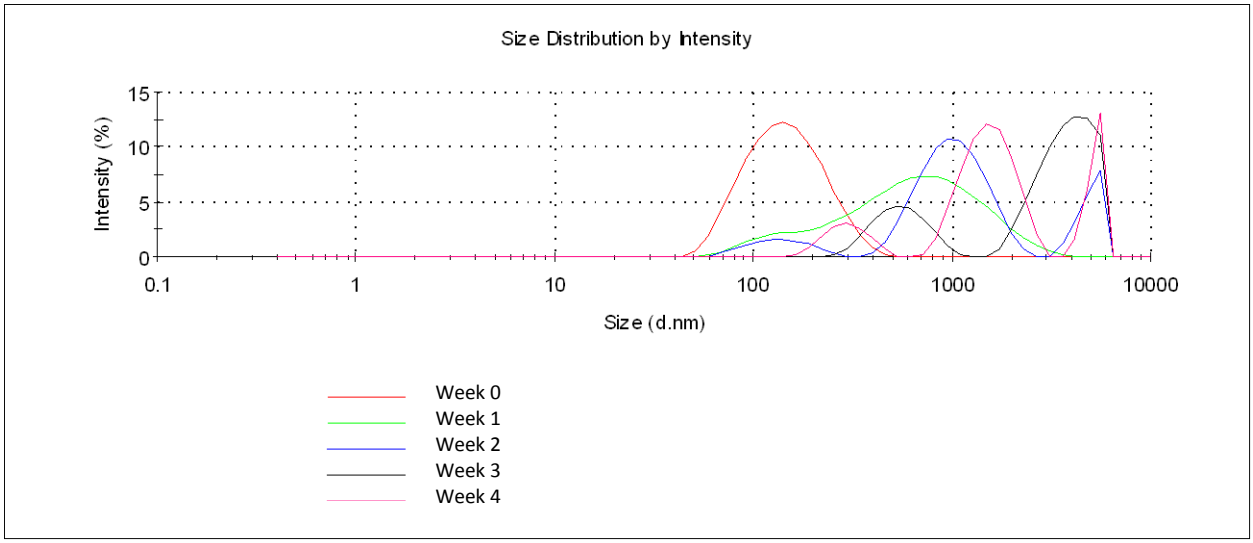

Figure 2.15 Variation in z-average distribution in samples formulated by ultrasonication after storage at 25°C for one month.

The multi modal distribution seen in the samples stored at 25°C shows the heterogeneity in the system and hence a reflection in the drastic changes in the Pdi recorded. The samples stored at

4°C always showed a unimodal distribution (representative of a more homogeneous system), in contrast to those stored at 25°C and confirming the observations made earlier.

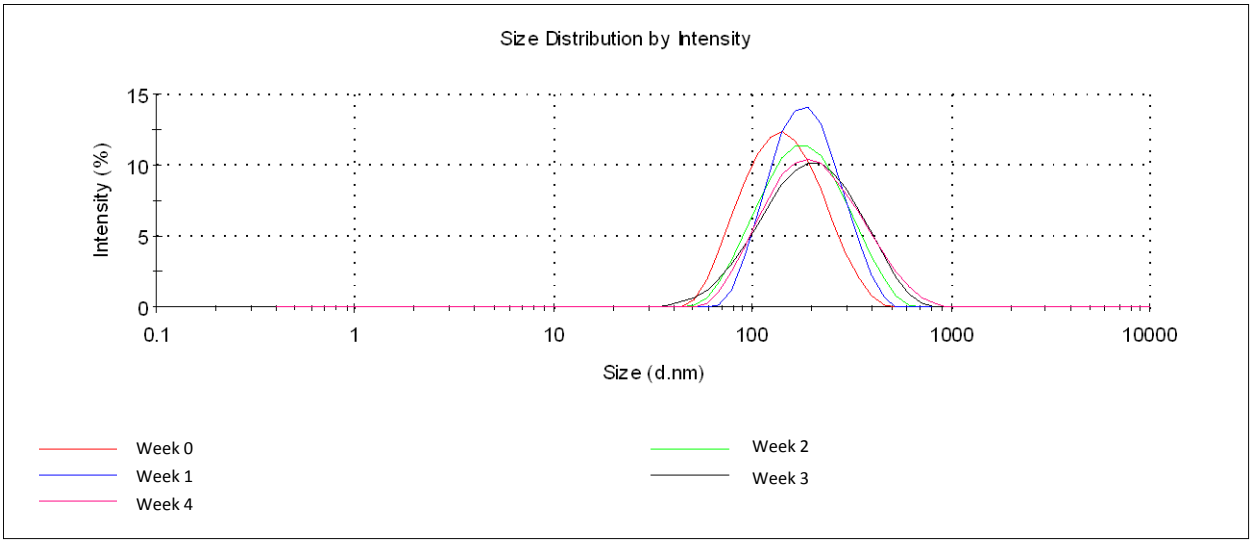

Figure 2.16 Variation in z-average distribution in samples formulated by ultrasonication after storage at 4°C for one month

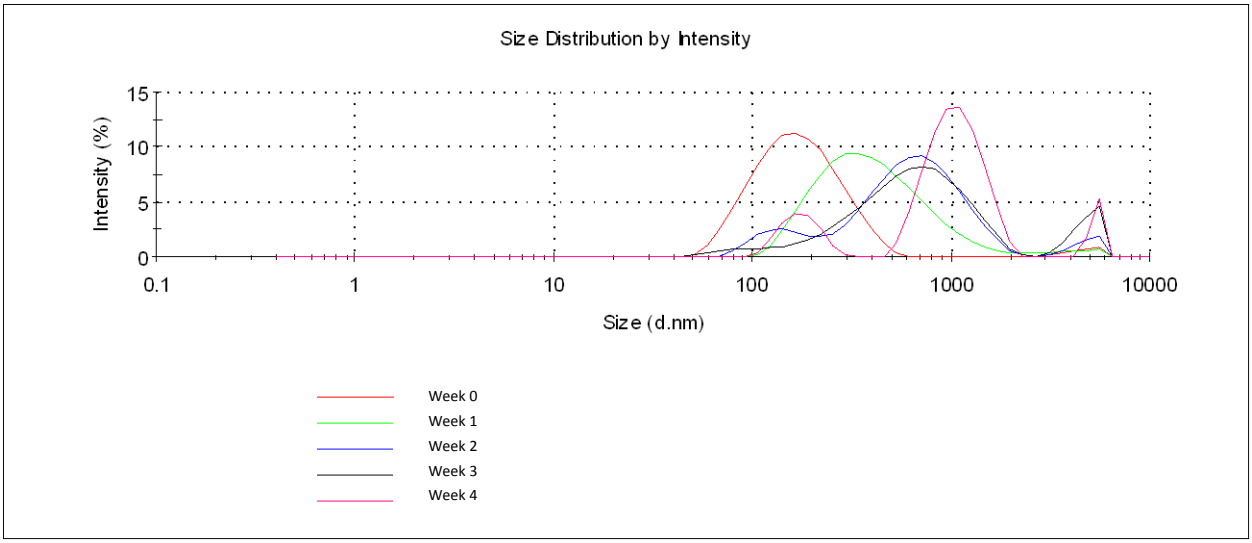

Figure 2.17 Variation in z-average distribution in samples formulated by magnetic stirring after storage at 25°C for one month.

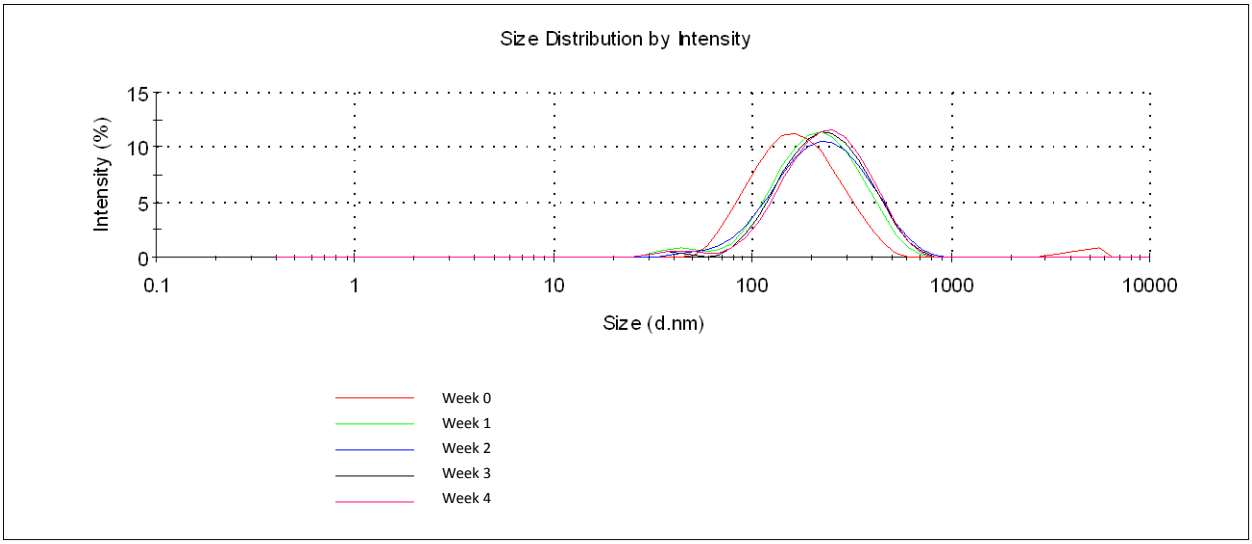

Figure 2.18 Variation in z-average distribution in samples formulated by magnetic stirring after storage at 4^{o}C for one month

2.7 CONCLUSION

It can be concluded that, the production of chitosan nanoparticles by ultrasonication is feasible. Prolonged ultrasonication causes significant rise in temperature, which appears to manifest in an increase in z-average. Increase in pH and also the amount of starting material causes increases in z-average of nanoparticle. However working concentrations between 1 mg/ml – 5 mg/ml of chitosan was found to produce consistent particle size, whilst concentrations above 10 mg/ml tended to produce precipitates and non-colloidal solutions. Nanoparticles produced by ultrasonication were less stable compared to those produced by magnetic stirring during storage for one month. On the other hand, the zeta potentials of both types of nanoparticles remained essentially unchanged during storage, although the values indicate low stability. The above data shows that temperature of storage provides a more meaningful data with regards to stability assessment that from zeta potential measurements.

CHAPTER 3

FUNCTIONALISATION OF CHITOSAN WITH PHENYLBORONIC ACID

3.1 Introduction

Chitosan is a natural cationic polysaccharide obtained from partial deacetylation of chitin and is the main constituent of the crustacean skeleton. It is non-toxic, biodegradable, biocompatible and easily modified by chemical and physical methods. It is widely used in encapsulation applications due to its ability to form gels in the presence of certain divalent cations such as calcium, barium, and other polyanions.

Chemical modification of chitosan can improve its bio-functionality and these modifications tend to preserve the original physicochemical and biochemical properties while rendering other application potential. A major drawback in the functionalisation and application of chitin and chitosan is their poor water solubility(Kittur *et al*. 2002). Major chitosan functionalisation could be carried out by: (1) substitution, introducing small groups into the back bone of the chitosan and (2) depolymerisation by chemical, physical or enzymatic treatments. Further chemical modification of the functionalised chitosan can be pursued to widen their application.

Chitosan has been modified with different chemical groups for use in the fields of drug delivery, medicine, food, chemical engineering and the agriculture industry. For example chitosan and alginate modified by acylation with palmitoyl chloride has been used to create an ideal encapsulation system for micronutrients to reduce the reactivity of the micronutrient in relation to the outside environment. This allowed maximal stability in acidic pH and gave resistance to extreme moisture conditions (Han *et al*. 2008).

Chitosan has also been modified by trimethylation to increase its water solubility and this trimethyl chitosan (TMC) has been synthesised and characterised by FTIR and NMR, where these quartenized derivatives of chitosan possess a positive charge and are soluble over a wide range of pH (Mourya and Inamdar 2009).

Chitosans have also been used as conjugates with bioactive excipients for the delivery of active ingredients such as calcitonin. Enzyme inhibitors of trypsin were conjugated to chitosan and this conjugation has demonstrated a potential in the delivery of small peptides by inhibiting the degradation of the encapsulated calcitonin by the enzymes (Guggi 2003). Smoum *et al*. (2006) developed a chitosan-pentaglycine-phenylboronic acid conjugate for the colon specific delivery of calcitonin. Novel chitosan gel modified by phenylboronate with selective glucose adsorption capacity was synthesised by Matsumoto *et al*. (2002) and these gels have demonstrated a potential for use in the recognition of saccharides.

Wu *et al.* (2011) have investigated the utilisation of phenyl boronic acid (PBA)-bonded chitosan nanoparticles as a vehicle for controlled insulin release and insulin release from the nanoparticles was attributed to the glucose sensitivity of the PBA moiety and the molecular weight of the polymer.

In the present project various methods and approaches were adopted to introduce the PBA group onto chitosan, these methods explored the chemistries of both chitosan and phenylboronic acid. Both physical and chemical methods were pursued and the successful functionalisation of the chitosan by PBA was thoroughly studied by various techniques in order to ascertain the degree of functionalisation.

3.2 Materials, methods and equipment

Low molecular weight chitosan was purchased from Sigma Aldrich (Missouri, USA); tripolyphosphate (TPP), phenylboronic acid (PBA), 4-formylphenyl boronic acid (4-FPBA) and sodium borohydride (Thermofischer Scientific New Jersey, USA), sodium hydroxide pellets (Merck, Darmstadt, Germany), acetic acid, methanol, acetonitrile and glucose (Thermofischer Scientific New Jersey, USA). All other chemicals were of reagent grade.

Bruker S4-Explorer X-ray fluorescence (XRF), Field emission scanning electron microscopy (FESEM) (Model Quanta 400F, FEI Company, USA) with an Energy dispersive x-ray detector (EDX) (EDAX Inc. U.S.A.), Perkin Elmer FTIR spectrometer (Spectrum RX 1), Time-of-flight secondary ion mass spectrometry (ToF-SIMS, ION-TOF equipped with a liquid metal, Bi ion gun, GmbH, Munster, Germany), Mettler Tolledo DSC system, CE440 Elemental analyzer (Exeter Analytical (UK) Ltd), CHRIST Freeze drier Alpha 1-2 10 plus S/N1-1521with Vacuubrand rotary vane vacuum pump R22.5 S/N 31219013.

3.2.1 Methods

3.2.1.1 Nanoparticle formulation via electrostatic interaction between chitosan and PBA

Chitosan was dissolved in 1% acetic acid under magnetic stirring and filtered. PBA was dissolved in water and its pH adjusted to 10.0 to make it anionic. The PBA was added drop wise into the chitosan solution whilst ultrasonicating for 1 minute as was done for the production of chitosan TPP nanoparticles in section 2.3.1. Various ratios of the chitosan to PBA were prepared, namely: chitosan:PBA ratios of 1:1, 1:2 and 1:3 respectively, and the z-average and Pdi of the nanoparticles were assessed by Zetasizer Nano ZS® (Malvern, UK) equipped with a 4Mw He-Ne laser (633 nm). Each analysis was carried out at 25^{o}C and performed in triplicate and data expressed as mean ± standard deviation. SEM imaging was performed by field emission scanning electron microscope (FESEM, Quanta 400F, FEI Company, USA) under low vacuum and at a viewing voltage of 20.0 kV.

3.2.1.2 Tagging of PBA electrostatically onto chitosan

It was theorised that, chitosan and PBA could be formulated into nanoparticles by cross linking with TPP. Therefore chitosan was 'functionalised' with the PBA by physical admixture and then formulated into nanoparticles using TPP as a cross-linker. Chitosan in 1% acetic acid and PBA dissolved in distilled water and pH adjusted to 10 were mixed together and stirred using a magnetic stirrer at a speed of 700 rpm, the stirring times were between 1 hour and 24 hours. Different amounts of chitosan and PBA were used and different stirring times were also investigated. The resulting solutions were either precipitated out by pH adjustment using 1M NaOH or collected without precipitation. In either case, the formulations were then freeze-dried. The presence of PBA within chitosan polymer was ascertained by-FTIR, DSC, XRF and EDX.

3.2.1.3 Formulation of chitosan TPP/PBA nanoparticles

Tagging of PBA electrostatically onto chitosan also appeared to be non-feasible. In a subsequent method, chitosan-TPP nanoparticles were produced as described in section 2.3.1 whilst PBA was entrapped or incorporated in the matrix.

PBA was dissolved in water, filtered and added to the chitosan solution and stirred for different times. Filtered TPP solution was then added to the PBA chitosan solution and ultrasonicated at 40% amplitude (300 Watts) for one minute to form the nanoparticles. Chitosan to PBA ratios of 1:1, 1:2 and 1:3 were studied and the ratio of chitosan to TPP was fixed at 3:1. The nanoparticles were then recovered by centrifugation at 10000 rpm, washed with water, and freeze-dried. The freeze-dried samples were subjected to FTIR and EDX analyses.

In an alternate procedure, chitosan was dissolved in 1% acetic acid. The TPP and the PBA were dissolved in deionised water together and filtered. The TPP/PBA solution was added to the chitosan solution and then ultrasonicated at 40% (300 Watts) for 1 minute (this time not chitosan-PBA alone but TPP being incorporated as a cross-linker). The nanoparticles were recovered by centrifugation at 10000 rpm, washed with deionised water, and then freeze-dried. The z-average of the particles produced was determined by Zetasizer Nano ZS® (Malvern, UK) equipped with a 4Mw He- Ne laser (633 nm). Each analysis was carried out at 25^{o}C and performed in triplicate and data expressed as mean ± standard deviation and images were viewed on the FESEM. The success of incorporation of PBA onto the nanoparticles was monitored by FTIR and EDX.

3.2.1.4 Synthesis and purification of chitosan-PBA conjugates by N-reductive alkylation

50 mg of chitosan (0.3 mmol of NH_2) was dissolved in 5 ml of 1% acetic acid and the mixture was stirred for 1 hour to obtain a 1% w/v solution. Various amounts of 4-formylphenylboronic acid (table 3.1) dissolved in 3ml of methanol were added to the chitosan solution, which was stirred at room temperature. After 1 hour, sodium borohydride ($NaBH_4$) (1.5%w/v) in 2 ml of methanol was added. The reaction mixture was then incubated for 24 hours at room temperature under continuous stirring. The precipitate formed was centrifuged and washed with methanol, ethanol and water thoroughly. The success of N-alkylation was monitored with FTIR, DSC, EDX, and ToF-SIMS.

Table 3.1 Quantities of starting material used in the production of chitosan-PBA conjugates by N-reductive alkylation

Formulation	Aldehyde equivalence(eq)	Aldehyde weight (mg)
F1	0.40	17.99
F2	0.80	35.98
F3	1.00	44.97
F4	1.50	67.45
F5	2.00	89.94
F6	3.00	134.91

Sample calculation

50 mg of chitosan has 0.300 mmol of NH_2 groups

Therefore: 0.40 equivalence of aldehyde converted to mmol = 0.300 x 0.40 = 0.12 mmol of aldehyde.

Molecular weight of 4 – formylphenylboronic acid = 149.90 $gmol^{-1}$

Amount of substance (n) = mass/ molecular weight

Therefore 0.12 mmol aldehyde = mass/149.9 $gmol^{-1}$

Mass = 0.12 mmol x 149.9 $gmol^{-1}$

= 0.017799 g = 17.99 mg

Same calculation was done for the rest of the formulae

Equation of the reaction

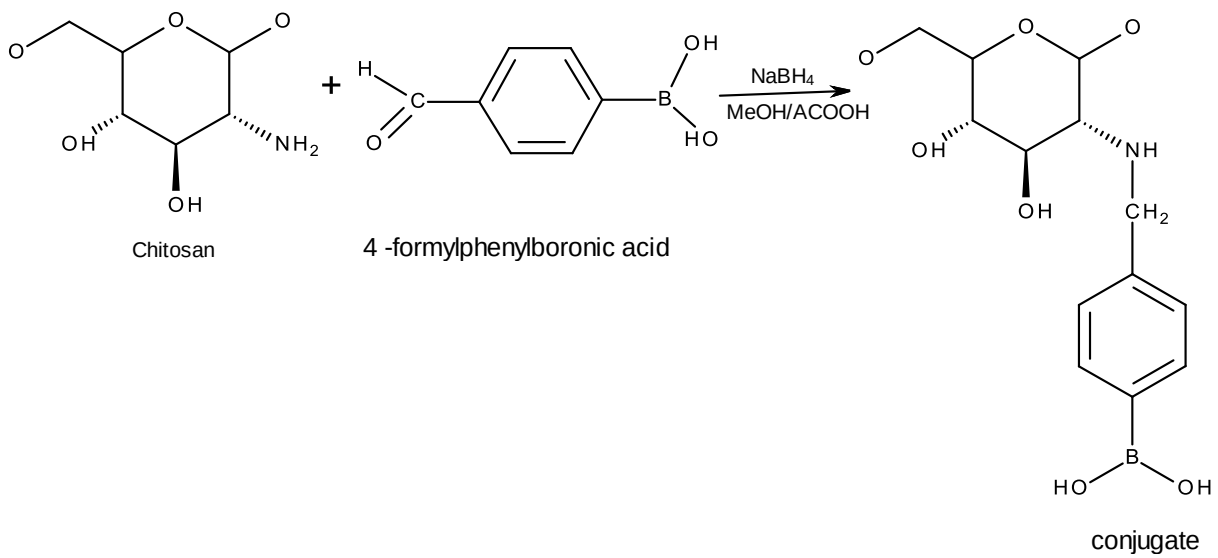

Figure 3.1 Equation of reaction between chitosan and 4-formylphenylboronic acid in the presence of $NaBH_4$

3.2.1.5 Fourier transform infra-red analysis

FTIR spectra of chitosan, TPP, chitosan-PBA conjugate and chitosan TPP PBA nanoparticles prepared by electrostatic tagging and N-reductive alkylation were obtained using a Perkin Elmer FTIR spectrometer, Spectrum RX 1. Lyophilised samples were gently mixed with about 250 mg of micronised KBr powder that was oven dried at 120^{o}C for 4 hours. The mixture was compressed at a pressure of 6 tons (5000 psi) and made into a disc, using a pneumatic table press. Spectra were collected in the range of 4000 – 400 cm^{-1}. All determinations were done in triplicate.

3.2.1.6 Differential scanning calorimetry

Thermograms were obtained using Mettler Tolledo DSC system, equipped with a STARe® software version 9.01. About 5 mg of the lyophilised powder was crimped in standard aluminum pans and heated from 25^{o}C to 500^{o}C at a constant heating rate of 10^{o}C/min under constant purge of nitrogen at 20 ml/min with an empty pan as the reference. The enthalpies for samples prepared by electrostatic tagging of PBA onto chitosan (as described in section 3.2.1.2 - 3.2.1.3) and samples of conjugate synthesised by N- reductive alkylation (as described in section 3.2.1.4) were determined using the STARe software.

3.2.1.7 Energy dispersive x-ray spectroscopy (EDX) analysis

The success of the tagging of boronic acid moiety onto chitosan was determined by the presence of boron. Samples mounted on a carbon tape were analysed using Field emission scanning electron microscopy (FESEM) (Model Quanta 400F, FEI Company, USA) with an Energy dispersive x-ray detector (EDX) (EDAX Inc. U.S.A.). EDX maps were collected for samples prepared by electrostatic tagging of PBA onto chitosan (as described in section 3.2.1.2 - 3.2.1.3) and samples synthesised via N- reductive alkylation (as described in section 3.2.1.4).

3.2.1.8 ToF-SIMS of functionalised chitosan

The success of tagging PBA onto chitosan via N-reductive alkylation was also monitored on Time-of-Flight Secondary Mass Ion Spectrometer (ToF-SIMS) IV (ION-TOF GmbH, Münster, Germany), equipped with a Bi ion gun (LMig). The presence of PBA onto chitosan was monitored based on the element boron and ionic fragments from boronic acid. These secondary

particles were analysed by mass spectroscopy (parallel acquisition with the time-of-flight analyser).

3.2.1.9 Determination of percentage yield

The percentage yield of conjugate recovered from synthesising via N-reductive alkylation was calculated based on the amount of functionalised chitosan recovered after freeze-drying for 48 hours as a percentage of the amount of chitosan (the initial weight of polymer) used at the start of the reaction. Analyses were performed in triplicate and expressed as the mean ± standard deviation.

$$\text{Percentage yield} = \frac{\text{Final weight of functionalised chitosan}}{\text{Initial weight of chitosan used}} \times 100\% \quad \textbf{..... Equation 3.1}$$

3.2.1.10 Elemental analysis of functionalised chitosan

The elemental composition of the functionalised chitosan was determined using CE440 Elemental analyser (Exeter Analytical (UK) Ltd). 1.7 mg of conjugate synthesised via N-reductive alkylation was weighed into aluminium capsules. The sample was injected into a high temperature furnace and combusted in pure oxygen under static conditions. At the end of the combustion period, a dynamic burst of oxygen was added to ensure total combustion of all inorganic and organic substances. The resulting combustion products were passed through specialised reagents to produce the elements carbon, hydrogen, and nitrogen; as the gases carbon dioxide (CO_2), water (H_2O) and nitrogen (N_2) and nitric oxides. Analysis was done in triplicate for each sample.

3.3 Results and Discussion

3.3.1 Electrostatic tagging of PBA onto chitosan

3.3.1.1 Formulation of chitosan-PBA nanoparticles

It was assumed that using pH adjustments, chitosan-PBA nanoparticles could be formulated. Table 3.2 shows z-average, Pdi and zeta potential of the chitosan-PBA nanoparticles formulated by electrostatic tagging onto chitosan. The z-averages recorded were all in the microparticle range. Figure 3.2 shows the SEM image of the chitosan-PBA nanoparticles produced at a ratio of chitosan to PBA of 1:2.

Table 3.2 Z-average, Pdi and zeta potential of chitosan-PBA nanoparticles

Formulation ratio of chitosan to PBA	Z-average (nm)	Pdi	Zeta potential (mV)
1:1	1417 ± 69.60	0.594 ± 0.24	40.9 ± 5.20
1:2	1245 ± 35.20	0.545 ± 0.38	42.5 ± 3.20
1:3	1017 ± 45.20	0.587 ± 0.14	44.9 ± 2.40

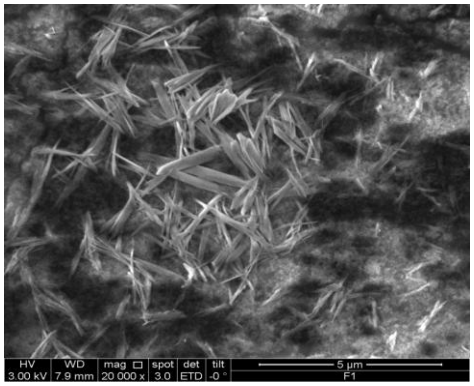

Figure 3.2 SEM image of chitosan phenylboronic acid nanoparticles

It can be seen that the structures are not spherical but appear to be spindle-shaped; such spindle-shaped structures have been reported by Harish and Tharanathan (2006) who attributed these to the structure of chitosan. It can therefore be concluded that, the spindle shaped structures seen are chitosan and that PBA did not electrostatically interact with chitosan as expected to produce nanoparticles.

3.3.1.2 Formulation of chitosan-PBA conjugates

In a refined approach, PBA was first made to react with chitosan by stirring for different times and the conjugates were precipitated out by addition of 1M NaOH, washed with deionised water and then freeze-dried, whilst a portion of the conjugates were also freeze-dried directly without precipitation and washing. The FTIR spectra and DSC thermograms of the freeze-dried conjugates (precipitated and non-precipitated) were compared to those from pure chitosan (figures 3.3 and 3.4).

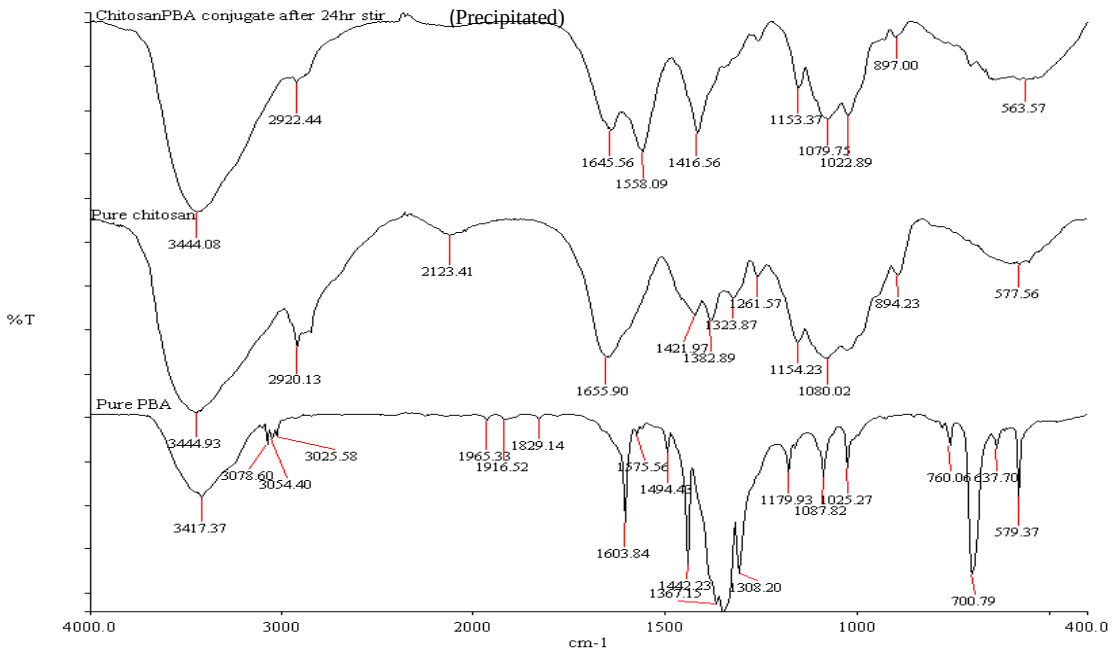

Figure 3.3 FTIR spectra of conjugate (formulated by stirring for 24 hours), chitosan and PBA

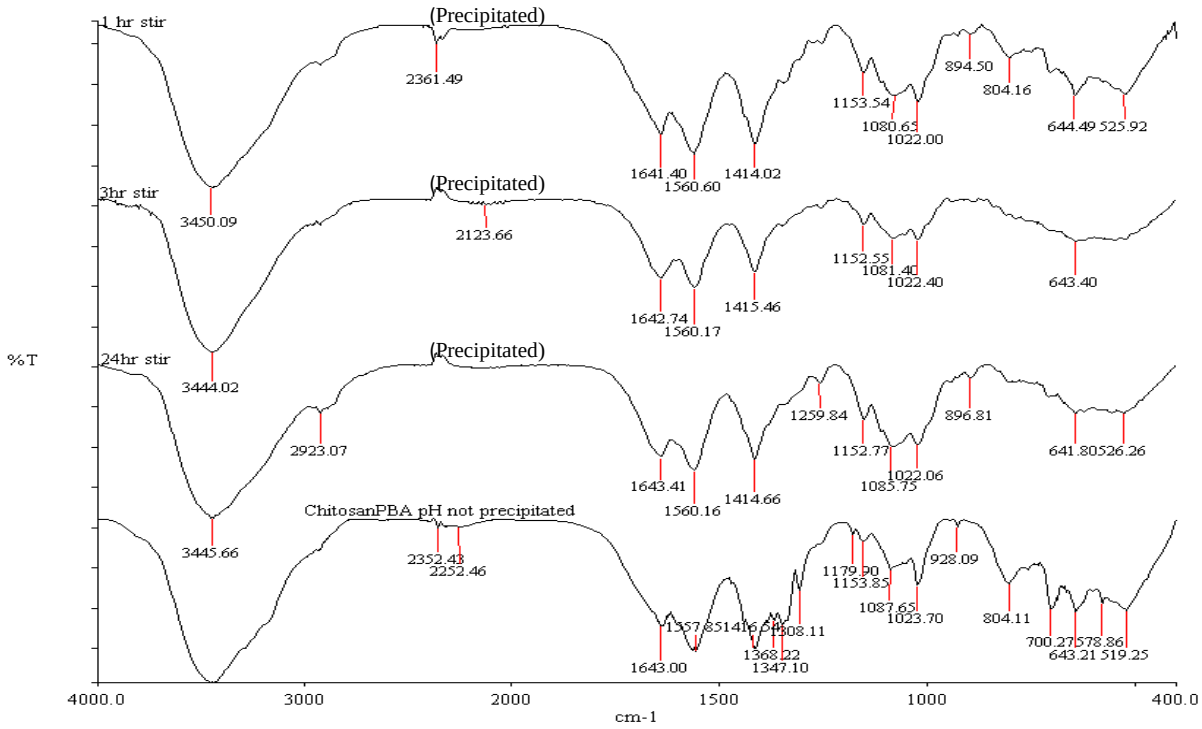

Figure 3.4 FTIR spectra of precipitated and non-precipitated conjugates stirred for different times

It is observed that conjugates recovered by the above mentioned methods, washed and freeze dried has similar spectra to that of chitosan. Characteristic peaks of PBA appearing at 1442 cm^{-1} has been attributed to a mixture of several motions including C-C and B-O stretching, while the band centred around 1367 cm^{-1} is likely due to vibrational modes involving B-O stretching motions and peaks at 1080-1110 cm^{-1} have been attributed to B-C stretching mode in arylboronic acid (Faniran and Shurvell 2011), these characteristic peaks are seen in the pure boronic acid and the conjugates that were not precipitated out (figure 3.3 and 3.4) (table 3.3), but none of the above mentioned peaks characteristic of PBA was seen in the conjugate that was precipitated out, washed and freeze dried (figure 3.3). The washing step in the procedure after precipitation might have washed all the unreacted PBA and hence no characteristic peak of PBA seen in the washed conjugate but the reverse is seen in the unprecipitated conjugate because the unreacted

PBA was not washed and hence the presence of characteristic boronic acid peaks in those conjugates (figures 3.3 and 3.4)

Figure 3.4 also shows the effect of stirring times on the tagging of boronic acid onto the chitosan, the spectra shows that increasing the stirring times of the reaction did not have significant effect on the extent of incorporation of the PBA into chitosan.

Table 3.3 FTIR peaks (cm^{-1}) of interest from chitosan, TPP, PBA and chitosan-PBA conjugates (n=3)

Possible assignment	Chitosan	TPP	PBA	Chitosan-PBA conjugate
-NH_2 and -OH stretching vibration	3459.69±12.97	-	-	3430.87±9.30
carbonyl ($CONH_2$)	1654.77±1.88	-	-	1652.77±1.20
Secondary amide	1380.31±0.73			
C-C and B-O stretching	-	-	1442.20±0.25	-
Vibrational modes involving B-O stretching	-	-	1367.64±0.51	-
B-C stretching mode in arylboronic acid	-	-	1086.92±14.98	-
Amine groups in Chitosan interaction with TPP	1637.57±0.50 1540.54±1.52		-	-
Characteristic absorption band of para-substituted benzene				1559.54±0.53 1514.85±0.43 830.90±0.37

Figure 3.5 shows the DSC thermogram of chitosan. There are two characteristic peaks at 95^{o}C which is endothermic and an exothermic peak at 310^{o}C. These peaks have also been reported by other researchers (Kittur *et al*. 2002; Mourya and Inamdar 2009; Sreenivasan 1996; Sarmento *et al.* 2006). Endothermic peak have been correlated with evaporation of water associated to hydrophilic groups of polymers, whilst the exothermic peaks have been related to degradation due to dehydration, depolymerisation and pyrolitic reactions.

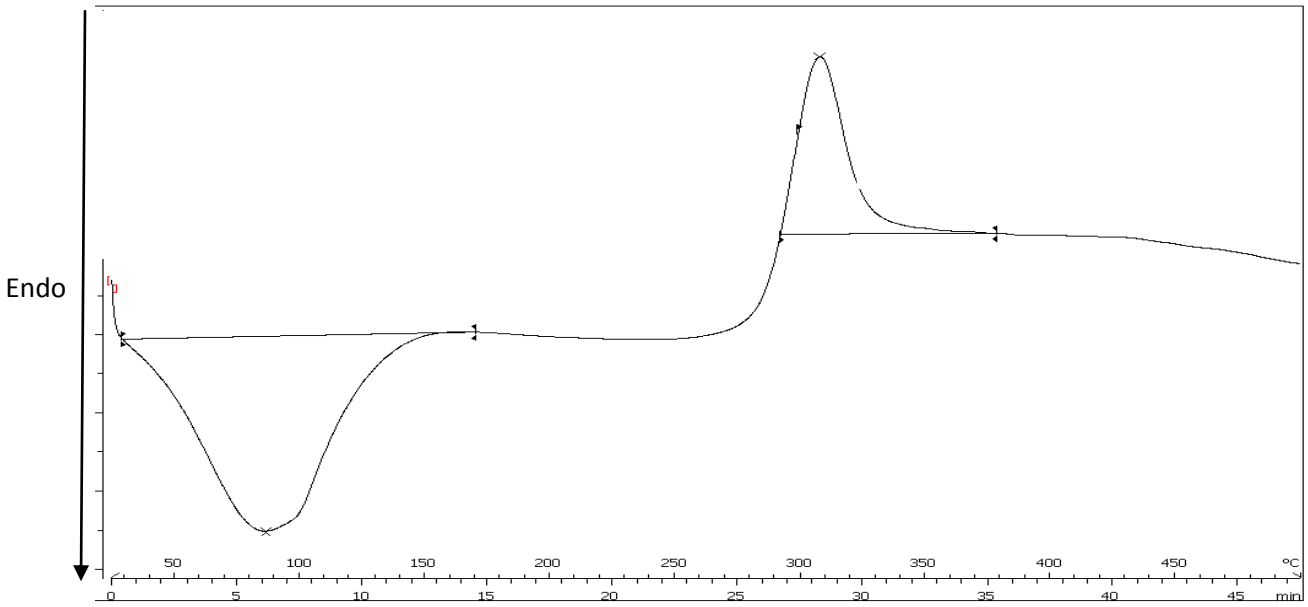

Figure 3.5 DSC thermogram of chitosan

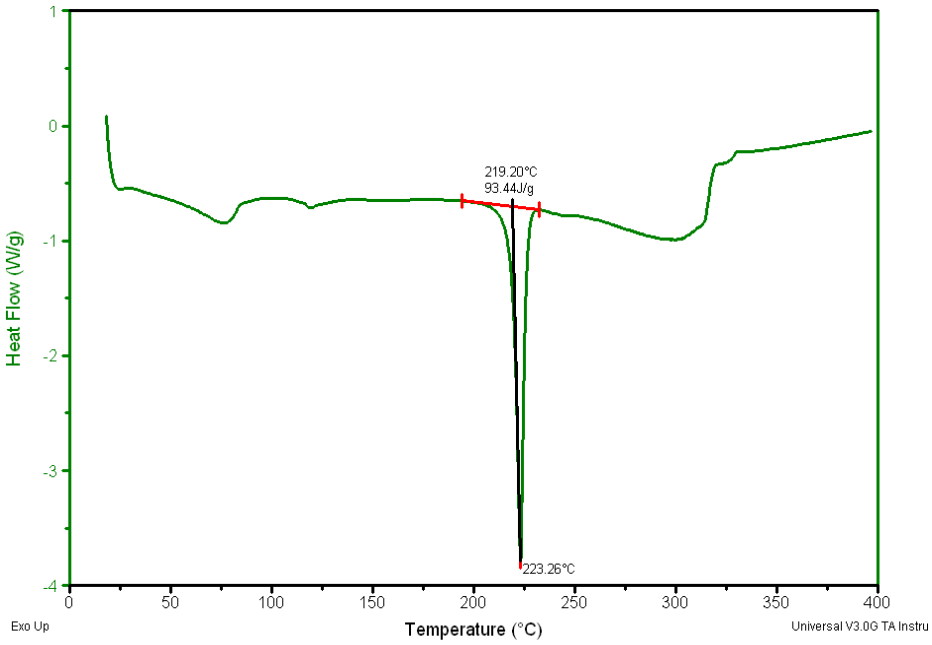

Figure 3.6 DSC thermogram of PBA

Figure 3.6 represents the DSC thermogram of pure PBA. There is a characteristic sharp endothermic peak at around 220^{o}C; endothermic peaks have been associated with melting points of chemicals. The melting point of PBA is reported to be in the range 219-222^{o}C (Sigma Aldrich, 2013), hence the endothermic peak at around 223^{o}C can be ascribed to the melting point of PBA.

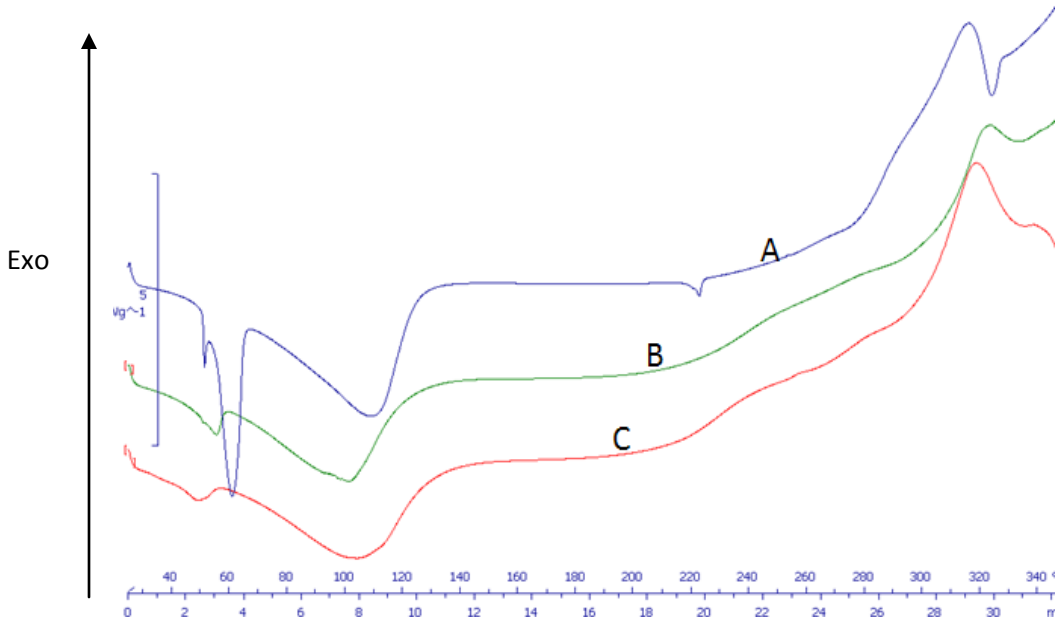

Figure 3.7 DSC thermogram of chitosan-PBA conjugate

A: DSC thermogram of unprecipitated chitosan phenylboronic acid conjugate
B/C: DSC thermogram of precipitated and washed chitosan phenylboronic acid conjugate

Figure 3.7 is the thermogram of the freeze-dried conjugates that were precipitated with sodium hydroxide and one that was not. It appears that the endothermic peak of chitosan has shifted to higher temperature (110^{o}C) whilst the exothermic peak appears to have been retained (figure 3.7 B and C). In addition, there appears to be two endothermic peaks, one at 60^{o}C and a smaller one at around 220^{o}C from the unprecipitated conjugate and these peaks (figure 3.7 A) may be akin to PBA. The endothermic peak at 60^{o}C is also present in the washed conjugate albeit somewhat smaller and shifted to lower temperatures, but the peak at around 220^{o}C disappears. It follows that the washing procedure is necessary in removing the unreacted PBA from the conjugate.

Table 3.4 XRF compositional analysis of conjugate weight percentage of sample PBA in oxide and elemental form

Oxide	Element	Concentration (%) Oxide	Concentration (%) Element
CO_2	C	95.00	26.00
Na_2O	Na	5.10	3.80
Cr_2O_3	Cr	0.10	0.07
Fe_2O_3	Fe	0.17	0.12
-	O	-	70.18
Total		100.37	100.17

X-Ray fluorescence spectroscopy (XRF) is used for detection of elements on the periodic table between beryllium (Be) and uranium (U). Conventional methods for elemental analysis are not sensitive enough to quantify elements such as boron. Since boron is a major element that can be monitored as prove presence of PBA on chitosan, boron content was measured by XRF. From table 3.4, the XRF data show that no boron was detected, except for C and O which is attributed to elements in chitosan. Traceable amounts of sodium and other elements were also found. This also shows that functionalisation of chitosan by electrostatic tagging for the preparation of chitosan-PBA conjugates was not successful.

3.3.1.3 Formulation of chitosan-TPP-PBA nanoparticles

The assumptive tagging of phenylboronic onto chitosan TPP nanoparticles was also attempted which was based on the premise that, the negatively charged boronic acid will seemingly react with the positively charged chitosan as TPP will do. The recovered nanoparticles prepared by ultrasonication were taken through FTIR analysis and EDX analysis to check the success of tagging by this method also. It was observed from the FTIR that there were no peaks attributable to PBA, but that of chitosan and TPP (figure 3.8).

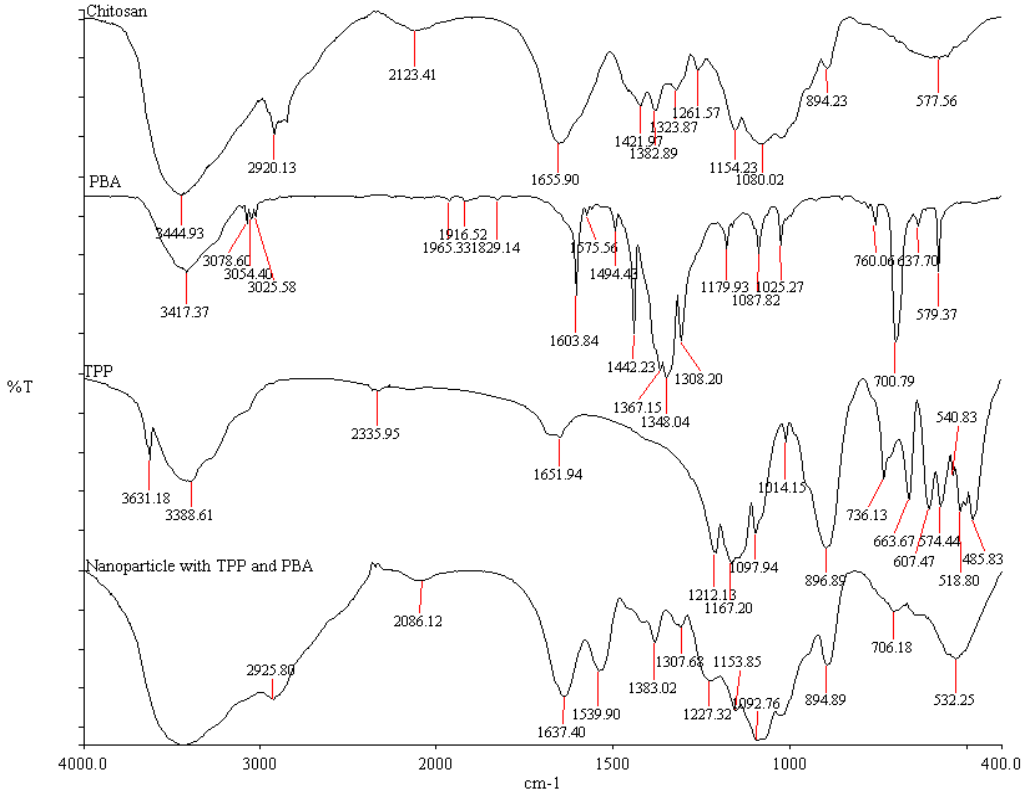

Figure 3.8 FTIR spectra of chitosan, PBA, TPP and chitosan TPP PBA nanoparticles

A broad peak around 3450 cm^{-1} in the chitosan TPP PBA nanoparticles is indicative of enhanced hydrogen bonding. The intensities of ($CONH_2$) band at 1655 cm^{-1} which can be observed in

chitosan decrease dramatically and two new sorption bands at 1637 and 1539 cm^{-1} (table 3.3) appear and this is indication that the ammonium groups in chitosan are cross-linked with tripolyphosphate molecules. Thus it is postulated that polyphosphoric groups of sodium polyphosphate interact with the ammonium groups of chitosan, which serves to enhance both the inter- and intramolecular interaction in chitosan nanoparticles (Qi *et al*. 2004).

The EDX for the plain carbon tape which was used to mount the samples also seem to have traces of boron as seen in figure 3.9 and table 3.5 and this implies that there would be a source of interference from the carbon tape.

Table 3.5 EDX of carbon tape

Element	Weight%	Atomic%
B K	6.41	7.41
C K	75.44	78.47
N K	0.00	0.00
O K	17.98	14.04
Al K	0.17	0.08
Totals	100.00	

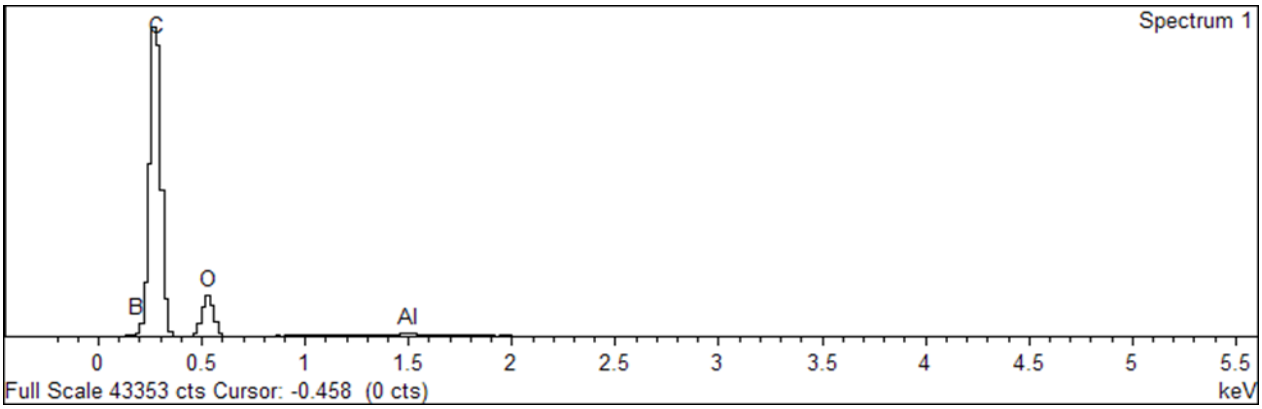

Figure 3.9 EDX of Carbon tape

The elements carbon, oxygen and phosphorous were detected by EDX for the chitosan TPP PBA nanoparticles (figure 3.10).

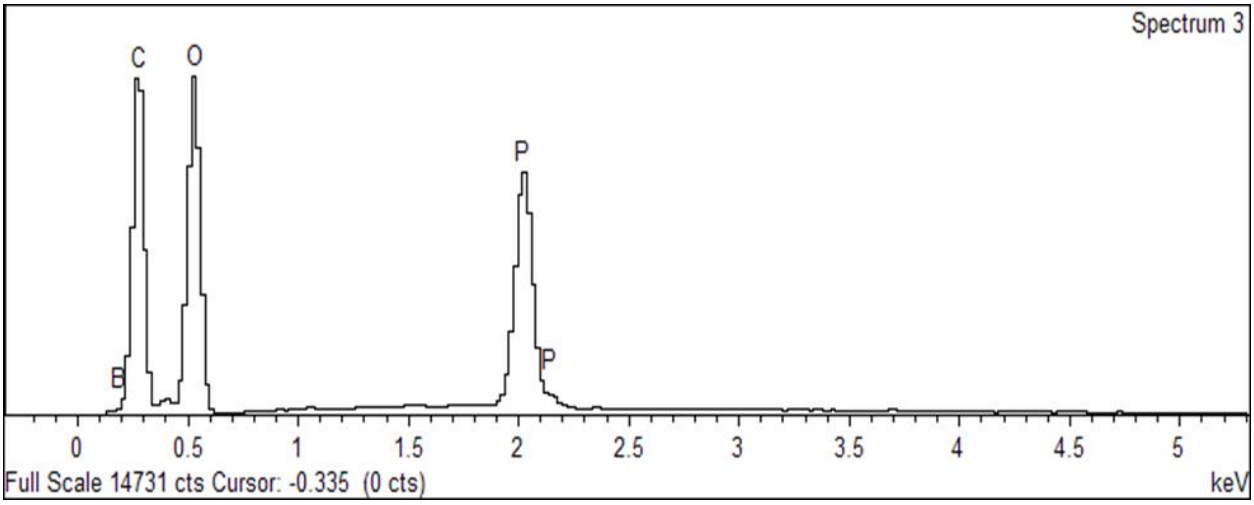

Figure 3.10 EDX of chitosan TPP PBA nanoparticles

The carbon and oxygen can be ascribed to chitosan whilst TPP contributes the phosphorous. The sodium present may also be from the TPP, because it comes as a sodium salt.

As seen in table 3.6 and 3.7 and figures 3.10 and 3.11, there is no difference between the EDX of chitosan TPP nanoparticles and chitosan TPP PBA nanoparticles. The percentage of boron seen is attributable to the traces of boron from the carbon tape.

From the above methods employed which were met with no success, it was inferred that, the electrostatic tagging of the phenylboronic acid to chitosan was not feasible.

Table 3.6 EDX of chitosan TPP PBA nanoparticles

Element	Weight%	Atomic%
B	6.73	8.62
C	46.51	53.58
O	40.40	34.94
Na	0.15	0.09
P	6.20	2.77
Totals	100.00	

Table 3.7 EDX of chitosan TPP nanoparticles

Element	Weight%	Atomic%
B	5.40	7.01
C	42.09	49.17
O	47.20	41.39
Na	0.16	0.10
P	5.14	2.33
Totals	100.00	

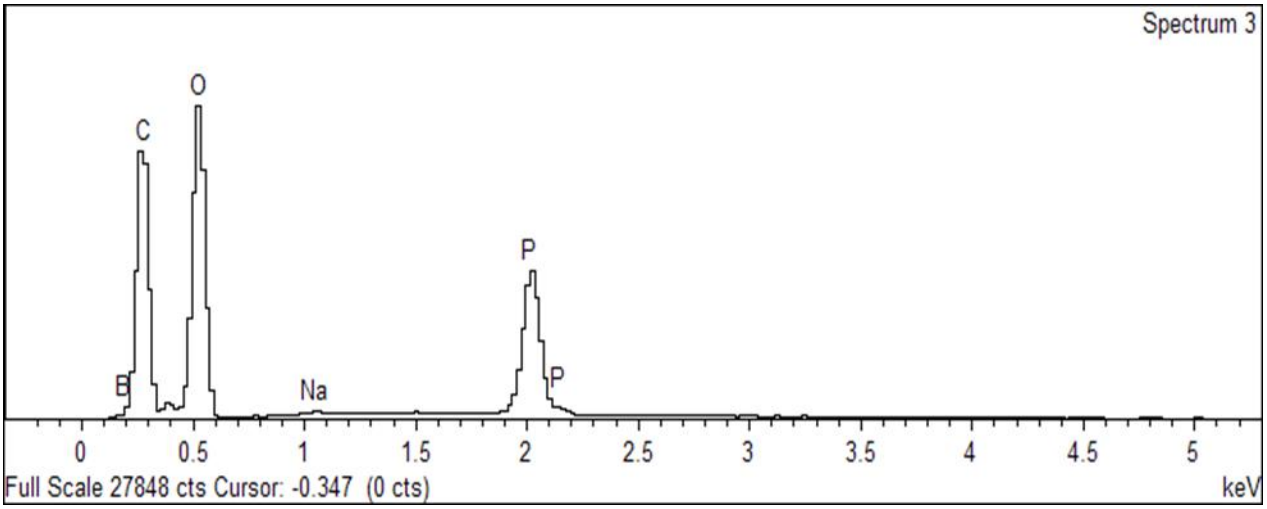

Figure 3.11 EDX of chitosan TPP nanoparticles

Nanoparticles cannot be produced from the positively charged chitosan and negatively charged phenylboronic acid alone. The method of incorporating the phenylboronic acid in the process of production of the chitosan TPP nanoparticles also does not bring about the tagging or the incorporation of the phenylboronic acid into the nanoparticulate system.

3.3.2 Tagging of PBA onto chitosan via N-reductive alkylation

After the unsuccessful attempts at electrostatic tagging phenylboronic acid onto chitosan, PBA was made to chemically react with chitosan. There are several methods in the literature that describe the tagging of PBA onto chitosan but the one most reviewed is based on the N-reductive alkylation of the amine groups within chitosan (Smoum *et al*. 2006). This same method was used also by Matsumoto *et al* (2002) to synthesise a novel chitosan gel modified by phenylboronate with selective glucose adsorption capacity. In the present study the tagging of the boronic acid group was done via the Schiff's base method where the phenylboronate group (p-formylboronic acid) was introduced into chitosan by reductive N-alkylation. A second method was also used by the same group to introduce the phenylboronic acid group onto chitosan. In that method the amino group in chitosan reacted with carboxyboronic acid to form the amide compound in the presence of thionyl chloride in dimethylformamide (figure 3.12b) and the resulting gels were then filtered, washed with methanol and ethanol, and dried in vacuo (Matsumoto *et al*. 2002).

The second pathway of reaction (figure 3.12b) had more steps in the reaction than the first pathway (figure 3.12a).

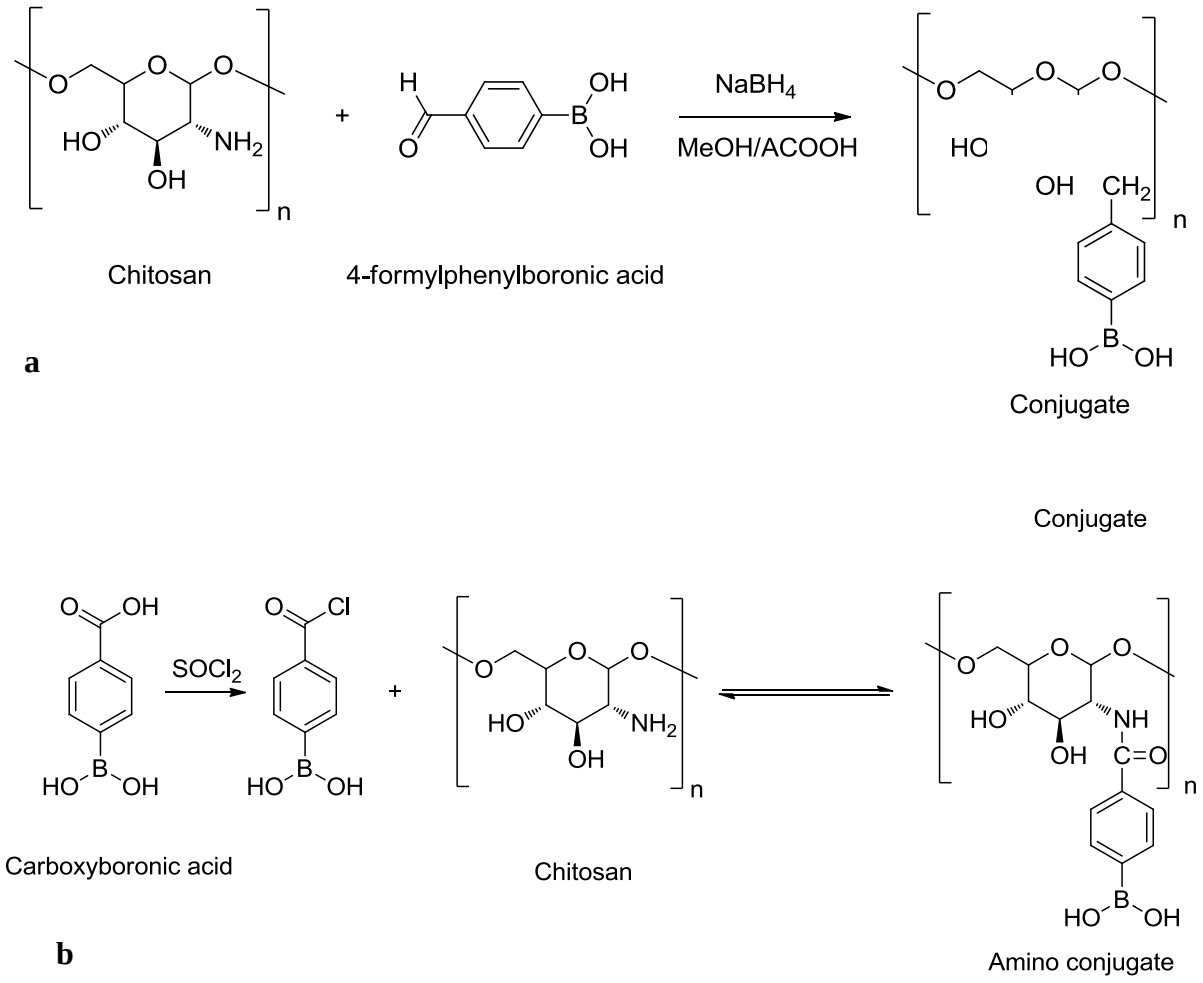

Figure 3.12 Reaction of N- reductive alkylation of chitosan, A- by the Schiff's base method and B- by amide bonding. (Smoum *et al*., 2006).

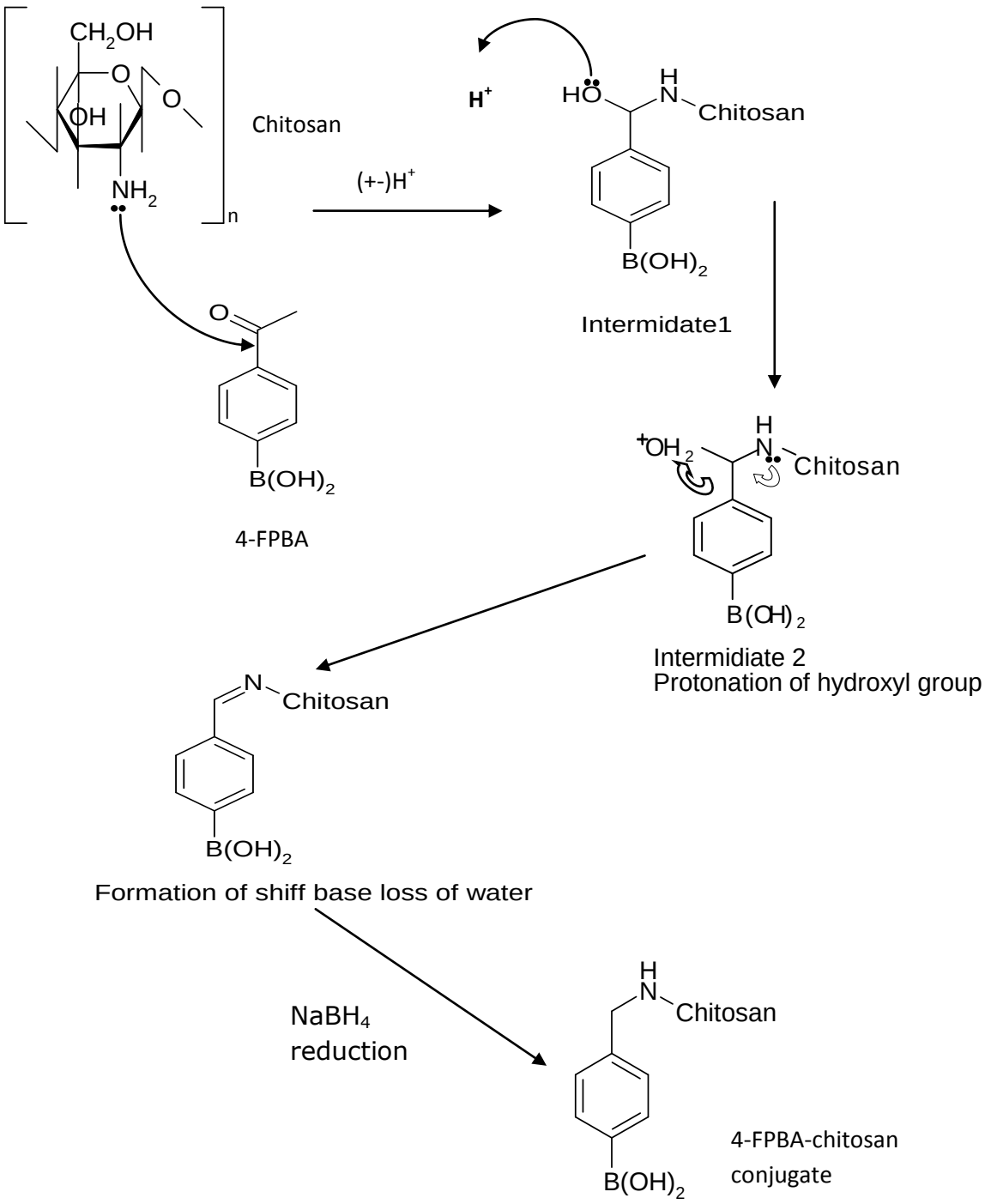

Figure 3.13 Reaction mechanism of a single chitosan monomer with (4-FPBA) via a schiff base intermediate.

Figure 3.13 outlines the chemical process of the N- reductive alkylation. The initial reaction of the chitosan with FPBA produces an imine intermediate which is further reduced to an amine by the sodium borohydride.

Moreover, based on the selective adsorption work done by Matsumoto *et al*. (2002), it was found out that the gels produced by the N– reductive alkylation via Schiff's base method had selective adsorption for glucose and since this current project is dealing with the development of a glucose responsive insulin delivery system, it was deemed appropriate to adopt the schiff base method. Chitosan derivatives were synthesised by direct reductive N-alkylation of chitosan with 4-formylphenylboronic acid and the degree of N-substitution could be controlled by increasing or decreasing the amount of the aldehyde (FPBA) in the reaction mixture (Table 3.1 in section 3.2.1.4)

3.3.2.1 Percentage yield

The percentage yield of the PBA functionalised chitosan was calculated using equation (3.1). Table 3.8 shows the average of yield of each formulation coded F1-F5.

Table 3.8 Percentage yield of the formulation F1 to F5 (see table 3.1) after centrifugation

Formulation	Percentage yield
F1	79.30 ± 1.80
F2	83.97 ± 4.70
F3	90.40 ± 2.59
F4	107.24 ±6.50
F5	112.42 ±3.06

Smoum *et al* (2006) used the filtering method for the recovery of the functionalised chitosan after production. In this current project, it was observed that the precipitate recovered after production was colloidal and sticky to the filter paper.

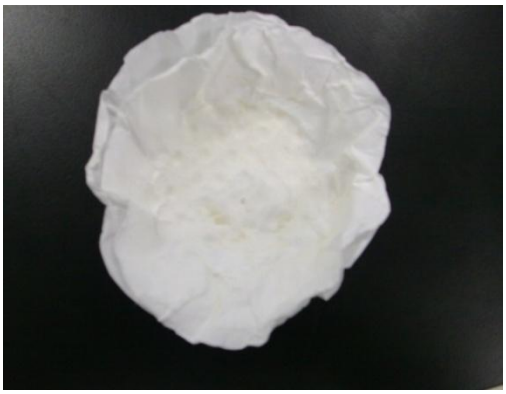

Figure 3.14 Image of precipitate of functionalised chitosan after filtration and drying in *vacuo*

Figure 3.14 is the image of functionalised chitosan recovered by filtration and dried in vacuo, the colloidal precipitate was difficult to recover from the filter paper and after vacuum drying samples stuck onto the filter and an attempt to remove it introduced contamination from the filter paper. Therefore the conjugates were recovered by centrifugation at 6000 rpm for 10 minutes with several washing cycles using methanol, ethanol and water. The yield from the recovery by centrifugation was better than Smoum *et al's* (2006) filter paper method. A minimum percentage yield of about 46% and a maximum of about 76% were recorded by Smoum *et al.* (2006). From table 3.8 above, there was a significant increase in the percentage yield. In this regard the method of centrifugation was considered a better way for recovering the precipitate than filtration because there is minimal loss in the process.

Also comparing the method of washing using methanol and ethanol only as employed by Matsumo *et al* (2002), in the production of chitosan phenylboronic acid conjugate for saccharide

recognition and that of Smoum *et al* (2006) using water and methanol, it was observed that, the process and solvents used in the washing of the conjugate had effect on the final appearance, texture and acetic acid solubility of the formulation. Therefore a combination of water, ethanol and methanol washings was employed in present study as an improvement on the previous methods used. F4 – F5 when washed with ethanol and methanol combination alone yielded a yellow crystalline material. Methanol, ethanol and water washings on these same formulations yielded an off white amorphous powder with better solubility in 1% acetic acid. Also the method of drying had an influence on the physical appearance of the conjugate. (Matsumoto *et al*. 2002) dried their conjugates in vacuo, but when this mode of drying was attempted in the present study, hard crystalline products with less solubility in 1% acetic acid were recovered. Freeze drying yielded near amorphous powders with good solubility in 1% acetic acid and hence this latter method of drying was used throughout the project.

Figures 3.15-3.19 show the production and the recovery process used for the synthesising the conjugates.

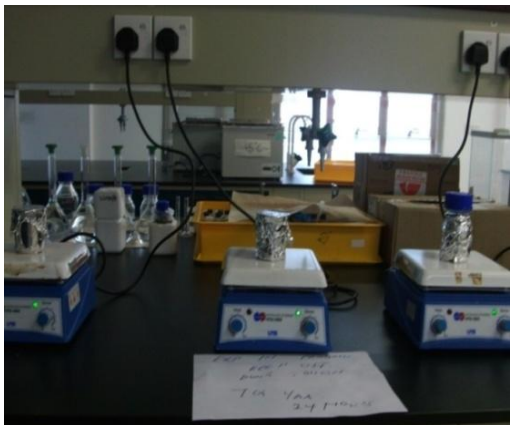

Figure 3.15 Image of the process of production of functionalised chitosan

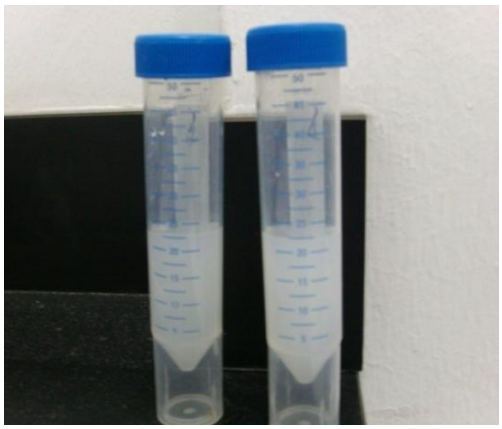

Figure 3.16 Image of precipitate of functionalised chitosan before centrifugation

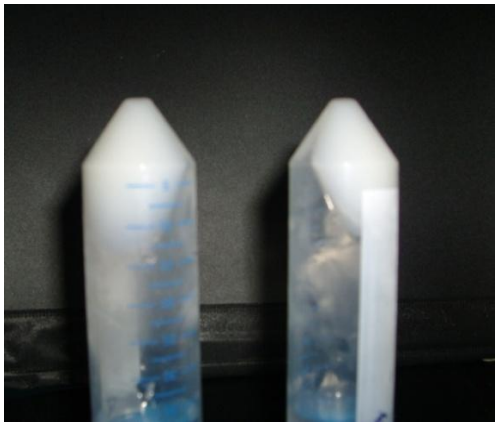

Figure 3.17 Image of functionalised chitosan after centrifugation

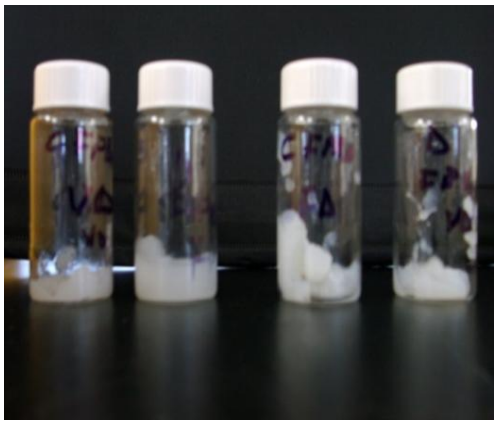

Figure 3.18 Image of functionalised chitosan before freeze drying

Figure 3.19 Image of functionalised chitosan after freeze drying

3.3.2.2 Elemental analysis of conjugates prepared by N-reductive alkylation

Elemental analysis is an experiment that determines the amount (typically a weight percent) of an element in a compound. Just as there are many different elements, there are many different experimental methods for determining elemental composition. The most common type of elemental analysis is for carbon, hydrogen, and nitrogen (CHN analyses). This type of analysis is especially useful for organic compounds (compounds containing carbon-carbon bonds).

Elemental analyses on the different functionalised chitosan revealed an increase in the carbon percentage as the amount of FPBA used in the initial reaction increased. From table 3.9, it can be seen that the percentage of carbon increased, indicating the addition of more chemical groups to the chitosan. The percentage of nitrogen (N) due to amine groups within the chitosan decreases because there are more carbon (C) groups (contributed by the formylphenylboronic acid substitution) being added to a fixed number of amine groups within chitosan. The difference in the composition of the various elements across the different formulation proves that, the degree of substitution of the boronic acid onto chitosan depend on the initial amount of the FPBA added.

Table 3.9 Elemental analyses of functionalised chitosan

Formulation	C (%)	H (%)	N (%)
Chitosan	40.29	6.58	7.22
F1	41.31	6.10	6.55
F2	42.20	6.14	6.19
F3	42.87	6.09	6.12
F4	44.34	5.78	5.50
F5	45.48	5.19	4.61

3.3.2.3 FTIR analysis of the conjugates prepared by N-reductive alkylation

In the FTIR spectra of chitosan (figure 3.20), the characteristic peak for chitosan appear at about 3430.24 cm^{-1} indicative of OH and NH_2 stretching vibrations and a peak at 1654.29 cm^{-1} attributable to an amide – linked carbonyl group (C=O) and the C-O bond peak appear at 1080 (table 3.3). The 1381.02 cm^{-1} corresponds to a secondary amide, most likely due to incomplete de-acetylation of chitosan (Osman and Arof 2003; Vandeveld and Kiekens 2004). These are in agreement with previous works done (Matsumoto *et al*. 2002; de Moura *et al*. 2008; Bruno Sarmento *et al*. 2006).

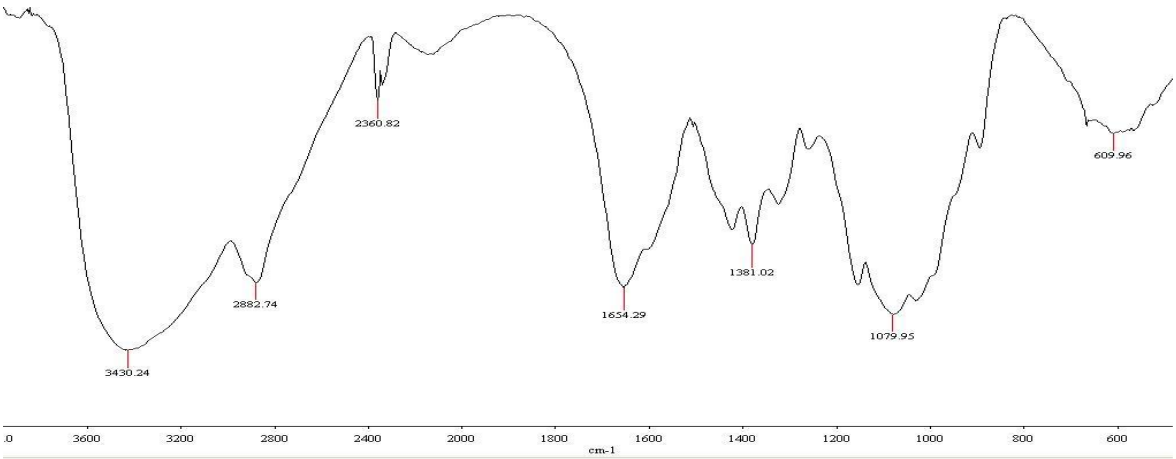

Figure 3.20 FTIR spectra of chitosan

The newly synthesised chitosan-PBA conjugates showed characteristic bands at 1559.54, 1514.85 and 830.90 cm^{-1}, (figure 3.21-3.23) (table 3.3) which are characteristic absorption bands of para substituted benzenes. These peaks are sharper and higher in intensity in proportion to the degree of substitution (figure 3.23). The conjugate with the highest amount of substitution showed the greatest peak.

The peak relating to the primary amine of chitosan at 1590 cm^{-1} became less apparent from F1 through F6 and virtually disappeared in F6 (figure 3.23). This strongly suggest that the PBA resides at the primary amine group ($-NH_2$). This confirms the successful functionalisation of chitosan with the boronic acid group (Smoum *et al*., 2006; Matsumoto *et al*., 2002).

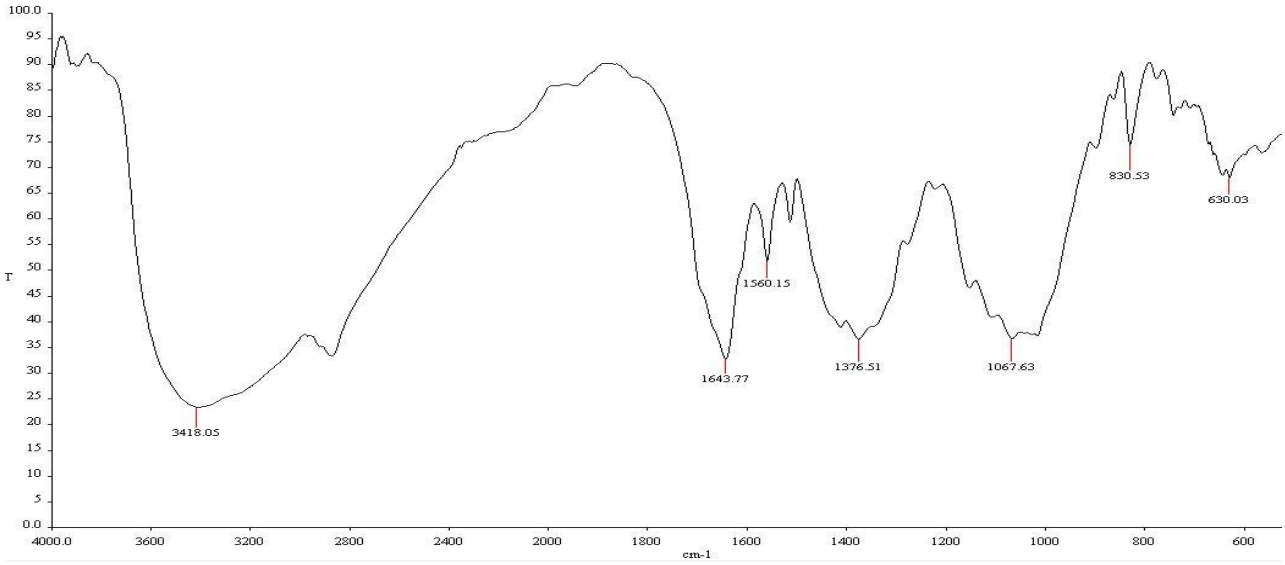

Figure 3.21 FTIR spectra of Conjugate F4

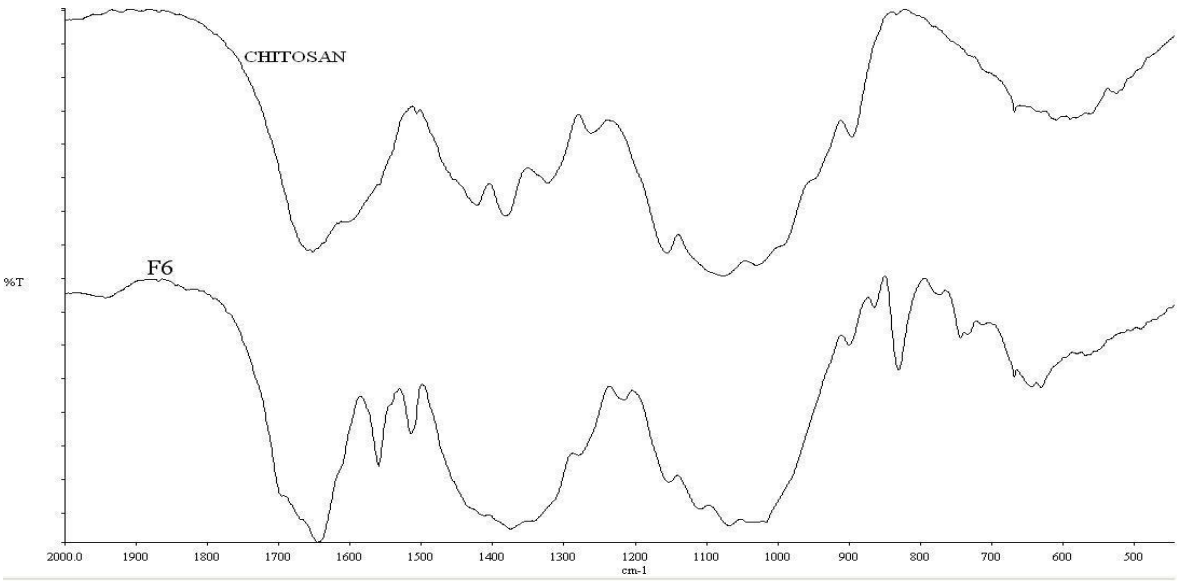

Figure 3.22 FTIR spectra of conjugate (F6) and chitosan

In figure 3.23, an increase in the intensities of the peaks of the para substituted benzene (1559, 1514, 831 and 647 cm^{-1} (table 3.3)) is observed as the degree of substitution increases.

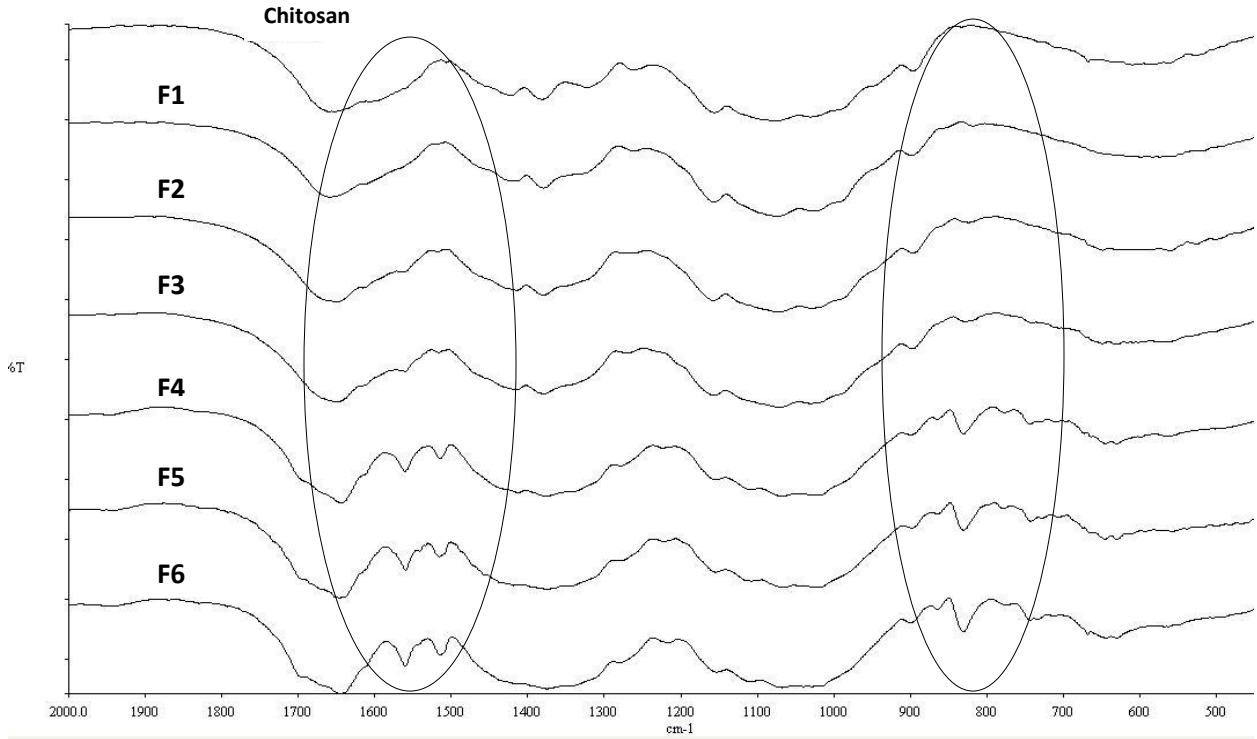

Figure 3.23 FTIR spectra of chitosan and conjugates F1 through F6

3.3.2.4 Differential scanning calorimetry (DSC) of conjugates prepared by N-reductive alkylation

To study the change in material organisation in chitosan due to bonding with FPBA, DSC analysis of the functionalised chitosan were performed and are presented in figures 3.24 -3.26. Thermograms of chitosan and the conjugates are very different as seen in figure 3.23 below. This indicates the presence of additional chemical functionality. Chitosan has an endothermic and exothermic peak and these are characterised at 80^{o}C and 300^{o}C respectively. Endothermic peak have been correlated with evaporation of water associated to hydrophilic groups of polymers, whilst the exothermic peaks have been related to degradation due to dehydration, depolymerisation and pyrolitic reactions (Bruno Sarmento *et al*. 2006; Bhumkar and Pokharkar 2006).

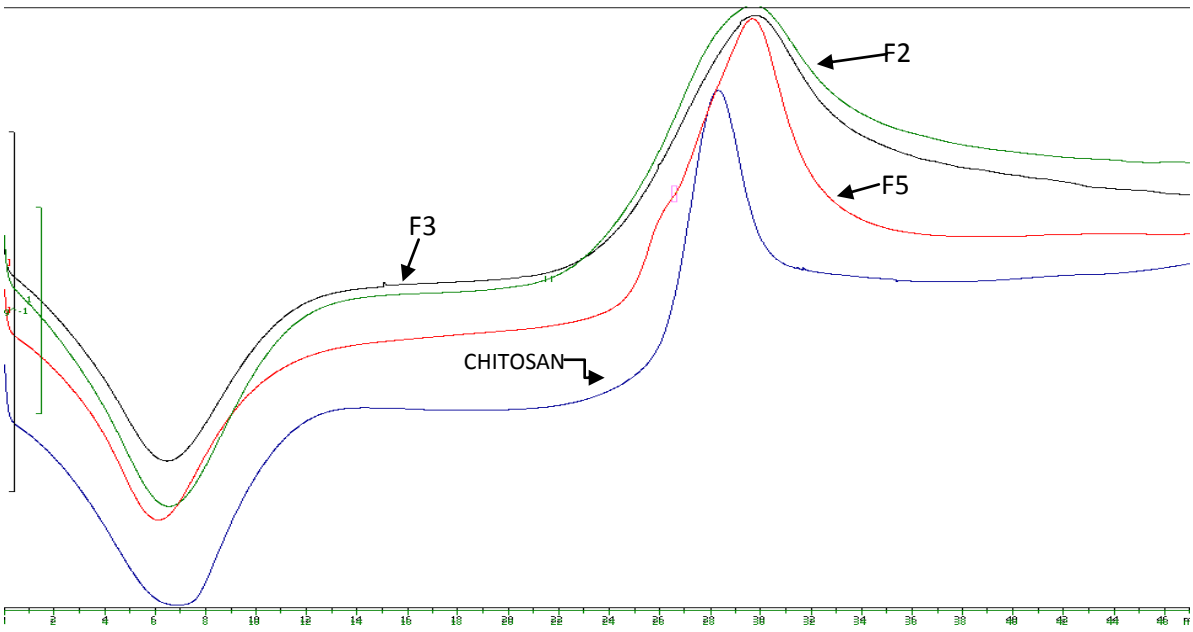

Figure 3.24 DSC Thermogram of conjugates (F2, F3 and F5) and chitosan

The thermograms of the new conjugates made by N-reductive alkylation exhibit a wide endothermic peak at around 75^{o}C which is slightly shifted from the endothermic peak of pure

chitosan at 83^{o}C. The exothermic peaks in the new conjugates are slightly shifted from the temperature where the chitosan peak occurs which is around 308^{o}C to 320^{o}C (figure 3.24). This is indicative of chemical modification of chitosan by another chemical group. The existence of the endothermic peak has always been attributed to the evaporation of water from hydrophilic groups of polymers and the existence of this peak in the conjugate shows that the polymeric nature of the new conjugate is retained. The existence and slight shift of the conjugate exothermic peaks can be related to degradation due to dehydration, depolymerisation and pyrolitic reactions as seen in chitosan. The shift can be attributed to the new group substitution onto chitosan making it more bulky a polymer than what it used to be and hence a higher temperature of degradation. There appears to be no report on chitosan-PBA conjugate thermogram in the literature and these are new observations that have been made.

In order to ascertain that the tagging of PBA to chitosan was successful and also monitor the purity of the conjugate, a physical admixture of pure chitosan and pure 4- FPBA was made and its thermogram taken. This thermogram was compared to that of pure chitosan, pure FPBA and the newly synthesised conjugates. The endothermic peak in pure FPBA is seen as two peaks (figure 3.25), a broader peak occurring around 125^{o}C and a sharp peak at around 155^{o}C and also two exothermic peaks occur around 300^{o}C and 350^{o}C.

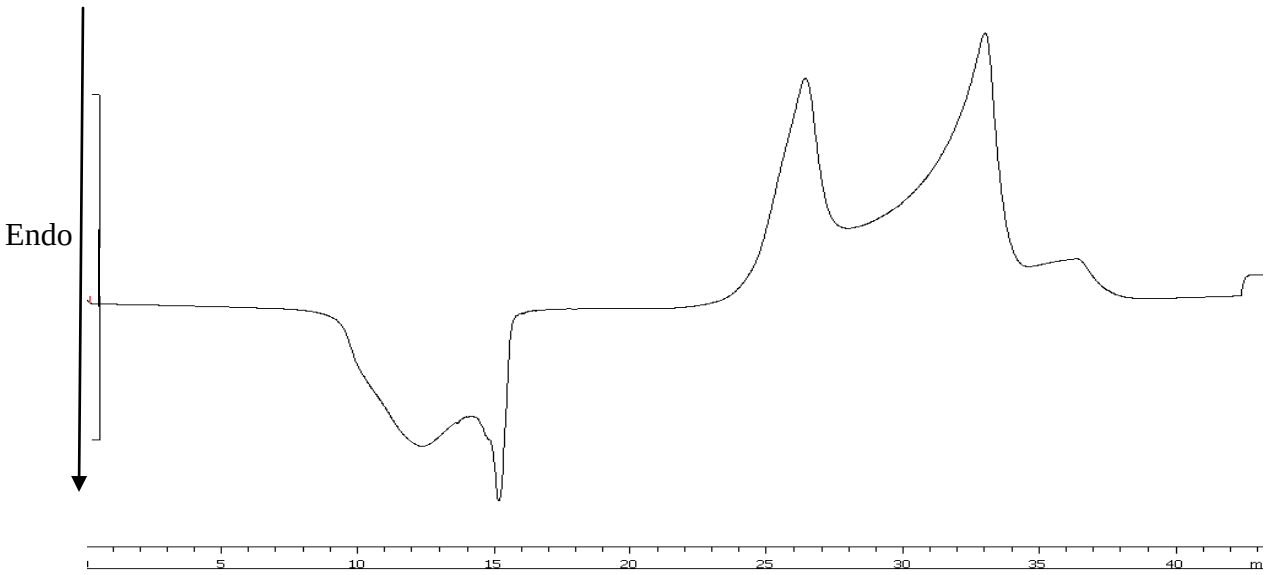

Figure 3.25 DSC Thermogram of pure 4-formylphenylboronic acid

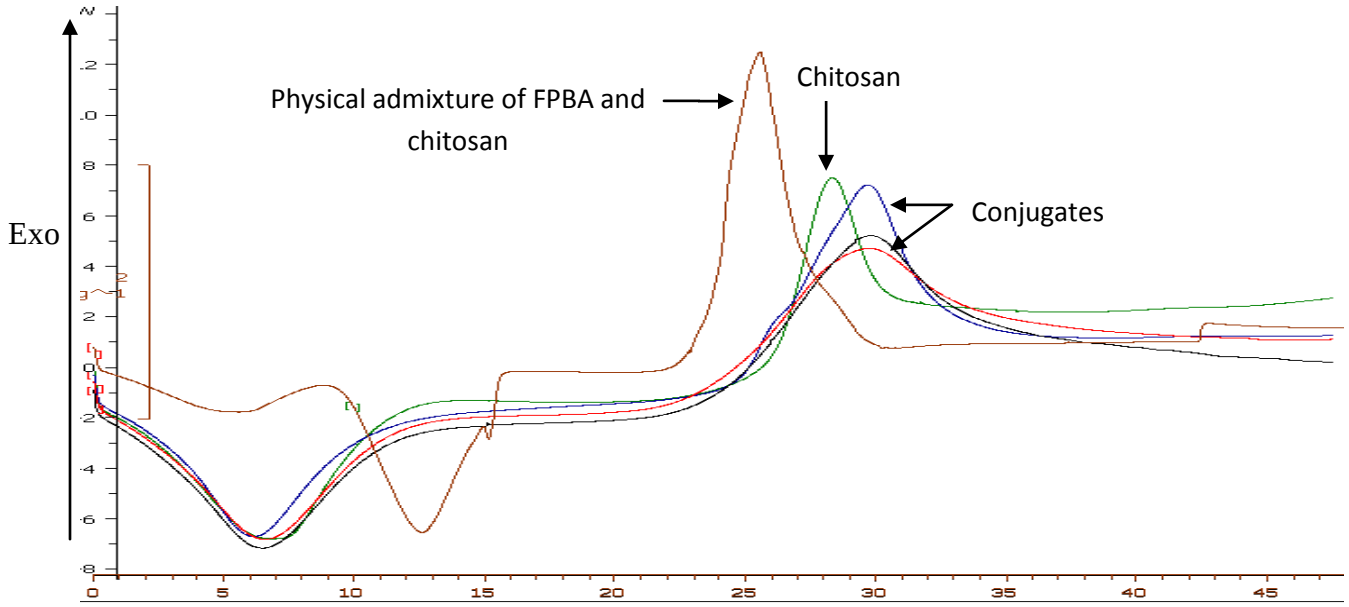

Figure 3.26 DSC Thermogram of conjugates, chitosan and FPBA admixed with chitosan

In the thermogram of the physical admixture (figure 3.26), there are three endothermic peaks and these peaks can be attributed to that of chitosan occurring around 70^{o}C and the broad peak of pure FPBA at 125^{o}C and the small sharp one at 155^{o}C. The endothermic peaks of FPBA at 125

and 155^{o}C are retained. The exothermic peak seen in the physical admixture is very unique and different from the exothermic peak of the chitosan or FPBA, the exothermic peak of chitosan and FPBA occur above 300^{o}C. The fusion of the exothermic peaks in the two compounds shows as a characteristic peak 270^{o}C as seen in figure 3.26. This is a confirmation that the new conjugates produced are a result of a definitive chemical reaction process, also the method used in the collection and purification of conjugate was effective, because if there was any unreacted FPBA it would have been seen in the new conjugate's thermogram as a broad endothermic peak with a small sharp one attached.

3.3.2.5 Time-of-flight secondary ion mass spectrometry (TOF-SIMS) of conjugates prepared by N- reductive alkylation

The FTIR data for F1 and F2 shown in figure 3.23 suggest a non- existent PBA functionality, i.e., at lower 4-FPBA loading, since the peaks representing the para di-substituted benzene is not apparent. The ToF-SIMS analysis, however (figure 3.27-3.29), revealed the presence BO and BH_2O_2 (boronic acid) fragments and the boron ions (B^-) at 11.0 m/z in F1, F3 and F5 (figure 3.28) also revealed the successful functionalisation of chitosan because the boron fragment was absent in chitosan.

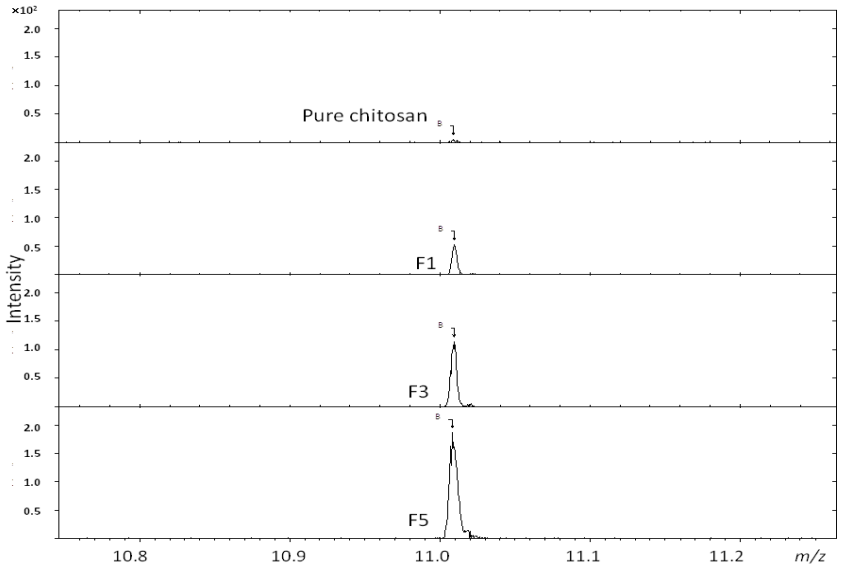

Figure 3.27 TOF-SIMS spectra of pure chitosan and selected conjugates

The intensities of the different fragments shown correlates with the FPBA load (figure 3.28 and 3.31). Thus the ToF-SIMS is in concert with the FTIR analysis in that there is a direct correlation between the degree of PBA bonding onto chitosan and the 4-FPBA loading during the reaction, albeit the ToF-SIMS is more sensitive than the FTIR.

A further analysis of boron oxide (BO^-), boron dioxide (BO_2^-) and boronic acid $(BO_2H_2)^-$ fragments confirms the presence of boronic acid moiety onto conjugates in proportion to the load at preparation (figure 3.28-3.30).

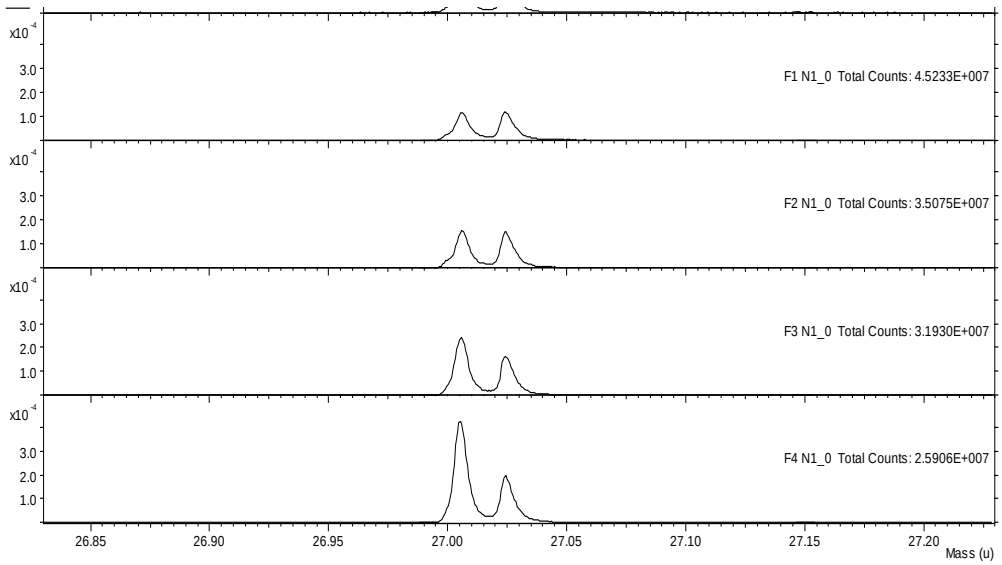

Figure 3.28 TOF-SIMS spectra of BO^- fragments of functionalised chitosan F1-F4

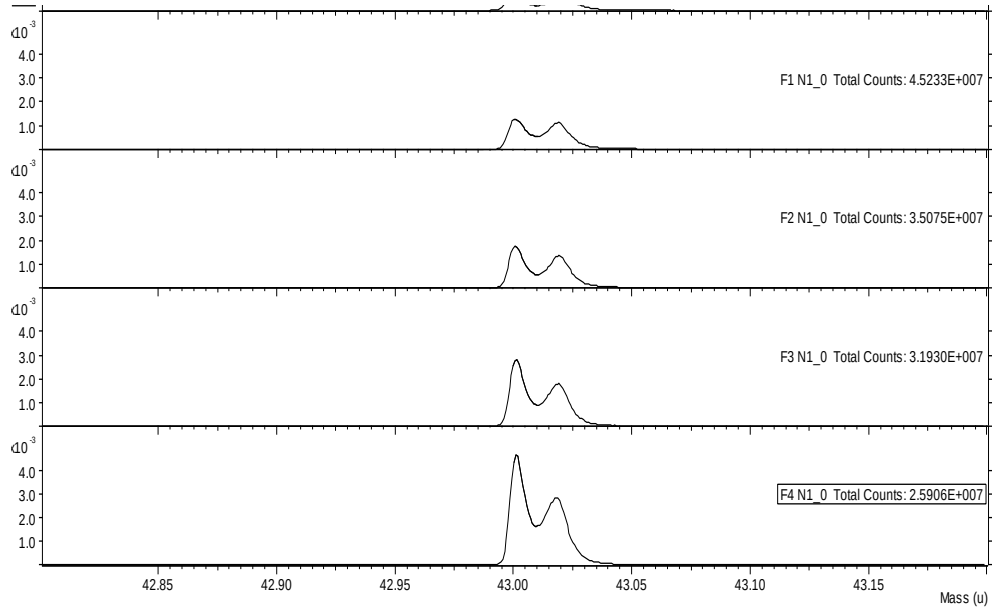

Figure 3.29 TOF-SIMS spectra of BO_2^- fragments of functionalised chitosan F1-F4

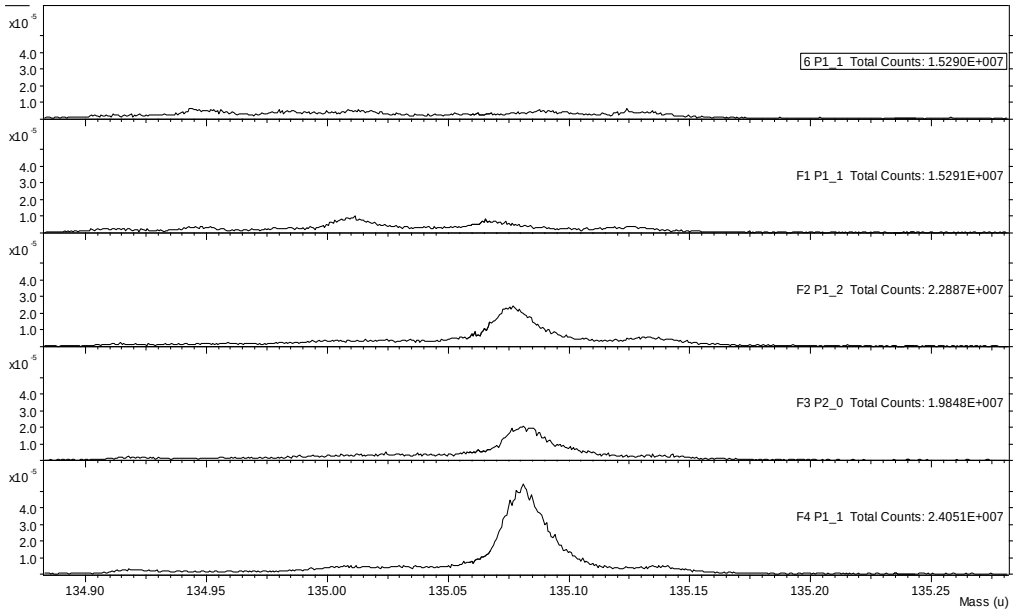

Figure 3.30 TOF-SIMS spectra of boronic acid+ fragments of chitosan and functionalised chitosan F1-F4

Figures 3.31 and 3.32 represents the total counts of $C_7BO_2H_8^+$ and BO_2^- for conjugate F1 to F4, the counts of ion fragments in the above conjugates increased as the degree of substitution of the FPBA on the chitosan increases. Figures 3.33 and 3.34 shows the colour of mapping of B^+ and $BH_2O_2^+$, the image brightness at each point is a function of the relative concentration of the mapped element or molecule. The brightness of the image increases as the concentration of BH_2O_2 fragment increase across the formulation F1 to F5, the lateral resolution is less than 0.1 μm for elements and about 0.5 μm for large molecules. Images are acquired to visualise the distribution of individual species on the surface and these chemical images are generated by collecting a mass spectrum at every pixel as the primary ion beam is rastered across the sample surface. The above data backs the FTIR showing that the degree of substitution of FPBA onto chitosan increases across as the initial amount of the FPBA aldehyde in the reaction is increased.

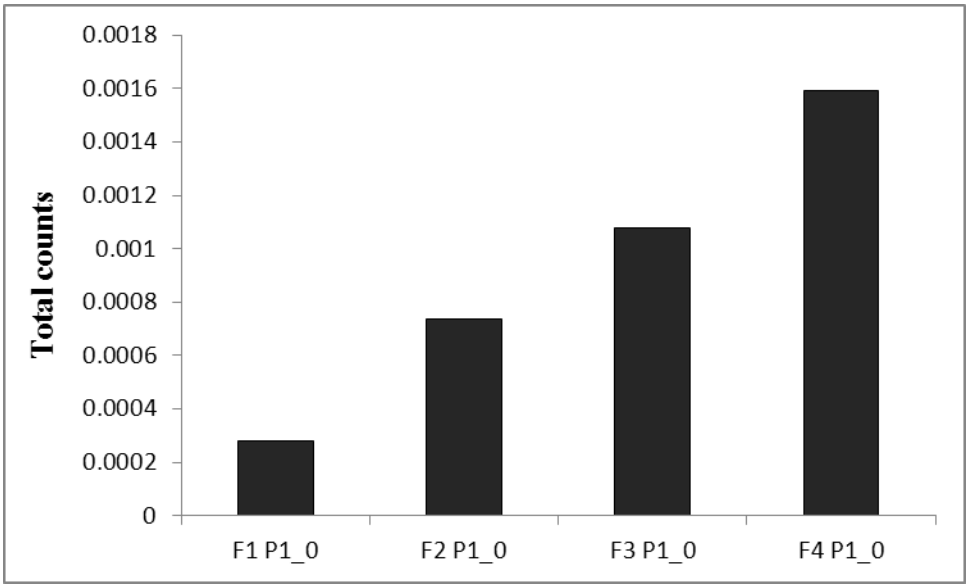

Figure 3.31 Total count of $C_7BO_2H_8^+$ fragments from F1 to F4

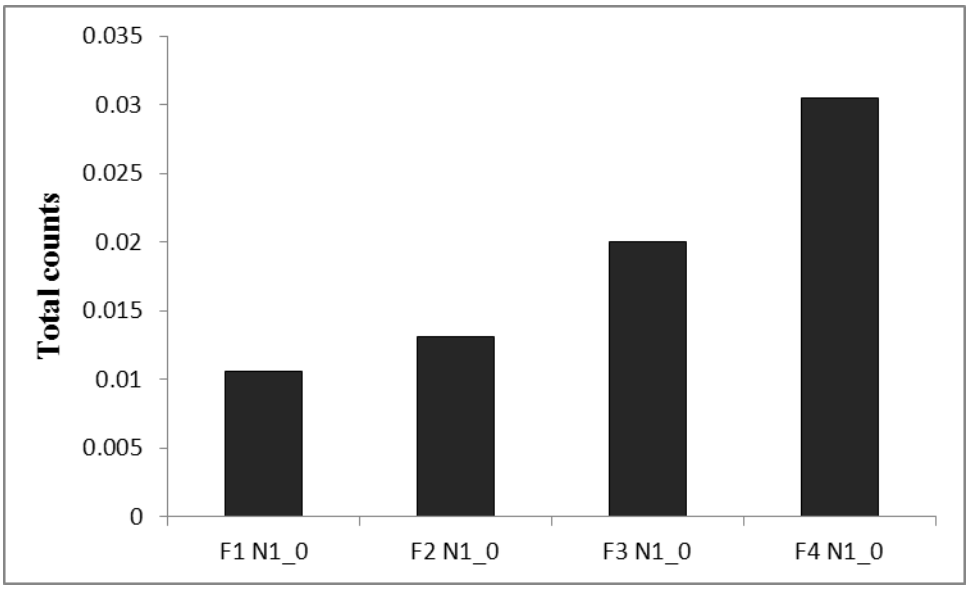

Figure 3.32 Total count of BO_2^- from F1 to F4

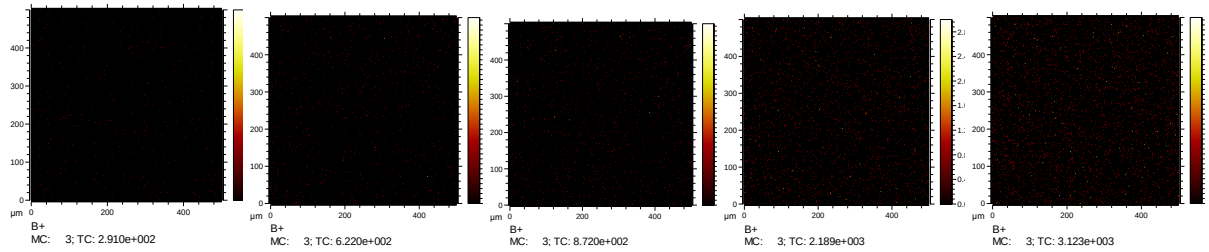

Chitosan F1 F2 F3 F4

Figure 3.33 B^+ data mapping of chitosan and conjugates F1-F4

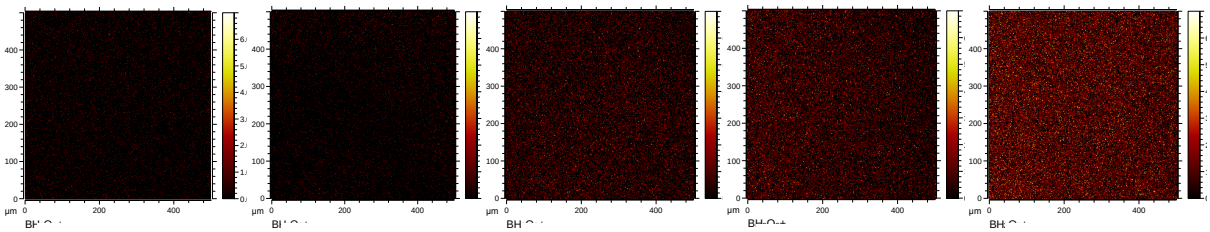

F1 F2 F3 F4 F5

Figure 3.34 $BH_2O_2^+$ data mapping of conjugates F1-F5

3.3.2.6 Energy Dispersive X-ray (EDX) of conjugate prepared by N-reductive alkylation

EDX was carried out to further confirm the success of tagging of the boronic acid onto the chitosan. In the previous EDX analysis done on the conjugates prepared by electrostatic tagging (figure 3.9 and 3.10), the EDX showed that PBA was not tagged onto chitosan. EDX was done on different conjugates prepared by N-reductive alkylation to ascertain the degree of substitution of the boronic acid group onto chitosan in each of the formulation in the series. There was a detectable amount of boron in the carbon tape on which the samples were mounted and from table 3.10 and figure 3.35 the amount of boron in the carbon tape was about estimated to be about 6% (weight percentage).

Table 3.10 EDX of carbon tape

Element	Weight%	Atomic%
B K	6.41	7.41
C K	75.44	78.47
N K	0.00	0.00
O K	17.98	14.04
Al K	0.17	0.08
Totals	100.00	

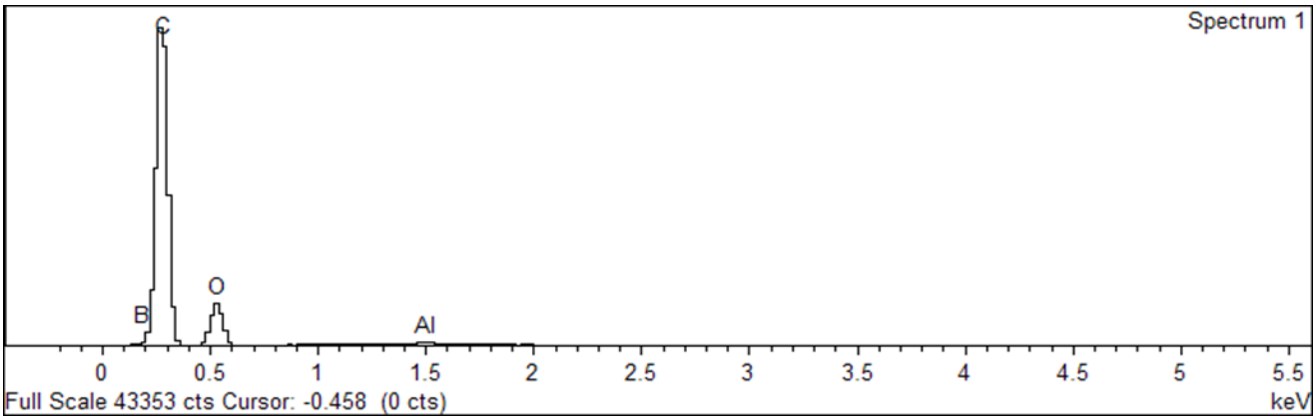

Figure 3.35 EDX of carbon tape

Table 3.11 EDX of conjugates prepared by N-reductive alkylation

Conjugate	Element	Weight%	Atomic%
F1	B K	10.95	13.06
	C K	54.65	58.69
	N K	5.59	5.15
	O K	28.44	22.92
	Al K	0.37	0.18
F2	B K	8.62	10.35
	C K	56.38	60.91
	N K	4.19	3.88
	O K	30.43	24.68
	Al K	0.28	0.13
	Si K	0.10	0.05
F3	B K	8.08	9.75
	C K	57.55	62.46
	O K	33.74	27.49
	Al K	0.62	0.30
F4	B K	9.59	11.43
	C K	60.02	64.36
	O K	29.59	23.82
	Na K	0.16	0.09
	Al K	0.64	0.30

F5	B K	9.55	11.39
	C K	58.05	62.32
	N K	2.87	2.64
	O K	29.05	23.41
	Na K	0.11	0.06
	Al K	0.37	0.18
F6	B K	9.42	11.26
	C K	57.51	61.88
	N K	3.15	2.91
	O K	29.22	23.60
	Na K	0.14	0.08
	Al K	0.56	0.27

From above table 3.11, the amount of boron measured increased in the conjugates in contrast to boron content in the plain carbon tape (table 3.9, figure 3.35) and this proves that there is an increase in the amount of a substituents that contributes to the increase of the concentration of carbon and this is in all likelihood is PBA. However the amount of boron does not appear to show any increasing pattern as expected and this might be due to the fact that the scanning of the samples during EDX is limited to the surface of the sample and amount of element picked is determined by the area being scanned and therefore the concentration of the element being determined in that sample in that specific area may not be a true representation of the entire elemental concentration within the sample. Since the scan is mainly limited to the surface of mounted sample, inner residing elements may not contribute to the analysis. We believe this is the source of the apparent lack in trend in the presence of Boron element in the samples.

3.4 CONCLUSION

The electrostatic tagging of PBA onto chitosan was not feasible. Functionalising chitosan with PBA was achieved via N- reductive alkylation and the conjugates were easily purified from excess reactants by washing with methanol, ethanol and water. The procedures used in the washing also affected the physical appearance of the functionalised chitosan which makes the conjugate either amorphous or crystalline. The process of centrifugation used in the recovery of the conjugates was better because higher yield was observed and there was minimisation of contamination and loss. Freeze-drying is also the best method for drying the conjugate other than in vacuo.

The characteristic FTIR spectra of the conjugates as compared to chitosan proved that the boronic group had been introduced and the DSC thermograms, though not conclusive gave information on the pure reactants and that of the new and showed that the conjugates produced were different from the physical admixture of chitosan and FPBA and also the purification process used was optimum after the synthesis of the new conjugate. The results from the EDX reflected an increase in the boron content more than the traces picked on the carbon tape further proved that another group had been introduced onto chitosan. The EDX was a qualitative tool and not a quantitative tool in this instance, since the results did not reflect the increasing amount of the boronic acid group in each conjugate. The TOF-SIMS data shows the trend of increment as the amount of boronic acid is increased in each formulation. The tagging of the boronic acid group onto chitosan was therefore successful and the functionalised chitosan has been rightly characterised by employing different analytical techniques and equipments. In the subsequent chapters, attempts would be made at further characterising the conjugates and then fabricating into nanoparticles accordingly.

CHAPTER 4

GLUCOSE ADSORPTION CAPACITY OF THE CONJUGATES

4.1 Introduction

Boronic acids have been used in the development of feedback controlled drug delivery polymers as saccharide sensors and their potential applications pharmaceutically have been widely explored (Yang *et al*. 2003).

Matsumoto *et al*. (2002) synthesised a novel chitosan gel modified by phenylboronate for the selective adsorption of glucose and these gels were synthesised via N-reductive alkylation and by the introduction of the phenylboronate by amide formation and their glucose adsorption capacities were determined. In an observation made by the group, the conjugates synthesised via N-reductive alkylation selectively adsorbed glucose whilst those produced by the introduction of the phenylboronate group by amide formation did not. The *m*-acrylamidophenylboronic acid needed for the amide reaction had to be synthesised and its microspheres were chemically unstable. Functionalised chitosan synthesised via N-reductive alkylation could easily be prepared with readily available commercial compounds and the resulting conjugates were chemically and physically stable. In the light of the above, the N-reductive alkylation method of introducing the phenylboronate onto chitosan was adapted and pursued in the present work as discussed in chapter 3.

The glucose adsorption capacities of the PBA functionalised chitosan were ascertained with the idea of correlating their glucose adsorption capacities to their potential glucose sensitivity and selectivity when used as sensors in a glucose responsive insulin delivery system. The adsorption capacity study was done to aid the selection of the conjugate(s) that would be further formulated

into a glucose responsive nanoparticulate insulin delivery system, since there was a possibility of correlating the glucose adsorbing capacity sensitivity of the functionalised chitosan to its potential use as a glucose sensor in the nanoparticulate delivery system.

The glucose adsorption capacities of the conjugates were determined by an HPLC method adapted from Lee *et al*. (2004). Glucose cannot be detected spectrophotometrically by ultra-violet (UV) light so the hexokinase reaction was used as an indirect way of quantifying glucose.

In this reaction the glucose is converted to phosphogluconate and nicotinamide adenine dinucleotide in the reduced from (NADH) in the presence of the enzyme hexokinase, the NADH can then be quantified spectrophotometrically at 340 nm. The amount of NADH produced in the reaction is directly proportional to the initial amount of glucose (figure 4.1).

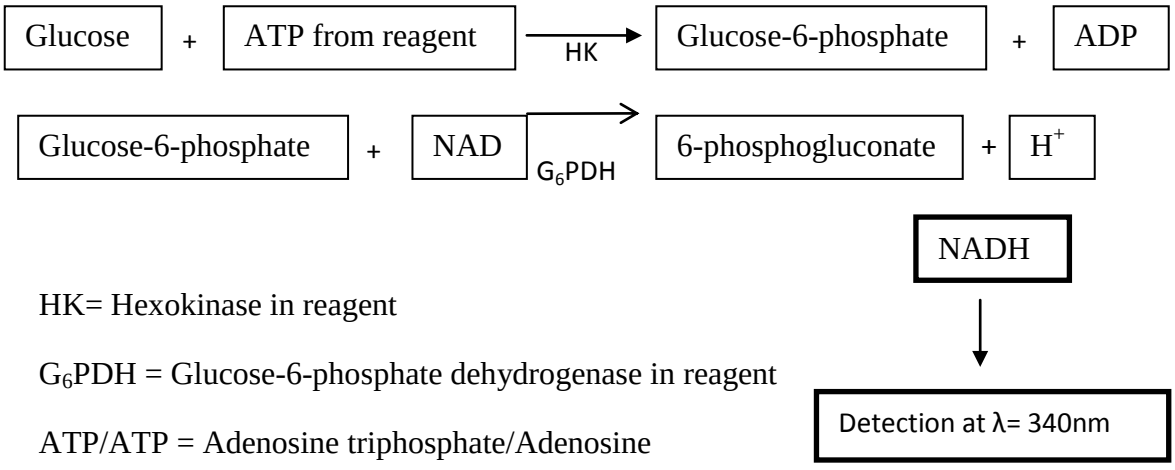

HK= Hexokinase in reagent

G_6PDH = Glucose-6-phosphate dehydrogenase in reagent

ATP/ATP = Adenosine triphosphate/Adenosine diphosphate

NAD = Nicotine adenine dinucleotide in reagent

Figure 4.1 Outline of glucose conversion to detectable NADH using the hexokinase reagent.

4.2 Materials and equipment

Functionalised chitosan (Chapter 3), HPLC grade acetonitrile and methanol, purchased from Thermofischer Scientific New Jersey, USA, Glucose hexokinase reagent set (Pointe Scientific Inc. USA), Type one ultrapure Milli-Q® water (18.2 ohms at 25˚C), D-glucose (R&M Chemicals). All other chemicals were of reagent grade.

HPLC system (PerkinElmer, Shelton, Connecticut, USA), Phenomenex Jupiter C_{18} column, 5 um with pore size 300Å, Beckman Coulter Microfuge 16 centrifuge and WiseCube WIS-20, precise shaking incubator, Sartorius basic pH meter PB-11.

4.3 Methods

4.3.1 HPLC analyses

The HPLC solvent system used consisted of 20 mM potassium dihydrogen phosphate (KH_2PO_4) solvent A and acetonitrile solvent B. The solvent composition was 95% of A and 5% of B, at a flow rate of 1 ml/min at a detection wavelength of 340 nm. The column used was a Phenomenex Jupiter C_{18} with pore size of 300Å.

The calibration curve was constructed from glucose solutions between 0.25 mg/ml – 10.00 mg/ml. Prior to injection into the HPLC system, 1 ml of glucose hexokinase reagent was measured into a 1.5 ml tube and 10 µl of various concentration of glucose was added and incubated for 10 minutes at room temperature and then 20 µl of the above solution was injected into the HPLC system. A graph of average peak area was plotted against concentration and the coefficient of determination (R^2) and the equation of the line determined. Each reading was done in triplicate.

4.3.2 Determination of optimum complete reaction time for hexokinase reagent and glucose

10 µl of the 1 mg/ml D-glucose solution was reacted with 1 ml of the hexokinase reagent and the reaction was allowed to go on for different times between 2-30 minutes and 20 µl of the reacted glucose converted to NADH was injected into the HPLC system (PerkinElmer, Shelton, Connecticut, USA) and the peak areas determined. The peak areas were converted to mass (using the calibration curve) to find the exact amount of glucose reacted at a specified time and hence the optimum time for complete reaction determined from data. Each experiment was done in triplicate.

4.3.3 Correlating the amount of glucose adsorbed as a function of pH using the functionalised chitosan conjugate (F3)

4.3.3.1 Preparation of buffers

Buffers were prepared according to the USP method for preparing a simple phosphate buffer, namely, a stock solution of 1000 ml of 0.2 M potassium phosphate was prepared by dissolving 27.22 g of monobasic potassium phosphate (mw = 136) in 18Ω millipore water. A stock solution of 1000 ml of 0.2 M NaOH was made by dissolving 8.0 g of NaOH pellets in Millipore water. 50 ml of the 0.2 M potassium phosphate solution was then measured into a 200 ml volumetric flask. Depending on the desired pH a specific volume of NaOH 0.2 M was added (table 4.1) before making up to 200 ml volume with millipore water.

Table 4.1 Volumes of NaOH required for making phosphate buffer solutions at various pH (USP)

Desired pH	5.8	6.0	6.2	6.4	6.6	6.8	7.0	7.2	7.4	7.6	7.8	8.0
Volume of NaOH (ml) to be added	3.6	5.6	8.1	11.6	16.4	22.4	29.1	34.7	39.1	42.2	44.5	46.1

Based on this method buffers at pH 6.0, 6.4, 6.8, 7.2, 7.4, 7.6, 8.0 were made up and the actual pH of the buffer was then recorded using the Sartorius basic pH meter PB-11.

4.3.3.2 Correlating the amount of glucose adsorbed by F3 conjugate as a function of pH

The adsorption of glucose by 20 mg of F3 was determined by dispersing conjugate in 1 ml of 1 mg/ml glucose and the amount of glucose adsorbed over a 2 hour period at pH of 6.4, 7.4 and 8.33 were recorded (as per method in section 4.3.2). The adsorption of glucose after 30 minutes was also monitored at recorded pH of 6, 6.40, 7.10, 7.4 and 8.33.

The amount of glucose adsorbed onto the conjugate was calculated based on the difference in the peak areas of NADH obtained from the initial 1 mg/ml glucose buffer without conjugate and the glucose buffer after its exposure to the conjugate. Each experiment was done in triplicate.

4.3.4 Glucose adsorption of conjugates

10 µl aliquot of the glucose solution (unexposed to conjugate) was reacted with the hexokinase reagent for 10 minutes and 20 µl of the resulting solution was injected into the HPLC to determine the baseline of glucose concentration. 5 – 40 mg of conjugate was weighed and dispersed in 1 ml of 1 mg/ml glucose solution buffered at various pH. The sample was then

equilibrated in the WiseCube WIS-20, precise shaking incubator at a speed of 100 rpm and at predetermined time intervals 50 µl supernatant glucose solution was isolated by centrifugation at 14000 rpm for 2 minutes. 10 µl of this supernatant glucose solution was reacted with the 1 ml of the hexokinase reagent and 20 µl of the reacted sample was injected into the HPLC (PerkinElmer, Shelton, Connecticut, USA). The amount of glucose adsorbed was determined by subtracting peak area of the buffered glucose solution after exposure to conjugate from the initial peak area of glucose before exposure to the conjugate and further calculations done using the calibration curve. Each experiment was done in triplicate.

4.4 RESULTS AND DISCUSSION

4.4.1 The glucose hexokinase reaction for the quantification of glucose

In the hexokinase reaction, adenosine triphosphate (ATP) is consumed when glucose is converted to glucose-6-phosphate and the ATP to adenosine diphosphate (ADP) in the presence of the enzyme hexokinase (HK). In the presence of NAD the enzyme glucose-6-phosphate dehydrogenase (G6PDH) oxidises glucose-6-phosphate to 6-phosphogluconate which in turn becomes reduced to NADH. The increase in NADH concentration is directly proportional to the glucose concentration. The formation of NADH causes an increase in absorbance at 340 nm and this increase is directly proportional to the amount of glucose in the sample.

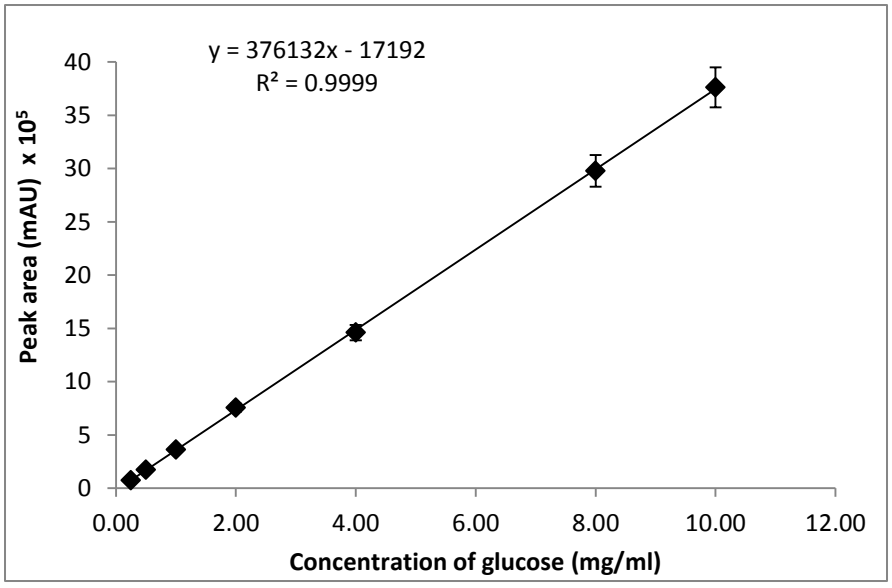

Figure 4.2 Calibration curve for the glucose hexokinase reaction

A calibration curve (figure 4.2) constructed by plotting the average peak area with the glucose concentration gave a calibration curve with good linearity which is reflected by the coefficient of determination (R^2) value of 0.999.

Two clearly resolved peaks were obtained in each chromatogram, one for a component of the hexokinase reagent (at 5.8 minutes) and the other for NADH (at 6.1 minutes) the area of which is directly proportional to the concentration of glucose in the sample (figure 4.3).

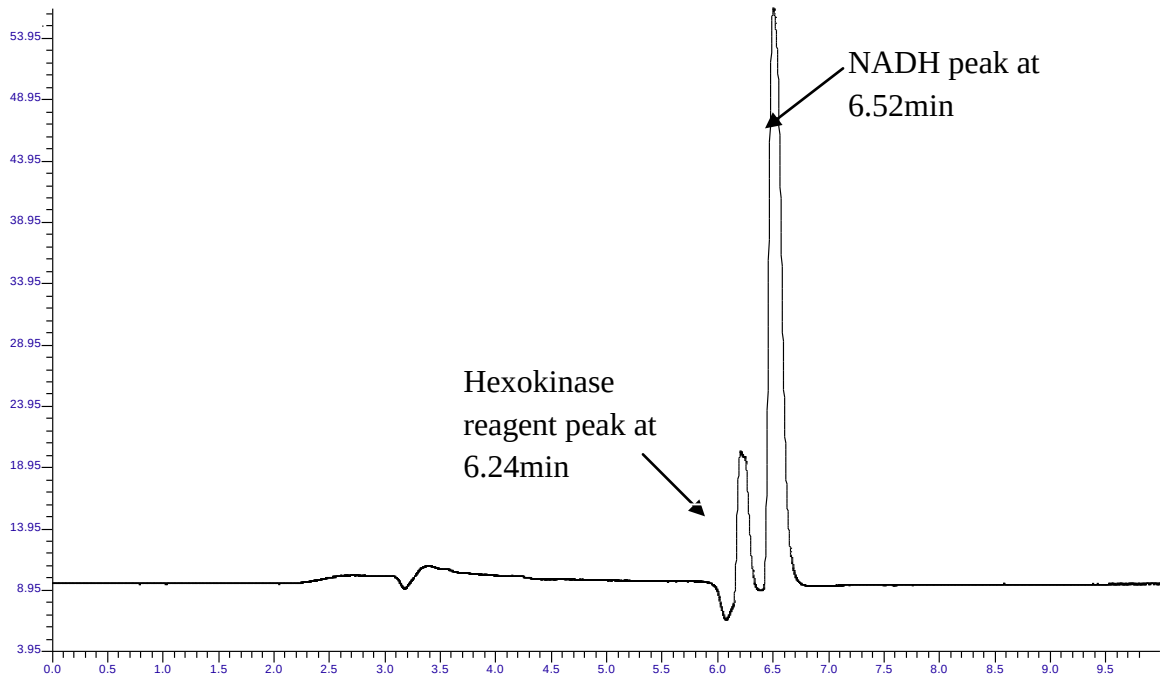

Figure 4.3 HPLC chromatogram showing peaks of NADH and hexokinase reagent

The hexokinase glucose reaction is an enzymatic reaction and since this method is an indirect way of quantifying the amount of glucose in solution, it will be expedient to have a complete reaction before the NADH is detected by HPLC, so that any errors due to incomplete reaction in the quantification process can be avoided. The molar ratio of glucose conversion to NADH is 1:1 and therefore an incomplete reaction will lead to errors in the quantification of glucose present. In the light of the above observation, the optimum reaction time for the complete glucose hexokinase reaction was determined by profiling the amount of glucose converted to NADH at specific times of reactions for a 1 mg/ml solution of glucose.

Figure 4.4 shows that, the complete conversion of glucose to NADH was before 10 minutes and this implies that a reaction time of 10 minutes was enough or optimum for a complete reaction before the sample was injected into the HPLC system. Therefore, a 10 minute reaction time was used for glucose hexokinase reaction prior to injection of samples into the HPLC system. The rate of an enzyme catalysed reaction depends directly on the proportion of the enzyme (Tzafriri 2003), in the current reaction the ratio of reagent to glucose used for the reaction was 100:1 and therefore the substrate concentration was very low and this implies that the reaction would be completed in a short time.

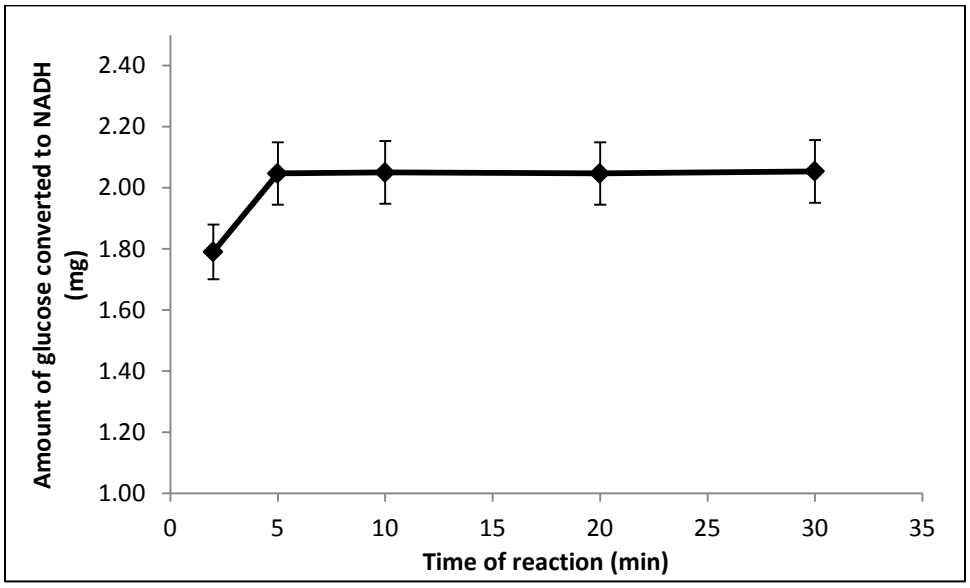

Figure 4.4 Amount of glucose converted to NADH over time

The Michaelis-Menten model for enzyme kinetics presumes a simple 2-step reaction: where step 1 involves the binding of substrate to the enzyme and step 2 being catalysis which is the substrate conversion to product and the initial amount of enzyme for a specific substrate if high, leads to a high turnover of product and also increases the velocity of the reaction (Tzafriri 2003). In this regard, the less amount of substrate present in comparison to the amount of enzyme is also a possible explanation for the reaction going to completion in less time. Also, since all the

substrate which was glucose was consumed within the reaction, the amount of product (NADH) plateaued as seen in figure 4.4.

The amount of detected NADH was stable over a 30 minutes period (figure 4.4), and this implied that, the products formed after the enzymatic reaction were stable and did not break down. Hence samples reacted earlier could also be quantified accurately, thus widening the time frame within which accurate quantification of the NADH could be done.

4.4.2 The effect of pH on the glucose adsorption capacity of the conjugates

For boronic acid to bind to diols, it is commonly believed that the higher the pH of the medium, the higher the binding constant between the boronic acid and the diol. Also other researchers suggest that the optimal pH for binding of a boronic acid to a diol must always be above the pKa of the boronic acid. The delivery system being developed in the present study is meant to be used at physiological pH and ideally the PBA in this system should be able to bind to glucose and cause the needed reaction which will lead to drug release at physiological pH. Therefore the correlation between the amount of glucose adsorbed on the conjugate and pH was studied by quantifying the amount of glucose adsorbed by F3 at different pHs.

At pH below 7 (figure 4.5), low glucose adsorption occurred with only 0.12 mg being adsorbed after 30 minutes at pH 6.40, lower pH of 6.0 showed even less adsorption of glucose. The low adsorption of glucose by F3 at the pH below 7 was related to the fact that at pH < 7, the pH of the system was below the pKa of 4-FPBA as calculated by Yan *et al*. (2004) to be 7.6. Although this value may be affected by conjugation to chitosan, gross deviation is unlikely as chitosan is neither strongly electron withdrawing or donating. At pH below the pKa, the boronic acid groups

will be in their protonated unionised form and therefore in a less favorable conformation for binding to glucose, hence the adsorption of glucose by conjugate F3 being minimal at those pH (figure 4.5).

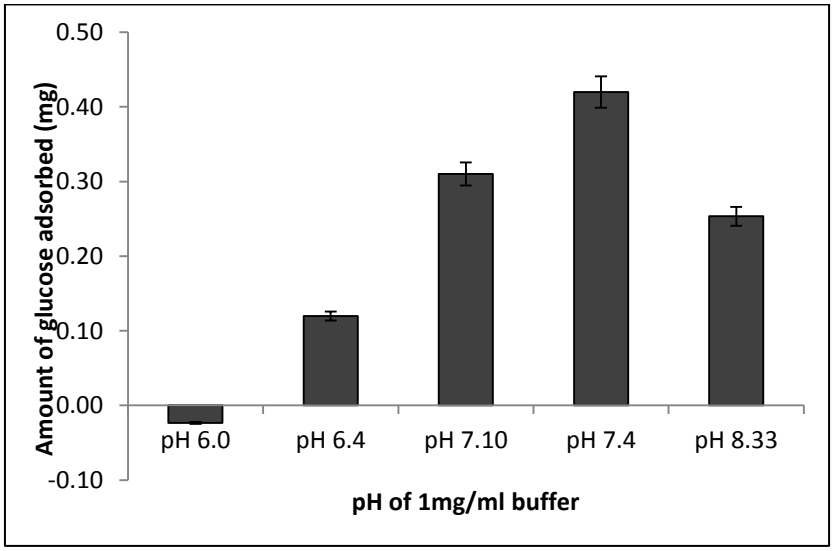

Figure 4.5 Adsorption of glucose by conjugate F3 after 30 minutes.

This agrees with a similar study by (Matsumoto *et al* 2002) which showed no adsorption of glucose by 4-FPBA chitosan conjugates in a similar adsorption study at pH 6.

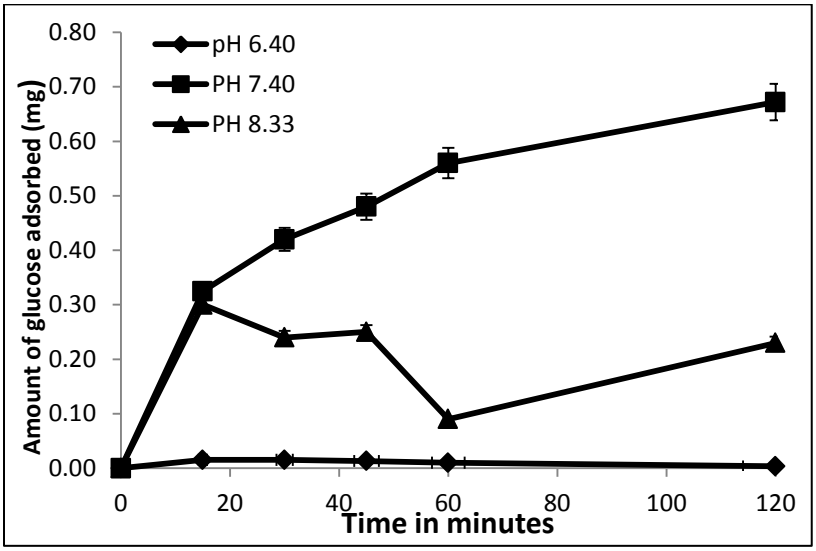

Figure 4.6 Adsorption of glucose by conjugate F3 over 120 minutes

Referring to figure 4.6, at pH 7.4 the quantity of glucose adsorbed increased over the two hour period peaking with 0.67 mg adsorption after 2 hours and the amount of glucose adsorbed at this pH was more than that adsorbed at pH 6.4 and 8.33 at equivalent time points and this supports data from figure 4.5 which shows optimum adsorption of glucose at pH 7.4 with 0.40 mg glucose adsorbed after 30 minutes. Clearly, at pH closer to the pKa of 4-FPBA the boronic acid groups can become ionised taking up a favourable conformation for glucose binding, hence glucose is adsorbed. This appears to be in disagreement with data from Matsumoto *et al*. (2002), as in their study, 4-FPBA gels could only adsorb glucose at pH in excess of pH 8. Work done by Springsteen *et al.* (2002) emphasised on the fact that the optimal pH for binding of boronic acids to diol was not always above the pKa of the boronic acid and that the nature, concentration of buffer and temperature could dramatically affect the boronic acid binding affinity. Whereas a buffer system based on potassium dihydrogen phosphate and sodium hydroxide at room temperature were used in this present study, the previous study by Matsumoto *et al*. (2002) utilised a buffer system based on potassium hydrogen phthalate solution and potassium hydroxide solution at 30˚C. Hence the results in the present work may have differed from results presented by Matsumo *et al.* (2002) because of the difference in experimental set ups.

In view of the above results it is important to note that, the binding affinity of a boronic acid at a given pH to a diol is not simply determined by the pKa of the boronic acid but also the nature of the buffers, solvent systems and temperature used in the study, taking also into consideration the nature of the different chemical groups bonded to the boronic acid (Springsteen and Wang 2002).

At a higher 8.33, the conjugate F3 could still adsorb about 0.23 mg of glucose after 30 minutes, but unexpectedly the amount of glucose adsorbed was less than the amount adsorbed at pH 7.4. At higher pH more of the boronic acid groups were expected to be ionised and so should be able

to bind more glucose. However from figures 4.5 and 4.6 it can be seen that less amount of glucose was adsorbed at pH above 8. In a detailed examination of boronic acid and diol binding by Springsteen *et al*. (2002) using the binding of Alizarin red (AR) with PBA as function of pH, they observed that, the AR binding with PBA increased with increase in pH from 4 to 7 but began to drop at pH above 7. They concluded that, the maximum binding pH for their system was around 7 and anything above this pH resulted in less binding and this finding gives a possible explanation to the observed decrease in adsorption of glucose on F3 at pH above 7.4 in this current work.

4.4.3 Comparative glucose adsorption capacities of functionalised chitosan conjugates

The glucose adsorption capacities of the conjugates were determined by the use of the same glucose hexokinase reagent method described in section 4.3.1.1 and the glucose adsorption capacities of the conjugates were studied in order to correlate the adsorption of glucose to the sensitivity and selectivity of the conjugate. This would guide our selection from the conjugates for their further development into glucose responsive nanoparticulate insulin delivery systems.

Different relationship exists between the binding of boronic acids and diols in relation to their pKa, pH and binding constants. The binding of boronic acids to diols are determined by various conditions and mostly these bindings are pH dependent. There is a general concept that the higher the pH of the medium, the higher the binding constant of the boronic acid and the diols, but this appears to be the case up to a point as observed in the present study.

From the results of the pH study on the conjugate F3, a pH of 7.4 was used for the study of the glucose adsorption by the conjugates (F1-F6).

Figure 4.7 is the adsorption curves of the different conjugate formulations which shows that the amount of the glucose adsorbed is dependent on the type of conjugate in respect to their of degree of substitution with boronic acid.

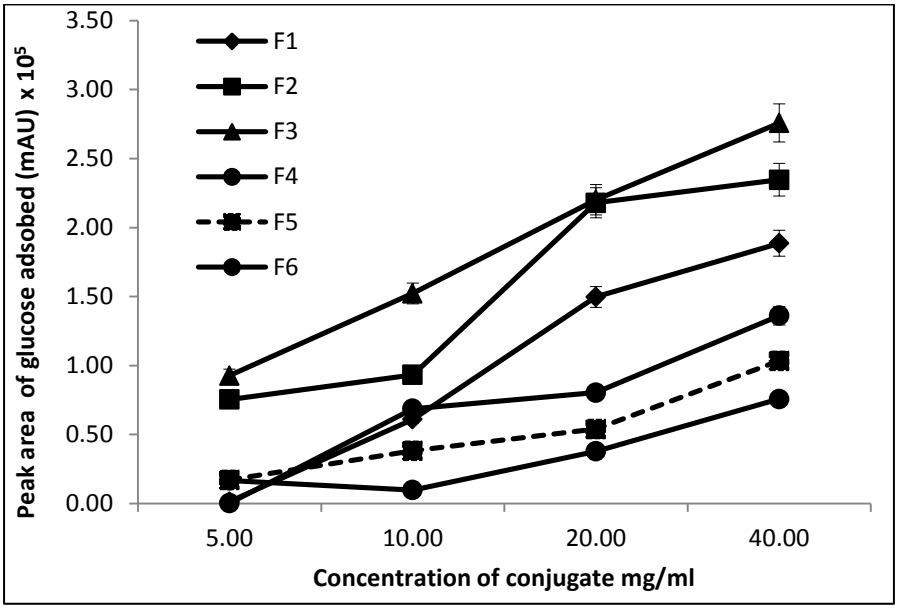

Figure 4.7 Glucose adsorption curves of the conjugates (F1-F6) compared

There appaears to be a direct correlation between the amount of boronic acid bonded chitosan with glucose adsorption sensitivity of F1, F2 and F3, conversely, the sensitivity to glucose adsorption on F4, F5 and F6 reduced in that order.

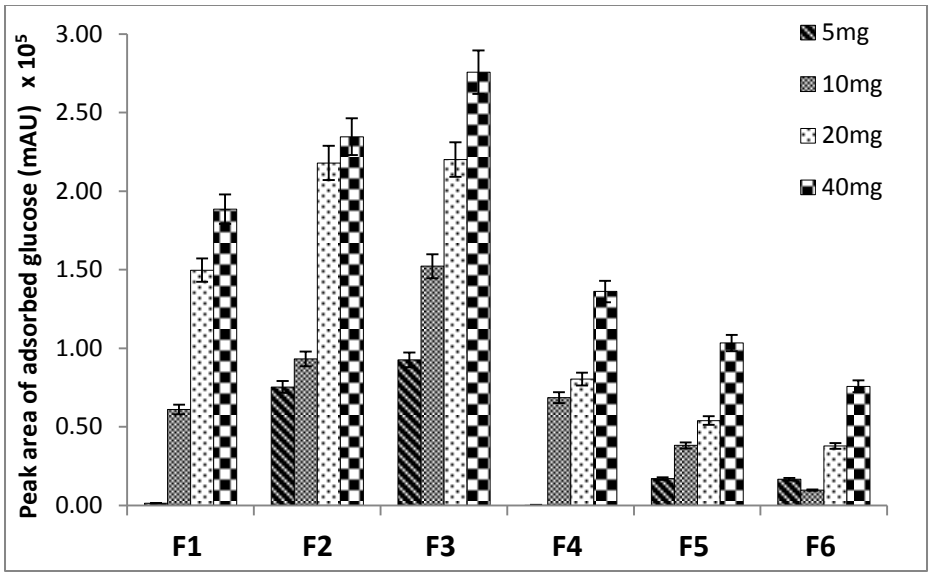

Figure 4.8 Adsorption of glucose as a function of the weight of conjugate

There was also an increase in amount of glucose adsorbed on the conjugates as the amount of conjugate was increased (figure 4.8). An increase in the amount of conjugate presents an increase in the amount of boronic acid groups available for interaction with glucose and hence more interaction of glucose with boronic acid leads to increased glucose adsorption.

In order to explain this unusual phenomenon whereby the highly boronic acid substituted conjugates showed the lowest adsorption propensity, the relationship between the surface topography and the degree of substitution was studied and used to correlate the adsorbing capacities of the conjugates. Visual examination of the various conjugates revealed that F1 to F3 had soft and fluffy textures, whilst F4 to F6 had coarse, gritty and crystalline texture.

Furthermore, SEM examination (figure 4.9) of the conjugates showed that, conjugates F1 to F3 had porous and spongy-looking surfaces whilst conjugates F4 – F6 (figure 4.9) showed flat hard surface images which looked more crystalline than those in the F1 to F3 series.

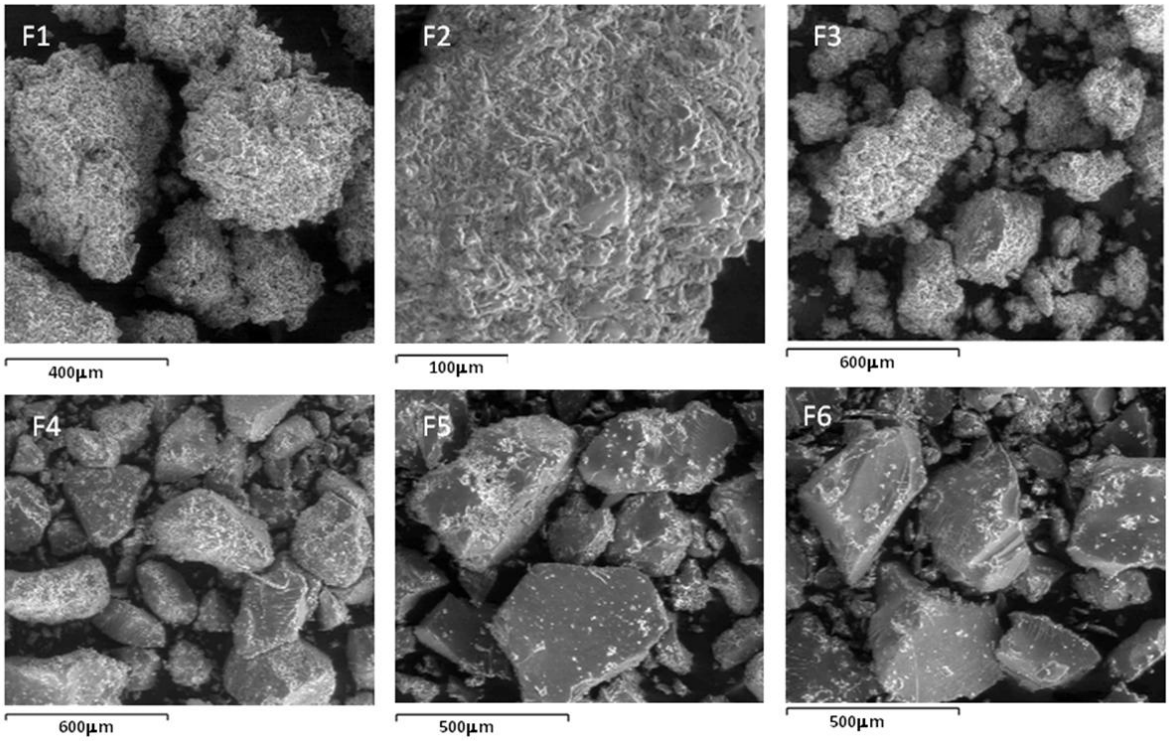

Figure 4.9 SEM images of conjugates F1 through F6.

The surface interaction of the boronic acidic with the glucose will certainly rely on the availability of the boronic acid group for interaction. The hard and crystalline nature of F4-F6 conjugates might have reduced the degree of interaction between glucose and the conjugates whilst the seemingly porous and fluffy nature of conjugate F1 –F3 might have contributed or promoted the interaction of boronic acid on them with glucose and hence the highest degree of adsorption exhibited by conjugates in this series. The seemingly porous nature of conjugates F1 – F3 meant that the surface area available for interaction between glucose and the boronic acid

moiety was enhanced. Conversely, in the series F4 – F6, fewer surfaces was available for interaction with glucose.

4.5 CONCLUSION

The conjugates demonstrated glucose adsorption capacity, with F3 showing the conjugate showing highest adsorption propensity. It appears that, the surface nature and stereochemistry of conjugate plays a role in the adsorption process wherein. The presence of PBA also modified the appearance of the conjugates from porous matrices to crystalline ones with increasing PBA bonding. The crystalline conjugates were less sensitive to glucose adsorption due to inaccessibility of glucose to the PBA moiety. Thus, sensitivity to glucose adsorption by the conjugates appears to require an optimum content of boronic acid, beyond which crystalline domains form which reduces access to glucose. These results have clear implications for the development of glucose sensing and in particular for delivery systems based upon boronic acid-tagged chitosan.

In Chapter 5, conjugates F1, F3 and F5 (representing low, medium and high load of phenylboronic acid respectively) will be selected and formulated into nanoparticles. The size changes prompted due to exposure to glucose will then be investigated. It is presumed that size increase would precede release of any encapsulated drug, in the present case insulin.

CHAPTER 5

DETERMINATION OF THE GLUCOSE RESPONSIVENESS OF FUNCTIONALISED CHITOSAN NANOPARTICLES

5.1 Introduction

Stimuli-responsive controlled-release systems have recently attracted much attention because of their potential applications in drug delivery. The incidence of *diabetes mellitus* is rising worldwide and is a condition that demands daily multiple injections (for type I diabetes) or oral therapy (for type II diabetes) to help maintain normal glycaemic levels (Kim *et al*. 2003). Due to the burden of multiple injections and associated trauma, much focus and attention have been directed to the development of glucose responsive insulin delivery systems which can respond to physiological glucose changes in the body and release insulin in return.

In the development of glucose responsive insulin delivery systems different sensing mechanisms have been proposed including those requiring the enzymatic reaction of glucose oxidase with glucose which causes the hydrogel to swell or shrink to release the encapsulated insulin *(Kost et al*. 2004; Kost and Langer 2001), or the of use of con A, a carbohydrate binding lectin formed into a matrix and used for the delivery of glycosylated insulin. Due to the preferential binding of glucose to con A, the release of the encapsulated insulin within the matrix is facilitated (Obaidat and Park 1996; Cefalu 2004; Brownlee and Cerami 1979).

Recently the use of boronic acids as potential glycol sensors has also attracted attention due to their selective reaction with 1,2 and 1,3 cis- diols in aqueous medium and these boronic acids when incorporated into polymers renders them glucose sensitive. The reaction of boronic acids

with glucose in these polymeric vehicles causes structural changes within the polymer which leads to the release of the encapsulated insulin (Yang *et al*. 2003; Cambre and Sumerlin 2011).

In the present project, our focus was on the development of glucose responsive nanoparticulate insulin delivery system out of the natural polymer chitosan which is biodegradable and biocompatible whilst employing phenylboronic acid as the sensing moiety. Figure 5.1 represents the proposed model for the release of insulin.

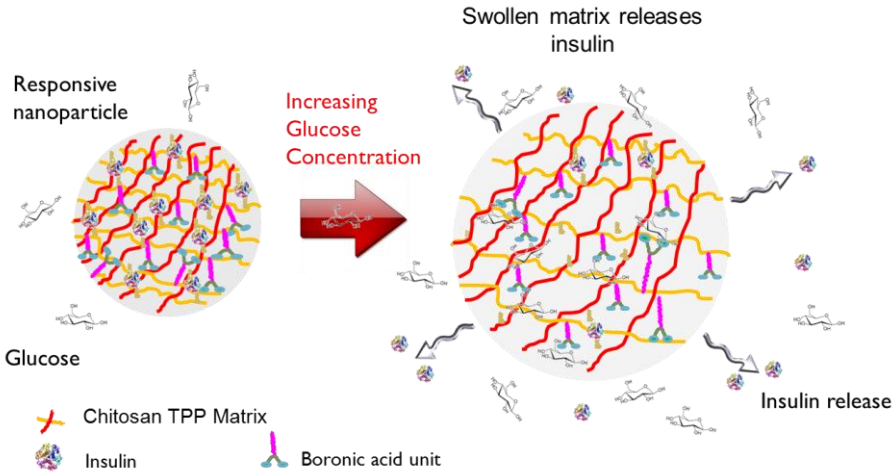

Figure 5.1 Proposed model of insulin release from the nanoparticles

Chitosan was functionalised with a phenylboronic acid group via N-reductive alkylation as described in chapter 4 and nanoparticles were produced using the ionotropic gelation method by cross-linking the functionalised with TPP. The glucose responsiveness of the nanoparticles was determined by the Nanosight nanoparticle tracking system (NTA). NTA is a technique that uses a laser light scattering microscopy coupled with a charged-coupled device (CCD) camera which enables visualisation and recording of nanoparticles in solution in real-time and an in-built software to identify and track individual particles moving under Brownian motion which then relates the movements to particle size.

Our aim was therefore to explore the potential of the NTA for the studies of the glucose responsive behaviour of the functionalised chitosan nanoparticles developed when they were exposed to different buffered sugar media. Size changes prompted by the addition of glucose were pursued and the mechanisms and findings are discussed.

5.2 Materials

PBA functionalised chitosan (F1, F3 and F5) were prepared as described in section 3.2.1.4. D-glucose and D-fructose were purchased from Sigma Aldrich (Missouri, USA); tripolyphosphate (TPP), 4-formylphenyl boronic acid, Dubelco phosphate buffered saline tablets and sodium borohydride from Thermofischer Scientific New Jersey, USA; acetic acid, methanol, acetonitrile were purchased from Thermofischer Scientific New Jersey, USA, Millipore 18 Ω pure water. All other chemicals were of reagent grade.

Field emission scanning electron microscope (FESEM, Quanta 400F, FEI Company, USA), Nanosight LM 10 with LM 14 viewing (Nanosight, Amesbury, United Kingdom), Ultrasonicator (Vibra Cell, Sonics, VCX 750, USA).

5.3 Methods

5.3.1 Preparation of functionalised chitosan TPP nanoparticles (FCTN)

2.5 mg/ml of functionalised chitosan (F1, F3, or F5) were dissolved in 1% v/v acetic acid and stirred overnight and filtered. To 5 ml of each conjugate solution the required amount of filtered TPP (table 5.1) dissolved in water was added drop wise whilst ultrasonicating at amplitude of 40% (300 Watts) over 1 minute. The resulting formulations were designated as FN1, FN3 and FN5. Freshly prepared samples were used each time for the glucose responsive study.

Table 5.1 Ratios of TPP to functionalised chitosan used in the formulation of nanoparticles

Formulation	Ratio of TPP to functionalised chitosan
FN1	1:3.0
FN3	1:4.2
FN5	1:5.0

5.3.2 Characterisation of nanoparticles

The z-average, Pdi and zeta potential of the FCTN were measured by photon correlation spectroscopy (PCS) (Zetasizer Nano ZS® (Malvern, UK) equipped with a 4Mw He- Ne laser (633 nm). Each analysis was carried out at 25^{o}C and performed in triplicate and data expressed as mean ± standard deviation.

Nanoparticle morphology was studied by mounting sample of nanoparticle in solution on carbon tape mounted on a metal stub and air-dried overnight at room temperature and examined on a Field Emission Scanning Electron Microscopy (FESEM).

5.3.3 Determination of glucose responsive propensities of PBA functionalised chitosan nanoparticles

5.3.3.1 Standardisation of nanoparticle tracking equipment

Different concentrations of glucose and fructose solutions in the concentration range of 0.1 mg/ml - 5 mg/ml were prepared using filtered phosphate buffer pH 7.4.

1 ml of buffer, glucose or fructose solution was measured into a small clean vial and 1 µl of polystyrene bead solution was added (1 in 1000 dilution was chosen because it gave particles concentration reading of 10^7-10^9/ml as required by the instrument for accurate measurement and analysis). Approximately 0.3 ml of the sample was injected into the viewing chamber (equipped with a 405 nm laser wavelength) with sterile syringe until the liquid reached the tip of the nozzle. All measurements were performed at room temperature. Videos lasting for 1 min 30 seconds were captured at 30 frames per second and analysed using the NTA software (figure 5.2 and 5.3). All measurements were performed at room temperature. The size distribution of the polystyrene beads in buffer and the different sugar media was studied and the distributions compared.

The rate of particle movement is related to a sphere equivalent hydrodynamic radius as calculated through using the Stokes-Einstein's equation.

$$(x, y)^2 = 2k_B T/3r_h \pi\eta \quad \text{……..} \quad \textbf{Equation 5.1}$$

Figure 5.2 Nanoparticle Tracking Analysis set up

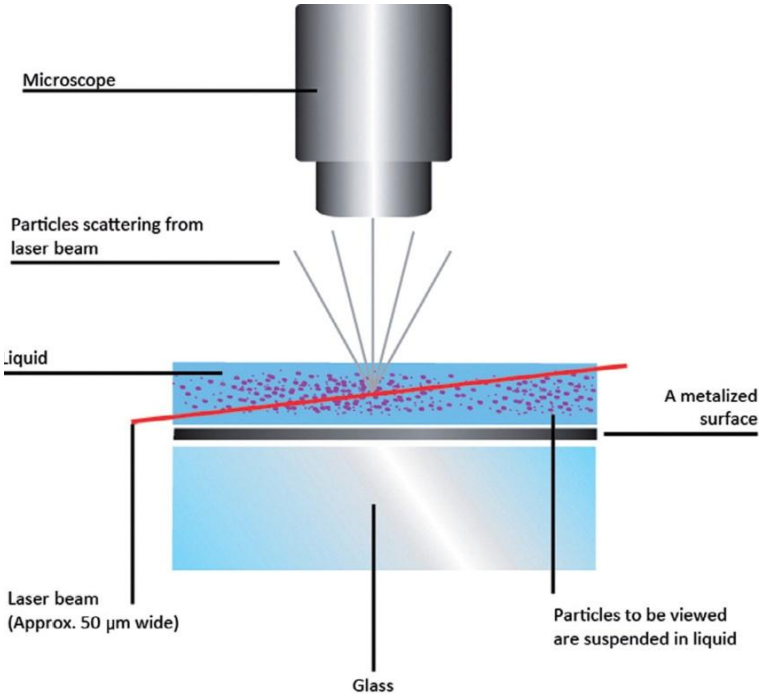

Figure 5.3 Schematic presentation of the operational mode of the NTA for size analysis (Malloy 2011)

5.3.3.2 Determination of glucose responsive behaviour of functionalised nanoparticles

Different glucose solutions in the concentration range of 0.1 mg/ml-5 mg/ml were prepared in filtered phosphate buffer pH 7.4.

1 ml of buffer or glucose solution was measured into a clean vial and 2-10 µl of the nanoparticulate suspension of each formulation (FN1, FN3 or FN5) was added to the plain buffer or buffered glucose solution and approximately 0.3 ml of the sample was injected into the viewing chamber (equipped with a 405 nm laser wavelength) with sterile syringe until the liquid reached the tip of the nozzle. Videos lasting for 1 min 30 seconds were captured at 30 frames per second and analysed using the NTA software. All measurements were performed at room temperature.

5.4 RESULTS AND DISCUSSION

5.4.1 Formulation of functionalised chitosan TPP nanoparticle (FCTN)

Chitosan-TPP nanoparticles have been studied by various groups in the delivery of drugs ranging from small (furosemide) to large molecules (proteins such as insulin) *(*Mao *et al. 2006;* Illum *et al*. 1994; Akbuğa and Durmaz 1994; Aktaş *et al*. 2005). This polymer has also been modified by different groups to impart specific desirable properties onto it for the delivery of specific drugs or for the performance of specific functions. The modified chitosan may be used as such or formulated into micro or nanoparticles. The process of formulation normally depends mostly on the inherent polycationic nature of chitosan and its ability to form cross-links with other polyanions or negatively charged molecules (De Moura *et al*. 2008; Mourya and Inamdar 2009; Mao *et al*. 2006; Smoum *et al*. 2006; Prego *et al*. 2006).

From the above works, the possibility of formulating nanoparticles from chitosan that has been modified by different groups is feasible and the feasibility of these methods has led to the exploration of chitosan modified by the attachment of phenylboronic acid as a potential for the development of glucose responsive nanoparticulate insulin delivery system. Matsumo *et al*. (2002) modified chitosan with a phenylboronic acid group via N- reductive alkylation and determined its ability to adsorb glucose and they observed that the chitosan made by Schiff's base method adsorbed D-glucose and not 1-methyl-α-D-glucoside. Since this functionalised chitosan made by N-reductive alkylation could selectively adsorb glucose, its potential as an insulin delivery vehicle could be explored.

The focus of this project was therefore the formulation of functionalised chitosan prepared by the N-reductive alkylation into nanoparticles for the delivery of insulin and this nanoparticle was

expected to be glucose responsive because of the selectivity in the adsorption of glucose. The novelty in the present approach lies in the formulation of the functionalised chitosan with a phenylboronic acid prepared by the above mentioned method into nanoparticles as this has not been studied before. The formation of nanoparticles should ensure a faster reaction time or sensitivity with glucose due to the larger surface area to volume ratio.

Figure 5.4 represents the SEM image of nanoparticles from formulation (FN3). It can be seen that the nanoparticles are spherical and well formed.

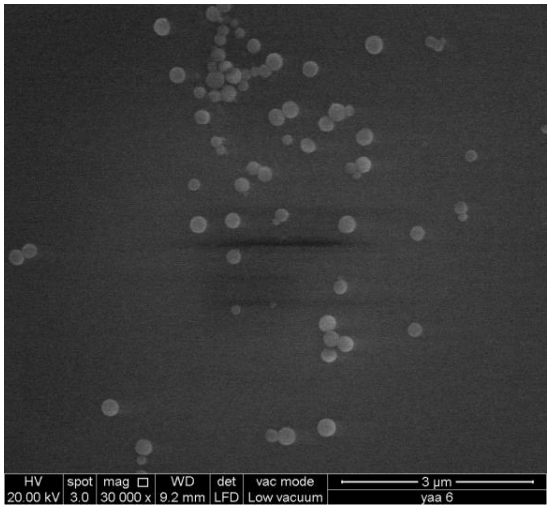

Figure 5.4 SEM of PBA functionalised chitosan TPP nanoparticles (FN3)

Table 5.2 Z-average, Pdi and zeta potential of the different functionalised chitosan TPP nanoparticle

Formulation	Z-average (nm)	Pdi	Zeta Potential (mV)
FN1	139.40 ±4.20	0.232±0.0078	21.06±0.18
FN3	147.57±8.50	0.239±0.0101	20.30±0.35
FN5	158.82±18.35	0.240±0.0058	20.46±2.45

Nanoparticles produced by ultrasonication out of the selected conjugates had average sizes between 110-160 nm (table 5.2). The sizes of the nanoparticles normally depend on formulation and processing parameters such as pH of the polymer and the cross-linker solution, the initial amount of polymer and the amount of cross linker used as thoroughly studied in chapter 2. This implies that desirable nanoparticle size can be obtained by varying the initial parameters as stated above in the production of the nanoparticles.

The Pdi of the different formulations was about 0.2 (table 5.2), values closer to 0 have been reported to be an indication of homogeneity and the data above shows that the formulations have some degree of homogeneity. Sizes of nanoparticles in a formulation can be in the nanometre range but one must bear in mind that the interparticulate difference is of much importance also, because a wide variability within the particle sizes may affect the drug loading and drug release of the delivery system.

Zeta potential values of chitosan-TPP nanoparticles are normally positive due to the positive charge contribution from the amine groups in chitosan. Not surprisingly, the zeta potential of the boronic acid-functionalised chitosan nanoparticles was about +20 mV (table 5.2) and the positive

magnitude is a result of the positive charge density from the amine groups of the chitosan. The zeta potential values obtained from the boronic acid-functionalised chitosan were however lower due to substitution of some of the amine groups in chitosan with the boronic acid.

5.4.2 Nanosight tracking analysis on the glucose responsive behaviour of the boronic acid-functionalised nanoparticles

Nanoparticle Tracking Analysis (NTA) is a unique methodology for visualising nanoparticles in suspension and the high resolution particle size against concentration distributions are derived through image analysis. The particle size is calculated using the Stokes-Einstein equation (equation 5.1). Its mode of particle size determination overrides some of the inherent errors and constraints in dynamic light scattering mode of particle size determination. The major advantages this technique presents for the measurement of particle size over that of dynamic light scattering (DLS) or photon correlation spectroscopy) is that, the latter has the inherent weaknesses of being heavily skewed towards the larger particles in the particle size distributions of a sample. This is due to the fact that DLS is strongly influenced by the intensity of light scattered from a particle and as such larger particles scatter significantly more light than smaller particles and the scattered light obscures the signal from the smaller particles. NTA on the other hand works by tracking the movement of each particle on a particle-by-particle basis and relates the degree of movement to the sphere-equivalent hydrodynamic diameter thus the biasing observed in DLS is overcomed. NTA also provides real-time monitoring of the subtle changes in the characteristics of particle populations with all of these analyses uniquely captured by visual validation.

With this idea in mind the NTA was used to study the behaviour of FCTN in different glucose concentration media and the certainty was that even minimal changes in the particle size as determined by the nature of the medium in which the particles were subjected to could be detected.

NTA requires several optimisation steps in order to be able to reproduce, capture and analyse the videos obtained for accurate size distribution determination. Therefore the effect of the concentrations of the buffers used was investigated on standard polystyrene beads. If size changes prompted by the nature of the buffers were seen in these polystyrene beads, then errors in the size profiles of the responsive nanoparticles was a possibility. From figure 5.5 it can be seen that the size of the standard 200 nm polystyrene beads in the different media did not show any changes. This implies that, the nature of the media has no effect on the size of these standard particles and hence any size distribution changes in our formulation when exposed to the different media would mainly be a result of the components of the nanoparticle reacting with the components of the buffer system.

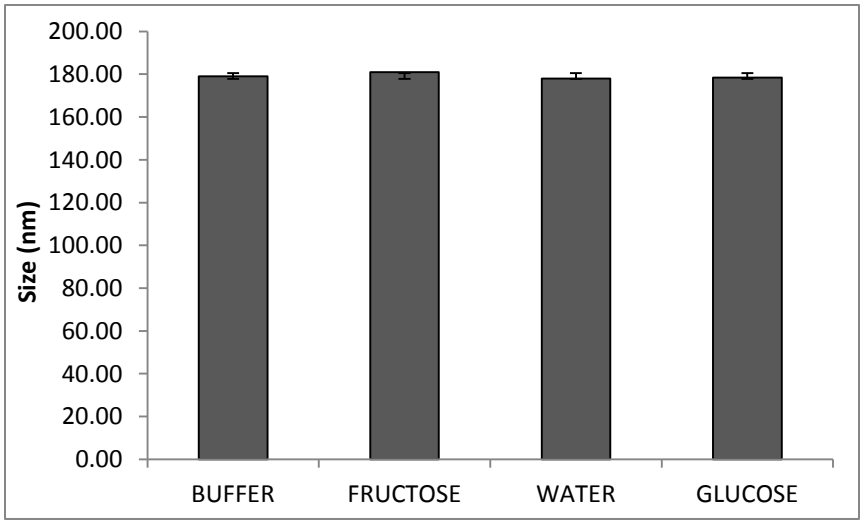

Figure 5.5 Size responses of standard 200 nm polystyrene beads in various media

One important parameter on the NTA software is the detection threshold. The effect of the detection threshold on the size distribution of standard polystyrene beads was also ascertained so as to know the right detection threshold to set for the detection of the functionalised nanoparticles. Wrong setting of the detection threshold can exclude some particles from the analysis by the NTA software. The sizes of standard 200 nm polystyrene beads were determined at different detection thresholds, the higher the threshold, the higher the probability that very small particles will not be counted and also very low detection threshold will result in the picking up noise and particle flurrying as particles and introduce error in the data analysis.

The size distribution of 200 nm polystyrene beads was analysed using different threshold of detection values and its effect of the mean particle sizes was compared. It can be seen from figure 5.6 that the detection threshold did not have significant effect on the average size of the polystyrene beads and the size of polystyrene beads did not change. This was not directly applicable to our sample.

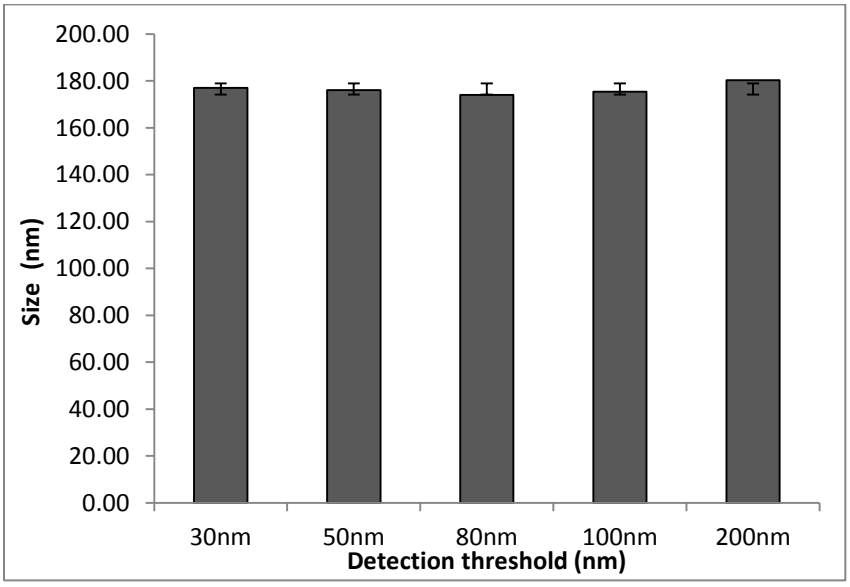

Figure 5.6 Size of standard 200 nm polystyrene determined at various detection thresholds

Laser scattering by colloidal polymeric nanoparticles such as FCTN are not intense as compared to that of polystyrene beads, so this implies that detection of polystyrene beads will be easier on the nanosight than detection of colloidal particles. Hence not all parameters optimised for studying the polystyrene beads distribution in the different media in this current experiment was directly applicable to the FCTN colloidal nanoparticles. In this regard, separate definite parameters were optimised for the colloidal nanoparticles so that instrumental errors due to wrong parameter settings when analysing the videos could be avoided. In the light of the above raised issues, the processing parameters for each video captured for the FCTN nanoparticles were carefully optimised to help in the accurate analysis of each of the videos.

The FCTN formulations also exhibited unique characteristics as their videos were captured and analysed, for example it was very challenging capturing and analysing videos for chitosan-TPP nanoparticles, but it was relatively easier with FCTN. The highest light intensity was used when capturing videos for formulation FN1 but the intensity had to be lowered when capturing for FN3 and FN5. In this regard, it could be concluded that, the degree of functionalisation of the conjugate also affected the light diffracting properties of their respective nanoparticulate formulations.

The introduction of the PBA moiety onto chitosan was expected to make the functionalised chitosan nanoparticles glucose sensitive, therefore an experiment was designed to ascertain the changes that occur in nanoparticles in response to different glucose concentration as the external media. The average normal post prandial blood glucose level of a human being is around 1.4 mg/ml (“Blood sugar level ranges, 2013) and this implies that any model of a glucose responsive

insulin delivery system must be able to sense and release insulin at glucose concentration above 1.4 mg/ml and not concentrations lower.

In these series of experiments, FCTN was introduced in to plain buffer and glucose buffer (0.1–5 mg/ml) at pH 7.40. A wide range of glucose concentrations was selected and studied to help ascertain the behaviour of the functionalised nanoparticulate formulation at, below and above physiological blood glucose concentration. Three different formulations FN1, FN3 and FN5 prepared via ionotropic gelation were studied for their behaviour in different concentrations of glucose media. Considering fact that the required physiological blood glucose concentration targets for non-diabetic and diabetic must be maintained at 0.72-1.6 mg/ml (table 5.3), it will be expedient that none of the aforementioned formulations show any significant response to low concentrations of glucose.

Table 5.3 Target levels of blood glucose for diabetic and non-diabetic patients

Target Levels	Pre-prandial glucose concentration (mg/ml)	Post prandial glucose concentration (mg/ml)
Non - diabetic	0.72-1.06	Under 1.40
Type I	0.72-1.26	Under 1.53
Type II	0.72-1.26	Under 1.62

(http://www.diabetes.co.uk/diabetes_care/blood-sugar-level-ranges.html)

Across all the formulations investigated none showed any size changes due to glucose at concentrations below 1 mg/ml. Figures 5.7 -5.11 are a representative and comparative size distribution profiles of the three selected formulations used to study the behaviour of the functionalised nanoparticles in the presence of plain buffer and glucose. The data shows that the nanoparticles under study were not responsive to glucose at the low glucose concentration and

this was desirable because the system being developed in this current project was purported to show significant response at glucose concentration above 1.4 mg/ml at which patients were considered diabetic.

FN1 among the series showed the least responsiveness to glucose at the different concentrations of glucose, possibly because the amount of boronic acid substituted on F1 was less that on FN3 and FN5 as seen from the elemental analyses results in table 3.8 (chapter 3). The lower amount of boronic acid substitution meant less interaction with glucose and hence less size changes in the particle matrix on interaction with glucose producing less change in the size distribution profile (figure 5.7).

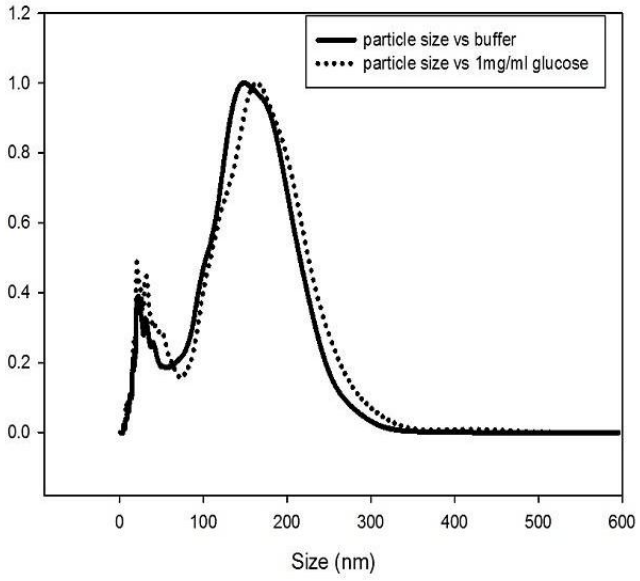

Figure 5.7 Particle size distribution of formulation FN1 after exposure to phosphate buffer and 1 mg/ml phosphate buffered glucose solution.

A histogram of size of distribution at different percentiles determined for the formulation FN1 (figure 5.8) showed that no significant changes were seen in the percentiles for glucose concentrations at 1 mg/ml to 5 mg/ml. This data was also in support of the fact that the lower degree of substitution of boronic acid in F1 caused it to be less responsive to glucose, which is also in concert with the results from the adsorption studies in section 4.4.3, where F1 showed the lowest glucose adsorption.

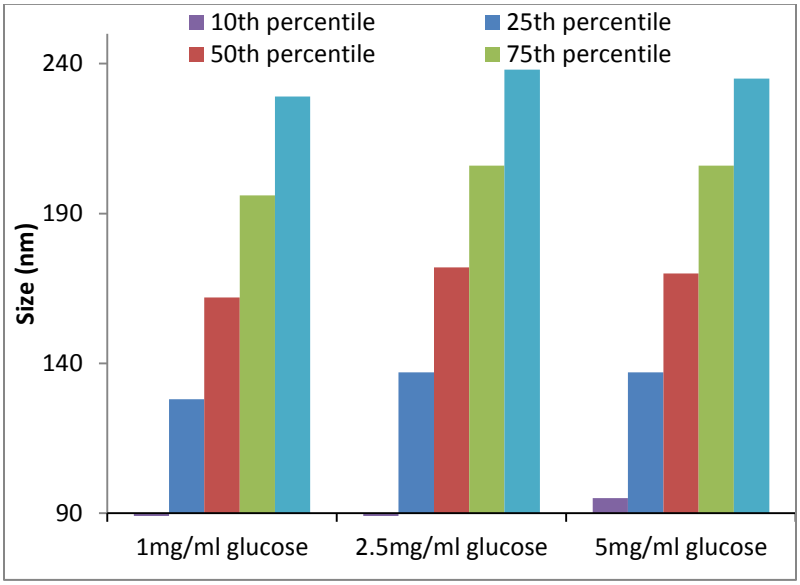

Figure 5.8 Percentiles of size distribution from FN1 in various concentrations of glucose

From the adsorption studies on conjugates in chapter 4 (section 4.43), F3 showed the highest glucose adsorbing capacity than F5 and we correlated the surface topography, crystallinity and possible orientation of the boronic acid within the conjugate to their glucose adsorbing capacities. The adsorption study was done using the solid powdered conjugates and therefore it was not automatic that the behaviour of the nanoparticulate formulations will follow the same trend as the solid conjugates. It would have been interesting to relate the behaviour of the solid conjugates directly with those of the nanoparticles made from them, although there was no

guarantee that exposure of the boronic acid to glucose within the nanoparticulate matrix in suspension and that of the solid conjugate will be directly related or exhibit the same behaviour. Hence F5 which showed a lower glucose adsorption capacity than F3 was also studied on the nanoparticulate level for its glucose responsiveness. F3 and F5 in the experiment showed size changes on interaction with glucose especially at a 2.5 mg/ml concentration (figure 5.9 and 5.10).

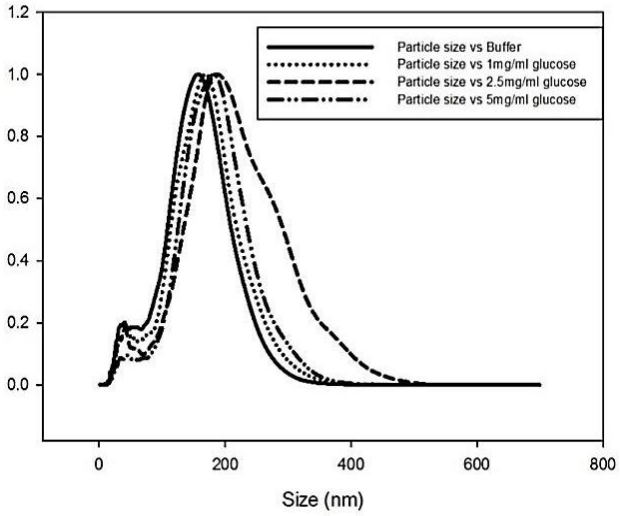

Figure 5.9 Particle size distribution of formulation FN3 after exposure to phosphate buffer and 1 mg/ml, 2.5 mg/ml and 5 mg/ml phosphate buffered glucose solution.

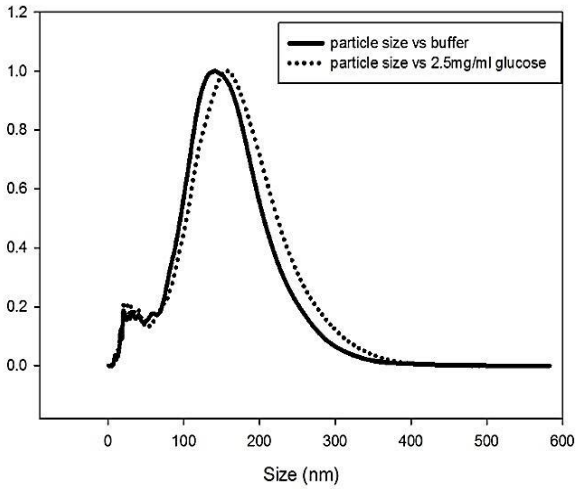

Figure 5.10 Particle size distribution of formulation FN5 after exposure to phosphate buffer and 2.5 mg/ml phosphate buffered glucose solution.

The histogram (figure 5.11) of the different percentiles of FN3 on exposure to different concentrations of glucose shows changes in the percentiles indicating that the particles gradually increased in size as they interacted with glucose.

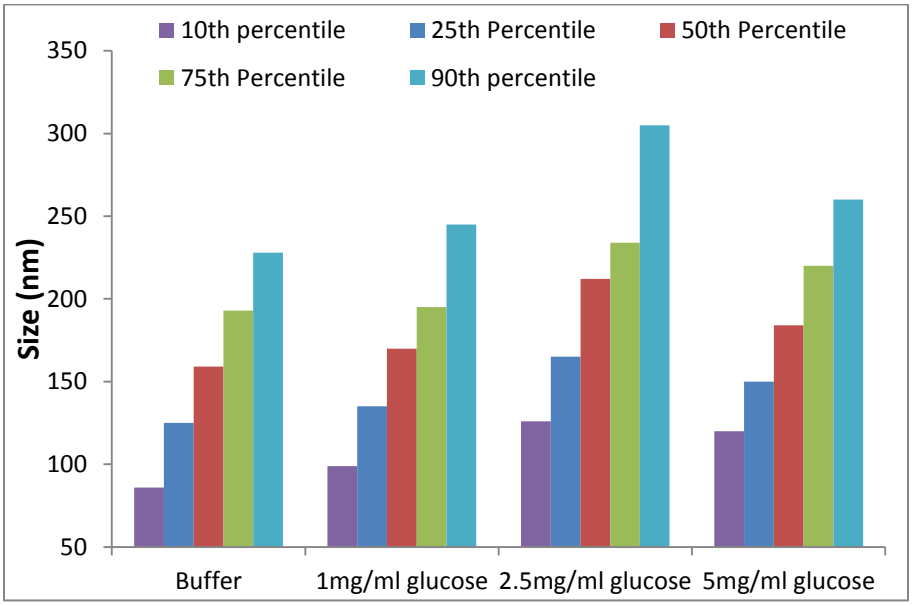

Figure 5.11 Percentiles of size distribution from FN3 in phosphate buffer and various concentrations of glucose

Though the different formulations have their characteristic properties, the changes in their size distribution profiles upon interaction with 2.5 mg/ml of glucose could not be over emphasised. It is evident that the statistics of the nanoparticles behaviour changes as the concentration of glucose changes. Though these changes might be small, they are significant because, these changes results from the behaviour of individual particles as they are tracked by the NTA, hence the overall changes in the size distribution profile of the particles is contributed by each individual particle that was tracked.

An increase in the specific percentage percentiles of the particle size across the different concentration of glucose as compared to that of the plain buffer (table 5.4) also proves that the presence of glucose does effect the particle size changes in the nanoparticles.

The responsive behaviour of polymeric nanoparticles is considered as a combination or sequence of several events: reception of an external signal (physical or chemical) followed by chemical reaction of the material or changes of the material's properties to release the encapsulated drug (Motornov *et al*. 2010). It is expected that, under normal circumstance nanoparticles which are glucose responsive demonstrates continuous size increase in their size distribution profile in the presence of increased amounts of glucose, but this was not so with the FCTN when they were exposed to increased concentrations of glucose. The size distribution profiles representing nanoparticles exposed to 5 mg/ml glucose did not show continuous increase in size in comparison with those exposed to glucose concentration of 2.5 mg/ml (figure 5.9 and 5.10) and this observation was made across all the formulations studied. The possible inference will be that, the nanoparticles under development have glucose dependent swelling ability, but this swelling ability is significantly affected by the concentration of glucose of the medium. Work done by Alexeev *et al.* (2003) suggests that, at high glucose concentration a bidentate complex is formed between the glucose and the boronic acid derivatives. In view of the bidentate binding of glucose by two boronic acid moieties, the glucose molecule in itself can act as a cross-linker and hence impede swelling (Asher *et al*. 2003; Jin *et al*. 2009; Alexeev *et al*. 2003). Results presented here therefore reinforce the above observation by Asher *et al* (2003). This glucose mediated cross-linking of the nanoparticle by glucose explains the decrease in size of nanoparticles at glucose concentration of 5 mg/ml in contrast to an increase in size at 2.5 mg/ml. From the above, it is apparent that the more boronic acid groups present within the nanoparticles,

the higher the chances of these groups interacting with glucose and the better the manifestation of the bidentate knitting of the nanoparticle matrix with glucose. This explains the constrained size increase in FN5 (figure 5.12) compared to that observed in FN3 or FN1.

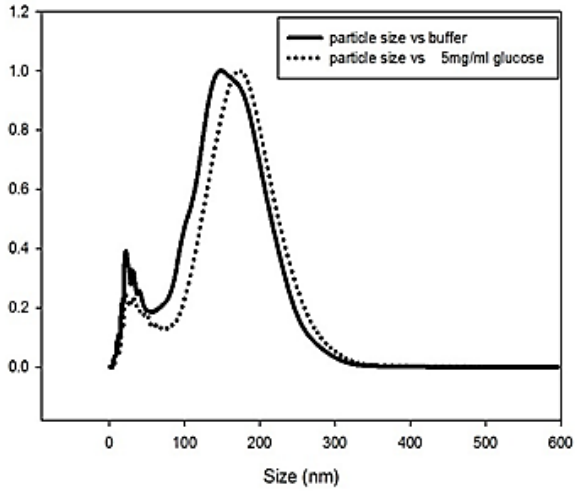

Figure 5.12 Particle size distribution of formulation FN5 in buffer and 5 mg/ml phosphate buffered glucose solution

5.5 CONCLUSION

Chitosan was successfully functionalised by boronic acid and nanoparticles were successfully formulated out of the functionalised chitosan via ionotropic gelation using ultrasonication and these nanoparticles have exhibited a glucose responsive behaviour. However, the increase in the size of the nanoparticles was dependent on both the amount of boronic acid groups present within the nanoparticles and also the concentration of glucose. The glucose acts as a cross-linking agent when its concentration is high and also when the boronic acid substitution within the nanoparticulate matrix increases.

In the subsequent chapter an attempt would be made to encapsulate insulin in the functionalized chitosan TPP nanoparticles matrices in the process of the fabrication of the nanoparticle and an attempt will be made to correlate the size changes as studied in this chapter with the amount of insulin released in different sugar media at physiological pH.

CHAPTER 6

ENCAPSULATION AND RELEASE OF INSULIN FROM FUNCTIONALISED CHITOSAN NANOPARTICLES

6.1 Introduction

Drug delivery involving the use of polymers has attracted much attention in recent years; in this regard the choice of polymers is often tailored to meet specific physiological challenges. Both biodegradable and non-biodegradable polymers have extensively been researched into and these polymers can be either synthetic or natural. Ideally a polymer for drug delivery must be biocompatible, biodegradable and easily modified for specific functionalities.

Of interest to the current project is the chitosan polymer, which a polysaccharide derived from the alkaline deacetylation of chitin, a natural cellulose derivative from crustaceans such as shrimps and crabs. It is mucoadhesive, enhances permeation of biomolecules across the epithelia and does not cause mucosal damage (Kumar 2000). Chitosans have been formulated into different pharmaceutical dosage forms such as beads, microparticles and nanoparticles and out of the above mentioned; nanoparticles have perhaps the widest applications in medicine.

It is possible to modify the chemical properties of chitosan by adding specific moieties and these chemical moieties may be tailored to achieve specific drug delivery outcomes. The concept of imparting stimuli responsive properties onto chitosan has also been pursued widely. For example chitosan as a pH responsive hydrogel (Goycoolea *et al*. 2003; Lin *et al*. 2009; Shantha and Harding 2000) or chitosan as a glucose responsive polymer by functionalising with glycol sensors such as con A (Yin *et al*. 2010), glucose oxidase (Wu *et al*. 2009) and boronic acids (Wu *et al*. 2011).

Micro and nano encapsulation methods have recently drawn attention as an attractive method for drug formulation since these delivery systems offer several advantages over conventional delivery systems. Site-specific drug delivery, controlled release, minimising side effects and protection of sensitive drugs (McGee 1995) are few of such attributes. Different methods have been employed in encapsulating proteins and peptides into chitosan nanoparticles and these methods include ionotropic gelation (Fernández-Urrusuno *et al*. 1999), polyelectrolyte complexation (Mao *et al*. 2006) and layer - by- layer adsorption (Fan *et al*. 2006).

Encapsulation of insulin into chitosan tripolyphosphate (TPP) nanoparticles via ionotropic gelation has been extensively studied and its feasibility has been proven beyond doubt. Trimethyl chitosan nanoparticles have also been formulated incorporating insulin using ionotropic gelation and polyelectrolyte complexation (Yin *et al*. 2009). Chitosan functionalised by an amino boronic acid has also been formulated into nanoparticles with insulin via polyelectrolyte complexation (Wu *et al*. 2011).

In the present project, exploration of the formulation of functionalised chitosan (chitosan phenylboronic acid conjugates) into glucose responsive nanoparticles employing ionotropic gelation and polyelectrolyte complexation will be explored with much focus and emphasis on the encapsulation efficiency, stability, ease of nanoparticles recovery and insulin release as a function of different external media. The choice of nanoparticle dosage form over other types stems from the fact that with nanoparticles, there is a higher surface area to volume index. This, we aim to exploit, so as to impart sensitivity and hope that insulin release from the eventual dosage form is fast and orchestrated. Since the addition of insulin was likely to perturb the previously established characteristics of nanoparticles by ionotropic gelation or polyelectrolyte

complexation, it was necessary to study how incorporation of insulin might modulate the responsiveness of the nanoparticles when exposed to glucose.

6.2 Materials

Functionalised chitosan (FC) was prepared as described in section 3.2.1.4, Human recombinant zinc insulin from *P. pastoris* (28.5 IU/mg) (Merck, Darmstadt, Germany), HPLC grade acetonitrile and methanol, (Thermofischer Scientific New Jersey, USA) and ultrapure Milli-Q® water (18.2 ohms at 25˚C). All other chemicals were of reagent grade

6.3 Methods

6.3.1 Preparation of functionalised chitosan TPP insulin nanoparticles (FCTIN) via ionotropic gelation

Functionalised chitosan (FC) was dissolved in 1% acetic acid at a concentration of 3.2 mg/ml and the pH adjusted to 4.50 and 5.50 with 4 M NaOH using a Sartorius basic pH meter PB-11. Insulin was dissolved in 0.01 N HCl at a concentration of 2.56 mg/ml and TPP was dissolved in deionised water at a concentration of 0.844 mg/ml. All three solutions were filtered through a 200 nm regenerated cellulose membrane.

A 0.5 ml aliquot of insulin was added to the required volume of TPP solution (table 6.1) and the mixture was added drop-wise into the 4 ml FC solution whilst stirring at 600 rpm on an HTS-1003 magnetic stirrer for 45 minutes at room temperature. The formulations were designated as NI (insulin containing), thus formulations made from F1-F5 conjugates, were labelled as F1NI - F5NI accordingly and DN (Dummy nanoparticle).

Table 6.1 Formulation of FCTIN via ionotropic gelation

Formulation	Polymer	Volume of TPP at 0.844 mg/ml (ml)	Ratio of FC to TPP
F1NI	F1	5.0	3.0:1
F2NI	F2	5.0	3.0:1
F3NI	F3	4.0	3.8:1
F4NI	F4	3.6	4.2:1
F5NI	F5	3.1	5.0:1

6.3.2 Preparation of functionalised chitosan insulin nanoparticles (FCIN) via polyelectrolyte complexation (PEC)

In addition to preparing nanoparticles by ionotropic gelation, nanoparticles were also prepared by PEC. In this procedure, 2 mg/ml of functionalised chitosan (F3 or F5) solution was prepared in 1% acetic acid, pH adjusted to 5.5 with a Sartorius basic pH meter PB-11 and then filtered. A 1 mg/ml solution of insulin was prepared in a mixture of 0.01 N HCl and 0.1 N Tris base at a ratio of 87:13, respectively and pH adjusted to 8.50 with 1 N NaOH. 1 ml of the functionalised chitosan solution was measured into a vial and 2 ml of 1 mg/ml insulin was added drop wise whilst stirring at room temperature at 600 rpm on an HTS-1003 magnetic stirrer for 20 minutes. The sample was allowed to stir for an additional 20 minutes. The samples were analysed visually where an opalescent dispersion was indicative of nanoparticle formation. The formulations were designated F3PN and F5PN accordingly. All experiments were performed in triplicate.

6.3.3 Characterisation of nanoparticles

Z-average, Pdi and zeta potential of the nanoparticles were assessed by Zetasizer Nano ZS (Malvern, UK) equipped with a 4Mw He- Ne laser (633 nm). Each analysis was carried out at 25^{o}C and performed in triplicate and data expressed as mean ± standard deviation. The morphological examination of NPs was performed by field emission scanning electron microscope (FESEM, Quanta 400F, FEI Company, USA) under low vacuum and at a viewing voltage of 20.0 kV.

6.3.4 Evaluation of encapsulation efficiency of NPs

The encapsulation efficiency (EE) of insulin was determined upon separation of NPs from the aqueous medium containing free insulin by centrifugation at 14000 rpm for 45 min at 15°C using a Beckman Coulter Microfuge 16 centrifuge. The amount of free insulin in the supernatant was measured using a Perkin Elmer quaternary HPLC system equipped with UV detector with detection wavelength set at 214 nm and the amount of the unencapsulated insulin was deduced from the calibration curve.

The insulin encapsulation efficiency within the nanoparticles was calculated as:

$$EE\% = \frac{\text{Total insulin in formulation} - \text{free insulin in supernatant}}{\text{Total insulin in formulation}} \times 100\% \quad \textbf{.....Equation 6.1}$$

6.3.5 Recovery of nanoparticle

6.3.5.1 FCTN recovery by centrifugation

1.5 ml of freshly prepared FCTN suspension was placed in a 2 ml eppendorf tube, and the Eppendorf microcentrifuge, (5417R) was operated at different speeds between 4000-14000 rpm for 45 minutes. The amount of nanoparticle recovered was weighed. The redispersibilty of the pellet was studied at the different speeds of centrifugation.

6.3.5.2 FCTIN recovery by ultrafiltration

40 ml of the F3NI suspension was concentrated to a volume of 1 ml using the Millipore stirred ultrafiltration cell (Model 8010) with a 25 mm regenerated cellulose membrane with molecular weight cut-off of 100 kDa. The system was operated under nitrogen pressure operated at 60psi with continuous magnetic stirring and the concentrate was washed repeatedly with deionised water to remove all the un-incorporated insulin and the concentrate was then used for further analyses.

6.3.6 Stability behaviour of FCIN

Formulation F3PN and F5PN were prepared according to the method described in section 6.3.2. Samples of the formulations were then stored at 25^{o}C and 4^{o}C and the z-average, Pdi and zeta potential were measured weekly over a period of one month.

6.3.7 *In vitro* insulin release studies

Insulin release from the nanoparticles was studied in (1) Phosphate buffer, pH 7.4 (2) glucose (1-5 mg/ml) buffered solution (pH 7.4) and (3) fructose (1-5 mg/ml) buffered solution (pH 7.4). Several replicas of 100 µl of F3PN were placed in eppendorf tubes containing 1 ml of the different release media mentioned above and incubated at 37 ± 0.20°C with horizontal shaking at 100 rpm on a WiseCube WIS-20, Precise Shaking Incubator. At predetermined time points, the seeded tube was taken and 100 µl of solution was centrifuged at 14000 rpm for 15 minutes using a Beckman Coulter Microfuge 16 centrifuge and the supernatant removed. 20 µl of the supernatant was injected into the Perkin Elmer quaternary HPLC system equipped with UV detector with detection set at 214 nm and the amount of insulin released was determined based on reference to the standard curve. The value reported is an average of triplicate readings.

6.3.8 HPLC analysis

The mobile phase consisted of 0.1% aqueous triflouroacetic acid (TFA) (A) and 0.1% TFA acetonitrile (B). Elution was gradient starting with 75% of A decreasing to 40% over 8 min at a flow rate of 1 ml/min with detection of insulin set at a wavelength of 214 nm. The columns used were an Agilent Zorbax 300SB-4.6 x 250 mm C_{18}, with particle size of 5 µm and pore size of 300 Å and Viva 2.1 x 150 mm C_{18} column (USP L1), with 3 µm particle size and pore size of 300 Å.

The calibration curve was constructed from pure insulin dissolved in 0.01 N HCl solutions at a concentration range of 0.625 µg/ml – 100 µg/ml. 20 µl of various concentrations of insulin solutions was injected into the HPLC system, each reading was done in triplicate. A graph of

average peak area was plotted against concentration and the coefficient of determination (R^2) and the equation of the line determined.

The effect of temperature on the retention time, peak height and area of insulin was studied on a Viva 2.1 x 150 mm C_{18} column (USP L1) with 3 µm particle size and pore size 300 Å by keeping the column at temperatures between 25^{o}C and 60^{o}C. 20 µl of 50 µg/ml of insulin dissolved in 0.01 N HCl was injected and the retention time, peak height and peak area at each temperature was recorded. Each reading was done in triplicate.

6.3.9 Study of size changes of F3PN prepared via PEC in different sugar media

F3PN was prepared according to method in section 6.3.2. 100 µl F3NP was added to 1 ml of freshly prepared and filtered buffer or buffered glucose or fructose solutions in the concentration range of 1–5 mg/ml at pH 7.4 in a capped zeta sizing cuvette. The z-average was recorded at different time points and the size changes in each media over the period of 60 minutes were recorded.

6.4 RESULTS AND DISCUSSION

6.4.1 Formulation of functionalised chitosan

The insulin containing nanoparticles were formulated by ionotropic gelation of the cationic FC polymer with TPP anions (FCTIN) and also by polyelectrolyte complexation of the cationic FC polymer with anionic insulin (FCIN). These mild techniques involve the mixing of aqueous solutions at ambient temperature and do not require the use of organic solvents and therefore favourable for preparing protein-loaded nanoparticles. In the attempt to incorporate insulin into the FCTIN, a 10% drug weight with reference to the polymer weight was used as the drug loading whilst in the formulation by PEC, the ratio of conjugate to insulin was 1:1.

All the conjugates (F1-F5) formulated by ionotropic gelation (NI series) were evaluated for insulin encapsulation efficiency however, only F3 and F5 conjugates formulated by PEC (PN series) were evaluated for insulin encapsulation efficiency. The z-average diameter of the dummy nanoparticles prepared by ionotropic gelation (DN) ranged between 140 nm -170 nm, the Pdi was around 0.2 and the zeta potential ranged from +17 mV to +21 mV (table 6.2). However on incorporation of insulin, there was an increase in the z-average of all the nanoparticles, with the average Pdi and the average zeta potential remaining essentially unchanged. The zeta potential for F3DN was lower than that of F3NI, but for the rest of the formulations studied the dummy nanoparticles had slightly higher zeta potential than the insulin loaded ones.

Table 6.2 Z-average, Pdi and zeta potential of PBA functionalised chitosan TPP insulin nanoparticles (FCTIN) formulated by ionotropic gelation

Formulation	Z-average (nm)	Pdi	Zeta potential (+mV)
F1DN	140.37±0.67	0.275±0.008	21.53±0.72
F2DN	170.77±1.53	0.280±0.005	18.67±0.50
F3DN	158.37±1.34	0.272±0.010	18.63±0.75
F4DN	167.00±1.15	0.242±0.024	19.60±0.92
F5DN	145.57±0.60	0.290±0.002	18.07±0.71
F1NI	183.77±8.17	0.265±0.024	18.80±0.85
F2NI	185.20±6.50	0.277±0.029	17.60±0.80
F3NI	189.57±5.39	0.210±0.012	21.57±1.27
F4NI	198.17±5.05	0.241±0.007	17.10±0.75
F5NI	171.37±3.74	0.257±0.060	17.27±1.75

DN = Dummy nanoparticles
NI = Insulin loaded nanoparticles

Table 6.3 Z-average, Pdi and zeta potential of PBA functionalised chitosan insulin nanoparticles (FCIN) formulated by polyelectrolyte complexation

Formulation	Z-average (nm)	Pdi	Zeta potential (+mV)
F5PN	151.6±11.75	0.172±0.02	17.50±0.95
F3PN	140.0±12.83	0.168±0.01	19.10±0.69

The nanoparticles produced by polyelectrolyte complexation for conjugates F3 and F5 showed slightly lower z-average than the insulin loaded ones produced by ionotropic gelation and the Pdi for the PEC's were lower than that from the ionotropic gelation series which is an indication of better homogeneity (table 6.3). The zeta potential values were almost identical to the NI formulations. The positive values of the zeta potential are attributable to the unsubstituted amine groups within the conjugates used in the formulation. The zeta potential values suggest a low stability since these are lower than |25| mV.

Figure 6.1 (a and b) shows a near spherical images of F3PN and F5PN and figure 6.2 (a and b) shows their respective unimodal size distributions.

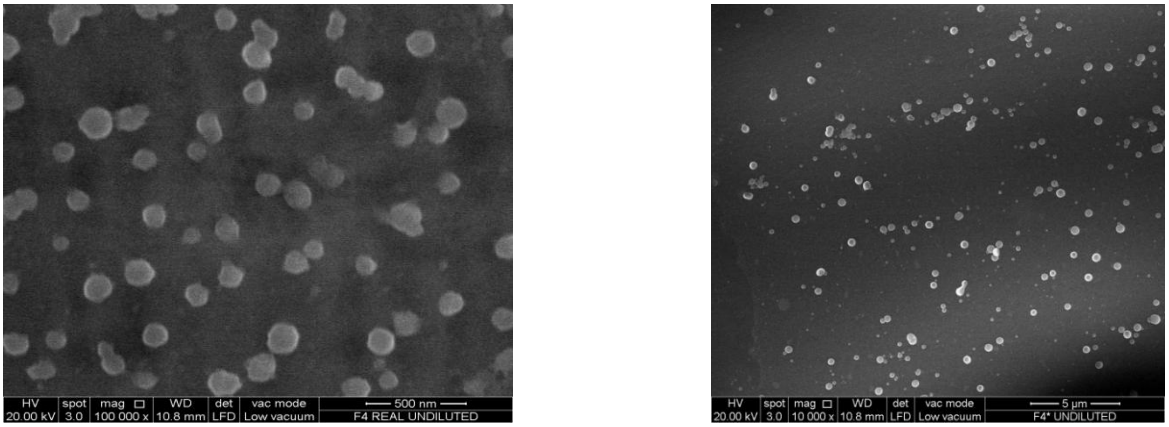

(a) **(b)**

Figure 6.1: SEM image F3PN (a) and F5PN (b)

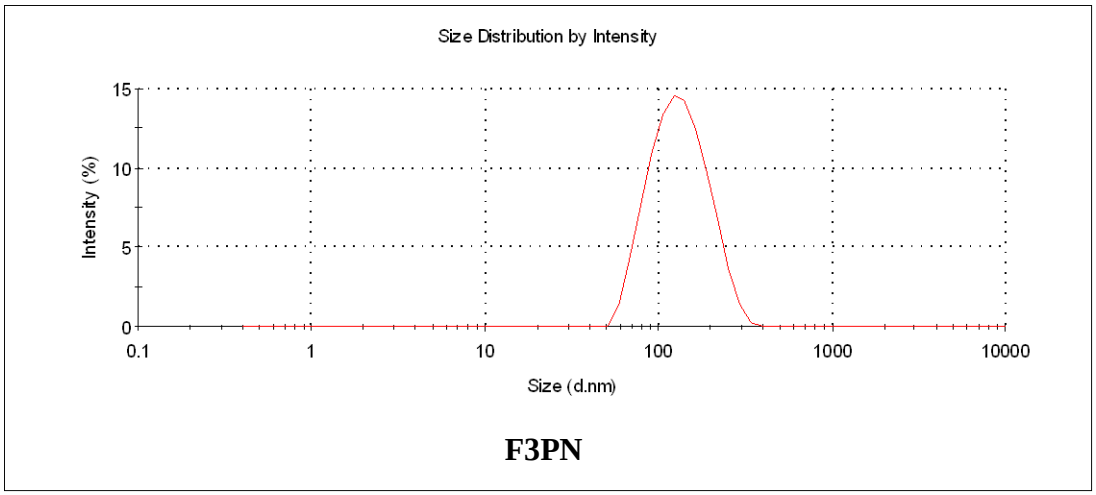

(a)

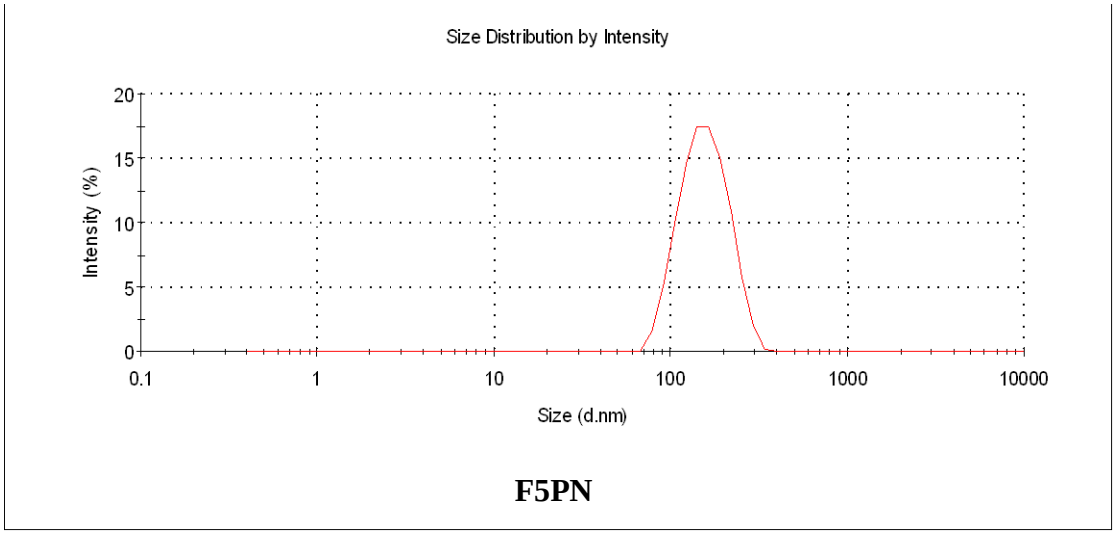

(b)

Figure 6.2 Size distribution profiles of F3PN (a) and F5PN (b)

Figure 6.3 also shows the representative zeta potential profile for F5PN. These figures corroborate with the data presented in table 6.3.

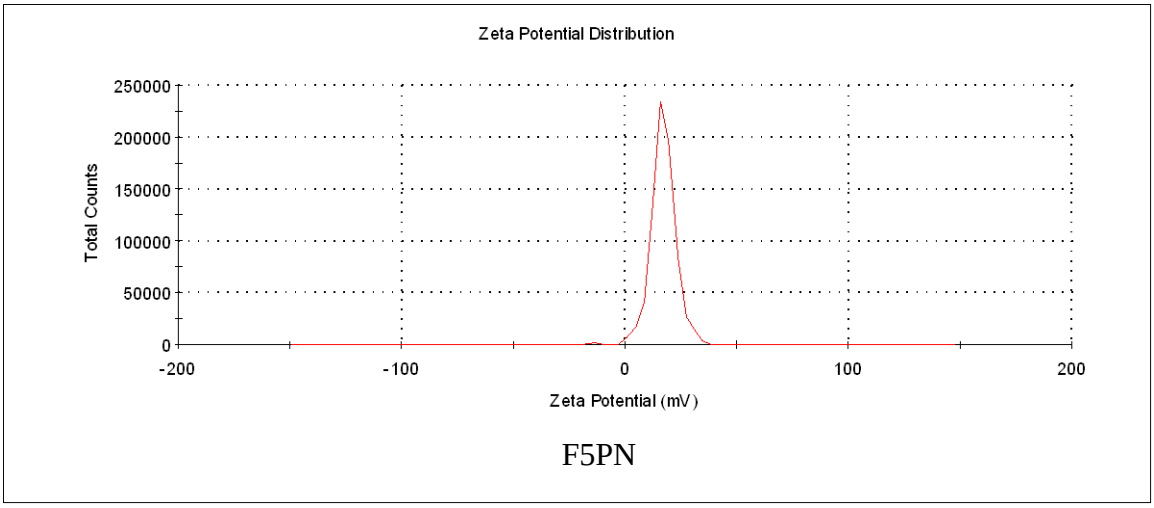

Figure 6.3 Zeta potential profile of F5PN

6.4.2 Stability behaviour of functionalised chitosan insulin nanoparticles (FCIN) produced via PEC

Encapsulation of insulin in chitosan TPP nanoparticles has been studied widely but in the present work, we optimised the method for the production of functionalised chitosan TPP insulin nanoparticles (FCTIN) and functionalised chitosan insulin nanoparticles (FCIN) via ionotropic gelation and polyelectrolyte complexation respectively. There was therefore a need to ascertain the stability of the nanoparticle formulations. The colloidal stability of FCIN produced by PEC was studied over a period of one month, however the FCTIN formulations were not studied because of low stability and low encapsulation efficiencies observed earlier. The samples to be studied were subjected to different storage conditions as described under 6.3.5 and the z-average, zeta potential and Pdi were then measured weekly. Much is not reported on the stability of chitosan TPP insulin nanoparticles, but the stability of dummy chitosan TPP nanoparticles has

been thoroughly studied (López-León *et al*. 2005). The stability studies for chitosan and some modified chitosan insulin PEC has also been done (Mao *et al*. 2006), hence the conjugate–insulin nanoparticles (FCIN) were also evaluated for stability.

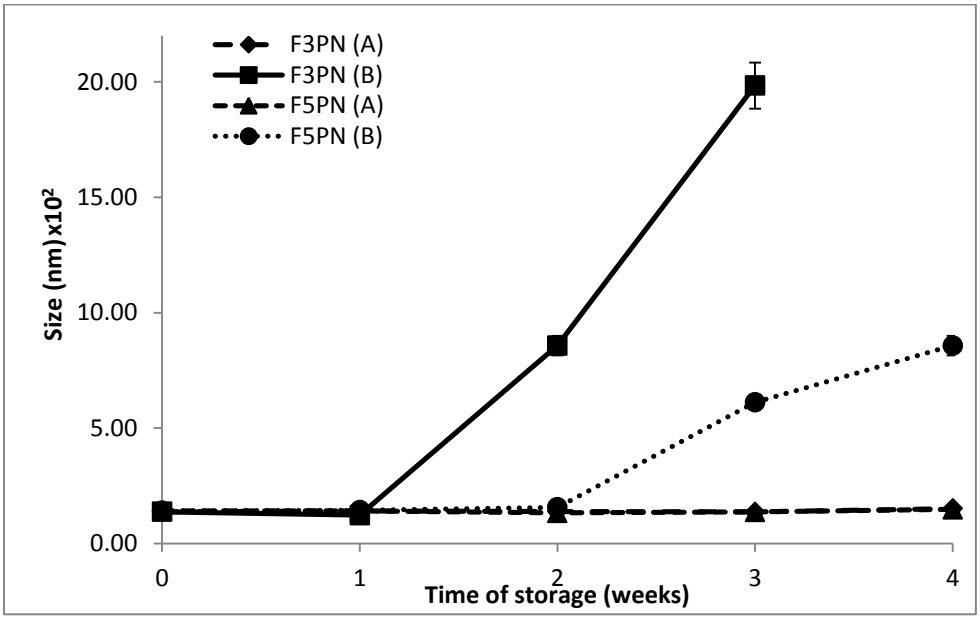

Figure 6.4 Average diameter of F3PN and F5PN stored at 25°C and 4°C as a function of time.

- (A) = Nanoparticles stored at 4°C
- (B) = Nanoparticles stored at 25°C

Figure 6.4 shows the z-averages of F3NP and F5NP stored at 25°C and 4°C. The particle size for nanoparticles stored at 25°C shows a significant increase in size over the weeks. By the end of week 3 the size increase in F3PN was more than 10 fold with a significant increase in the Pdi (figure 6.5). Further evaluations were halted for F3PN stored at 25°C because of the presence of large aggregates and microbial growth.

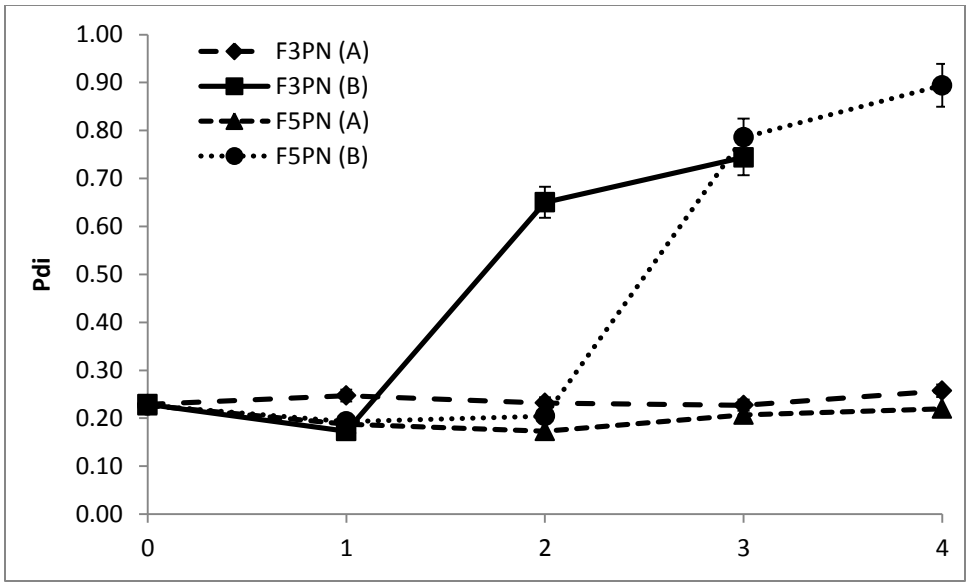

Figure 6.5 Average Pdi of F3PN and F5PN stored at 25^{o}C and 4^{o}C as a function of time.

- (A) = Nanoparticles stored at 4^{o}C
- (B) = Nanoparticles stored at 25^{o}C

The increase in size seemed more pronounced in the F3PN nanoparticles compared to the F5PN nanoparticles for samples stored at 25^{o}C and the progression of size increase was slower for the F5PN nanoparticles. The significant increase in the Pdi of both formulations at 25^{o}C is indicative of heterogeneity in the formulations and this is also confirmed by the size distribution profiles. Heterogeneous systems are not favourable in drug delivery because this will affect the drug release.

In figures 6.4 and 6.5 it is apparent that samples stored at 4^{o}C showed better stability than samples stored at 25^{o}C. Furthermore, the size and Pdi changes of both formulations stored at 4^{o}C did not change significantly. Although the zeta potential measured are below 25 mV (suggesting poor stability), when samples were stored at 4^{o}C they retained their stability for one month. Temperature relationship with Brownian motion of particles has been used to explain possible

aggregation in nanoparticulate systems (Tsai *et al*. 2011). Lower temperatures reduce the Brownian motion of particles, thereby reducing their kinetic energy. These reductions lead to an increase in interparticulate distance which reduces the tendency for particles to collide with each other and aggregate. Hence this may explain the significant difference seen in size profiles for the samples stored at 25^{o}C with those stored at 4^{o}C.

Zeta potential is a parameter that ascertains the state of the nanoparticle surface charge and help in predicting the long term stability of the nanoparticle formulation. Nanoparticulate systems with zeta potential values above |25| mV are considered stable and those having values below, are liable to aggregation caused by van der Waal inter – particle attractions. The zeta potential of both formulations was about +18 mV, which is clearly below the required |25| mV threshold. However, the zeta potential of both formulations stored at 4^{o}C remained essentially unchanged during the one month of storage (figure 6.6)

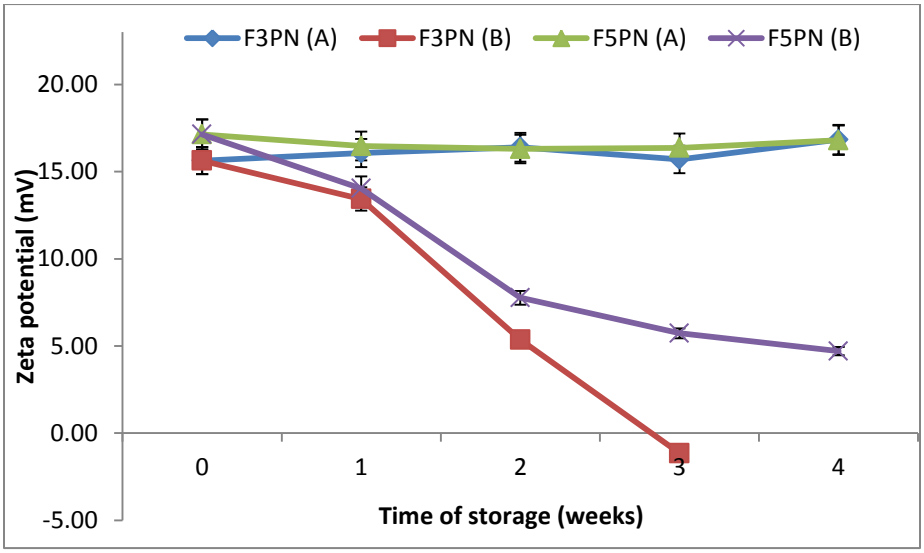

Figure 6.6 Average zeta potential of F3PN and F5PN stored at 25^{o}C and 4^{o}C as a function of time.

- (A) = Nanoparticles stored at 4^{o}C
- (B) = Nanoparticles stored at 25^{o}C

The zeta potential of F3PN and F5PN stored at 25^{o}C showed large variation after storage over 1 month. The zeta potential of the formulations stored at 25^{o}C decreased drastically as the weeks progressed. Chitosan–insulin PEC studied by Mao *et al* (2006) were susceptible to aggregation when stored at room temperature (25^{o}C) or at 4°C over just 2 days, but in contrast, some modified chitosan such as TMC and PEGylated TMC insulin complexes showed no indication of aggregation even within a month of storage at room temperature. The improvement in stability in those formulations was attributed to the higher hydrophilicity of the modified polymer surface (Jintapattanakit *et al*. 2007). They hypothesised that the surface coupling of polyethylene glycol (PEG) increases the hydrophilicity of the complexes and lower their surface free energy, thereby enhancing their physical stability in aqueous media. In the light of the above, our functionalised nanoparticles which showed a downward trend in the zeta potential as a function of storage time may be probably due to the enhancement of the hydrophobicity of the complexes in aqueous media by boronic acid moieties, thereby increasing surface free energy and thus increasing this tendency to agglomerate. The fall in zeta potential values of both formulations stored at 25^{o}C can be attributed to the agglomeration that results due to increased Brownian movement as explained earlier. Such increase in kinetic energy is likely to cause more collisions between particles with increased chances of particles becoming agglomerated. The agglomeration would lead to charge condensation and consequently, a reduction in zeta potential. Albeit the progression was slower in the F5PN than the F3PN so probably the degree of boronic acid substitution may also have a role to play in the stabilisation of the nanoparticle matrices.

Figure 6.7 (a and b) shows images of samples stored at 25^{o}C and 4^{o}C for 4 weeks for F3PN and F5PN. Figure 6.7 a and b shows the appearance of F3PN and F5PN respectively after 4 weeks of storage, it is evident that the samples stored at 25^{o}C appear more opalescent than the same samples stored at 4^{o}C in the figure 6.7 c and d. The F3PN sample stored at room temperature also showed signs of microbial growth with F5PN showing no such sign (figure 6.7 a and b) but the initial clear opalescence of F5PN was lost which manifested as an increase in the turbidity and this is indicative of the presence of larger aggregates in samples.

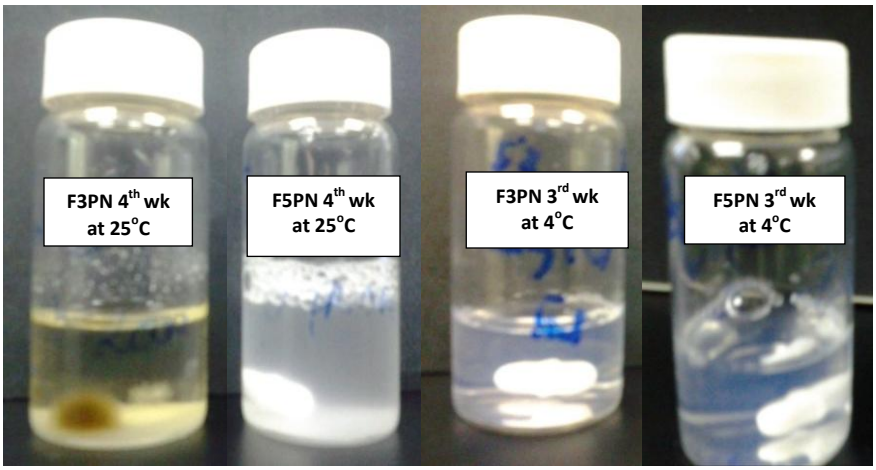

(a) (b) (c) (d)

Figure 6.7 Visual images of F3PN and F5PN during 1 month of storage. F3PN stored at 25^{o}C (a), F5PN stored at 25^{o}C (b), F3PN stored at 8^{o}C (c) and F5PN stored at 8^{o}C (d)

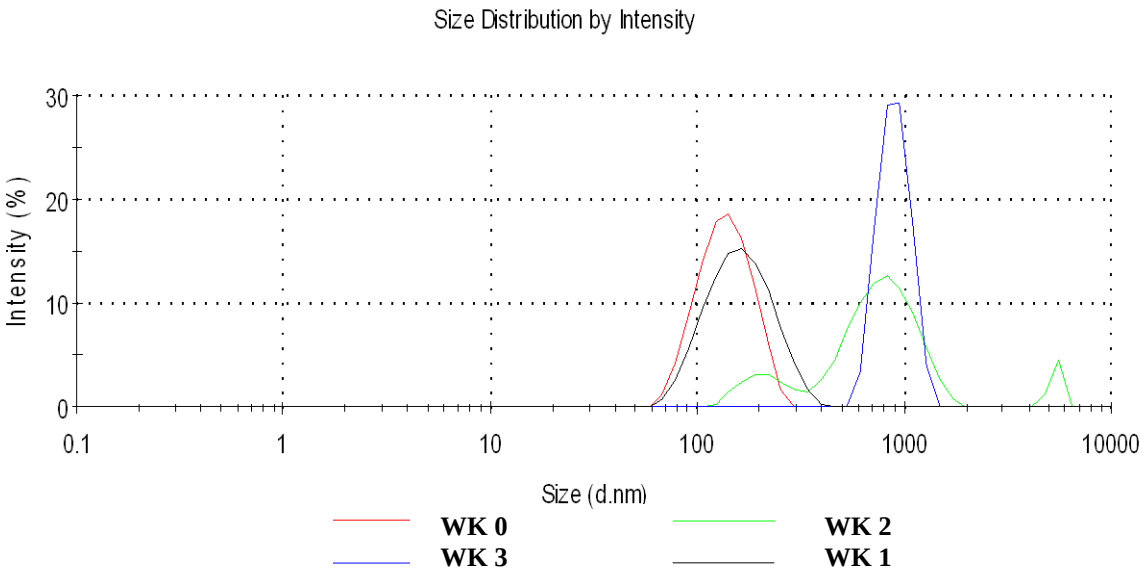
Size Distribution by Intensity
Intensity (%)
30
20
10
0
0.1
1
10
100
1000
10000
Size (d.nm)
WK 0
WK 3
WK 2
WK 1

(a)

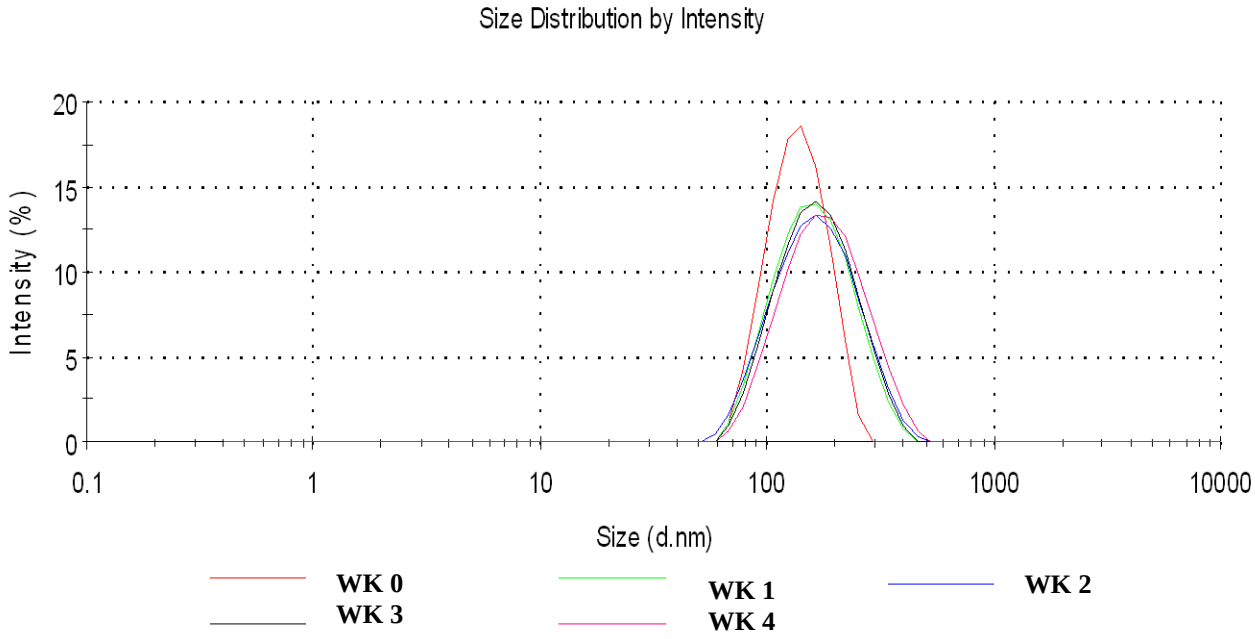
Size Distribution by Intensity
Intensity (%)
20
15
10
5
0
0.1
1
10
100
1000
10000
Size (d.nm)
WK 0
WK 3
WK 1
WK 4
WK 2

(b)

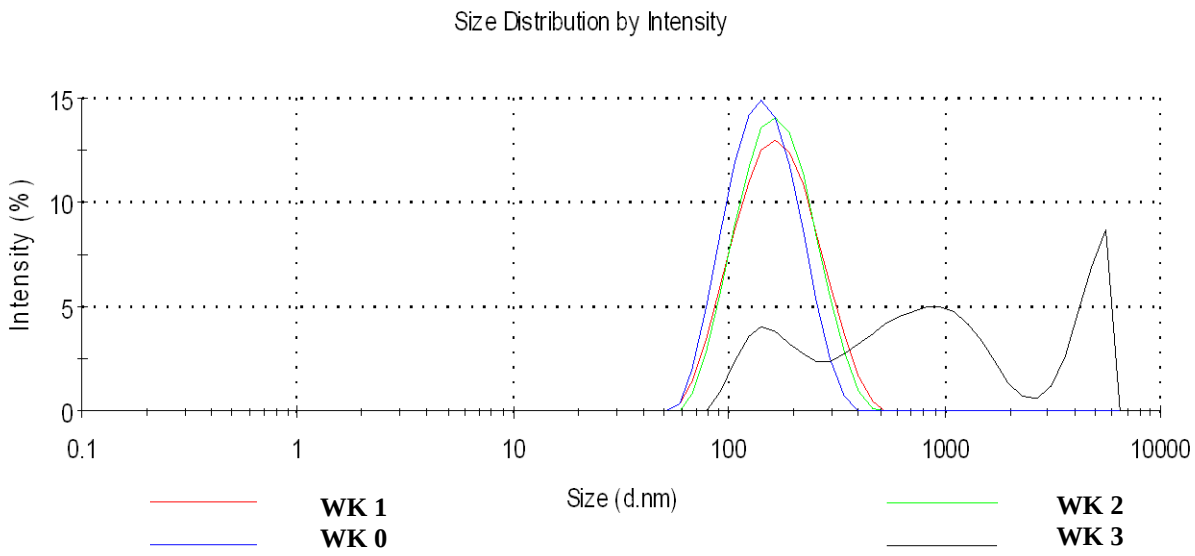

(c)

Figure 6.8 Size distribution of F3PN stored at 25°C (a), 8°C (b) and F5PN stored at 25°C(c) over 3 weeks

Figure 6.8 (a-c) shows the size distribution by intensity of the formulations stored at the different temperatures over the period one month. The multi modal distribution of the size profile seen in the samples stored at 25°C shows heterogeneity in the system and hence a reflection in the drastic changes in the Pdi recorded (figure 6.5). The samples stored at 8°C always showed a unimodal size distribution profile, in contrast to those stored at 25°C also confirming the observations made earlier in the Pdi (figure 6.5). Therefore to preserve the stability of these formulations they would require storage at 8°C, where stability is retained for up to 4 weeks.

6.4.3 Percentage encapsulation efficiency (%EE)

The amount of drug incorporated into the matrix of nanoparticle is important in assessing the release profile, functionality and cost effectiveness of pursuing the formulation to a developmental stage.

Incorporating insulin into chitosan nanoparticle that has been modified by different chemical groups has been studied by several researchers and has proven successful. Zhang *et al*, (2008) incorporated insulin into a polyethylene glycol grafted chitosan and nanoparticles produced gave an encapsulation efficiency greater than 78.6% whilst Zhu *et al.* (2007) synthesised PEG modified *N*-trimethylaminoethylmethacrylate chitosan nanoparticles in which insulin was encapsulated with %EE ranging from 10-84.0% depending on the initial weight of polymer used. This implies that modification of chitosan with different chemical groups to impart specific functionality does not necessarily impede its insulin encapsulating potential when formulated into nanoparticles.

In the present study, chitosan functionalised by PBA was used to formulate insulin containing nanoparticles via ionotropic gelation and PEC. The PEC method was pursued further since the ionotropic gelation formulations method yielded formulations with low stability (evidenced by precipitation and aggregation with slight pH changes) and low encapsulation efficiencies. The %EE varied within not only the formulations studied but also according to the method used for the formulation.

Table 6.4 shows the %EE for the different functionalised chitosan nanoparticles prepared by ionotropic gelation, where the values ranged between 12-32% depending on the chitosan conjugate in the series F1-F5 being used. There appeared to be a gradual increase in the %EE as the degree of substitution of boronic acid unto the chitosan increased from F1 to F5, hence the possibility of the presence of the boronic acid groups in enhancing insulin association or incorporation into the nanoparticle matrix is apparent.

Table 6.4 Percentage encapsulation of insulin in functionalised chitosan nanoparticles prepared by ionotropic gelation as a function of pH

Formulation (pH 5.5)	% Encapsulation(pH of FC solution 4.50)	% Encapsulation (pH of FC solution 4.50)
F1NI	12.05±5.61	9.05±7.53
F2NI	18.87±7.99	-
F3NI	15.04±4.53	12.04±3.69
F4NI	34.36±8.14	-
F5NI	32.51±8.69	24.51±9.65

A pH of 5.5 has been considered as the optimum pH for formulating chitosan TPP nanoparticles by ionotropic gelation, because at this pH, it is believed that about 90% of the amine groups are protonated (NH_4^+) to facilitate interaction with TPP (Csaba *et al*. 2009). A of pH 5.5 was therefore used initially to formulate the nanoparticles, but formulation made at this pH became easily aggregated. Though the pKa of chitosan is around 6.5 and chitosan seem to precipitate out of solution only at pH above 6.0, our formulation easily precipitated at pH 5.5 (especially F5NI). There is a possibility that, the substituted boronic acid on the chitosan modifies pKa of the polymer and hence nanoparticles produced from the pure chitosan tend to show greater stability

towards aggregation with pH changes than nanoparticles produced from the functionalised chitosan at the same pH. In the light of the above constraint the pH was reduced to 4.5 and its effect was studied on three of the formulations.

Table 6.4 shows that when the pH was reduced to 4.50 the encapsulation efficiency decreased. This pH dependent %EE has also been reported by Ma *et al*, (2002). In the series of experiments performed by that group in attempting to encapsulate insulin in chitosan nanoparticles, they observed that a %EE of 57-62% at pH of 6.1 dropped sharply to 12-13% at pH around 5.7 and at lower pH of 3 the %EE dropped to about 7%. Higher pH may have favoured interaction between chitosan and insulin because proteins are known to adsorb efficiently unto polymers at pH around their isoelectric point because of the minimisation of the electrostatic repulsion, increased conformational stability, coupled with smaller specific surface area of protein molecules *(Ma et al*. 2002). The association of chitosan with insulin has also been attributed to hydrogen bonding and hydrophobic interactions and such interactions are considered labile, hence the equilibrium rapidly shifts towards dissociation with small changes in the pH. The above explanation may also account for the decreased %EE as the pH was reduced in our formulation.

The polyelectrolyte complexation method of making chitosan and modified chitosan insulin nanoparticles has also been widely explored (Sadeghi *et al*. 2008; Jintapattanakit *et al*. 2007; Wu *et al.* 2011). However, this method utilises the cationic nature of chitosan and the anionic nature of insulin for the formation of nanoparticles. Due to the lower %EE, lower stability and difficulty in the purification of the FCTIN (purification will be discussed in the next heading), the method of PEC was adapted to help increase the encapsulation efficiency of insulin and also improve ease of formulation and stability.

In the development of 3-aminophenylboronic acid grafted chitosan as a sensitive vehicle for controlled release of insulin using a caboxyacyl chitosan, Wu *et al*. (2011) achieved a %EE between 49.4-59.4 using the PEC method and the %EE depended on the initial amount of insulin used and the molecular weight of the polymer. In the present study, the PEC method was used to formulate nanoparticles from conjugates F3 and F5 (F3PN and F5PN respectively). The highest encapsulation efficiencies: 81% for F3PN and 91% for F5PN (table 6.5) were achieved. Furthermore, %EE increased as the initial pH of the FC solution was increased gradually and this implies that, the amount of insulin encapsulated within the nanoparticle matrix is pH dependent.

Table 6.5 Percentage encapsulation (%EE) of insulin in formulation F3PN and F5PN

pH	F3PN	F5PN
4.50	s68.00±2.08	76.49±1.99
5.00	78.04±2.19	86.25±3.16
5.50	81.39±2.24	91.31±0.96

An increase in pH causes more of the residual amine groups within the FC polymer to become more protonated and hence enhances the interaction between the cationic amine groups and the anionic insulin. However, when the pH of the FC solution was raised above 5.50, it led to precipitation of the nanoparticles, because further increase in pH causes the FC to become deprotonated and since protonation is necessary to keep the FC in solution, precipitation occurs as a consequence.

It was also observed that during that formulation process, the F5 series was prone to precipitation with slight pH changes compared to the F3 series and since F5 had higher degree of substitution of the boronic acid (chapter 3) there is also a possibility that the degree of the PBA substitution

affected the pKa of the polymer and its stability in aqueous formulations. Hence the degree of boronic acid substitution on the polymer might also dictate their behaviour towards pH changes.

6.4.4 Recovery and purification of nanoparticles

Recovery of nanoparticles is one of the most important parameters that need thorough consideration in the process of developing a formulation. The recovery of colloidal nanoparticles poses more challenges than the recovery of solid nanoparticles, because colloidal nanoparticles have lower mass densities and are also more liable to structural deformation in the recovery process. Different methods have been used to recover nanoparticles from solutions depending on different properties of the nanoparticles. For example, Leo *et al.* (2004) recovered and purified polylactic acid nanoparticles containing a lipophilic drug by gel-filtration chromatography. Other methods including (Leo *et al*. 2006) and cross-flow filtration (Ma *et al*. 2005) but sometimes combinations of methods are used . The process of cross-flow filtration used by Ma *et al.* (2005) to remove free ions and insulin molecules from the chitosan–insulin nanoparticle dispersion. Cross-flow filtration was used because of the instability of the dispersion to centrifugation.

The method of centrifugation is the most widely used method in the purification and recovery of colloidal nanoparticles like chitosan TPP nanoparticles. These colloidal nanoparticles which encapsulate different drugs are normally recovered and redispersed in deionised water and used as suspensions or freeze-dried with or without cryoprotectant before further analyses. In the course of the present study, different methods were evaluated for suitability in the recovery of the nanoparticles. In each method, the benefits and constraints are discussed.

The method of dialysis attempted was unsuccessful because the cationic nature of the chitosan polymer caused most of the nanoparticles to stick onto the membrane due to the electrostatic interaction between the dialysis membrane and the cationic chitosan. This made nanoparticle recovery seemingly impossible.

The method of centrifugation (high speed or ultra) is the widely reported method for the purification and recovery of insulin loaded chitosan and modified chitosan nanoparticles encapsulating insulin. The major setback with this method is the variability in the centrifugal speeds and forces used to separate nanoparticles from solution by different researchers, wherein the difference in these parameters will be dependent on the properties of the nanoparticles being formulated. The process of centrifugation with speeds ranging from 3000- 45000 rpm and 10000 – 74200g have been used in separating chitosan TPP nanoparticle encapsulating insulin (Damgé *et al*. 2007; Bruno Sarmento *et al*. 2006; Fernández-Urrusuno *et al*. 1999; Amidi *et al*. 2006). Some of the centrifugation was also done on a glycerol bed, where the pellet was then redispersed in purified water or freeze-dried and used for further analysis.

In the present work, we observed that centrifugation did not help in the recovery, though the speed of centrifugation had a direct relationship with the amount of substance recovered (figure 6.9).

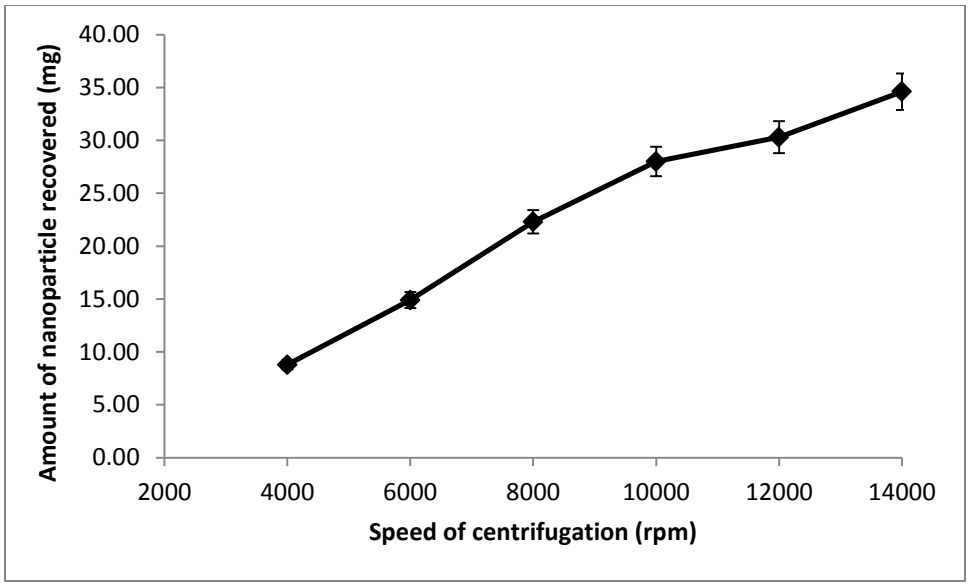

Figure 6.9 Amount of nanoparticle recovered at different speeds of centrifugation

Though this increase in speed with high recovery is plausible, one must be cognisant of the effect of speed of centrifugation on the redispersibilty of the nanoparticle pellet and the accompanying possible morphological changes that can occur. Dummy nanoparticle formulation of the F1NI was centrifuged at speeds between 4000-14000 rpm and the ease of redispersibilty of the recovered pellet at the various centrifugal speeds was studied. It was observed that nanoparticles recovered at speed 4000-6000 rpm were easily dispersed by vortexing or shaking but speeds above 6000 rpm produced a pellet that was difficult to redisperse. Few researchers have given highlights on the non-dispersible cakes or pellet formed when nanoparticles are recovered by high speed centrifugation (Leo *et al*. 2006). An attempt to recover the FCTN and FCTIN by centrifugation was met with minimal success because the pellet recovered at high speeds (speed which gave the highest weight of nanoparticle recovered) was not redispersible. The pelletization may have led to a possible destruction of the spherical morphology of the nanoparticles and this would eventually affect any further studies on the recovered nanoparticles.

Figure 6.10 shows the particle size distribution of nanoparticle formulation prior to and after centrifugation at 4000 rpm, where it was observed that at that speed most of the nanoparticles did not pellet out. As seen in the figure the intensity in the two distributions did not change significantly indicating that a lot of the particles were still remaining in suspension in the supernatant after centrifugation and the shift of the distribution towards the smaller particles (green label) also indicate recovery of only larger particles leaving the smaller particles still in suspension within the supernatant. In this regard any attempt to use the recovered nanoparticle for further study will affect the data in terms of accurate quantification of released drug as a function of the initial amount encapsulated, because we cannot tell whether more of the drug is encapsulated within the smaller particles or the larger ones.

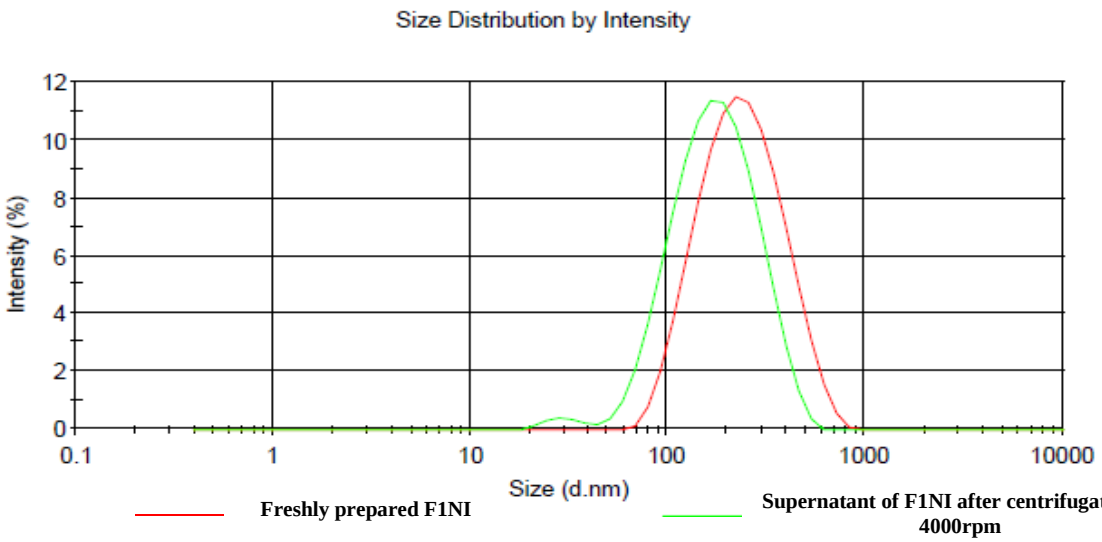

Figure 6.10 Size distributions of nanoparticle before centrifugation and the supernatant after centrifugation

An attempt was also made to freeze dry the recovered pellet and redisperse after, but freeze-dried nanoparticles were not dispersible in deionised water. The use of common cryoprotectants which are mostly sugars or sugar derivatives (Abdelwahed *et al*. 2006) for the process of freeze drying

was avoided in our work. This is because the boronic acid groups in the nanoparticle matrices are known to be sensitive to different diols and the effect of these cryoprotectants on the stability of the nanoparticles and their potential effect on the insulin release could not be predicted.

In the light of the above difficulties encountered with nanoparticle recovery by dialysis and centrifugation, a mild and simple method was sought after to help recover and purify the fragile insulin loaded nanoparticles. It was speculated that, the method of centrifugation was harsh and therefore led to the destruction of the colloidal nanoparticle because of the non dispersibility of the pellet recovered after centrifugation.

The Amicon® ultrafiltration system equipped with a membrane with molecular cut-off 100 kDa was therefore studied for its application in the recovery of nanoparticles. This system is used for protein purification and recovery and has the ability to concentrate formulations into small volumes whilst preserving the constituents and integrity of the formulations.

Figure 6.11 (a and b) is a representation of the setup of the ultrafiltration system, the internal magnetic stirring bar prevents the aggregation of the particle during filtration because as the volume of the medium decreases the nanoparticles occupy a small volume and the stirring action of the magnetic bar prevents aggregation.

(a)

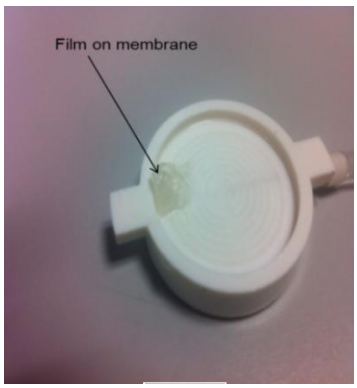

(b)

Figure 6.11 (a and b) Set up for Amicon ultrafiltration system for the recovery of nanoparticles

Though the process of recovery and purification was successful, other factors such as film formation on the membrane also limited the use of the above method. During the process of purification it was observed that a thin film formed on the membrane (figure 6.11b), thereby reducing the filtration rate. Some of the excess insulin and polymer still remained in the concentrate above and an attempt to clear the film from the membrane to enhance the filtration rate damaged the membrane. These membranes though reusable could not be used again and therefore added more cost to the process.

Table 6.6 % EE of insulin in F1NI and F3NI versus expected encapsulation as determined by ultrafiltration

	Determined % encapsulation after centrifugation	% of insulin in filtrate	Expected encapsulation (%)
F1NI	14.30	60.42	39.60
F3NI	23.60	84.40	15.60

Table 6.6 shows the encapsulation efficiency determined by centrifugation and from the filtrate after concentration using the Amicon® filter. The determined encapsulation for F1NI by centrifugation was 14.3%, whilst the amount of unencapsulated insulin in the filtrate from the ultrafiltration was 60.42%, and this implies that about 26% of insulin was not accounted for. During the filtration process the film formed on the membrane as explained earlier, may have prevented the unassociated insulin from going into the filtrate. Therefore any further analysis with the concentrate will not be a true reflection of any determined parameters of the initial formulation. Also another constraint was the length of time it took to concentrate 12 ml volume to 1 ml, where approximately 2 hours was required to achieve the above mentioned concentrate and this implied the practicality of the upward scaling was in question.

Therefore though the process of ultrafiltering was feasible and yielded concentrated nanoparticles, it will be advisable to thoroughly determine the molecular weight of the polymer and also ascertain the correlation between the sizes of the nanoparticles with the molecular weight cut-off of the membrane. This determination will help in choosing the right molecular weight cut-off for the membrane so that all the insulin loaded nanoparticles are retained in suspension but the excess drug and polymer filter out with less restriction making the process scalable and cost-effective.

6.4.5 Insulin release studies in various media

The formulation of the functionalised chitosan into insulin containing nanoparticle was successful as discussed earlier, therefore the release profiles of the formulation were assessed in different media. The formulations made by PEC had proven to be superior in terms of stability and %EE. Therefore those formulations were used in the study of insulin release. The demonstration of a glucose dependent swelling of the nanoparticles warranted an assessment of the insulin releasing properties from the nanoparticles in different external media to help correlate the glucose dependent swelling behaviour with the insulin release profiles. To establish the insulin release profile from the insulin loaded nanoparticles (F3PN) phosphate buffer, glucose and fructose buffers at pH 7.4 were used.

6.4.5.1 HPLC method for quantifying proteins

The HPLC method used for quantifying proteins has been adapted by different researchers, which is also applicable for insulin analyses with the detection system as UV. A number of researchers utilised fluorescence detection mode, using fluorescein isothiocyanate (FITC) labelled insulin as the flourophore (Damgé *et al*. 2007).

The amount of insulin encapsulated within the matrix were analysed by comparing with a constructed calibration curve as shown in figure 6.12. The retention time for insulin was about 6 minutes and the HPLC method was validated with regards to linearity and the correlation coefficient value (R^2) was 0.9995.

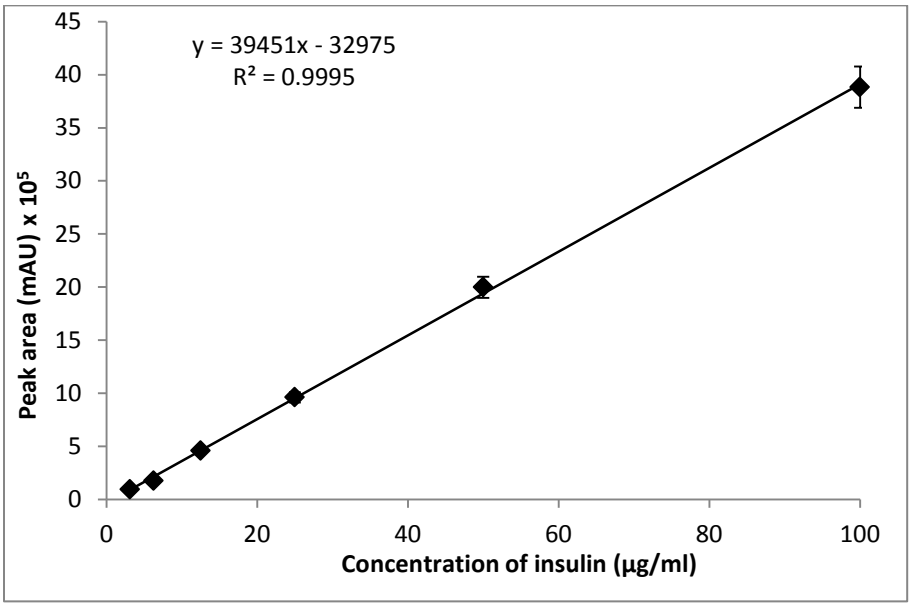

Figure 6.12 Standard calibration curve of peak area of insulin

In the analysis of proteins larger bore columns are known to be more efficient and they tend to give better peak resolution. This conventional column uses large volumes of solvent in comparison to the new narrow bore columns.

The effect of temperature on elution of insulin was studied on the elution of insulin using a 2.1 mm i.d Viva C_{18} column a narrow bore column. It was observed that peak area did not change much as the temperature was increased, but peak height did change at 60^{o}C where, the peaks were sharper than the peaks at 25^{o}C (figure 6.13). This implies that peak resolution and sharpness is enhanced when temperature is increased and this observation has also been reported by Ye *et al*. (2001).

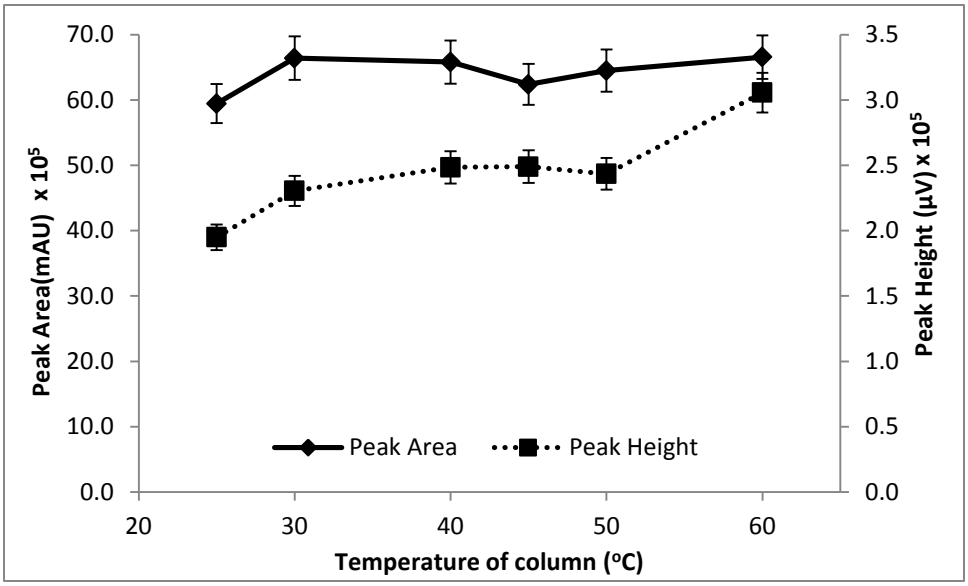

Figure 6.13 Effect of temperature on peak height and peak area

Figure 6.14 is a representative chromatogram of the insulin peaks detected at different temperatures.

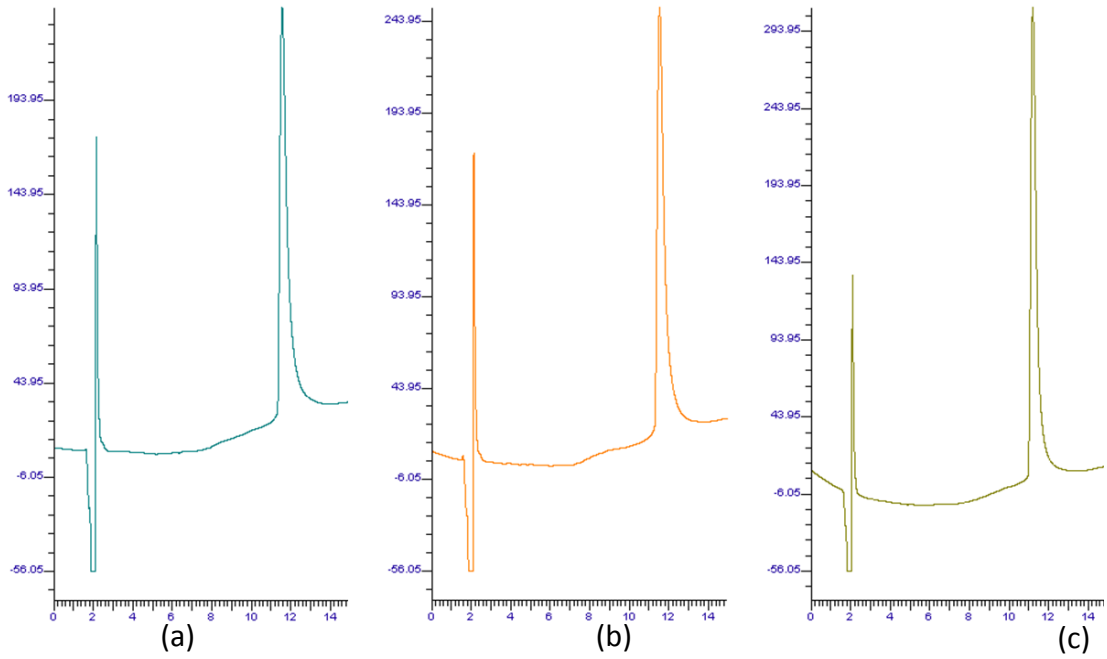

Figure 6.14 Representative chromatograms of insulin (50 µg/ml) detected at 25°C (a), 50°C (b) and 60°C (c)

The intensity scale shows an increment in height as the temperature is increased. The intensity reading at 25^{o}C was 194.95 µV, that of 50^{o}C was 243 µV and that of 60^{o}C was 293 µV. Increased peak height with minimal changes in the peak area (as depicted in figure 6.13) is indicative of better peak resolution and sharpness.

Furthermore an increase in the temperature led to a decrease in column pressure (figure 6.15). Temperature has an indirect relationship with viscosity; temperature increment in fluids known to cause a decrease in their viscosity. Hence as the temperature was increased, flow of the mobile phase was enhanced thereby reducing the pressure in the column and the tubes. The retention time of about 11 min was not affected by the changes in temperature.

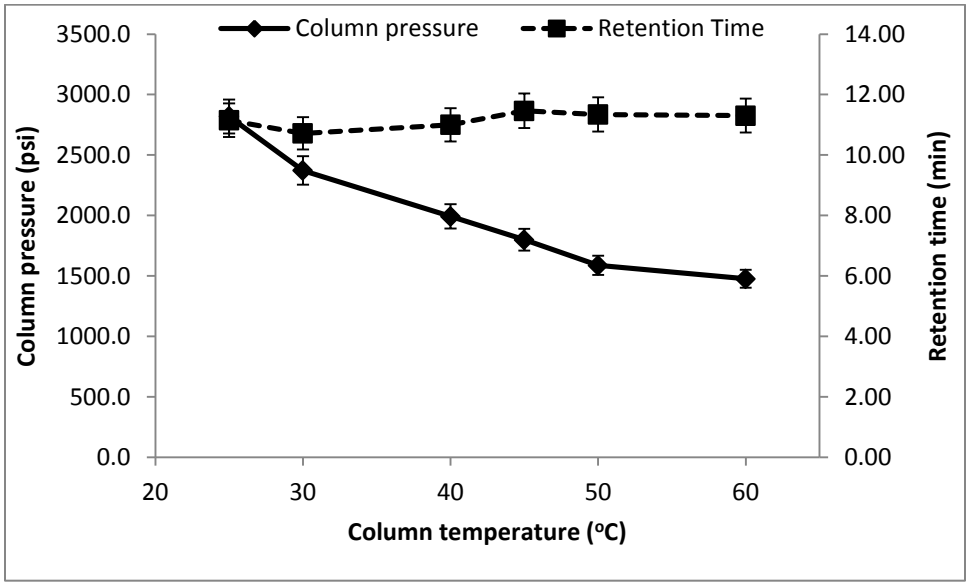

Figure 6.15 Effect of temperature on column pressure and peak retention time

6.4.5.2 *In vitro* insulin release

The insulin release profile from nanoparticles is usually affected by the method of formulation, the ionic interaction between the drugs, auxiliary ingredients, regional residence (incorporation or by adsorption within the matrix) and the chemical composition of the release medium.

The analysis of insulin released was performed using an Agilent C_{18} column as described in section 6.3.8. With this column, shorter retention times were recorded using the optimised parameters for analysis on the Viva C· column. Figure 6.16 (a and b) is a representative chromatogram of pure insulin and insulin after release in buffer medium respectively. The retention time was about 6 minutes and it is can be seen that the peaks were completely resolved and free from interference from extraneous material. More importantly, the release study suggests that no degradation of insulin occurred as these would have registered other chromatographic peaks.

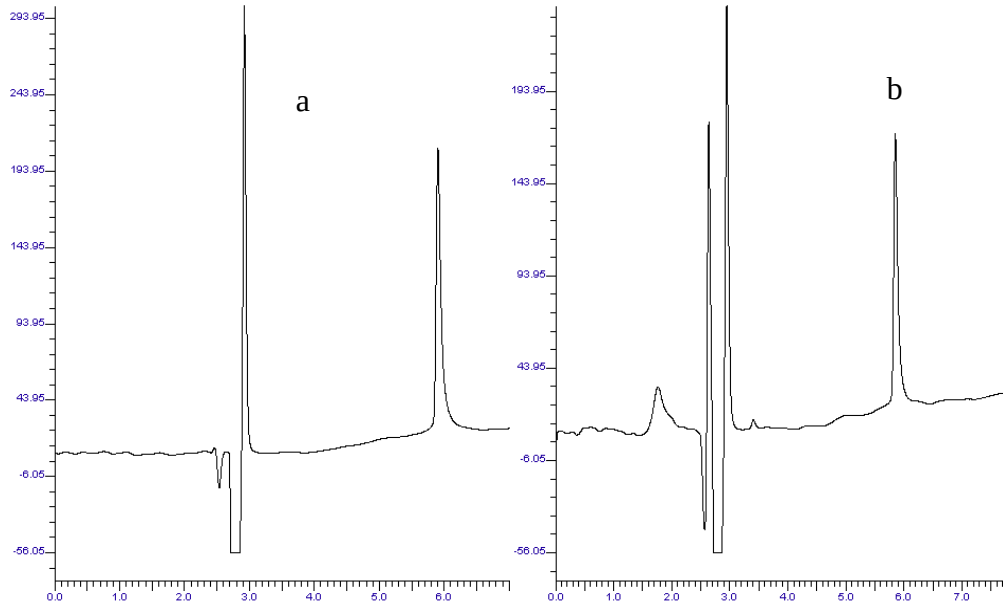

Figure 6.16 Chromatogram of pure insulin (a) and after release from formulation in buffer pH 7.4 media (b)

Other studies have however indicated the manifestation of degradation products of insulin following formulation into nanoparticles (Oliva *et al*. 2000).

Characteristic insulin release profiles usually reported by different groups in insulin release studies from different formulation is characterised by an initial burst release phase (due to drug desorption from particle surface), followed by a plateau attributed to the diffusion of the drug through the matrix and lastly a constant sustained release of the remaining drug attributed to the diffusion of insulin through the polymer wall as well as its erosion (Wu *et al*. 2011).

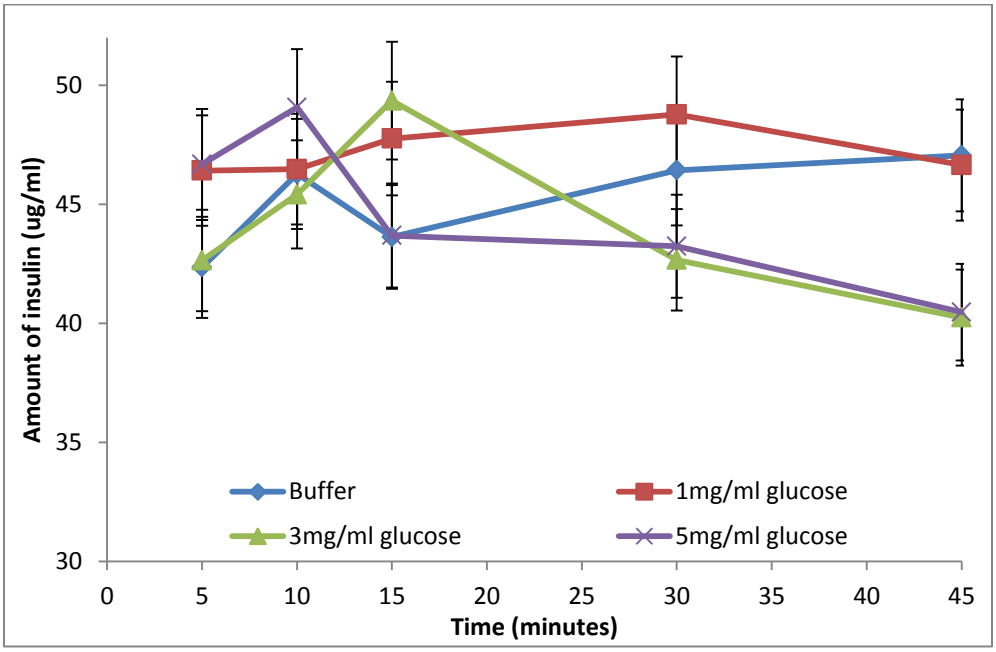

Figure 6.17 Release profiles of insulin from F3PN in phosphate buffer and various concentrations of phosphate buffered glucose solution

Figure 6.17 is the representative release profile for insulin in buffer pH 7.4 and different glucose media, namely 1, 3, and 5 mg/ml glucose. At 1 mg/ml glucose, the release of insulin was more sustained, peaking slightly at 30 minutes. In 3 mg/ml of glucose, insulin release from the nanoparticles was manifested by an initial burst release which peaked 15 minutes followed by a

fall. A similar trend was observed in the 5 mg/ml glucose, with insulin release peaking at 10 minutes. It is apparent from the foregoing that the higher the glucose concentration, the more interactions there are with the PBA groups within the nanoparticle matrices. Such interactions lead to an increase in the diameter of the matrices as discussed in chapter 5. The increase in size then allows permeation of insulin into the media. The speed and the extent of interaction of glucose with boronic acid is slowest at 1 mg/ml.

In all the cases however, there is an apparent dip in insulin release, following the peak. This dip can be attributed to the bidentate interaction between the OH moieties of the boronic acid with glucose. In this regard, a sustained interaction of boronic acid groups with glucose leads to "knitting" of the nanoparticle matrix by glucose, which restricts further diffusion of insulin.

From figure 6.17, it is also noticed that there was a significant release of insulin in buffer and this release profile shows an initial burst release which then tends to increase with time. This is in contrast to insulin release from the matrices in glucose media and suggests a different mechanism responsible for insulin release. Since insulin and the polymer are held in place by electrostatic interaction, it is apparent that ions contributed by the buffer effectively quenches these interactions. Consequently, the release of insulin continues to rise due to the loss of the integrity of the matrices. Fernández-Urrusuno *et al*, (1999) made a striking observation in a study on the profile of the insulin release from chitosan TPP nanoparticles in water and buffer. They observed that only 30% of the encapsulated insulin was released in water after 2 hours, but there was a 90% release in buffer in the same time frame. Hence they concluded that the dissociation of ionic complex within the nanoparticulate matrices caused by the components of the buffer was what governed the above observation. Therefore the role of buffer in aiding insulin release cannot be overlooked.

Studies have shown that fructose has a higher affinity for boronic acid than glucose (Springsteen and Wang 2002). The concept of the binding is related to the pKa of the sugar boronate ester in aqueous medium, where the pKa of the fructose boronate and glucose boronate esters have been determined to be 4.6 and 6.8 respectively. The lower pKa of the fructose boronate ester favours the reaction with PBA. Though the concentration of fructose in the blood of a diabetic patient is <10 mM (Yao *et al*. 2012), concentration of fructose used in this current study was intentionally made the same as that used for the glucose studies in order to compare molecular affinities. This choice was to help gain a better understanding into the mechanism of insulin release from the sensitive matrix due to the complexity of the release profile portrayed by glucose.

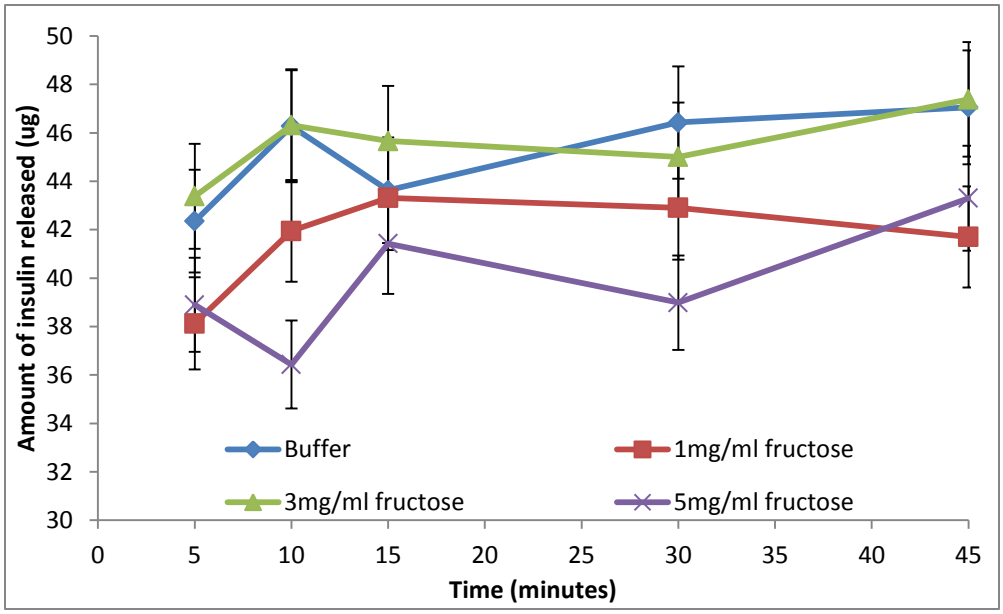

Figure 6.18 Release profiles of insulin from F3PN in phosphate buffer and various concentrations of phosphate buffered fructose solution

Figure 6.18 shows that, at an initial low concentration of fructose (1 mg/ml) insulin release was less than that from 3 mg/ml, indicating that the binding of fructose with boronic acid moieties within the nanoparticles caused more release of the insulin as observed with glucose. However as

the concentration of fructose was increased to 5 mg/ml, the release was significantly lowered. This implies that, the high concentration of fructose makes more interactions possible between the boronic acid and the fructose molecule leading to the formation of more bidentate interactions which then tends to knit the nanoparticle matrix together and causes retention which retains the integrity of the matrix. Ultimately, this restricts further release of insulin. The buffer also has a role to play since it appears that whilst the buffer may be causing disruption of the matrix, the fructose also works to keep the matrix intact. But obviously the effects of fructose supersedes. Comparing insulin release from the matrices in glucose and fructose, it is apparent that more insulin was released from matrices in glucose media than identical concentrations in fructose media. The reason for this is clearly due to the stronger affinity that fructose has with the boronic acid OH groups compared to glucose. In other words fructose is better at knitting the matrices than glucose through bidentate interactions.

In order to study the effect of buffer on insulin release further, three different buffers were used at pH 7.4: phosphate buffered saline (PBS), tris (tris (hydroxymethyl)aminomethane) (TRIS) and HEPES (4-(2-hydroxyethyl)-1-piperazineethanesulfonic acid). TRIS is one of the most widely used buffers in molecular biology and cell culture due to its low toxicity, stability, buffering capacity and its useful buffer range of (7-9) coincides with the physiological pH typical of most living organisms. HEPES (4-(2-hydroxyethyl)-1-piperazineethanesulfonic acid) is a zwitterionic organic chemical buffering agent and HEPES is widely used in cell culture, largely because it is better at maintaining physiological pH. Phosphate-buffered saline (PBS) is set to have a pH within the range of 7 ~ 7.6, and often set to be 7.4 as the pH of blood nears 7.4, a value referred to as the physiological pH in biology and medicine. Aside the maintenance of constant pH, PBS

is known to have an osmolarity that matches those of the human body (isotonic) and is non-toxic to the cells and hence most release studies are done in PBS.

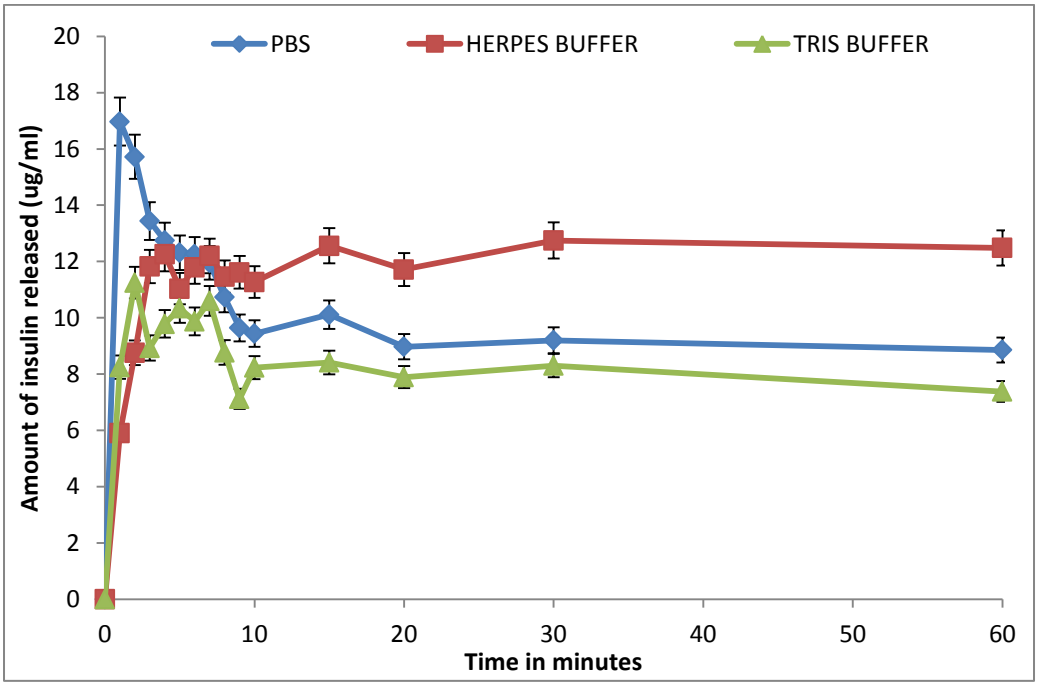

Figure 6.19 Release profile of insulin from F3PN in different buffers at pH 7.4

The release of insulin in these buffers was characterised by an initial burst release with the highest burst release recorded in PBS and the initial release in HEPES and Tris exhibiting almost a similar pattern (Figure 6.19). The release then plateaus with the highest release occurring in HEPES buffer, in this regard, the role of the individual components of the different buffers as contributors to insulin release from nanoparticle particles cannot be overlooked and must be considered when they are used in this kind of studies.

Springsteen *et al*. (2002), tested two buffer systems phosphate buffer and HEPES buffer for its effect on the binding constants of a phenylboronic acid – alizarin red (PBA/ARS) complex. They observed that the binding constants dropped dramatically with increasing buffer concentrations,

while the binding constant for the fructose/PBA complex stayed fairly constant. In HEPES buffer the PBA/ARS complex binding constant was independent of the buffer concentration over the tested range (0–0.1 M). However, the binding constant obtained at a given pH was different for the two buffer system. Therefore, if one is designing an experiment or comparing data from different experiments, the buffer composition and concentration needs to be thoroughly considered. The change in buffer system used will also have another effect. The difference and complexity of the release profile exhibited by the two diols in the above results might have resulted from a complex interplay between the effect of the buffer on the binding of the diol to boronic acid and the binding affinity of the different diols to boronic acid.

6.4.6 Size changes of FCIN (F3PN) in different diol media

Nanoparticles produced by the ionotropic gelation have been studied for their glucose-dependant swelling behaviour in Chapter 5. The release profile of insulin in the data above prompted more investigations into the behaviour of the PEC formulation (FCIN) in buffer and the diol media studied. In this regard, size changes prompted by the introduction of nanoparticles into buffer, fructose and glucose (1-5 mg/ml) over the course of time were studied for the PEC formulation. Because there is a significant release of insulin in the buffer and less in high concentration of fructose, the sugar-dependent size changes of the FCIN were investigated.

Size changes of F3PN in buffer and different concentrations of glucose and fructose is shown in figure 6.20. The size changes in buffer was more pronounced than those in glucose media, hence it is possible to assume that particles also swells in buffer and may lead to difficulties in deciphering any size changes prompted by glucose or fructose.

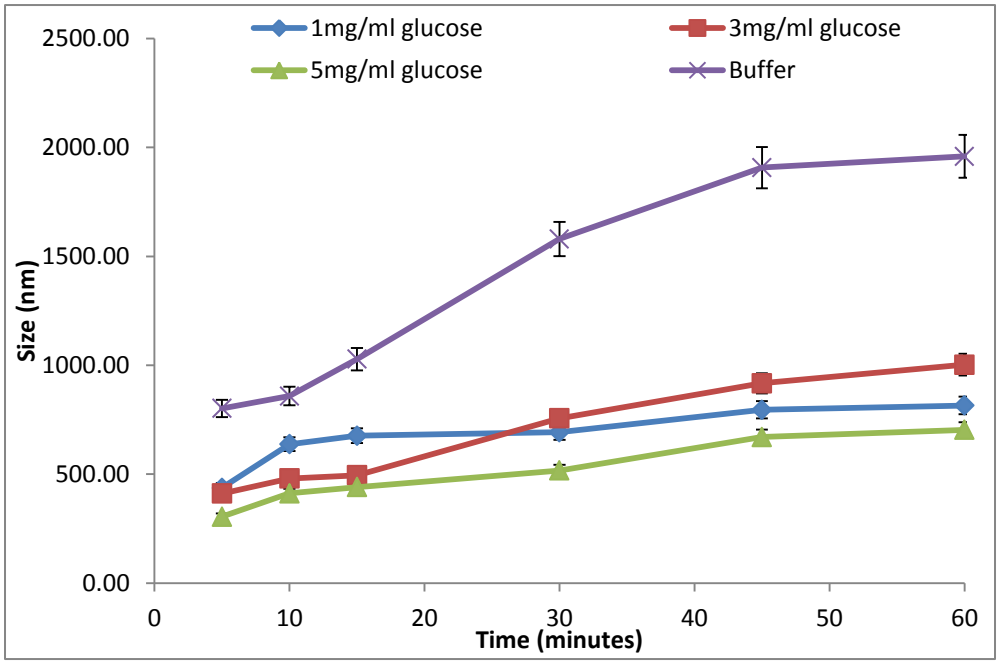

Figure 6.20 Size changes in F3PN in buffer and various concentrations of glucose

The progression of size increase in the nanoparticles at the different glucose concentration shows a slower progression as the glucose concentration was increased from 1 mg/ml to 5 mg/ml. The modulation of this size increase as the glucose concentration increased can be attributed to the interaction of the glucose with boronic acid moieties. The rate of size change in buffer was faster as compared to that in the glucose and in this regard, the buffer might be thought of as causing disruption of the matrices whilst the glucose might be working through bidentate interactions to keep them intact. This observation corroborates the insulin release studies described in section 6.4.5.2. It must also be noted that, size changes in buffer or any media does not directly depict

swelling because photon correlation analysis measures anything considered as particles, whether these are fragments or intact particles.

Figure 6.21 and 6.22 shows the z-average distribution profile of the nanoparticles after exposure to buffer and 3 mg/ml glucose respectively. The Pdi measured in buffer was much higher than in glucose and further points to the fact that an increase in polydispersity is occurring and as reflected in the multi modal nature of the size distribution.

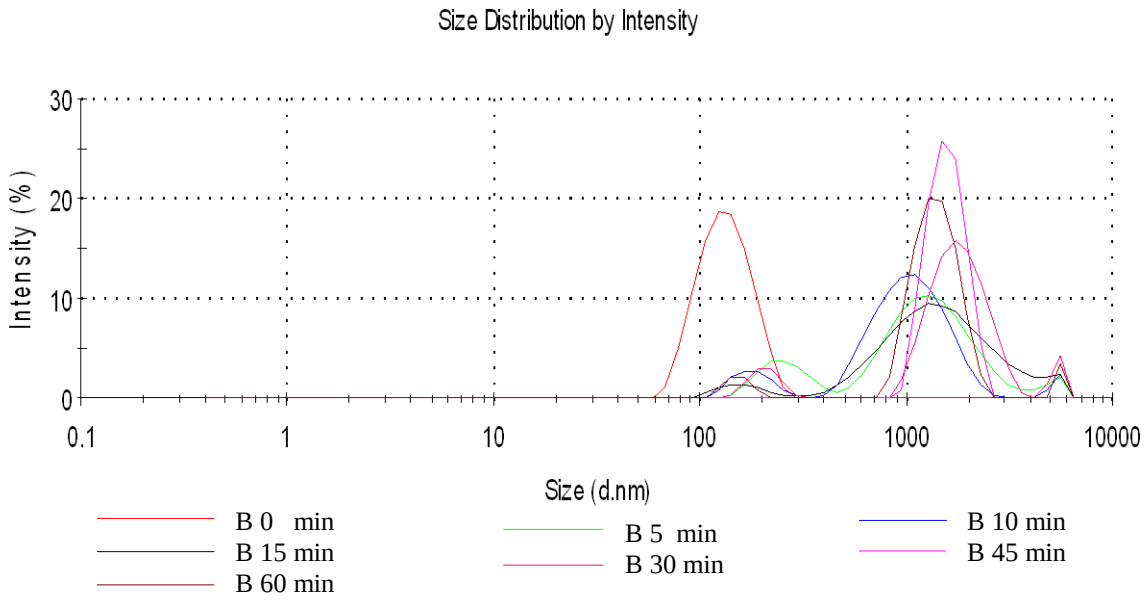

Figure 6.21 Size distribution profile of F3PN in buffer over 60 minutes

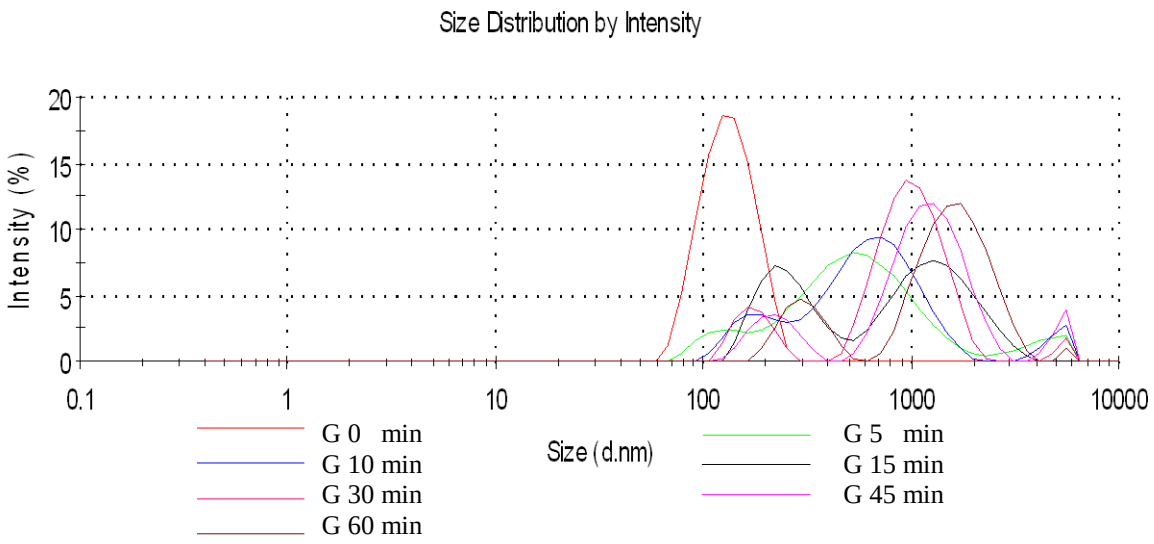

Figure 6.22 Size distribution profile of F3PN in 3mg/ml of glucose over 60 minutes

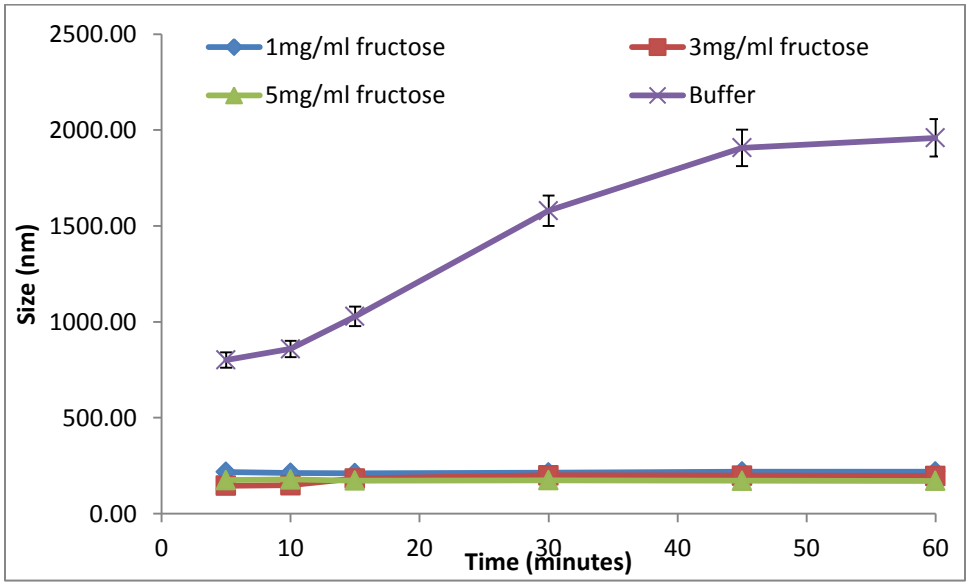

Figure 6.23 Size changes in F3PN in buffer and various concentrations of fructose

Figure 6.23 shows changes in the size of F3PN in fructose and figure 6.24 shows a unimodal size distribution of samples exposed to fructose. The size change of the F3PN in glucose over 60 minutes was significant whilst the change in buffer was drastic.

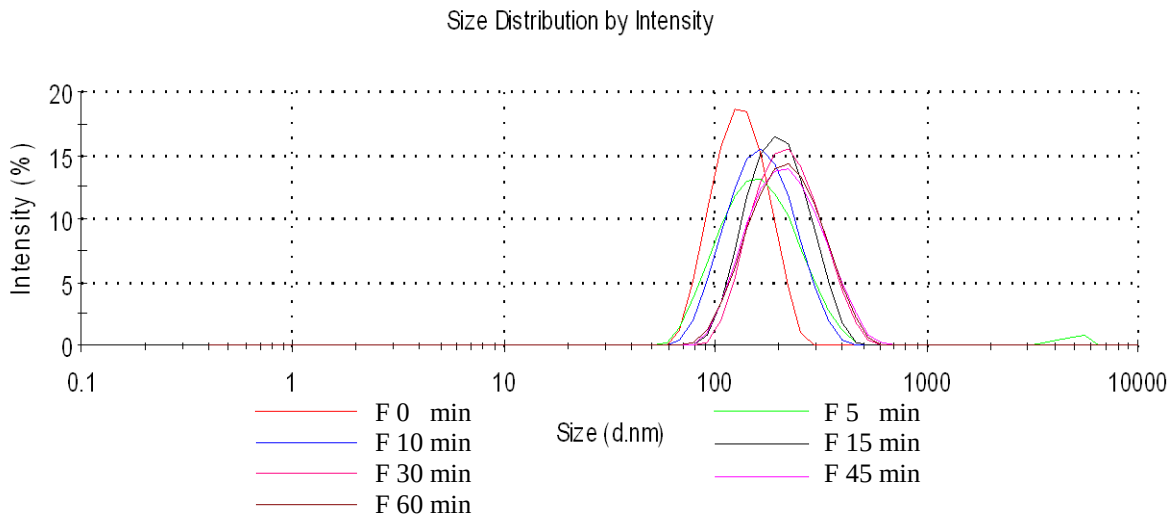

Figure 6.24 Size changes in F3PN in buffer and various concentrations of fructose

Figure 6.25 depicts a clear contrast between the two sugars with the measured Pdi after 15 minutes. The size change of nanoparticles in buffer is higher than in the sugar media. This trend seems to confirm a modulation of the size changes by the nature of the sugar present in the medium.

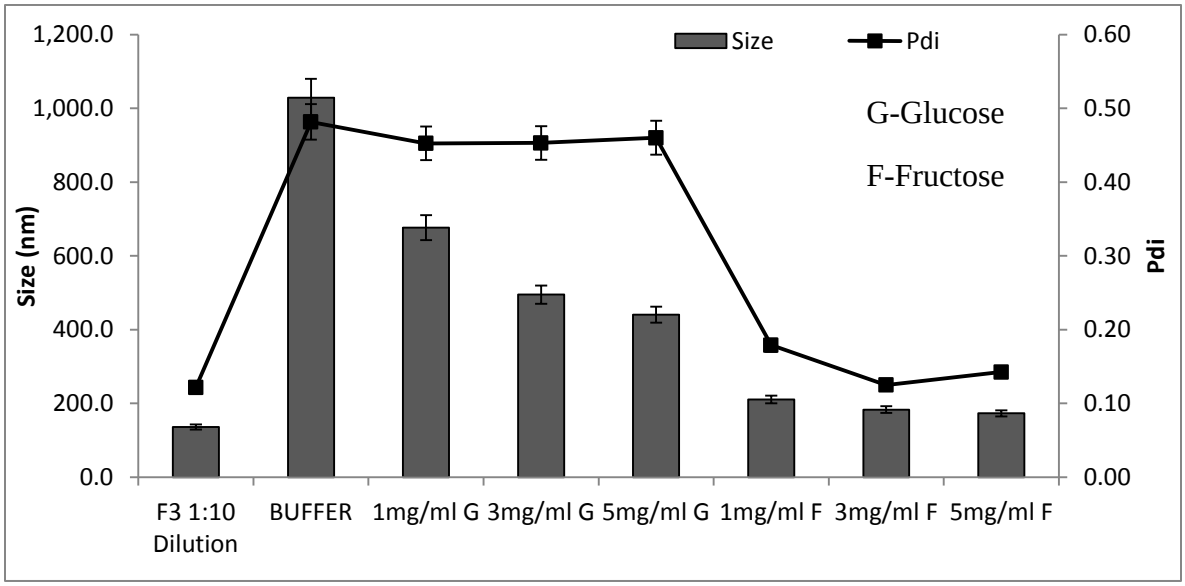

Figure 6.25 Size changes in F3 in buffer and various concentrations glucose and fructose at 15 minutes exposure

The higher affinity of fructose for boronic acid than glucose might have accounted for the slow changes of the particle size in the fructose medium. Furthermore, the decrease in size of the nanoparticles placed in fructose was accompanied by lower Pdi values compared to those observed in glucose. This also confirms that the knitting effect on the nanoparticles by fructose is more pronounced than glucose. It also suggest that the buffer effects on the nanoparticles are somewhat negated in the presence of fructose than glucose.

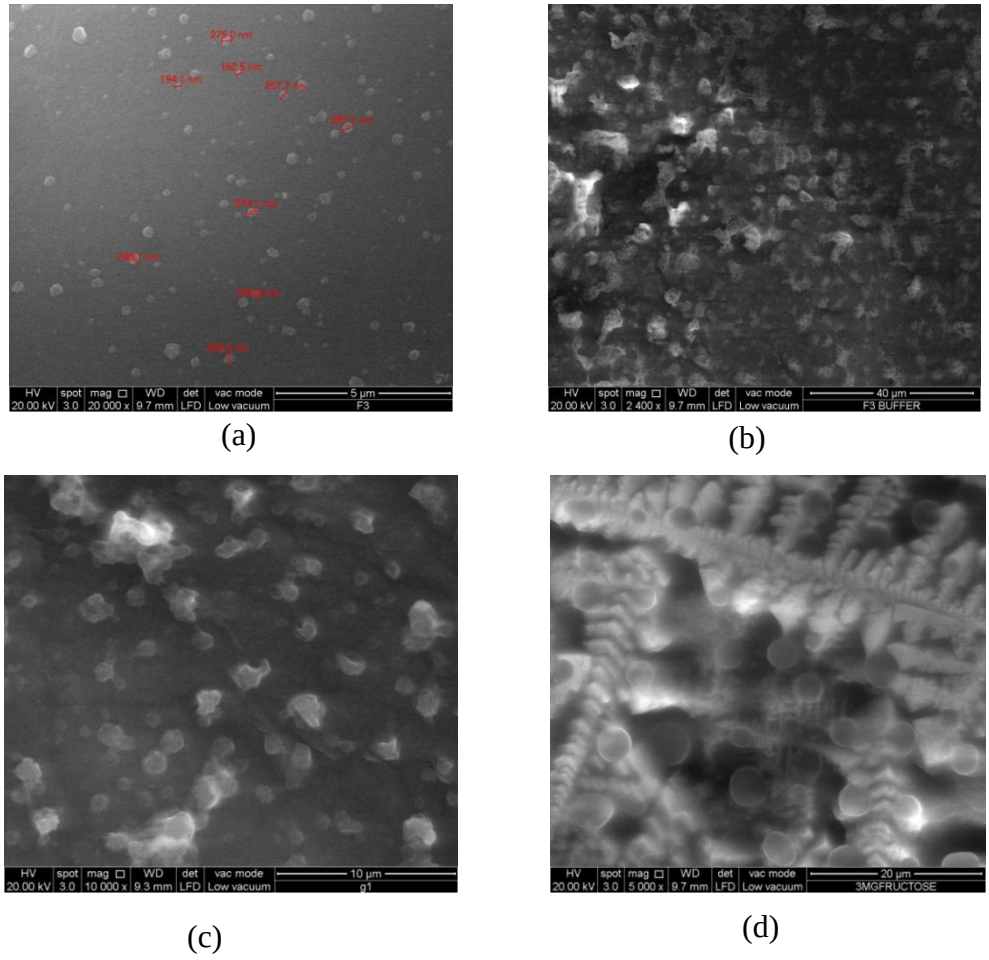

(a) (b)

(c) (d)

Figure 6.26 SEM image of F3PN before (a) after exposure to buffer (b), after exposure TO 3 mg/ml glucose (c) and after exposure to 3 mg/ml fructose (d)

Figure 6.26 (a-d) are images of F3PN before and after exposure to glucose and fructose, it can be seen from 6.26b that the particles that were exposed to buffer were fragmented and appear to

have lost their integrity. Hence these images correlate with the photon correlation data. This implies that the size increase in the after buffer exposure was due to a combination of swelling and fragmentation of the particles matrices. Because the interaction of insulin and the polymer in the formation of the nanoparticle matrices are electrostatic in nature, any changes in the ionic environment will cause disruption of the matrices easily. This disruption will also lead to significant drug release. These images tend to shed more light on the results obtained in the insulin release studies.

The presence of glucose and fructose seemed to help keep the structure intact, though there was an increase in the size of the nanoparticle initially. Thus the matrices were stabilised and not fragmented. Figure 6.26 (c and d) are the SEM images showing the appearance of the particles after exposure to glucose and fructose respectively. The nanoparticles exposed to glucose were a bit fragmented as compared to those exposed to fructose. There are crystals of fructose appearing in figure 6.26 (d) but the nanoparticles present are very spherical and appear to have retained their structure. This data is in concert with the nanosight data in chapter 5 where dummy nanoparticles prepared by ionotropic gelation showed a lesser degree of glucose dependent swelling in high concentration of glucose than lower concentration. It follows that a higher concentration of diol will not induce more swelling over the course of time but rather a reduced swelling at a point due to bidentate interaction between the sugar and the boronic acid moiety.

The higher affinity of fructose for boronic acids than glucose is established (Springsteen and Wang 2002; Hall 2006), in this regard the better protection of the nanoparticulate matrix offered by fructose is related to its affinity for boronic acid, this high affinity of the fructose for boronic acids than by glucose is related to the position of the cis diol in both sugars.

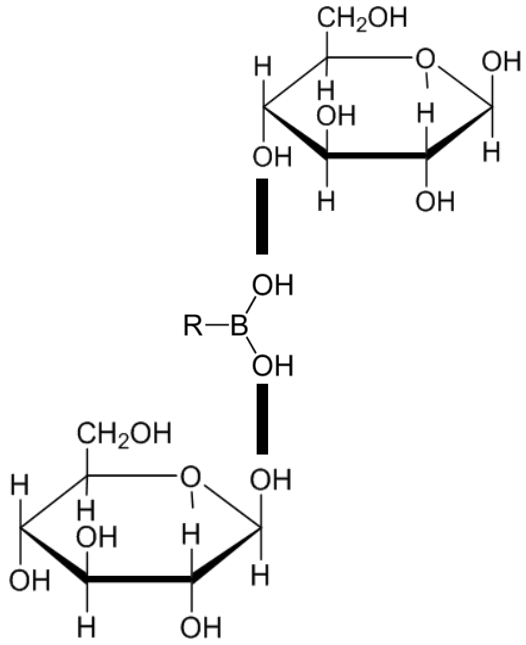

Possible glucose - boronic acid bidentate orientation

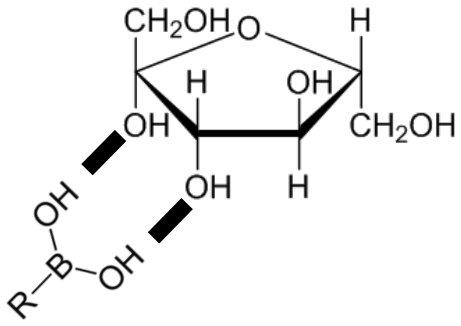

Possible fructose - boronic acid bidentate orientation

Figure 6.27 Structure of glucose and fructose and their possible interaction with boronic acid

Figure 6.27 shows the structure of glucose and fructose and their possible molecular interaction orientation with boronic acid. The position of the two OH groups in the fructose makes it more favourable and easy for enhanced interaction with the boronic acid leading to the formation of the bidentate bond. It can be observed that for free interaction between the OH groups of glucose and those of boronic acid; it would require possibly, two molecules of the glucose to be oriented far apart and free from steric hindrance. It would be a lot more constrained for one molecule of glucose to align in order for its two OH groups to react with the two OH groups of boronic acid. This positioning of the OH groups within the sugar molecules may explain why fructose aids in

retaining the structure of the nanoparticles through bidentate interactions better than glucose and hence lower rates of insulin release in fructose media than glucose.

6.5 CONCLUSION

The functionalised chitosan was successfully formulated into insulin containing nanoparticles via ionotropic gelation and polyelectrolyte complexation method. The nanoparticles produced by PEC method were smaller in size and showed higher insulin encapsulation efficiency. The individual steps in the formulation process parameters have significant effect on the encapsulation efficiency of the system.

The release of insulin from the nanoparticles depended on a complex interplay between the buffer effects and the sugar effects and hence choice of buffer for such studies must be carefully selected and its effects must also be rightly assessed. Though there was glucose and fructose dependent insulin release, the release is affected by the concentration of the sugar.

High concentrations of sugars favour the retention of the nanoparticle integrity through interactions with the boronic acid moiety. This is particularly pronounced with fructose, where bidentate association with boronic acid ensures that the particle remain intact by a seemingly knitted matrix. This results in a diminished permeation of insulin into the media.

CHAPTER 7

SUGGESTIONS FOR FUTURE WORK

The search for alternative insulin delivery systems have led to the developement of various novel systems in *diabetes mellitus* therapeutics. However, extensive research needs to take place before any new formulation can finally reach clinical trails. As an extension from this current project, a few suggestions for futher work are discussed below.

1. **Molecuar weight and degree of deacytyalation of chitosan**

In the present study, low molecular weight chitosan was used throughout the study. Many studies on polymers have shown that, their molecular weight and chemical properties do affect the ease of functionalization and also their formulation properties (Huang *et al*. 2004; Xu and Du 2003). It will be worthwhile studying the effect of molecular weight, degree of deacetylation and the effect of source (type of crustacean used in the process of chitosan production) on the tagging of boronic acid and how these parameters affect the degree of substitution of the boronic acid unto the chitosan and its effect on the glucose adsorption capacity, glucose sensitivity and selectivity

The process of standardising a method for the production of consistent molecular weight and viscosity of chitosan should also be pursued. The molecular weight quoted by Sigma Aldrich as low molecular weight chitosan is in the range of 50,000 - 190,000 Daltons and the viscosity 20-300 cP, (1 wt. % in 1% acetic acid at 25 °C, using a Brookfield viscometer). The range is very wide and it is already established that molecular weight of chitosan affect size and different properties of nanoparticles, hence to get consistent products the starting polymer must have almost the same properties.

2. **Stability studies of the solid and solution of functionalized chitosan conjugates**

The commercial production of chitosan yields different deacetylation grades, molecular weights and viscosities and this chitosan powder is normally stored at room temperature until used. Studies have shown that during storage certain changes occur in the viscosity and moisture content of the chitosan and thus influence the functional properties of the chitosan (No and Prinyawiwatkul 2009). This may lead to inter batch variations when used in formulation.

The dissolution of chitosan in dilute acetic acid is also the start of most applications of chitosan and there have been reports of hydrolysis of chitosan in acetic acid if the acetyl content and molecular weight is high. It will therefore be worthwhile investigating into the effect of the degree of substitution of boronic acid on the stability of the polymer and also subject the functionalized chitosan to different environmental stress and assess stability with time.

We noted that, some solutions of the functionalized chitosan stored at room temperature in vials started showing discolorations after about 30 days of storage and these colour changes were prominent in the F4 and F5 formulations. Hence, the solution of the functionalized chitosan should also be studied at different storage conditions so that appropriate storage conditions can be prescribed.

3. **Cytotoxic studies of functionalised chitosan and functionalised chitosan insulin nanoparticles**

The biocompatibility of chitosan and some modified chitosan such as trimethyl chitosan and thiolated trimethyl chitosan has already been established (Yin *et al*. 2009; Mao *et al*. 2005). The non-cytotoxicity of the chitosan nanoparticles have also been reported by different groups and are known to be biocompatible and biodegradable. It will therefore be in the right direction to study the cytotoxic and biodegradation properties of the new chitosan PBA conjugates and their nanoparticulate insulin formulation to establish its safety for use as a drug delivery system.

4. **Tailoring the chemistry of the conjugate to make the system more glucose responsive**

The glucose and fructose swelling behaviour of the polyelectrolyte complexes showed that the boronic acid in the nanoparticles do interact with the diols, but the effect of fructose was more pronounced than that of glucose. The insulin release profiles of fructose gave a better understanding into the interpretation of the release data than glucose which seemed inconclusive. The chemistry of the conjugates could be looked at again in terms of the introduction of specific chemical groups into the conjugate that can help tailor the sensitivity of the nanoparticles more towards glucose. The conjugates produced by the Schiff's base method by Matsumoto *et al*, (2002) showed selective glucose adsorption than the commercial one used and this selectivity was between glucose and 1-alpha methyl glucoside. On this basis this method was used in making the conjugates to be used for the development of the glucose responsive nanoparticles. The selectivity of the conjugate for fructose was not reported. In this current work the non-selectivity of the conjugate for fructose and glucose with fructose behaviour being more

pronounced have been reported. Therefore tailoring the chemistry of the conjugate to be more glucose sensitive will be worth exploring.

5. **Recovery of the insulin containing nanoparticles**

In order to improve the physical and chemical stability nanoparticulate suspensions, water must be removed. The major obstacle that limits the use of these nanoparticles in aqueous suspensions for extended periods is their physical instability (aggregation/particle fusion) and chemical instability (hydrolysis of polymer materials forming the nanoparticles, drug leakage of nanoparticles and chemical reactivity of medicine during the storage). The most commonly used process which allows for the conversion of solutions or suspensions into solids of sufficient stability for distribution and storage is freeze-drying.

In the course of the project different processes were assessed for the possibility of recovering the colloidal nanoparticles. The method of centrifugation as reported did not work for our system and freeze drying without a cryoprotectant gave undispersible nanoparticles. Freeze drying with a cryoprotectant was also not attempted, because most of the cryoprotectants reported are sugars or derivatives of it (Abdelwahed *et al*. 2006). The reactivity of the boronic acid moieties in the nanoparticle matrix with some sugars has already been established. The possibility of reaction of these cryoprotectants with the boronic acid in the nanoparticle matrix and its effect on insulin release therefore needs to be assessed critically. Pursuing this formulation into making it solid will be plausible, because solid formulation will exhibit more stability than suspension.

6. **Assessing different polymers for possible tagging with boronic acid**

Chitosan is a natural polymer of interest to many researchers because of its availability, biocompatibility and biodegradability. Though this polymer is widely explored as a vehicle for drug delivery, the exploration of other biocompatible polymers both synthetic and natural for the possibility of functionalizing them with boronic acid moieties and their potential use as a glucose responsive insulin delivery system could also be pursued.

APPENDIX

List of Publication and Presentations

Asantewaa, Y.; Aylott, J.; Burley, J.C.; Billa, N.; Roberts, C.J. Correlating Physicochemical Properties of Boronic Acid-Chitosan Conjugates to Glucose Adsorption Sensitivity. *Pharmaceutics* **2013**, *5*, 69-80

Y Asantewaa, JW Aylott, JC Burley, CJ Roberts and N Billa (2011). Development of a chitosan based nanoparticulate glucose responsive insulin delivery system. UK PHARMSCI 2011, 31st August – 2nd September, 2011, East Midlands Conference Centre Nottingham. Page 24.

REFERENCES

Abdelwahed, W., Degobert, G., Stainmesse, S., Fessi, H., 2006. Freeze-drying of nanoparticles: formulation, process and storage considerations. *Advanced Drug Delivery Reviews*, 58(15), pp.1688–713.

Agnihotri, S.A., Mallikarjuna, N.N. & Aminabhavi, T.M., 2004. Recent advances on chitosan-based micro- and nanoparticles in drug delivery. *Journal of Controlled Release*, 100(1), pp.5–28.

Akbuğa, J. & Durmaz, G., 1994. Preparation and evaluation of cross-linked chitosan microspheres containing furosemide. *International Journal of Pharmaceutics*, 111(3), pp.217–222.

Aktaş, Y., Andrieux, K., Alonso, M.J., Calvo, P., Gürsoy, R. N., Couvreur, P. & Capan,Y., 2005. Preparation and in vitro evaluation of chitosan nanoparticles containing a caspase inhibitor. *International Journal of Pharmaceutics*, 298(2), pp.378–83.

Albin, G., Horbett, T.A. & Ratner, B.D., 1985. Glucose sensitive membranes for controlled delivery of insulin: Insulin transport studies. *Journal of Controlled Release*, 2, pp.153–164.

Albin, G.W., Horbett, T.A., Miller, S.R. & Ricker, N.L., 1987. Theoretical and experimental studies of glucose sensitive membranes. *Journal of Controlled Release*, 6(1), pp.267–291.

Alexander, S. K., Azencott, R., Bodmann, B. G., Bouamrani, A., Chiappini, C., Ferrari, M., Liu, X. & Tasciotti, E., 2009. SEM image analysis for quality control of nsanoparticles. In *Computer Analysis of Images and Patterns*. Springer Berlin Heidelberg, pp. 590–597.

Alexeev, V.L., Sharma, A.C., Goponenko, A.V., Das, S., Lednev, I.K., Wilcox, C.S., Finegold, D.N., & Asher, S.A., 2003. High ionic strength glucose-sensing photonic crystal. *Analytical Chemistry*, 75, pp.2316 – 2323.

Amidi, M., Romeijn, S.G., Borchard, G., Junginger, H.E. Hennink, W.E. & Jiskoot, W., 2006. Preparation and characterization of protein-loaded N-trimethyl chitosan nanoparticles as nasal delivery system. *Journal of Controlled Release*, 111(1-2), pp.107–16.

Amos, A.F., McCarty, D.J. & Zimmet, P., 1997. The rising global burden of diabetes and its complications: estimates and projections to the year 2010. *Diabetic Medicine : A Journal of the British Diabetic Association*, 14 Suppl 5, pp.S1–85.

An, B. & Reinhardt, R.R., 2003. Effects of different durations of breath holding after inhalation of insulin using the AERx® insulin diabetes management system. *Clinical Therapeutics*, 25(8), pp.2233–2244.

Anthonsen, M.W., Vårum, K.M. & Smidsrød, O., 1993. Solution properties of chitosans: conformation and chain stiffness of chitosans with different degrees of N-acetylation. *Carbohydrate Polymers*, 22(3), pp.193–201.

Asher, S.A., Alexeev, V.L., Goponenko, A.V., Sharma, A.C., Lednev, I.K., Wilcox, C.S. & Finegold, D.N. 2003. Photonic crystal carbohydrate sensors: low ionic strength sugar sensing. *Journal of the American Chemical Society*, 125(11), pp.3322–9.

Aydın, R.S.T. & Pulat, M., 5-Fluorouracil encapsulated chitosan nanoparticles for ph-stimulated drug delivery: evaluation of controlled release kinetics. *Journal of Nanomaterials*, Volume 201, pp.1–10.

Bae, Y.H., Okano, T. & Kim, S.W., 1989. Insulin permeation through thermo-sensitive hydrogels. *Journal of Controlled Release*, 9(3), pp.271–279.

Bailey, C.J., 1993. Metformin—An update. *General Pharmacology: The Vascular System*, 24(6), pp.1299–1309.

Balfour, J.A. & McTavish, D., 1993. Acarbose. An update of its pharmacology and therapeutic use in diabetes mellitus. *Drugs*, 46(6), pp.1025–54.

Banga, A.K. & Chien, Y.W., 1988. Iontophoretic delivery of drugs: Fundamentals, developments and biomedical applications. *Journal of Controlled Release*, 7(1), pp.1–24.

Bayat, A., Larijani, B., Ahmadian, S., Junginger, H.E., Rafiee-Tehrani, M., & Junginger, H.E., 2008. Preparation and characterization of insulin nanoparticles using chitosan and its quaternized derivatives. *Nanomedicine : Nanotechnology, Biology, and Medicine*, 4(2), pp.115–20.

Beautiful Proteins. Available at: http://beautifulproteins.blogspot.com/. [Accessed October 16, 2013].

Behl, C.R., Kumar, S., Malick, A.W., DelTerzo, S., Higuchi, W.I. & Nash, R. A., 1989. Iontophoretic drug delivery: Effects of physicochemical factors on the skin uptake of nonpeptide drugs. *Journal of Pharmaceutical Sciences*, 78(5), pp.355–60.

Bendayan, M., Ziv, E., Gingras, D., Ben-Sasson, R., Bar-On, H. & Kidron, M. 1994. Biochemical and morpho-cytochemical evidence for the intestinal absorption of insulin in control and diabetic rats. Comparison between the effectiveness of duodenal and colon mucosa. *Diabetologia*, 37(2), pp.119–26.

Berger, J., Reist, M., Mayer, J.M., Felt, O., Peppas, N.A. & Gurny, R., 2004. Structure and interactions in covalently and ionically crosslinked chitosan hydrogels for biomedical applications. *European Journal of Pharmaceutics and Biopharmaceutics*, 57(1), pp.19–34.

Bhumkar, D.R. & Pokharkar, V.B., 2006. Studies on effect of pH on cross-linking of chitosan with sodium tripolyphosphate: a technical note. *AAPS PharmSciTech*, 7(2), p.E50.

Blood Sugar Level Ranges. Available at: http://www.diabetes.co.uk/diabetes_care/blood-sugar-level-ranges.html [Accessed March 6, 2013].

Boonsongrit, Y., Mueller, B.W. & Mitrevej, A., 2008. Characterization of drug-chitosan interaction by 1H NMR, FTIR and isothermal titration calorimetry. *European Journal of Pharmaceutics and Biopharmaceutics*, 69(1), pp.388–95.

Bornstein, J., 1950. A technique for the assay of small quantities of insulin using alloxan diabetic, hypophysectomised adrenalectomised rats. *Australian Journal of Experimental Biology and Medical Science*, 28, pp.87–97.

Brown, L., Siemer, L., Munoz, C. & Langer, R., 1986. Controlled release of insulin from polymer matrices. In vitro kinetics. *Diabetes*, 35(6), pp.684–91.

Brownlee, M. & Cerami, A., 1979. A glucose-controlled insulin-delivery system: semisynthetic insulin bound to lectin. *Science*, 206(4423), pp.1190–1191.

Calvo, P., Remuñan-López, C., Vila-Jato, J.L. & Alonso, M.J. 1997. Chitosan and chitosan/ethylene oxide-propylene oxide block copolymer nanoparticles as novel carriers for proteins and vaccines. *Pharmaceutical Research*, 14(10), pp.1431–6.

Cambre, J.N. & Sumerlin, B.S., 2011. Biomedical applications of boronic acid polymers. *Polymer*, 52(21), pp.4631–4643.

Cefalu, W.T., 2004. Concept, Strategies, and Feasibility of Noninvasive Insulin Delivery. *Diabetes Care*, 27(1), pp.239–246.

Chasin, M. & Langer, R., 1991. Biodegradable Polymers as Drug Delivery Systems. Drugs and the Pharmaceutical Sciences (45), pp.572.

Chien, Y.W. Siddiqui, O., Sun, Y., Shi, W.M. & Liu, J.C. 1987. Transdermal iontophoretic delivery of therapeutic peptides/proteins. I: Insulin. *Annals of the New York Academy of Sciences*, 507, pp.32–51.

Chuah, L.H., 2013, Development of a curcumin-containing mucoadhesive nanoparticulate delivery system for the potential treatment of colorectal cancer. Ph.D Thesis, University of Nottingham, Malaysia

Couvreur, P., Dubernet, C. & Puisieux, F., 1995. Controlled drug delivery with nanoparticles : current possibilities and future trends. *European Journal of Pharmaceutics and Biopharmaceutics*, 41(1), pp.2–13.

Creque, H.M., Langer, R & Folkman, J., 1980. One month of sustained release of insulin from a polymer implant. *Diabetes*, 29(1), pp.37–40.

Csaba, N., Köping-Höggård, M. & Alonso, M.J., 2009. Ionically crosslinked chitosan/tripolyphosphate nanoparticles for oligonucleotide and plasmid DNA delivery. *International Journal of Pharmaceutics*, 382(1-2), pp.205–14.

Dakhara, S. & Anajwala, C., 2010. Polyelectrolyte complex: A pharmaceutical review. *Systematic Reviews in Pharmacy*, 1(2), p.121.

Damgé, C., Maincent, P. & Ubrich, N., 2007. Oral delivery of insulin associated to polymeric nanoparticles in diabetic rats. *Journal of Controlled Release*, 117(2), pp.163–70.

De Moura, M.R., Aouada, F.A. & Mattoso, L.H.C., 2008. Preparation of chitosan nanoparticles using methacrylic acid. *Journal of Colloid and Interface Science*, 321(2), pp.477–83.

DiPiro, J., Talbert, R.L., Yee, G., Matzke, G., Wells, B. & Posey, L.M., 2005. *Diabetes mellitus*. In *Pharmacotherapy: A Pathophysiologic Approach*. New York: McGraw-Hill, pp. 1347–52.

Dong, L.C. & Hoffman, A., 1989. Drug delivery from environmentally sensitive hydrogels. In *2nd Topical Conference on Emerging Technologies in Materials*. San Francisco, pp. 192H.

Du, L., Jin, Y., Zhou, W. & Zhao, J., 2011. Ultrasound-triggered drug release and enhanced anticancer effect of doxorubicin-loaded poly(D, L-lactide-co-glycolide)-methoxy-poly(ethylene glycol) nanodroplets. *Ultrasound in Medicine and Biology*, 37, pp.1252–1258.

Edelman, E.R., Kost, J., Bobeck, H. & Langer, R. 1985. Regulation of drug release from polymer matrices by oscillating magnetic fields. *Journal of Biomedical Materials Research*, 19(1), pp.67–83.

Fajans, S.S., 1990. Scope and heterogeneous nature of MODY. *Diabetes Care*, 13(1), pp.49–64.

Fan, Y.F.G., Wang, Y.N. & Ma, J.B., 2006. Preparation of insulin nanoparticles and their encapsulation with biodegradable polyelectrolytes via the layer-by-layer adsorption. *International Journal of Pharmaceutics*, 324(2), pp.158–67.

Faniran, J.A. & Shurvell, H.F., 2011. Infrared spectra of phenylboronic acid (normal and deuterated) and diphenyl phenylboronate. *Canadian Journal of Chemistry*, 1968, 46(12), pp. 2089-2095.

Fernández-Urrusuno, R., Calvo, P., Remuñán-López, C., Vila-Jato, J.L. & Alonso, M.J. 1999a. Enhancement of nasal absorption of insulin using chitosan nanoparticles. *Pharmaceutical Research*, 16(10), pp.1576–1581.

Fildes, F.J.T., 1976. British patent 1. 400,217.

Fisher, B. V & Smith, D., 1986. HPLC as a replacement for the animal response assays for insulin. *Journal of Pharmaceutical and Biomedical Analysis*, 4(3), pp.377–87.

Fleige, E., Quadir, M.A. & Haag, R., 2012. Stimuli-responsive polymeric nanocarriers for the controlled transport of active compounds: concepts and applications. *Advanced Drug Delivery Reviews*, 64(9), pp.866–84.

Gerstein, H.C. & Haynes, R.B., 2001. *Evidence-Based Diabetes Care*, PMPH-USA. Available at: http://books.google.com/books?hl=en&lr=&id=pNR_ue_1bjkC&pgis=1 [Accessed June 11, 2012].

Goldberg, M. & Gomez-Orellana, I., 2003. Challenges for the oral delivery of macromolecules. *Nature reviews. Drug discovery*, 2(4), pp.289–95.

Goycoolea, F.M., Heras, A., Aranaz, I., Galed, G., Fernández-Valle, M.E. & Argüelles-Monal, W., 2003. Effect of chemical crosslinking on the swelling and shrinking properties of thermal and ph-responsive chitosan hydrogels. *Macromolecular Bioscience*, 3(10), pp.612–619.

Grobelny, J., DelRio, F.W., Pradeep, N., Kim, D., Hackley, V.A., & Cook, R.F. 2011. Size measurement of nanoparticles using atomic force microscopy. *Methods in Molecular Biology (Clifton, N.J.)*, 697, pp.71–82.

Groen, J., Kamminga, C. E., Willebrands, A. F. & Blickman, J. R., 1952. Evidence for the presence of insulin in blood serum. A method for an approximate determination of the insulin content of blood. *Journal of Clinical Investigation*, 31, pp.97–106.

Gu, Z., Dang, T.T., Ma, M., Tang, B.C., Cheng, H., Jiang, S., Dong, Y., Zhang, Y. & Anderson, D.G ., 2013. Glucose-responsive microgels integrated with enzyme nanocapsules for closed-loop insulin delivery. *ACS Nano*, 7(8), pp.6758–66.

Guntu, V.P. & Dhand, R., 2007. Inhaled insulin: extending the horizons of inhalation therapy. *Respiratory Care.*, 52(7), pp.911–22.

Guthrie, R., 1997. Treatment of non-insulin-dependent diabetes mellitus with metformin. *The Journal of the American Board of Family Practice*, 10(3), pp.213–21.

Hales, C.N. & Randle, P.J., 1963. Immunoassay of insulin with insulin-antibody precipitate. Available at: http://www.biochemj.org/bj/088/0137/bj0880137_browse.htm [Accessed October 19, 2013].

Hall, D.G., 2006. Structure, Properties, and Preparation of Boronic Acid Derivatives. Overview of Their Reactions and Applications. In G. D. Hall, ed. *Boronic Acids: Preparation and applications in organic synthesis and medicine*. Weinheim, Germany KGaA, Weinheim, FRG.: Wiley-VCH Verlag GmbH & Co., pp. 1–99.

Hall, J.B., Dobrovolskaia, M.A., Patri, A.K. & McNeil, S.E. 2007. Characterization of nanoparticles for therapeutics. *Nanomedicine (London, England)*, 2(6), pp.789–803.

Han, J., Guenier, A., Salmieri, S. & Lacroix, M., 2008. Alginate and chitosan functionalization for micronutrient encapsulation. *Journal of Agricultural and Food Chemistry*, 56(7), pp.2528–35.

Harish Prashanth, K. V & Tharanathan, Rudrapatnam N., 2006. Crosslinked chitosan--preparation and characterization. *Carbohydrate Research*, 341(1), pp.169–73.

Hasanovic, A., Zehl, M., Reznicek, G. & Valenta, C. 2009. Chitosan-tripolyphosphate nanoparticles as a possible skin drug delivery system for aciclovir with enhanced stability. *The Journal of Pharmacy and Pharmacology*, 61(12), pp.1609–16.

Hassan, C.M., Doyle, Francis J. & Peppas, Nikolaos A., 1997. Dynamic Behavior of Glucose-Responsive Poly(methacrylic acid- g -ethylene glycol) Hydrogels. *Macromolecules*, 30(20), pp.6166–6173.

He, Ping, Davis, Stanley S. & Illum, Lisbeth, 1998. In vitro evaluation of the mucoadhesive properties of chitosan microspheres. *International Journal of Pharmaceutics*, 166(1), pp.75–88.

Heinemann, L., 2008. The failure of exubera: are we beating a dead horse? *Journal of Diabetes Science and Technology*, 2(3), pp.518–29.

Hirokawa, Y. & Tanaka, T., 1984. Volume phase transition in a nonionic gel. *The Journal of Chemical Physics*, 81(12), pp.6379–6380.

Huang, M., Khor, E. & Lim, L.-Y., 2004. Uptake and Cytotoxicity of Chitosan Molecules and Nanoparticles: Effects of Molecular Weight and Degree of Deacetylation. *Pharmaceutical Research*, 21(2), pp.344–353.

Hollinger, J.O. ed., 1995. *Biomedical Applications of Synthetic Biodegradable Polymers*, Boca Raton, FL: CRC Press.

Hovgaard, L. & Brøndsted, H., 1995. Dextran hydrogels for colon-specific drug delivery. *Journal of Controlled Release*, 36(1-2), pp.159–166.

Huffman, A.S., Afrassiabi, A. & Dong, L.C., 1986. Thermally reversible hydrogels: II. Delivery and selective removal of substances from aqueous solutions. *Journal of Controlled Release*, 4(3), pp.213–222.

Illum, L, Farraj, N.F. & Davis, S S., 1994. Chitosan as a novel nasal delivery system for peptide drugs. *Pharmaceutical Research*, 11(8), pp.1186–9.

Insulin Basics - American Diabetes Association®. Available at: http://www.diabetes.org/living-with-diabetes/treatment-and-care/medication/insulin/insulin-basics.html. [Accessed October 23, 2013].

Insulin: Martindale: The Complete Drug Reference. Available at: http://www.medicinescomplete.com/mc/martindale/2009/7202-e.htm [Accessed October 6, 2013].

Janes, K.A., Fresneau, M.P., Marazuela, A., Fabra, A. & Alonso, M.J., 2001. Chitosan nanoparticles as delivery systems for doxorubicin. *Journal of Controlled Release*, 73(2-3), pp.255–267.

Jin, X., Zhang, X., Wu, Z., Teng, D., Zhang, X., Wang, Y., Wang, Z. & Li, C., 2009. Amphiphilic random glycopolymer based on phenylboronic acid: synthesis, characterization, and potential as glucose-sensitive matrix. *Biomacromolecules*, 10(6), pp.1337–45.

Jintapattanakit, A., Junyaprasert, V.B., Mao, S., Sitterberg, J., Bakowsky, U. & Kissel, T., 2007. Peroral delivery of insulin using chitosan derivatives: a comparative study of polyelectrolyte nanocomplexes and nanoparticles. *International Journal of Pharmaceutics*, 342(1-2), pp.240–9.

Jovanovic, L., 2001. Gestational Diabetes Mellitus. *JAMA: The Journal of the American Medical Association*, 286(20), pp.2516–2518

Jung, T., Kamm, W., Breitenbach, A., Kaiserling, E., Xiao, J.X. & Kissel, T., 2000. Biodegradable nanoparticles for oral delivery of peptides: is there a role for polymers to affect mucosal uptake? *European Journal of Pharmaceutics and Biopharmaceutics.* 50(1), pp.147–60.

Kataoka, K., Miyazaki, H., Okano, T. & Sakurai, Y., 1994. Sensitive glucose-induced change of the lower critical solution temperature of poly[n,n-(dimethylacrylamide)-co-3-(acrylamido)-phenylboronic acid] in physiological saline. *Macromolecules*, 27(4), pp.1061–1062.

Kean, T. & Thanou, M., 2010. Biodegradation, biodistribution and toxicity of chitosan. *Advanced Drug Delivery Reviews*, 62(1), pp.3–11.

Kennedy, F.P., 1991. Recent developments in insulin delivery techniques. Current status and future potential. *Drugs*, 42(2), pp.213–227.

Kikuchi, A., Suzuki, K., Okabayashi, O., Hoshino, H., Kataoka, K., Sakurai, Y. & Okano, T., 1996. Glucose-sensing electrode coated with polymer complex gel containing phenylboronic Acid. *Analytical chemistry*, 68(5), pp.823–8.

Kim, C., Newton, K.M. & Knopp, R.H., 2002. Gestational Diabetes and the Incidence of Type 2 Diabetes: A systematic review. *Diabetes Care*, 25(10), pp.1862–1868.

Kim, D., Mudaliar, S., Chinnapongse, S., Chu, N., Boies, S.M., Davis, T., Perera, A.D., Fishman, R.S., Shapiro, D.A. & Henry, R. 2003. Dose-response relationships of inhaled insulin delivered via the Aerodose insulin inhaler and subcutaneously injected insulin in patients with type 2 diabetes. *Diabetes care*, 26(10), pp.2842–7.

Kimiko, M., Seminoff, L.A., Holmberg, D.L., Gleeson, J.M., Wilson, D. E. & Mack, E.J., 1990. Self-regulated glycosylated insulin delivery. *Journal of Controlled Release*, 11(1-3), pp.193–201.

King, H., Aubert, R.E. & Herman, W.H., 1998. Global burden of diabetes, 1995-2025: prevalence, numerical estimates, and projections. *Diabetes care*, 21(9), pp.1414–31.

Kisel, M.A., Kulik, L.N., Tsybovsky, I.S., Vlasov, A.P., Vorob'yov, M.S., Kholodova, E.A. & Zabarovskaya, Z.V., 2001. Liposomes with phosphatidylethanol as a carrier for oral delivery of insulin: studies in the rat. *International Journal of Pharmaceutics*, 216(1-2), pp.105–14.

Kitagawa, T., Owada, M., Urakami, T. & Yamauchi, K., 1998. Increased incidence of non-insulin dependent diabetes mellitus among japanese schoolchildren correlates with an increased intake of animal protein and fat. *Clinical Pediatrics*, 37(2), pp.111–115.

Kitagawa, T., Owada, M., Urakami, T. & Tajima, N., 1994. Epidemiology of type 1 (insulin-dependent) and type 2 (non-insulin-dependent) diabetes mellitus in Japanese children. *Diabetes Research and Clinical Practice*, 24, pp.S7–S13.

Kitano, S., Hisamitsu, I., Koyama, Y., Kataoka, K., Okano, T. & Sakurai, Y., 1991. Effect of the incorporation of amino groups in a glucose-responsive polymer complex having phenylboronic acid moieties. *Polymers for Advanced Technologies*, 2(5), pp.261–264.

Kittur, F.S., Harish Prashanth, K.V., Udaya Sankar, K. & Tharanathan, R.N. 2002. Characterization of chitin, chitosan and their carboxymethyl derivatives by differential scanning calorimetry. *Carbohydrate Polymers*, 49(2), pp.185–193.

Kopeček, J., Vacík, J. & Lím, D., 1971. Permeability of membranes containing ionogenic groups. *Journal of Polymer Science Part A-1: Polymer Chemistry*, 9(10), pp.2801–2815.

Kost, J., Horbett, T.A., Ratner, B.D. & Singh, M., 2004. Glucose-sensitive membranes containing glucose oxidase: activity, swelling, and permeability studies. *Journal of Biomedical Materials Research*, 19(9), pp.1117–33.

Kost, J. & Langer, R., 2001. Responsive polymeric delivery systems. *Advanced Drug Delivery Reviews*, 46(1-3), pp.125–148.

Kost, J., Leong, K. & Langer, R., 1989. Ultrasound-enhanced polymer degradation and release of incorporated substances. *Proceedings of the National Academy of Sciences of the United States of America*, 86(20), pp.7663–6.

Kost, J., Leong, K. & Langer, R., 1988. Ultrasonically controlled polymeric drug delivery. *Makromolekulare Chemie. Macromolecular Symposia*, 19(1), pp.275–285.

Kost, J., Wolfrum, J. & Langer, R., 1987. Magnetically enhanced insulin release in diabetic rats. *Journal of Biomedical Materials Research*, 21(12), pp.1367–73.

Kumria, R. & Goomber, G., 2011. Emerging trends in insulin delivery: Buccal route. *Journal of Diabetology*, 2(1), pp.1–7.

Kunkel, A., Günter, S., Dette, C., & Wätzig, H., 1997. Quantitation of insulin by capillary electrophoresis and high-performance liquid chromatography method comparison and validation. *Journal of Chromatography A*, 781(1-2), pp.445–455.

Langer, Robert, 1993. Polymer-controlled drug delivery systems. *Accounts of Chemical Research*, 26(10), pp.537–542.

Leo, E., Contado, C., Bortolotti, F., Pavan, B., Scatturin, A., Tosi, G., Manfredini, S., Angusti, A. & Dalpiaz, A., 2006. Nanoparticle formulation may affect the stabilization of an antiischemic prodrug. *International Journal of Pharmaceutics*, 307(1), pp.103–13.

Leo, E., Brina, B., Forni, F. Vandelli, M.A., 2004. In vitro evaluation of PLA nanoparticles containing a lipophilic drug in water-soluble or insoluble form. *International journal of pharmaceutics*, 278(1), pp.133–41.

Leprince, L., Dogimont, A., Magnin, D. & Demoustier-Champagne, S. 2010. Dexamethasone electrically controlled release from polypyrrole-coated nanostructured electrodes. *Journal of Material Science: Material in Medicine*, 21, pp.925–930.

Levy, D., Kost, J., Meshulam, Y. & Langer, R., 1989. Effect of ultrasound on transdermal drug delivery to rats and guinea pigs. *The Journal of Clinical Investigation*, 83(6), pp.2074–8.

Lin, Y.-H., Chang, C.-H., Wu, Y.-S., Hsu, Y.-M., Chiou, S.-F. & Chen, Y.-J. 2009. Development of pH-responsive chitosan/heparin nanoparticles for stomach-specific anti-Helicobacter pylori therapy. *Biomaterials*, 30(19), pp.3332–42.

Liu, H. & Gao, C., 2009. Preparation and properties of ionically cross-linked chitosan nanoparticles. *Polymers for Advanced Technologies*, 20(7), pp.613–619.

López-León, T., Carvalho, E.L.S., Seijo, B., Ortega-Vinuesa, J.L. & Bastos-González, D., 2005. Physicochemical characterization of chitosan nanoparticles: electrokinetic and stability behavior. *Journal of Colloid and Interface Science*, 283(2), pp.344–51.

Ma, Z., Lim, T.M. & Lim, L.-Y., 2005. Pharmacological activity of peroral chitosan-insulin nanoparticles in diabetic rats. *International Journal of Pharmaceutics*, 293(1-2), pp.271–80.

Ma, Z., Yeoh, H.H. & Lim, L.-Y., 2002. Formulation pH modulates the interaction of insulin with chitosan nanoparticles. *Journal of Pharmaceutical Sciences*, 91(6), pp.1396–404.

Makino, K., Mack, E.J., Okano, T. & Kim, S.W., 1991. Self-regulated delivery of insulin from microcapsules. *Biomaterials, Artificial Cells, and Immobilization Biotechnology*, 19(1), pp.219–28

Malloy, A., 2011. Count, size and visualize nanoparticles. *Materials Today*, 14(4), pp.170–173.

Mao, H.Q., Roy, K., Troung-Le, V.L., Janes, K.A. Lin, K.Y. Wang, Y., August, J.T. & Leong, K.W. 2001. Chitosan-DNA nanoparticles as gene carriers: synthesis, characterization and transfection efficiency. *Journal of Controlled Release*, 70(3), pp.399–421.

Mao, S., Bakowsky, U., Jintapattanakit, A. & Kissel, T. 2006. Self-assembled polyelectrolyte nanocomplexes between chitosan derivatives and insulin. *Journal of Pharmaceutical Sciences*, 95(5), pp.1035–48.

Mao, S., Germershaus, O., Fischer, D., Linn, T., Schnepf, R. & Kissel, T. 2005. Uptake and transport of PEG-graft-trimethyl-chitosan copolymer-insulin nanocomplexes by epithelial cells. *Pharmaceutical Research*, 22(12), pp.2058–68.

Marks, H.P., 1925. The biological assay in insulin preparations in comparison with a stable standard. *British Medical Journal*, 2, pp.1102–1104.

Matsumoto, A., Ikeda, S., Harada, A. & Kataoka, K., 2003. Glucose-responsive polymer bearing a novel phenylborate derivative as a glucose-sensing moiety operating at physiological pH conditions. *Biomacromolecules*, 4(5), pp.1410–6.

Matsumoto, M., Shimizu, T. & Kondo, K., 2002. Selective adsorption of glucose on novel chitosan gel modified by phenylboronate. *Separation and Purification Technology*, 29(3), pp.229–233.

McClean, S., Prosser, E., Meehan, E., O'Malley, D., Clarke, N., Ramtoola, Z. & Brayden, D., 1998. Binding and uptake of biodegradable poly-dl-lactide micro- and nanoparticles in intestinal epithelia. *European Journal of Pharmaceutical Sciences*, 6(2), pp.153–163.

Mercolini, L., Musenga, A., Saladini, B., Bigucci, F., Luppi, B., Zecchi, V. & Raggi, M.A., 2008. Determination of insulin in innovative formulations by means of LC coupled to fluorescence detection. *Journal of Pharmaceutical and Biomedical Analysis*, 48(5), pp.1303–9.

Mesiha, M.S., Ponnapula, S. & Plakogiannis, F., 2002. Oral absorption of insulin encapsulated in artificial chyles of bile salts, palmitic acid and alpha-tocopherol dispersions. *International Journal of Pharmaceutics* 249(1-2), pp.1-5.

Miyata, T., Uragami, T. & Nakamae, K., 2002. Biomolecule-sensitive hydrogels. *Advanced Drug Delivery Reviews*, 54(1), pp.79–98.

Moslemi, P., Najafabadi, A.R. & Tajerzadeh, H., 2003. A rapid and sensitive method for simultaneous determination of insulin and A21-desamido insulin by high-performance liquid chromatography. *Journal of Pharmaceutical and Biomedical Analysis*, 33(1), pp.45–51.

Motornov, M., Roiter, Y., Tokarev, I. & Minko, S., 2010. Stimuli-responsive nanoparticles, nanogels and capsules for integrated multifunctional intelligent systems. *Progress in Polymer Science*, 35(1-2), pp.174–211.

Mourya, V.K. & Inamdar, N.N., 2009. Trimethyl chitosan and its applications in drug delivery. *Journal of Materials Science. Materials in Medicine*, 20(5), pp.1057–79.

Nakamae, K., Miyata, T., Jikihara, A. & Hoffman, A.S., 1994. Formation of poly(glucosyloxyethyl methacrylate)-concanavalin A complex and its glucose-sensitivity. *Journal of Biomaterials Science. Polymer edition*, 6(1), pp.79–90.

No, H.K. & Prinyawiwatkul, W., 2009. Stability of chitosan powder during long-term storage at room temperature. *Journal of Agricultural and Food Chemistry*, 57(18), pp.8434–8.

Obaidat, A. A. & Park, K., 1996. Characterization of glucose dependent gel-sol phase transition of the polymeric glucose-concanavalin A hydrogel system. *Pharmaceutical Research*, 13(7), pp.989–95.

Obaidat, A.A. & Park, K., 1997. Characterization of protein release through glucose-sensitive hydrogel membranes. *Biomaterials*, 18(11), pp.801–806.

Okabe, K., Yamaguchi, H. & Kawai, Y., 1986. New iontophoretic transdermal administration of the beta-blocker metoprolol. *Journal of Controlled Release*, 4(2), pp.79–85.

Okano, T., Bae, Y.H. & Kim, S.W., 1990. Temperature responsive controlled drug delivery. In J. Kost, ed. *Pulsed and Self-regulated Drug Delivery*. Boca Raton, FL: CRC Press, pp. 17–46.

Oliva, A., Fariña, J. & Llabrés, M., 2000. Development of two high-performance liquid chromatographic methods for the analysis and characterization of insulin and its degradation products in pharmaceutical preparations. *Journal of Chromatography. B, Biomedical Sciences and Applications*, 749(1), pp.25–34.

Osman, Z. & Arof, A.., 2003. FTIR studies of chitosan acetate based polymer electrolytes. *Electrochimica Acta*, 48(8), pp.993–999.

Owens, D.R., Zinman, B. & Bolli, G., 2003. Alternative routes of insulin delivery. *Diabetic Medicine : A Journal of the British Diabetic Association*, 20(11), pp.886–98.

Parker, R.S., Doyle, F J & Peppas, N A., 1999. A model-based algorithm for blood glucose control in type I diabetic patients. *IEEE Transactions on Bio-medical Engineering*, 46(2), pp.148–57.

Paul McGee, J., 1995. Zero order release of protein from poly(-lactide-co-glycolide) microparticles prepared using a modified phase separation technique. *Journal of Controlled Release*, 34(2), pp.77–86.

Phenylboronic acid purum, ≥97.0% (HPLC) | Sigma-Aldrich. Available at: http://www.sigmaaldrich.com/catalog/product/fluka/78181?lang=en&region=MY. [Accessed October 16, 2013].

Pinto Reis, C., Neufeld, R. J., Ribeiro, A.J. & Veiga, F., 2006. Nanoencapsulation I. Methods for preparation of drug-loaded polymeric nanoparticles. *Nanomedicine : Nanotechnology, Biology, and Medicine*, 2(1), pp.8–21.

Prego, C., Torres, D., Fernandez-Megia, E., Novoa-Carballal, R., Quiñoá, E. & Alonso, M.J., 2006. Chitosan-PEG nanocapsules as new carriers for oral peptide delivery. Effect of chitosan pegylation degree. *Journal of Controlled Rrelease*, 111(3), pp.299–308.

Qi, L., Xu, Z., Jiang, X., Hu, C. & Zou, X., 2004. Preparation and antibacterial activity of chitosan nanoparticles. *Carbohydrate Research*, 339(16), pp.2693–700.

Qi, W., Yan, X., Fei, J., Wang, A., Cui, Y. & Li, J., 2009. Triggered release of insulin from glucose-sensitive enzyme multilayer shells. *Biomaterials*, 30, pp.2799–2806.

Rave, K.M., Heise, T., Pfutzner, A., Steiner, S. & Heinemann, L., 2000. Results of a dose–response study with a new pulmonary insulin formulation and inhaler. *Diabetes*, 49(Suppl. 1), p.A7.

Ravi Kumar, M.N., 2000. A review of chitin and chitosan applications. *Reactive and Functional Polymers*, 46(1), pp.1–27.

Reis, C.P. & Damgé, C., 2012. Nanotechnology as a promising strategy for alternative routes of insulin delivery. *Methods in Enzymology*, 508, pp.271–94.

Riesler, P., 1967. *Insulin membranes and metabolism*, Baltimore.: Williams and Wilkins C.

Richter, B. & Neises, G., 2003. "Human" insulin versus animal insulin in people with diabetes mellitus. *The Cochrane database of systematic reviews*, (3), p.CD003816.

Sadeghi, A.M.M., Dorkoosh, F.A., Avadi, M.R., Saadat, P., Rafiee-Tehrani, M. & Junginger, H.E., 2008. Preparation, characterization and antibacterial activities of chitosan, N-trimethyl

chitosan (TMC) and N-diethylmethyl chitosan (DEMC) nanoparticles loaded with insulin using both the ionotropic gelation and polyelectrolyte complexation methods. *International Journal of Pharmaceutics*, 355(1-2), pp.299–306.

Saltiel, A.R. & Horikashi, H., 1995. Thiazolinediones are novel insulin-sensitising agents',. *Current Opinion in Endocrinology and Diabetes*, 2, pp.341–347.

Sarmento, B., Ferreira, D., Veiga, F. & Ribeiro, A., 2006. Characterization of insulin-loaded alginate nanoparticles produced by ionotropic pre-gelation through DSC and FTIR studies. *Carbohydrate Polymers*, 66(1), pp.1–7.

Sarmento, B., Martins, S., Ferreira, D. & Souto, E.B., 2006. Development and characterization of new insulin containing polysaccharide nanoparticles. *Colloids and surfaces. B, Biointerfaces*, 53(2), pp.193–202.

Sato, J., Kitahara, K., Sato, T., Inamura, T., Kanazawa, M., Notoya, Y. & Hayashi, T., 1996. Measurement of insulin content at different sites of insulin preparation vial. *Currrent Therapeutic Research*, 57(8), pp.579–588.

Sawicka, K., Sahota, T,. Taylor, M.J., & Tanna, S. 2006. Development of a reversed-phase high-performance liquid chromatography method for the analysis of components from a closed-loop insulin delivery system. *Journal of Chromatography. A*, 1132(1-2), pp.117–23.

Schmidt, D.J., Moskowitz, J.S. & Hammond, P.T., 2010. Electrically triggered release of a small molecule drug from a polyelectrolyte multilayer coating. *Chemistry of Matrerials*, 22, pp.6416–6425.

Seda Tığlı Aydın, R. & Pulat, M., 2012. 5-Fluorouracil Encapsulated Chitosan Nanoparticles for pH-Stimulated Drug Delivery: Evaluation of Controlled Release Kinetics. *Journal of Nanomaterials*, 2012, p.10.

Shah, N.K., Deeb, W.E., Choksi, R. & Epstein, B.J., 2012. Dapagliflozin: A Novel SGLT2 Inhibitor for Type 2 DM: Safety and Tolerability. *Pharmacotherapy*, 32(1), pp.80–94.

Shantha, K.L. & Harding, D.R.K., 2000. Preparation and in-vitro evaluation of poly[N-vinyl-2-pyrrolidone-polyethylene glycol diacrylate]-chitosan interpolymeric pH-responsive hydrogels for oral drug delivery. *International Journal of Pharmaceutics*, 207(1-2), pp.65–70.

Shaw, J.E., Sicree, R.A. & Zimmet, P.Z., 2010. Diabetes Atlas Global estimates of the prevalence of diabetes for 2010 and 2030. *Diabetes Research and Clinical Practice*, 87, pp.4–14.

Shiino, D., Murata, Y., Kubo, A., Kim, Y., Kataoka, K., Koyama, Y., Kikuchi, A., Yokoyama, M., Sakurai, Y. & Okano, T. 1995. Amine containing phenylboronic acid gel for glucose-responsive insulin release under physiological pH. *Journal of Controlled Release*, 37(3), pp.269–276.

Smoum, R., Rubinstein, A. & Srebnik, M., 2006. Chitosan-pentaglycine-phenylboronic acid conjugate: a potential colon-specific platform for calcitonin. *Bioconjugate Chemistry*, 17(4), pp.1000–7.

Soppimath, K.S., Aminabhavi, T.M., Kulkarni, A. R., & Rudzinski, W.E., 2001. Biodegradable polymeric nanoparticles as drug delivery devices. *Journal of Controlled Release*, 70(1-2), pp.1–20.

Soppimath, K.S., Aminabhavi, T.M., Dave, A.M., Kumbar, S.G. & Rudzinski, W.E. 2002. Stimulus-responsive "smart" hydrogels as novel drug delivery systems. *Drug Development and Industrial Pharmacy*, 28(8), pp.957–74.

Springsteen, G. & Wang, B., 2002. A detailed examination of boronic acid–diol complexation. *Tetrahedron*, 58(26), pp.5291–5300.

Sreenivasan, K., 1996. Thermal stability studies of some chitosanmetal ion complexes using differential scanning calorimetry. *Polymer Degradation and Stability*, 52(1), pp.85–87.

Structural Biochemistry/Protein function/Insulin - Wikibooks, open books for an open world. Available at: http://en.wikibooks.org/wiki/Structural_Biochemistry/Protein_function/Insulin. [Accessed October 23, 2013].

Tang, E.S.K., Huang, M. & Lim, L.Y., 2003. Ultrasonication of chitosan and chitosan nanoparticles. *International Journal of Pharmaceutics*, 265(1-2), pp.103–114.

Traitel, T., Cohen, Y. & Kost, J., 2000. Characterization of glucose-sensitive insulin release systems in simulated in vivo conditions. *Biomaterials*, 21(16), pp.1679–87.

Transmission Electron Microscope and Scanning Electron Microscopes - Nuclear Engineering Division (Argonne). Available at: http://www.ne.anl.gov/facilities/sems_tem/. [Accessed October 24, 2013].

Tsai, M.-L., Chen, R.-H., Bai, S.-W. & Chen, W.-Y., 2011. The storage stability of chitosan/tripolyphosphate nanoparticles in a phosphate buffer. *Carbohydrate Polymers*, 84(2), pp.756–761.

Tzafriri, A.R., 2003. Michaelis–Menten Kinetics at High Enzyme Concentrations. *Bulletin of Mathematical Biology*, 65, pp.1111–1129. .

Uner, M. & Yener, G., 2007. Importance of solid lipid nanoparticles (SLN) in various administration routes and future perspectives. *International Journal of Nanomedicine*, 2(3), pp.289–300.

Vandeveld, K. & Kiekens, P., 2004. Structure analysis and degree of substitution of chitin, chitosan and dibutyrylchitin by FT-IR spectroscopy and solid state C NMR. *Carbohydrate Polymers*, 58(4), pp.409–416.

Vila, A., Sánchez, A., Janes, K., Behrens, I., Kissel, T., Jato, J.L.V. & Alonso, M.J., 2004. Low molecular weight chitosan nanoparticles as new carriers for nasal vaccine delivery in mice. *European Journal of Pharmaceutics and Biopharmaceutics*, 57(1), pp.123–131.

Weiss, A.M. & Grodzinsky, A.J. Yarmush, M.L., 1986. Chemically and electrically controlled membranes: size specific transport of fluorescent solutes through PMMA membranes. *AICHE Symp. Ser.*, 82(250), pp.85–98.

WHO | Diabetes. Available at: http://www.who.int/mediacentre/factsheets/fs312/en/index.html [Accessed June 26, 2012].

Winegrad, A. & Renold, A.E., 1958. Studies on rat adipose tissue in vitro. *Journal of Biological Chemistry*, 233, pp.267–272.

Wright, P.H., 1960. Plasma-insulin activity in acromegaly and spontaneous hypoglycaemia. *Lancet*, 1(7131), pp.951–4.

Wu, H., Wang, J., Kang, X., Wang, C., Wang, D., Liu, J., Aksay, I.A. & Lin, Y.. 2009. Glucose biosensor based on immobilization of glucose oxidase in platinum nanoparticles/graphene/chitosan nanocomposite film. *Talanta*, 80(1), pp.403–6.

Wu, S., Tao, Y., Zhang, H. & Su, Z., 2011. Preparation and characterization of water-soluble chitosan microparticles loaded with insulin using the polyelectrolyte complexation method. J*ournal of Nanomaterials*, 2011(1-6).

Wu, Y., Yang, W., Wang, C., Hu, J. & Fu, S., 2005. Chitosan nanoparticles as a novel delivery system for ammonium glycyrrhizinate. *International Journal of Pharmaceutics*, 295(1-2), pp.235–45.

Wu, Z., Zhang, S., Zhang, X., Shu, S., Chu, T. & Yu, D., 2011. Phenylboronic acid grafted chitosan as a glucose-sensitive vehicle for controlled insulin release. *Journal of Pharmaceutical Sciences*, 100(6), pp.2278–86.

Xu, Y. & Du, Y., 2003. Effect of molecular structure of chitosan on protein delivery properties of chitosan nanoparticles. *International Journal of Pharmaceutics*, 250(1), pp.215–226.

Yang, W., Gao, X. & Wang, B., 2003. Boronic acid compounds as potential pharmaceutical agents. *Medicinal Research Reviews*, 23(3), pp.346–68.

Yao, Y., Zhao, L. & Yang, J.J., 2012. Glucose-Responsive Vehicles Containing Phenylborate Ester for Controlled Insulin Release at Neutral pH. *Biomacromolecules*, 13(6), pp.1837–44.

Ye, L., Landen, W.O. & Eitenmiller, R.R., 2001. Comparison of the Column Performance of Narrow-Bore and Standard-Bore Columns for the Chromatographic Determination of α-, β-, γ-, and δ-Tocopherol. *Journal of Chromatographic Science*, 39, pp.1–6.

Yin, L., Ding, J., He, C., Cui, L., Tang, C. & Yin, C., 2009. Drug permeability and mucoadhesion properties of thiolated trimethyl chitosan nanoparticles in oral insulin delivery. *Biomaterials*, 30(29), pp.5691–700.

Yin, R., Han, J., Zhang, J. & Nie, J., 2010. Glucose-responsive composite microparticles based on chitosan, concanavalin A and dextran for insulin delivery. *Colloids and Surfaces. B, Biointerfaces*, 76(2), pp.483–8.

Zhang, X., Zhang, H., Wu, Z., Wang, Z., Niu, H. & Li, C., 2008. Nasal absorption enhancement of insulin using PEG-grafted chitosan nanoparticles. *European Journal of Pharmaceutics and Biopharmaceutics*, 68(3), pp.526–34.

Zhu, S., Qian, F., Zhang, Y., Tang, C. & Yin, C., 2007. Synthesis and characterization of PEG modified N-trimethylaminoethylmethacrylate chitosan nanoparticles. *European Polymer Journal*, 43(6), pp.2244–2253.

Zimmet, P., Alberti, K.G. & Shaw, J.E., 2001. Global and societal implications of the diabetes epidemic. *Nature*, 414(6865), pp.782–7.